BELGIQUE
CANADA
DANMARK
DEUTSCHLAND
ELLÁS
FRANCE
ISLAND
ITALIA
LUXEMBOURG
NEDERLAND
NORGE
PORTUGAL
TURKIYE
UNITED KINGDOM
UNITED STATES

AGARDograph 35

10

AGARDograph

A SUMMARY OF DESIGN TECHNIQUES FOR AXISYMMETRIC HYPERSONIC WIND TUNNELS

BY
Ying-Nien Yu

FC

NOVEMBER 1958

NORTH ATLANTIC TREATY ORGANIZATION
ADVISORY GROUP FOR AERONAUTICAL RESEARCH AND DEVELOPMENT
Palais de Chaillot, Paris 16

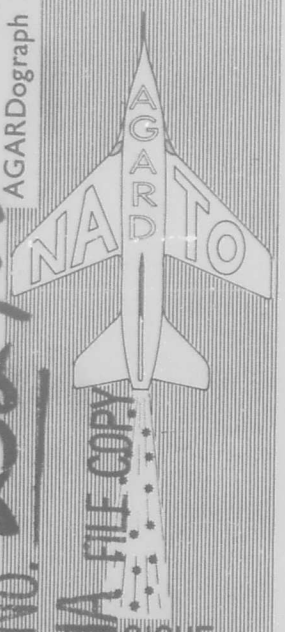

BELGIQUE
CANADA
DANMARK
DEUTSCHLAND
ELLÁS
FRANCE
ISLAND
ITALIA
LUXEMBOURG
NEDERLAND
NORGE
PORTUGAL
TURKIYE
UNITED KINGDOM
UNITED STATES

AGARDograph 35

(10)

AGARDograph

A SUMMARY OF DESIGN TECHNIQUES FOR AXISYMMETRIC HYPERSONIC WIND TUNNELS

BY
Ying-Nien Yu

FC

NOVEMBER 1958

NORTH ATLANTIC TREATY ORGANIZATION
ADVISORY GROUP FOR AERONAUTICAL RESEARCH AND DEVELOPMENT
Palais de Chaillot, Paris 16

AGARDograph 35

NORTH ATLANTIC TREATY ORGANIZATION

ADVISORY GROUP FOR AERONAUTICAL RESEARCH AND DEVELOPMENT

A SUMMARY OF DESIGN TECHNIQUES FOR AXISYMMETRIC HYPERSONIC WIND TUNNELS

by

Ying-Nien Yu

November 1958

SUMMARY

A family of perfect fluid coordinates for axisymmetric effusers with the exit Mach number range of 5 to 20 has been computed by the method of characteristics. A conical source flow front and a centerline Mach number distribution are used as initial conditions. Design techniques and other related problems of interest in the development of hypersonic facilities are summarized.

SOMMAIRE

Une famille d'axes de coordonnées d'un fluide parfait pour les souffleries axe-symétriques avec nombre de Mach sortie depuis 5 jusqu'à 20 est calculée par la méthode des caractéristiques. Un écoulement du ecoulement du source conique et une distribution des nombres de Mach d'axe sont employés comme les conditions initiales. Les techniques de dessin et les autres problèmes d'interêt apparentés dans le développement des facilités hypersoniques sont récapitulés.

533.6.071:533.6.011.55

3b8c2c

CONTENTS

LIST OF TABLES

LIST OF FIGURES

NOTATION

a	local speed of sound
a, a_0, a_1, a_2	coefficients (Sections 3.2.2.2 and 3.2.2.4)
a_0	speed of sound at stagnation conditions
c_f	local skin friction coefficient
c, d	exponents in temperature function
f	function
g	acceleration of gravity
h_g	gas side film coefficient
k	function of specific heat ratio
$k_1 k_2$	factors in Mach number distribution function
n, n_1, n_2, n_3	exponents
p	points along source flow front and exit characteristic
q	velocity ratio (Sec. 3.2.1.2)
q	rate of heat transfer (Sec. 5)
r.f.	temperature recovery factor
r	nozzle ordinate (r = 0 along axis of symmetry)
s	transfer function in Laplace transform
t_0	total temperature in boundary layer
u, v	velocity components (u in z-direction, v in r-direction)
w	weight flow rate
x,y	expansion region coordinates (Sec. 3.2)
x, y	local coordinates in boundary layer (Sec. 3.3)
z	nozzle abscissa (z = 0 at origin of source flow)
A	area

A/A^*	one-dimensional area ratio
A, B, C, D	coefficients in flow equation ((Sec. 3.2.1.1)
C_1, C_2, C_3, C_4	coefficients in response equation
E	Young's modulus of elasticity
F, G	iteration functions
H	boundary layer shape factor
J, J_0, J_1, J_2	right-running characteristic line notation
K_A	loop gain factor
L	minimum nozzle length
M	Mach number
N	characteristic net size
P	pressure
Q	iteration function (Sec. 3.2.1.2)
Q	unknown point in wall point calculation (Sec. 3.2.3.2)
P, Q	coefficients in boundary-layer growth equation
R	gas constant
R	radius of source flow front
R_0	radius of source flow front at Mach 1
Re	Reynolds number per unit length
Re_θ	Reynolds number based on momentum thickness
S, S′	intersections of characteristic lines with stream lines
T	temperature; also local static temperature in boundary layer
T_1	temperature at which thermal stress is zero
T_2	temperature at which thermal stress is desired
U, V, W	points in wall coordinate calculation (Sec. 3.2.3.2)
V	volume

V	velocity (Sec. 3.2.1.2)
V_M	maximum speed obtainable by expanding the flow to zero absolute temperature
W	weight of gas
ΔW	change in weight of gas
α	Mach angle
α	coefficient of thermal expansion (Sec. 5)
β_1, β_2	exponents in response equation
γ	ratio of specific heats
δ	boundary-layer thickness
δ^*	boundary-layer displacement thickness
η_1, η_2	quantities used in wall coordinate calculation
θ	flow angle with respect to (z, r) coordinate system
θ	boundary-layer momentum thickness (Sec. 3.3)
λ	Mach number function
μ	coefficient of absolute viscosity
ν	Poisson's ratio
π	partial cancellation region length factor
ρ	density
$1/\rho_t$	nozzle wall curvature at throat
σ	temperature function (Sec. 3.3)
σ	thermal stress (Sec. 5)
τ	time
ϕ	velocity potential
ψ	Prandtl-Meyer angle
ω	exponent in skin friction equation
Δ	thermal boundary-layer thickness

Subscripts

a	refers to adiabatic conditions
e	refers to diffuser exit conditions
i	refers to numerical index (Sec. 3.2.4)
i	refers to initial conditions
p	refers to points along source flow front and exit characteristic
r, z, ṙ	refers to partial derivatives
s	refers to storage conditions
t	refers to nozzle throat
W	refers to wall values
A, B, C	refers to nozzle points
L, R	refers to left and right running characteristics respectively
L	refers to laminar sub-layer thickness (Sec. 3.3)
0	refers to stagnation conditions
1	refers to nozzle test section conditions
∞	refers to conditions at outer edge of boundary layer
1, 2, 3	refers to points in characteristic net iteration (Sec. 3.2.2.1)
$(\dot{})$, $(\ddot{})$	refers to derivatives
$(\bar{})$	refers to average value (Sec. 3.2.2.1)
$(\bar{})$	refers to function of momentum thickness (Sec. 3.3)
$(\,)^*$	refers to values at nozzle throat

A SUMMARY OF DESIGN TECHNIQUES FOR AXISYMMETRIC HYPERSONIC WIND TUNNELS

Ying-Nien Yu*

1. INTRODUCTION

Due to the rapid increases in flight speeds of vehicles in the past decade, aeroscientists and engineers are confronted with many unsolved problems associated with high speed flow. Experimental information must be gathered to overcome the lagging theoretical treatment of these newly created problems and to correlate theories under development. The use of supersonic wind tunnels for testing flight vehicles or objects at lower Mach numbers has provided much valuable information for scientists and engineers. For vehicles traveling at hypersonic speeds, valuable design information will also be available through wind-tunnel testing even though complete simulation of free flight may not be achieved.

The methods employed in supersonic wind tunnel design are well known, for installations of supersonic wind tunnels of varying sizes and types are common throughout the world. References 1 through 3 describe the design and development of various types of supersonic wind tunnels.

Most of the techniques developed for supersonic wind tunnel design are equally applicable to hypersonic wind tunnels. For Mach numbers greater than 5, higher supply pressures and temperatures are necessary to expand the gas to test region Mach number and to accomplish this without gas liquefaction. As the Mach number increases, the required supply energy will be higher accordingly. For example, to obtain the test region Mach number of 14, if the gas is air to be expanded to atmospheric pressure, a supply pressure of 24,000 lb/in^2 and supply temperature of 3000°R may be required. The simultaneous generation of high supply energy, and the resulting thermo-structural problems from the high temperature and pressure in various parts of the tunnel circuit, necessitate additional techniques for the development of hypersonic wind tunnels.

The nozzle or effuser section of the supersonic wind tunnel is usually two-dimensional since the contoured nozzle can be made either flexible or semi-flexible to permit variable Mach number operation. Due to the limitation of test section size, and the large ratio between exit and throat areas, the two-dimensional nozzle becomes impractical at Mach numbers greater than 8. The test section area is usually limited by the supply energy available, thus limiting the mass flow rate. The larger test area requires greater energy sources, hence it is economically impractical. A limited test area combined with large area ratio results in a very small throat area, which means a very small throat height for the two-dimensional nozzle. For example, a Mach 8.0 nozzle with a perfect fluid exit height of 8 inches will have a throat height of only 0.042 inches.

Structurally, such a small throat is not only difficult to fabricate, but will create disturbances in the flow field downstream, since thermal distortion results from high heat transfer rates to the large wetted throat surface. Aerodynamically, the hypersonic boundary layer growth for the two-dimensional nozzle is difficult to estimate. The boundary layer displacement thicknesses are larger than those of supersonic nozzles, and the presence of different transverse pressure gradients, as well as longitudinal pressure gradients, along the contoured walls

*Sandberg-Serrell Corporation, Pasadena, California, U.S.A.

and the side walls results in a non-uniform boundary layer build-up. It becomes necessary to diverge or perhaps contour the side walls to compensate for the boundary layer growth in addition to adjusting the contoured walls. This introduces difficult sealing problems along the corners of the walls. Finally, despite all the adjustments, the non-uniform boundary layer build-up will still result in a non-uniform flow distribution in the test section such as shown in Figure 1(a).

There are obvious advantages in making the nozzle rotationally symmetric. The throat height, or diameter, as compared to the two-dimensional nozzle with the same test section Mach number and height, is larger; higher temperatures can be permitted at the throat since thermal expansion is small and uniform due to axial symmetry; and, with the same pressure gradient along the meridians, boundary layer growth is uniform, resulting in a symmetric flow pattern in the test section as shown in Figure 1(b).

The contoured surface of the nozzle must be made very smooth in order to prevent flow disturbances that will focus on the center-line and reflect downstream to the test region. Included in this report is a discussion on the fabrication of axisymmetric nozzle by electro forming, a technique by which the nozzle walls can be made extremely smooth.

Despite the inherent limitation to fixed Mach number, axisymmetric nozzles must replace conventional two-dimensional nozzles for the high Mach number range.

The major portion of this report is devoted to the design techniques for axi-symmetric nozzles. In particular, a family of 46 perfect fluid contours was computed by the IBM Type 704 electronic digital computer using the method formulated. The contours have a Mach number range of 5 to 20 at expansion angles of 6^{o} and 10^{o}. Specific heat ratios of 6/5 and 5/3 in addition to 7/5 (for air), were used in computing contours for Mach numbers greater than 9. The gas in all cases was assumed to be at frozen equilibrium. The coordinates of these 46 contours are tabulated in Appendix I.

In Appendix II perfect fluid contour coordinates computed by the NASA*, are included. The exit Mach number of one of the contours is 27.

Computations of axisymmetric nozzle contours are also being made at the Wright Aeronautical Development Center. The report on these contours will be published soon.

In the discussion on aerodynamics, methods for calculating boundary layer growth are given. The remainder of this report is a summary of design techniques for axisymmetric hypersonic wind tunnels.

2. COMPONENTS OF HYPERSONIC WIND TUNNELS

2.1 General Arrangement of Wind Tunnel Circuits

In conventional supersonic wind tunnels, the steady flow duration governs the physical arrangement of the tunnel circuit. For continuous operation, the circuit will be closed, and the tunnel will be driven by a continuously operating compressor system. The flow duration for the intermittent type of wind tunnel ranges from a few seconds to a few minutes. There are generally three possible arrangements for intermittent wind tunnels: the blowdown, the drawdown, and a combination of blowdown and drawdown.

In general, a heater and thermal equalizer in the supply sections and an aftercooler downstream of the diffuser are required for a hypersonic tunnel in addition to the components of the supersonic tunnel. To

*National Aeronautics and Space Administration, formerly NACA.

generate high pressure ratios during starting for continuous flow tunnels, an auxiliary evacuating device may be added to the circuit. For economical and practical reasons, the majority of intermittent hypersonic wind tunnels are a combination of blowdown and drawdown. It is often advantageous to make use of an ejector system instead of an expensive vacuum tank to evacuate the gas downstream of the diffuser. Figure 2 shows typical arrangements for continuous and intermittent hypersonic wind tunnel circuits.

2.2 Supply Sections

As shown in Figure 2, the supply sections for continuous-operation tunnels contain a drying system for inlet air, a compressor system, a heater section, and a thermal mixer. For intermittent tunnels, high-pressure vessels are required to store the compressed gas. Extensive theories and data on air drying systems and compressors for high speed wind tunnels are reported in References 4 and 5, respectively.

2.2.1 *Storage Tanks*

In general, the storage tanks are located upstream of the heater section. The volume and energy level of the storage tank are functions of the run duration desired. The decrease in gas weight in the storage tank by the end of a run is

$$\Delta W = \frac{V_s P_{si}}{R T_{si}}\left[1 - \left(\frac{P_0}{P_{si}}\right)^{\frac{1}{n}}\right] = \dot{w}_1 \tau_1 \quad (1)$$

$\dot{w}$, remains constant during a run since the stagnation pressure and temperature are usually constant. Therefore, the running time, τ, varies directly with $V_s P_{si}$, if the tank initial temperature, T_{si}, and stagnation pressure, P_0, are given.

In selecting storage tanks, consideration must be given to cost, available space, safety, etc. Usually, high-pressure vessels require welding, stress-relieving and inspection before assembly. Such operations are costly to perform in the field, therefore it is economical to fabricate the tanks in the shop and install in the field, i.e., if the tanks can also be made transportable. Sometimes, due to space limitations, a single tank is not feasible, but can be replaced by connecting a parallel row of tanks to a common manifold. Code requirements for high pressure vessels should be observed for safety.

2.2.2 *Heaters*

As pointed out in the Introduction, to maintain liquefaction-free flow at high Mach numbers in the test region, the stilling chamber gas must be raised to a high temperature level. Figure 3 shows computed stagnation temperatures vs test section Mach numbers at various stagnation pressures. The exact behavior of gas liquefaction is extremely complicated and relatively unknown. Detailed treatment of this subject is available in References 6 and 7.

Most of the hypersonic facilities in the United States are still in the development stage, and the design of the heaters is one of the major problems associated with this development work. For operation up to approximately Mach 14, heat can be transferred by convection. For operation at Mach numbers greater than 14, high temperature and pressure can be achieved simultaneously by compressing the gas adiabatically.

Convection heaters may be of continuous or intermittent types to match the tunnel circuit arrangement. Electric heaters are suitable for continuous operation. The gas temperature is limited by the heating element temperature obtainable. Nichrome, with an operating element temperature of 2000°R, is often used for electric heaters. It is reported in Reference 8 that electric heaters using Kanthal elements have produced air temperatures in excess of 2500°R.

When it is desirable to reduce electric power requirements, the gas can be heated by convection in two stages. The first stage heater can be gas or oil-fired to achieve a

gas temperature of about 1400°R. The second stage is usually an electric heater.

It is more desirable to use storage heaters for intermittent operation, although direct heating by electric heaters may also serve the purpose. Storage heaters are commonly of the pebble-bed type. Before each run, thermal energy is accumulated at a low rate and stored in the pebbles which are usually made of aluminum or zirconium oxide. In general, pebble-beds can be heated electrically or by gas-firing. A typical gas-fired pebble-bed heater is shown in Figure 4. The design and operation of pebble bed heaters suitable for hypersonic wind tunnel operations are reported in References 9 through 13. The operating temperature for aluminum oxide is about 3000°R and for zirconium oxide is about 4500°R.

In Reference 14, a new type of heater using the principle of adiabatic compression is discussed. The heater consists of a vertical cylinder with a free-travelling diaphragm which divides the cylinder into two chambers. The bottom chamber connecting with the nozzle is filled with gas of predetermined initial pressure and temperature. Cold air at high pressure in the top chamber moves the diaphragm downward and compresses the gas in the bottom chamber to a high pressure and temperature level. A sketch of the compression heater is shown in Figure 5. A temperature of 6000°R can be realized with an initial temperature of 3000°R. This is illustrated in the ideal performance graph for the compression heater in Figure 6, which is duplicated from Reference 15. These high temperatures will allow tunnel operation up to Mach 20.

2.2.3 Thermal Mixers

The purpose of the thermal mixer is to remove the temperature stratification due to mixing of hot and cold air streams or uneven heating. Experience has shown that successful mixing can be achieved by: 1) long mixing length, 2) swirling motion of the streams, or 3) coarse grid screens or perforated plates.

An efficient mixer usually causes high pressure losses. A typical thermal mixer design is shown in Figure 7.

2.3 Nozzles

The objection to the use of two-dimensional nozzles for high Mach number operations was stated in the Introduction. One of the main difficulties is unsymmetrical thermal distortion in the throat region, which is caused by the high heat transfer rates which result from turbulent boundary layer growth at the throat. Many complicated engineering problems in cooling and fabrication of the throat section result from this process.

It has been stated that the advantage in using the two-dimensional nozzle is the achievement of variable Mach number with one pair of flexible walls. However, in hypersonic flow the high temperature gradients in the throat region necessitate minute adjustments in throat height to compensate for distortion; this introduces sealing, insulation, and motion problems which are not easily overcome.

Moreover, the three-dimensional thermal distortion in the two-dimensional throat section (which may be reinforced with ribs or without ribs as shown in Figure 8) can generate disturbances downstream in the test region. Therefore, the two-dimensional nozzle is impractical for high Mach number applications.

The axisymmetric nozzle has a minimum wetted surface area at the throat; the heat load, therefore, is lower than that of the two-dimensional nozzle. The smaller throat surface results in less thermal expansion which will not disturb the test region flow appreciably.

The methods for computing perfect fluid contours, boundary layer growth, and related aerodynamic problems for the rotationally symmetric nozzles are discussed comprehensively in Section 3.

2.4 Test Sections

The general requirements for the test section design are as follows:-

(a) It must be possible to mount a model support of minimum blockage area securely so that it will provide multi-degrees of freedom with all models to be tested.

(b) It must be possible to install viewing windows for observation of the flow.

Since no difficulty exists in mounting the viewing windows in the two-dimensional nozzles, the test sections can be made closed. At Mach numbers above 5, flat windows can be mounted in a closed test section for an axisymmetric nozzle, since the disturbances created by the resulting discontinuities cross well downstream of the model. For axisymmetric nozzles at Mach numbers below 5, however, it is sometimes necessary to mount curved windows, which are not only impractical from an engineering standpoint, but optically undesirable. However, by making a free-jet test section, flat windows can be easily installed. The temperature on the windows will probably rise slightly above ambient due to the small amount of mass transfer from the boundary of the jet. Figure 9 illustrates a typical free-jet test section.

Certain other advantages are obvious in using the free-jet test section:

(a) There is more space for maneuvering models. Thus, models can be ejected outside the test region during starting and stopping.

(b) With a larger test area, the mechanical and structural design of the model support is relatively simple.

(c) By regulating the plenum-chamber pressure, desirable jet expansion may be obtained.

Experience has indicated that larger pressure ratios are usually required to start and run a free-jet nozzle in comparison with a closed-jet nozzle. Discussion of the two modes of operation will be given in Section 3.

2.5 Diffusers

2.5.1 General Considerations

The theoretical aspects of supersonic and subsonic diffuser processes are still relatively unknown. The geometry of supersonic diffusers is arbitrarily based, therefore, on the best experimental data available. Converging-diverging diffusers are commonly used for supersonic wind tunnel circuits. Such configurations usually provide the best recovery and stability in the test section flow because the shock system in the diffuser can be located near the second throat region.

Diffusers can be either fixed or adjustable. Fixed diffusers are economical, but undesirable if the tunnel has a large Mach number range and the objects under test vary considerably in size and shape. For maximum recovery, it is always desirable to use the variable diffuser. However, the cost of adjustable diffusers is many times the cost of fixed ones.

The design procedures for diffusers in hypersonic operation are similar to those for supersonic wind tunnels except that the diffuser walls should be thermally protected because of the high supply temperatures required for hypersonic operation.

In addition to the thermal protection of the diffuser walls, the recovered flow should be cooled to a desirable temperature level for exhaust to the atmosphere or return to the compressor inlet in continuous operation.

2.5.2 Fixed Diffusers

The simplest geometry for a fixed diffuser is a straight circular pipe 8 to 15 diameters in length. This simple diffuser can easily

be connected to the pick-up scoop of the free-jet test section regardless of whether the nozzle exit is two-dimensional or rotationally symmetric. In a closed test section, a transition piece will be required if the nozzle is two-dimensional.

A more effective diffuser is the conical fixed-diffuser. A gradually converging cone is followed by a straight section of approximately two to ten diameters in length. This section is followed by a diverging section as shown in Figure 10(a). With this configuration, a fixed second throat is provided.

2.5.3 *Adjustable Diffusers*

Since the mixing of the flow in the diffuser is a very complex process, solutions have not been found except on empirical bases. The existing technique of adjusting the second throat area to optimize starting and running ratios seems to be quite successful. For a particular tunnel circuit, however, better recoveries may be obtained with additional adjustments in the other parts of the diffuser. This usually involves laborious research and high cost in fabrication, and the configuration so obtained in a particular tunnel cannot generally be applied to other tunnels.

The second throat area in conical diffusers can be adjusted by sliding a center body cone along the axis of symmetry. However, little success has been reported with this configuration.

The conventional two-dimensional adjustable diffuser with single jacks at the second throat is still a favorable design. Experience indicates that the design criteria for the most efficient two-dimensional variable diffuser suitable for hypersonic operation are as follows:

(a) Total length of the diffuser should be at least ten times the entrance height.

(b) Contraction-ratio range, that is, the diffuser entrance height to second throat-height ratio, should be from five to ten.

(c) Total contraction - angle range should be about 15° to 18°.

(d) Total expansion angle downstream of the second throat should be below 12°, preferably 6° to 8°.

(e) Exit area should be about one and one-half times the tunnel test section area.

The geometry of a typical two-dimensional adjustable diffuser is illustrated in Figure 10(b).

2.6 Ejectors

One of the main requirements for operating a hypersonic wind tunnel is a high pressure ratio (P_0/P_e) between the stilling chamber and diffuser exit. With efficient diffusers, experimental data, which will be discussed in the performance section, indicate that hypersonic tunnels with empty test section can be started at slightly higher than the normal-shock pressure ratio of the test section Mach number, i.e., one may assume one-dimensional flow with a normal shock separating the flow fields. The running ratios will usually be below the normal shock ratios.

As Mach number increases, the normal-shock ratio increases at a much larger rate. For air ($\gamma = 1.4$)

$$\frac{P_0}{P_e} = \left(\frac{M_1^2 + 5}{6M_1}\right)^{7/2}\left(\frac{7M_1^2 - 1}{6}\right)^{5/2} \qquad (2)$$

For example, at $M_1 = 2.0$, P_0/P_e is only 1.19; while at $M_1 = 10.0$, P_0/P_e is 328. This implies that a stagnation pressure of 328 times the atmospheric pressure will be necessary to start a Mach 10 nozzle if the air is expanded to atmospheric pressure at the exit of a blowdown wind tunnel. The

storage pressure P_s must be greater than P_0 if appreciable run times are to be achieved in blowdown operation. Such high pressure levels result in high cost compressor systems and pressure vessels; blowdown to atmospheric pressure, therefore, is impractical.

High pressure ratios can be easily achieved by ejecting the exit pressure P_e below atmosphere. One of the convenient methods is to provide a vacuum chamber or sphere at the exit. However, for large test section areas the vacuum spheres required become enormous. Perhaps an ejector or ejector system is most expedient for the purpose. The primary advantage in the use of ejectors is in the variability of P_e. In this case, optimized starting and running ratios are possible.

Ejector applications in various engineering and chemical fields are numerous. Design criteria at the present state of the art, however, are largely of an empirical nature due to the complicated mixing and diffusion processes involved and the many associated parameters which are not yet related rigorously by theory.

An ejector system generally consists of a supply of primary gas, a throttling valve, and a Laval nozzle or group of nozzles. The most efficient and common gas for the primary flow is steam; compressed air or other gases are, however, also utilized. About 3lb of steam are required to eject 2 pound of air and possibly 7 lb of air are required to eject 1 lb of air. Since the relationships are complicated, References 16 and 17 should be consulted before any design is undertaken.

The location of the ejector with respect to the tunnel circuit deserves careful consideration. Generally, the ejector is placed downstream of the diffuser; nevertheless, it is quite feasible to locate the system immediately downstream of the test section or in the second throat region. The first location is convenient from mechanical and structural standpoints because of the larger space available. If the system is placed near the test section or the second throat region, higher efficiency may be achieved, but this requires extensive research.

The number of ejector nozzles required can be related to the range of operation. Multiple nozzles always improve the downstream mixing as well as the control characteristics of the system. The mass flow rate ratio of primary and induced flows usually determines the value of P_e, it is, therefore, an important parameter.

It should be pointed out that ejectors may also be used advantageously in continuous tunnels, even though the tunnel circuit efficiency will necessarily be lowered. The advantage, of course, is to increase the pressure ratios, thus permitting extension of the Mach number range without increase in capacity of the compressor system. To accomplish this, gas is by-passed from the exit of the compressor to serve as a primary flow for the ejector. An arrangement of the ejector by-pass in the continuous circuit is shown in Figure 11.

3. AERODYNAMICS OF AXISYMMETRIC WIND TUNNEL NOZZLES

3.1 Perfect Fluid Contours - General Discussion

3.1.1 Nozzle Aerodynamic Regions

There are four aerodynamic regions in a supersonic wind tunnel nozzle. The contraction section lies between the supply section and the throat. In this section the flow is accelerated from subsonic speed to the speed of sound at the throat. The expansion region is downstream of the throat and extends to the point on the wall where the maximum wall angle is reached. Here the flow is expanded from sonic to supersonic speed. The wall point corresponding to this maximum wall angle is sometimes called the point of inflection. Downstream of the expansion region is the transition region;

here the flow is straightened to become uniform and parallel and it reaches the design Mach number at the exit characteristic line. The last region is the test region. Wall coordinates of the first, second, and third regions form a perfect fluid contour. The flow regions described are shown in Figure 12.

3.1.2 *Validity of Perfect Fluid Theory for Nozzle Design*

In order to achieve uniform and parallel flow at the design Mach number in the test region of a wind tunnel, the nozzle wall should be aerodynamically contoured. The shape of the portion of the contour downstream of the nozzle throat in the supersonic flow region is especially important.

Experience has shown that the classical perfect fluid theory, even at very high Mach numbers, is valid for calculating the supersonic flow regions of the nozzle, except, of course, in the viscous layer near the wall, which must be treated by other means.

Due to the high supply energy in the case of hypersonic nozzles, imperfect gas behavior will be introduced in the flow field. This real gas effect is small and can usually be neglected, except when the supply energy is extremely high. Even with extremely high supply energy, however, imperfect gas behavior occurs only near the throat region where the high free stream temperature and pressure cause deviations in the specific heat ratio. It will be shown later that by assuming an initial source-flow front, the difficulty in computing the expansion region coordinates can be avoided. Further, the selection of a low expansion angle for the computation of a hypersonic contour will tend to minimize the flow errors. Since real gas behavior at very high supply energy is relatively unknown, the use of perfect fluid theory is imperative. Fortunately, for most engineering applications the theory is valid.

In general, there are two methods used to establish the initial conditions for computing the nozzle coordinates:

Method I. The computation is begun at the throat by assuming the shape of the sonic surface and either

(a) expanding the flow through a finite angle at the throat, or

(b) prescribing the wall coordinates for a distance downstream of the throat, or

(c) prescribing the Mach number distribution along the axis of symmetry of the nozzle.

Method II. The coordinates are computed by assuming source flow at the inflection point and either

(a) expanding the flow without partial cancellation, or

(b) prescribing the shape of the wall in the partial cancellation region, or

(c) prescribing the Mach number distribution in the partial cancellation region along the axis of symmetry.

Figures 13(a), 13(b) and 13(c) illustrate Method I. In Figure 13(a) the flow is expanded through a finite angle at the throat. If plane sonic flow is assumed at the throat, in axially symmetric flow, the expansion through a finite angle behaves in the same manner as that in the two-dimensional case. Therefore, the expansion region can be established by expanding the flow through the corner until the design Mach number is reached on the axis. In Figure 13(b) an arbitrary expansion curve for the wall shape starting at the throat is prescribed. Instead of expanding the flow at the throat corner, the expansion region is constructed along the prescribed curve until the exit characteristic point on the axis is reached. The two approaches are analyzed in Reference 18.

The third approach is shown in Figure 13(c). Here the centerline Mach number distribution is used to calculate the expansion flow field. A flow net can be constructed with the given Mach number distribution and the assumption of a plane sonic surface. From the flow net, the wall streamline can be calculated. This method was first used in Reference 19 and is actually the inverse of the second approach.

It is also plausible to assume a curved sonic surface instead of the plane sonic surface to compute expansion regions in the three approaches discussed. The theory for calculation of the curved sonic surface is given by Sauer in Reference 20.

In Method II the flow up to the inflection point is assumed to be source flow, illustrated in Figures 14(a), 14(b) and 14(c). As in Method I, there are three ways to expand the flow to the exit Mach number. In the case of maximum expansion, shown in Figure 14(a), the downstream end of the source flow front coincides with the exit characteristic point, and the wall coordinates may be expressed analytically by Foelsch's method[21], or the partly graphical and partly analytical method of Sauer[22]. In Figure 14(b) the source flow front does not expand immediately to the exit characteristic, so that a partial cancellation region exists. This region can be specified by prescribing a monotonic wall curve as the boundary of the transition region. This results in a comparatively longer nozzle than that of Figure 14(a). The third approach, shown in Figure 14(c), is the one used in computing the family of perfect fluid contours for this report. In this approach, as in Method II b, the source flow front is not fully expanded. The Mach number distribution along the axis is prescribed from the end of the source flow front to the exit characteristic. From these conditions the flow net in the partial cancellation region can be constructed.

Each method of computing contours has its advantages. Whenever the flow is expanded through an angle at the throat (Method I a) or maximum expansion is assumed (Method II a), the nozzles will be shorter than those computed by the alternate methods. Prescription of the wall coordinates or partial cancellation region in Methods I b and II b yields more accurate results in the sense that iteration processes are not necessary and other conditions are less arbitrary. Whenever the centerline Mach number distribution is prescribed (Methods I c and II c), the nozzle length is immediately and accurately known from a simple relation.

3.1.3 Formulation of Axisymmetric Nozzle Design Method

The first method discussed involves the computation of flow expansion starting at the throat of the nozzle. Earlier, it was pointed out that, due to the high supply energy, imperfect gas behavior exists near the throat region. Hence the use of perfect fluid theory no longer holds in this region. Other difficulties arise near the sonic line. The flow equations are discontinuous at Mach 1. Moreover, it is known that the sonic line is not straight, and it is doubtful that the proper curvature of the sonic line can be accurately estimated. All these uncertainties indicate that to establish the initial conditions by the first method, i.e., prescribing values near the throat, is at least precarious.

The assumption of conical source flow has obvious advantages. First, the calculation of the expansion region coordinates is reduced to the problem of fitting a monotonic curve to match the throat geometry. Figures 15(a) and 15(b) show two types of curves which may be used as expansion curves. A circular arc followed by a straight line is one type shown in Figure 15(a) and a cubic parabola with origin at the point of inflection is the second type shown in Figure 15(b). Secondly, the expansion angle can be specified as a design parameter. This cannot be done if the computation starts from the throat. Because the ratio of throat diameter to expansion region length is smaller in the hypersonic case, the requirement for the

assumption of source flow is more nearly satisfied.

The second method gives three approaches to establish initial conditions by using the source flow assumption. The first approach yields the shortest nozzle; however, a discontinuity in wall curvature will result due to the discontinuity in the Mach number gradient along the centerline. A discontinuity in wall curvature is undesirable for the following reasons:

(a) Fabrication of a discontinuity is difficult, as is measurement for checking the work. Furthermore, the point of discontinuity is near the throat where space is considerably restricted.

(b) Aerodynamically, the occurrence of gas flow to conform with the design condition is hardly possible since any imperfect gas behavior, such as changes in the ratio of specific heats, changes in gas components, condensation or inaccurate boundary layer growth estimates, can cause the perfect gas characteristic pattern to shift. Such a shift, especially in the transition region, will cause focusing of compression waves on the centerline reflecting downstream to the test region. The effect of such a shift may be reduced only if the wall curvature is continuous and small. Further discussion on focusing effects will be given in Section 3.5.

In References 3 and 23 the auxiliary boundary conditions for continuous wall curvature in the two-dimensional nozzles are derived. Reference 3 suggests a prescribed contour for the partial cancellation region and Reference 23 uses a centerline Mach number distribution for the same purpose. The application of these auxiliary conditions is valid for axially symmetric flow, although the proof may not be obtained explicitly due to the complexity of the equations involved. The two approaches shown in Figures 14(b) and 14(c) show the applications of these auxiliary boundary conditions.

The advantage in using the prescribed curve for the partial cancellation region, as discussed in Reference 3, is that continuity in higher order derivatives of the wall coordinates can be obtained in addition to the continuity in curvature. This higher order continuity is necessary in flexible wall design. However, the axisymmetric nozzle is always fixed; therefore there is no particular need for continuity beyond the second order derivatives. Since continuous curvature is desirable and since nozzle length is often an important factor, the method illustrated in Figure 14(c) is chosen for the nozzle contours listed in this report. The analysis work necessary to establish these contours is presented in Section 3.2 of this report.

3.1.4 Contraction Contour

The contraction region contour should be a continuous curve, preferably designed according to potential theory to attain uniform flow at the throat. Such a method is given in References 24 and 25. The contour should give rapid acceleration of the flow when approaching the throat in order to avoid excessive boundary layer growth.

In practice, the design criteria for a satisfactory contraction contour may be summarized as follows:

(a) A large contraction ratio (of the order of more than 10 to 1) between inlet and the throat. This reduces the turbulence level and smooths the flow.

(b) A smooth curve with curvature continuity at the throat.

(c) Damping screens (about 3 to 5, spaced about 200 wire diameter apart) should be placed at the inlet to reduce the turbulence whenever possible.

With the above considerations, an arbitrary curve preserving continuity at the throat will serve as a contraction contour.

3.2 Perfect Fluid Contours - Computation

3.2.1 Method of Characteristics for Axisymmetric Flow

3.2.1.1 Theory. It is convenient to use a cylindrical coordinate system (z, r) for axisymmetric flow. The scalar form of Euler's equations of motion can then be written in the form

$$\left.\begin{aligned} u\frac{\partial u}{\partial z} + v\frac{\partial u}{\partial r} &= -\frac{1}{\rho}\frac{\partial P}{\partial z} \\ u\frac{\partial v}{\partial z} + v\frac{\partial v}{\partial r} &= -\frac{1}{\rho}\frac{\partial P}{\partial r} \end{aligned}\right\} \qquad (3)$$

For isentropic conditions the terms on the right hand side of (3) become

$$\left.\begin{aligned} \frac{\partial P}{\partial z} &= a^2\frac{\partial \rho}{\partial z} \\ \frac{\partial P}{\partial r} &= a^2\frac{\partial \rho}{\partial r} \end{aligned}\right\} \qquad (4)$$

where a is the local speed of sound which is related to the stagnation value a_0 by the equation

$$a^2 = a_0^2 - \frac{\gamma-1}{2}(u^2 + v^2) \qquad (5)$$

The continuity equation for compressible steady flow in cylindrical coordinates is

$$\frac{\partial(\rho u)}{\partial z} + \frac{\partial(\rho v)}{\partial r} + \frac{\rho v}{r} = 0 \qquad (6)$$

The condition of irrotationality gives the following relation

$$\frac{\partial v}{\partial z} - \frac{\partial u}{\partial r} = 0 \qquad (7)$$

This allows introduction of the velocity potential ϕ:

$$\left.\begin{aligned} \phi_z &= \frac{\partial \phi}{\partial z} = u \\ \phi_r &= \frac{\partial \phi}{\partial r} = v \\ \text{and} \quad \phi_{zr} &= \phi_{rz} \end{aligned}\right\} \qquad (8)$$

Combining Equations (3) through (8), the partial differential equation for axisymmetric, supersonic, irrotational, isentropic and steady flow is obtained:

$$(a^2 - \phi_z^2)\phi_{zz} - 2\phi_z\phi_r\phi_{zr} + (a^2 - \phi_r^2)\phi_{rr} + \frac{a^2}{r}\phi_r = 0 \qquad (9)$$

Substitution of A, B, C and D for the coefficients in (9) gives

$$A\phi_{zz} + 2B\phi_{zr} + C\phi_{rr} = D \qquad (10)$$

Equation (10) is a non-linear partial differential equation of the second order with two independent variables, and is sometimes called a quasi-linear differential equation because the derivatives of the highest order are linear.

The solutions of Equation (10) consist of three types depending on the signs of the quantity $B^2 - AC$:

(1) Hyperbolic Type: $B^2 - AC > 0$

(2) Parabolic Type: $B^2 - AC = 0$

(3) Elliptic Type: $B^2 - AC < 0$

In supersonic steady flow such as in Equation (9), the equation is of hyperbolic type. The hyperbolic differential equation can be solved by the well-known method of characteristics.

The fluid properties are continuous in the supersonic flow regime, therefore it is permissible to express the derivatives of the velocity components, ϕ_z and ϕ_r, in terms of the physical coordinates:

$$\left.\begin{aligned} d\phi_z &= \phi_{zz}dz + \phi_{zr}dr \\ d\phi_r &= \phi_{zr}dz + \phi_{rr}dr \end{aligned}\right\} \qquad (11)$$

It can be shown that the characteristic curves obtained as solutions to Equation (9) correspond to Mach lines which are generated in the actual flow.

These curves are known as hodograph characteristics when expressed in terms of the velocity components (ϕ_z, ϕ_r) and physical characteristics when expressed in terms of the space coordinates (z, r).

The solutions sought to Equation (9) are lines across which discontinuities in velocity can exist. These are obtainable by solving for the derivatives in Equations (10) and (11):

$$\left.\begin{aligned} A.\phi_{zz} + 2B.\phi_{zr} + C.\phi_{rr} &= D \\ dz.\phi_{zz} + dr.\phi_{zr} &= d\phi_z \\ dz.\phi_{zr} + dr.\phi_{rr} &= d\phi_r \end{aligned}\right\} \qquad (12)$$

These may be regarded as simultaneous linear algebraic equations in the variables ϕ_{zz}, ϕ_{zr} and ϕ_{rr}, as shown in Equation (12). Solution of the system for ϕ_{zz}, ϕ_{zr} and ϕ_{rr} gives

$$\phi_{zz} = \frac{D.dr^2 + C(dz.d\phi_z - dr.d\phi_r) - 2B.dr.d\phi_z}{A.dr^2 - 2B.dz.dr + C.dz^2} \qquad (13a)$$

$$\phi_{zr} = \frac{A.dr.d\phi_z - D.dz.dr + C.dz.d\phi_r}{A.dr^2 - 2B.dz.dr + C.dz^2} \qquad (13b)$$

$$\phi_{rr} = \frac{A(dr.d\phi_r - dz.d\phi_z) + D.dz^2 - 2B.dz.d\phi_r}{A.dr^2 - 2B.dz.dr + C.dz^2} \qquad (13c)$$

When the numerators and denominators of Equations (13) vanish simultaneously, ϕ_{zz}, ϕ_{zr} and ϕ_{rr} are indeterminate, and thus may be discontinuous.

Equating the denominator in Equations (13) to zero and solving for dr/dz gives

$$\left(\frac{dr}{dz}\right)_{R,L} = \frac{B \pm \sqrt{B^2 - AC}}{A} \qquad (14)$$

where R and L refer to the 'right-running' and 'left-running' characteristic curves corresponding to the positive and negative signs in Equation (14). Equation (14) is the differential equation for the projections of the characteristic curves in the physical plane. By substitution of values for A, B and C from Equation (9), (14) becomes

$$\left(\frac{dr}{dz}\right)_{R,L} = \frac{-uv \pm a\sqrt{u^2 + v^2 - a^2}}{a^2 - u^2} \qquad (15)$$

In a similar manner $d\phi_r/d\phi_z$ can be found by equating the numerator of any of Equations (13) to zero. For example, solving (13b):

$$\left.\begin{aligned} \left(\frac{d\phi_r}{d\phi_z}\right)_{R,L} &= -\frac{A}{C}\left(\frac{dr}{dz}\right)_{R,L} \pm \frac{D}{C}\left(\frac{dr}{d\phi_z}\right)_{R,L} \\ &= -\frac{B \pm \sqrt{B^2 - AC}}{C} + \frac{D}{C}\left(\frac{dr}{d\phi_z}\right)_{R,L} \end{aligned}\right\} \qquad (16)$$

Substitution for A, B, C, and D gives

$$\left(\frac{dv}{du}\right)_{R,L} = \frac{uv \pm a\sqrt{u^2 + v^2 - a^2}}{a^2 - v^2} - \frac{a^2 v}{a^2 - v^2}\frac{1}{r}\left(\frac{dr}{du}\right)_{R,L} \qquad (17)$$

Equation (17) gives the slopes of characteristic curves in the velocity plane in terms of ϕ_z, ϕ_r and r.

The solution of (9) is now reduced to solving the four simultaneous characteristic equations given by (15) and (17). Examination of these equations indicates that direct solutions are unobtainable, therefore numerical methods are necessary.

3.2.1.2 Numerical procedure. It is convenient to express the velocity components u and v in terms of V and θ where V is the local fluid velocity and θ is the direction of the velocity vector with respect to the (z,r) coordinate system as shown in Figure 16a). Thus:

$$\left.\begin{aligned} u &= V\cos\theta \\ v &= V\sin\theta \end{aligned}\right\} \qquad (18a)$$

and

$$\left.\begin{aligned} du &= \cos\theta.dV - V\sin\theta.d\theta \\ dv &= \sin\theta.dV + V\cos\theta.d\theta \end{aligned}\right\} \qquad (18b)$$

Substitution of (18a) and (18b), and of $\sin\alpha = a/V$ into (15) and (17), gives, after simplification, along 'right-running' characteristics:

$$\frac{dr}{dz} = \tan(\theta-\alpha) \qquad (19a)$$

$$d\theta + \frac{\cot\alpha}{V}dV - \frac{\sin\theta.\sin\alpha}{\sin(\theta-\alpha)}\frac{dr}{r} = 0 \qquad (19b)$$

and, along 'left-running' characteristics:

$$\frac{dr}{dz} = \tan(\theta+\alpha) \qquad (20a)$$

$$d\theta - \frac{\cot\alpha}{V}dV + \frac{\sin\theta.\sin\alpha}{\sin(\theta+\alpha)}\frac{dr}{r} = 0 \qquad (20b)$$

Equations (19) and (20) can be solved by the so-called 'lattice-point method', that is, by the construction of a Mach net in the physical plane. The procedure given in Reference 26 is used.

Introducing $q = V/V_M$

and

$$Q = \frac{\cot\alpha}{q} = \frac{\sqrt{M^2-1}}{q} \qquad (21)$$

$$F = \frac{\sin\theta.\sin\alpha}{\sin(\theta+\alpha)} \qquad (22a)$$

$$G = \frac{\sin\theta.\sin\alpha}{\sin(\theta-\alpha)} \qquad (22b)$$

where

$$M = \sqrt{\frac{2}{\gamma-1}\left(\frac{q^2}{1-q^2}\right)} \qquad (23a)$$

$$\alpha = \sin^{-1}\left(\frac{1}{M}\right) \qquad (23b)$$

and replacing the differentials in (19b) and (20b).

$$\left.\begin{aligned} &(\theta_3 - \theta_1) - Q_1(q_3 - q_1) + \\ &\qquad + \frac{F_1}{r_1}(r_3 - r_1) = 0 \\ &(\theta_3 - \theta_2) + Q_2(q_3 - q_2) - \\ &\qquad - \frac{G_2}{r_2}(r_3 - r_2) = 0 \end{aligned}\right\} \qquad (24)$$

where the subscript '1' refers to a known point on a 'left-running' characteristic, subscript '2' refers to a known point on a 'right-running' characteristic and subscript '3' refers to the point of intersection of the two characteristics, which is to be determined as shown in Figure 16(b).

At a 'general point', that is where $r_1 \neq r_2 \neq 0$, illustrated in Figure 16(b), the first approximation for point 3 is as follows: Solve for z_3 in Equation (25), which is (19a) and (20a) combined:

$$z_3 = \frac{r_2 - r_1 - z_2 \tan(\theta_2 - \alpha_2) + z_1 \tan(\theta_1 + \alpha_1)}{\tan(\theta_1 + \alpha_1) - \tan(\theta_2 - \alpha_2)} \tag{25}$$

and then γ_3 is obtained from either of the equations

$$\left.\begin{aligned} r_3 &= r_1 + (z_3 - z_1)\tan(\theta_1 + \alpha_1) \\ r_3 &= r_2 + (z_3 - z_2)\tan(\theta_2 - \alpha_2) \end{aligned}\right\} \tag{26}$$

q_3 can now be found by eliminating θ_3 from (24). Thus, q_3 is found from

$$q_3 = \frac{1}{Q_1 + Q_2}\left[q_1Q_1 + q_2Q_2 + \frac{F_1}{r_1}(r_3 - r_1) + \frac{G_2}{r_2}(r_3 - r_2) + \theta_2 - \theta_1\right] \tag{27}$$

Knowing q_3, θ_3 can be easily obtained from either of the relations

$$\left.\begin{aligned} \theta_3 &= \theta_1 + Q_1(q_3 - q_1) - \frac{F_1}{r_1}(r_3 - r_1) \\ \theta_3 &= \theta_2 - Q_2(q_3 - q_2) + \frac{G_2}{r_2}(r_3 - r_2) \end{aligned}\right\} \tag{28}$$

M_3 and α_3 are found from Equations (23a) and (23b) using q_3 from (27).

The quantities q_3, M_3, α_3 etc. represent first approximations to the solution. Iterations are necessary to converge to the solution. The number of iterations required depends on the grid size of the net. The rules for iteration are the following:

1. Calculate average quantities at points 1 and 2 designated by $\bar{}$

$$\left.\begin{aligned} \bar{\alpha}_1 &= \frac{\alpha_3 + \alpha_1}{2} \qquad \bar{\alpha}_2 = \frac{\alpha_3 + \alpha_2}{2} \\ \bar{\theta}_1 &= \frac{\theta_3 + \theta_1}{2} \qquad \bar{\theta}_2 = \frac{\theta_3 + \theta_2}{2} \\ \bar{r}_1 &= \frac{r_3 + r_1}{2} \qquad \bar{r}_2 = \frac{r_3 + r_2}{2} \end{aligned}\right\} \tag{29}$$

2. Evaluate $\bar{Q}_1$, $\bar{Q}_2$, $\bar{F}_1$ and $\bar{G}_2$ from (21), (22), (23) and (29).

3. The new quantities at point 3 can then be calculated using the average values in Equations (25) through (28). This procedure may be repeated as many times as necessary to bring the values of the differences of M_3 and θ_3 between a given pair of iterations to within desired tolerances.

Equation (24) becomes indeterminate when point 1 and point 2 are on the axis of symmetry, where $r_1 = r_2 = \theta_1 = \theta_2 = 0$. However, the last terms of (24) may be readily evaluated from the relations

$$\left.\begin{aligned} \lim_{\substack{r_1 \to 0 \\ \theta_1 \to 0}} \frac{F_1}{r_1}(r_3 - r_1) &= \theta_3 \\ \lim_{\substack{r_2 \to 0 \\ \theta_2 \to 0}} \frac{G_2}{r_2}(r_3 - r_2) &= \theta_3 \end{aligned}\right\} \tag{30}$$

Thus, the first approximation for point 3 becomes

$$q_3 = \frac{q_1Q_1 + q_2Q_2}{Q_1 + Q_2} \tag{31}$$

$$\left.\begin{aligned} \theta_3 &= \frac{Q_1(q_3 - q_1)}{2} \\ \theta_3 &= -\frac{Q_2(q_3 - q_2)}{2} \end{aligned}\right\} \qquad (32)$$

After the first approximation, the iteration procedure is the same as outlined for the 'general point' due to the averaging procedure used in Equation (29).

In case either point 1 or point 2 is on the axis of symmetry, the equations for the first approximations for q_3 and θ_3 can be derived in a similar manner.

The numerical procedure described here allows a step-by-step computation of the flow net once the initial conditions are known.

3.2.2 Initial Conditions

3.2.2.1 Nozzle design parameters. The design method formulated in Section 3.1.4 allows flexibility in selecting the nozzle design parameters. These parameters are

a. Test section Mach number, M_1

b. Nozzle expansion angle, θ_A

c. Length of partial cancellation region, π

d. Specific heat ratio at frozen equilibrium, γ.

In general, the Mach number in axisymmetric supersonic isentropic flow is associated with the expansion angle which equals one-half the value of the Prandtl-Meyer expansion angle. The Prandtl-Meyer relation is

$$\psi = \sqrt{\frac{\gamma+1}{\gamma-1}}\tan^{-1}\sqrt{\frac{\gamma-1}{\gamma+1}}\sqrt{M^2-1} - \tan^{-1}\sqrt{M^2-1} \qquad (33)$$

As in two-dimensional nozzles, there is a maximum allowable expansion angle $\psi_{A\,max}$ associated with the exit value ψ_1, in axisymmetric nozzles. This angle, according to Reference 21, is equal to

$$\psi_{A\,max} = \frac{\psi_1}{4} = \theta_{A\,max} \qquad (34)$$

Therefore θ_A should always be less than $\psi_1/4$ for an axisymmetric supersonic nozzle.

If the length of the nozzle is defined as the shortest nozzle shown in Figure 14(a), then with the origin at the source point

$$L = z_B + \sqrt{M^2 - 1} \qquad (35)$$

where $$z_B = \frac{1}{2}\csc\left(\frac{\theta_A}{2}\right) = R_0\left(\frac{A}{A^*}\right)_B^{\frac{1}{2}} \qquad (36)$$

and $$R_0 = \frac{1}{2}\csc\left(\frac{\theta_A}{2}\right)\left(\frac{A^*}{A}\right)_1 \qquad (37)$$

In the case of the shortest possible nozzle, point B on the axis coincides with C, and is the exit characteristic point; $(A/A^*)_B^{\frac{1}{2}}$, there, equals $(A/A^*)_1^{\frac{1}{2}}$ as shown in Figure 17(b).

We may conveniently choose the length of the partial cancellation region as πL. Thus, the total length of the nozzle is $(1 + \pi)L$ as shown in Figure 17(a).

If the gas is different from air, the appropriate specific heat ratio must be used to compute the contour.

3.2.2.2 Centerline Mach number distribution It has been stated that the auxiliary boundary condition for achieving curvature continuity at the wall is continuity in Mach number gradient along the axis of symmetry. It is also desirable to make $(d^2M/dz^2)_B$ continuous in addition to $(dM/dz)_B$. It requires only a slight amount of extra labor

to fit such a function between BC, as shown in Figure 17(a). Intuitively, this additional condition tends to refine the continuity properties along the wall contour.

Experience in computing a number of contours indicates that almost any function satisfying the conditions mentioned is suitable for the centerline Mach number distribution.

The method used in this report is illustrated in Figure 17. Once π is chosen, the length of BC is $2\pi L$; and

$$z_B = \frac{1}{2}\csc\left(\frac{\theta_A}{2}\right) \cdot \pi L \qquad (38)$$

Also, due to the source flow assumption

$$z_B = R_0\left(\frac{A}{A^*}\right)_B^{\frac{1}{2}}$$

$$= \frac{R_0}{M_B^{\frac{1}{2}}}\left[\frac{2}{\gamma+1} + \frac{\gamma-1}{\gamma+1}M_B^2\right]^{\frac{\gamma+1}{4(\gamma-1)}} \qquad (39)$$

M_B can be found from (39) by Newton's method.

It should be observed that there is an upper limit in choosing the π for given M_1 and θ_A. This limit is such that $\pi < (z_B - R_0)/L$.

Successive differentiations of (39) give the following expressions:

$$\dot{M}_B = \left(\frac{dM}{dz}\right)_B =$$

$$= \frac{2}{\frac{z_B}{M_B}\left[\left\{\left(\frac{R_0}{z_B}\right)^2\frac{1}{M_B}\right\}^{2k}M_B^2 - 1\right]} \qquad (40a)$$

$$\ddot{M}_B = \left(\frac{d^2M}{dz^2}\right)_B = \frac{1}{2}\dot{M}_B^2\left[\frac{1}{M_B}\left\{1 - \left(\frac{z_B}{M_B}\right)\dot{M}_B\right\} - \left\{\left(\frac{R_0}{z_B}\right)^2\frac{1}{M_B}\right\}^{2k}(M_B)\left\{(1-4k) - \left(\frac{z_B}{M_B}\right)\dot{M}_B(1-2k)\right\}\right] \qquad (40b)$$

where $k = \dfrac{\gamma-1}{\gamma+1}$

At the exit characteristic, point C,

$$\left.\begin{aligned} z_C &= \frac{1}{2}\csc\left(\frac{\theta_A}{2}\right) + \pi L \\ M_C &= M_1 \end{aligned}\right\} \qquad (41)$$

A fifth degree polynomial may be fitted in the interval (BC) along which the flow angle equals zero:

$$M = M_1 - \left[a_0(z_C - z)^3 + a_1(z_C - z)^4 + a_2(z_C - z)^5\right] \qquad (42)$$

For evaluating the coefficients of (42) the boundary conditions are as follows:

$$\left.\begin{aligned} z &= z_B \\ M &= M_B \\ \dot{M} &= \dot{M}_B \\ \ddot{M} &= \ddot{M}_B \end{aligned}\right\} \qquad \left.\begin{aligned} z &= z_C \\ M &= M_1 \\ \dot{M} &= 0 \\ \ddot{M} &= 0 \end{aligned}\right\} \qquad (43)$$

Therefore, a_0, a_1 and a_2 can be found from three linear algebraic equations resulting from (42) and (43):

$$\left.\begin{aligned} k_2^3 a_0 + k_2^4 a_1 + k_2^5 a_2 &= k_1 \\ 3k_2^2 a_0 + 4k_2^3 a_1 + 5k_2^4 a_2 &= \dot{M}_B \\ 6k_2 a_0 + 12k_2^2 a_1 + 20k_2^3 a_2 &= -\ddot{M}_B \end{aligned}\right\} \quad (44)$$

where $k_1 = M_1 - M_B$, $k_2 = z_c - z_B$

It is more convenient to solve (44) by the matrix method for the purpose of programming a digital computer. Expressing (44) by a matrix equation, we have

$$\begin{bmatrix} k_2^3 & k_2^4 & k_2^5 \\ 3k_2^2 & 4k_2^3 & 5k_2^4 \\ 6k_2 & 12k_2^2 & 20k_2^3 \end{bmatrix} \begin{bmatrix} a_0 \\ a_1 \\ a_2 \end{bmatrix} = \begin{bmatrix} k_1 \\ \dot{M}_B \\ -\ddot{M}_B \end{bmatrix} \quad (45)$$

The solution of (45) is

$$\begin{bmatrix} a_0 \\ a_1 \\ a_2 \end{bmatrix} = \begin{bmatrix} k_2^3 & k_2^4 & k_2^5 \\ 3k_2^2 & 4k_2^3 & 5k_2^4 \\ 6k_2 & 12k_2^2 & 20k_2^3 \end{bmatrix}^{-1} \begin{bmatrix} k_1 \\ \dot{M}_B \\ -\ddot{M}_B \end{bmatrix} \quad (46)$$

Hence a_0, a_1 and a_2 can be easily obtained by inversion of the matrix in (46), whence

$$\left.\begin{aligned} a_0 &= \frac{1}{k_2}\left(\frac{10k_1}{k_2^2} - \frac{4\dot{M}_B}{k_2} - \frac{\ddot{M}_B}{2}\right) \\ a_1 &= \frac{1}{k_2^2}\left(-\frac{15k_1}{k_2^2} + \frac{7\dot{M}_B}{k_2} + \ddot{M}_B\right) \\ a_2 &= \frac{1}{k_2^3}\left(\frac{6k_1}{k_2^2} - \frac{3\dot{M}_B}{k_2} - \frac{\ddot{M}_B}{2}\right) \end{aligned}\right\} \quad (47)$$

Figure 17(a) shows the Mach number distribution found by this method.

3.2.2.3 Conical source flow front. It is shown in Figure 17(b) that the flow angle of the conical source flow front varies from zero at point B (on the axis) to θ_A at the point of inflection A. The relation between the local angle and the Prandtl-Meyer angle is simply

$$\theta_p = \frac{\psi_B}{2} - \frac{\psi_p}{2} \quad (48)$$

ψ_B may be calculated from (33) and (39). Therefore,

$$\frac{\psi_A}{2} = \frac{\psi_B}{2} - \theta_A \quad (49)$$

Knowing θ_A, M_A may be obtained by Newton's method from (33). Thus, ψ_p can be found from

$$M_p = M_B - \frac{p}{N}(M_B - M_A) \quad (50)$$

where $M_A \leq M_p \leq M_B$ and p varies from zero to N, which represents the number of divisions of the flow front used in developing the characteristic net.

The coordinates along the source flow front are given by:

$$\left.\begin{aligned} z_p &= R_p \cos\theta_p \\ r_p &= R_p \sin\theta_p \end{aligned}\right\} \quad (51)$$

where $R_p = R_0\left(\frac{A}{A^*}\right)_p^{\frac{1}{2}}$ as given by Reference (21).

θ_p in (51) is calculated from (48) for a given M_p obtained from Equation (50).

3.2.2.4 Expansion curve. By assuming the existence of a source flow front, the expansion region curve is arbitrary as long as the curve is continuous and monotonic and meets the following boundary conditions:

$$\left.\begin{array}{ll} z = z_t & z = z_A \\ r = r_t & r = r_A \\ \dfrac{dr}{dz} = 0 & \dfrac{dr}{dz} = \tan\theta_A \\ & \dfrac{d^2r}{dz^2} = 0 \end{array}\right\} \quad (53)$$

The simplest curve satisfying (53) is used for the computations presented in this report. This curve is a cubic parabola in the (x, y) coordinate system about A, as shown in Figure 15(b):

$$y = a x^3 \quad (54)$$

The coefficient a can be obtained readily from the condition

$$a = \frac{\sin^3\theta_A \sec\theta_A}{6.75(r_A - r_t)^2} \quad (55)$$

and the coordinates in the (z, r) system are

$$\left.\begin{array}{l} z = z_A - (\chi\cos\theta_A + y\sin\theta_A) \\ r = r_A - (\chi\sin\theta_A - y\cos\theta_A) \end{array}\right\} \quad (56)$$

The curvature at the throat is

$$\frac{1}{\rho_t} = \left(\frac{4}{3}\right)\frac{\tan\theta_A \sin\theta_A}{(r_A - r_t)(1 + \tan^2\theta_A)^{3/2}} \quad (57)$$

Another convenient curve may be used for the expansion region, as illustrated in Figure 15(a). The advantage of this curve is that the curvature can be specified beforehand. However, the intersection of the circular arc and the straight line results in a curvature discontinuity which may not be desirable.

3.2.3 Transition Region Computation

3.2.3.1 Flow net. Having established the initial conditions, the transition region can be computed by constructing a Mach net using the procedure formulated in Section 3.2.1.2.

A new 'right-running' line J_i can be established by starting with the Mach numbers along the centerline and the source flow front J_0. A succeeding line J_2 may be constructed with a new point on the axis and the previously computed values of J_1. The flow net can be completed by stepwise computation of the J's until the exit of the nozzle is reached. In the beginning, the computation of each 'right-running' line starts from the axis of symmetry. When the axial distance of the first point on the J line equals z_c the computation of the next J line begins from the 'exit characteristic'. Hence, the lengths of J's decrease as they approach the nozzle exit. The coordinates for the 'exit characteristic' are calculated from the formula

$$\left.\begin{array}{l} z_p = z_c + \dfrac{p}{N}\sqrt{M_1^2 - 1} \\ r_p = \dfrac{p}{N} \end{array}\right\} \quad (58)$$

Along the 'exit characteristic', the Mach number equals M_1 and the flow angles are zero; therefore the line is straight. The construction of the flow net is shown in Figure 17(b).

3.2.3.2 Wall coordinates. Since the flow angle at the point of inflection (z_A, r_A) is known, initial direction of the wall streamline is known. The wall coordinates may be computed starting from the initial direction proceeding downstream crossing the 'right-running' and 'left-running' characteristics in the flow net until the exit characteristic is reached as shown in Figure 17(b).

The present method assumes a first order approximation or linear variation in the unit quadrilateral net. The flow conditions at points U, V and W are given as shown in Figure 18. To start the computation, U is equal to point A, and, in general, the flow condition at U has been obtained through computation of the previous quadrilateral. V and W may be the intersections on the

quadrilateral of either the J lines or the K lines; i.e., the 'right-running' or the 'left-running' lines, depending on the wall streamline paths of S and S'. Q is the unknown point to be calculated, and it becomes a new point on the wall streamline subsequent to U. In the computation of the next quadrilateral Q becomes U. The process is illustrated in Figure 18. The calculation is written as follows:

$$\frac{M_Q - M_W}{M_V - M_W} = \frac{r_Q - r_W}{r_V - r_W} = \frac{z_Q - z_W}{z_V - z_W} =$$

$$= \frac{\tan\theta_Q - \tan\theta_W}{\tan\theta_V - \tan\theta_W} \qquad (59)$$

$$\frac{r_Q - r_U}{z_Q - z_U} = \frac{1}{2}(\tan\theta_Q + \tan\theta_U) \qquad (60)$$

Solving (59) and (60)

$$z_Q = \tfrac{1}{2}(\eta_1 \pm \sqrt{\eta_1^2 - 4\eta_2}) \qquad (61)$$

where

$$\eta_1 = (z_U + z_W) +$$

$$+ \frac{1}{(\tan\theta_V - \tan\theta_W)}[2(r_V - r_W) -$$

$$- (z_V - z_W)(\tan\theta_U + \tan\theta_W)] \qquad (62a)$$

$$\eta_2 = z_U z_W +$$

$$+ \frac{1}{(\tan\theta_V - \tan\theta_W)}[2(z_V - z_W)(r_U - r_W) +$$

$$+ 2(r_V - r_W)z_W -$$

$$- z_U(z_V - z_W)(\tan\theta_U + \tan\theta_W)] \qquad (62b)$$

The unknown z_Q lies between z_V and z_W; therefore it is necessary to calculate the z_Q's from all the combinations of η_1 and η_2 and scan for the correct z_Q. With a high speed computer this can be easily done. M_Q, r_Q and $\tan\theta_Q$ may be obtained from substitution of z_Q into (59).

When V and W are on the exit characteristic line, a new formula should be used to replace (61) because of indeterminacy:

$$z_Q = \frac{\left((z_V - z_W)[2(r_U - r_W) - (\tan\theta_U + \right.}{\left. + \tan\theta_W)z_U] + 2(r_V - r_W)z_W\right)}{\left(2(r_V - r_W) - \right.} \qquad (63)$$
$$\left. - (z_V - z_W)(\tan\theta_U + \tan\theta_W)\right)$$

3.2.4 *Wall Coordinates at Equal Axial Increments*

The coordinates of the expansion region and the transition region constitute the perfect fluid coordinates from throat to exit of the nozzle. For fabrication it is desirable to have the coordinates listed in equal axial interval increments instead of the interval increments resulting from the computation.

One method of achieving equal spacing of coordinates is to interpolate by third order divided differences. This is equivalent to fitting a cubic through four adjacent points, and solving for radii at equal intervals along the axis. The interpolation for each group of four points is performed in the middle interval except in the first and last groups. To express this mathematically, consider four adjacent points, (z_i, r_i) $\ldots.(z_{i+3}, r_{i+3})$, the points corresponding to equal axial intervals in z where $z_{i+1} \leqslant z \leqslant z_{i+2}$ are found from

$$r = f_i + (z - z_i)f_{i,i+1} +$$

$$+ (z - z_i)(z - z_{i+1})f_{i,i+1,i+2}$$

$$+ (z - z_i)(z - z_{i+2})(z -$$

$$- z_{i+3})f_{i,i+1,i+2,i+3} \qquad (64)$$

where

$$f_i = r_i$$

$$f_{i,i+1} = \frac{r_{i+1} - r_i}{z_{i+1} - z_i}$$

$$f_{i,i+1,i+2} = \frac{f_{i+1,i+2} - f_{i,i+1}}{z_{i+2} - z_i} \qquad (65)$$

$$f_{i,i+1,i+2,i+3} = \frac{f_{i+1,i+2,i+3} - f_{i,i+1,i+2}}{z_{i+3} - z_i}$$

This procedure is illustrated in Figure 19.

3.2.5 *Computation of a Family of Perfect Fluid Contours*

3.2.5.1 Computer routine. It was soon found that manual computation of axisymmetric perfect fluid contours using the method of this report is a most laborious task. However, the procedure is readily programmed in a high speed electronic digital computer (e.g. the IBM 704). For example, an abbreviated flow chart describing the computing sequence is given in Figure 20.

The average machine time required per nozzle contour is slightly over two minutes, using:

(a) N = 20 along the source flow front and the exit characteristic line.

(b) All numerical operations carried to eight significant figures, i.e., the full accuracy of the computer routine.

(c) M_3 and θ_3: tolerance of 5×10^{-6} in the flow net computation, thus resulting in about three iterations per flow net point. It is estimated that manual computation of a typical contour would require more than one man-year.

3.2.5.2 Description of tabulated data. In Appendix I, 46 perfect fluid contour coordinates are listed. The first three lines contain the design parameters and other constants of interest. Column headings define the other quantities listed.

At the beginning of each table the coordinates which contain no information in the Mach number column are the coordinates in the expansion region, i.e., from the throat to the point of inflection. These coordinates are computed from Equations (48) through (52). The subsequent coordinates with the Mach number entries are the transition region coordinates computed using Equations (59) through (62).

All the coordinates listed are in uneven axial spacings. The equal-spaced coordinates have also been computed, and can be obtained upon request. Only one sample of the equally spaced wall coordinates together with the first and second differences is listed. The design parameters for the contour are $M_1 = 6.0$, $\theta_A = 10^0$, and $\gamma = 1.4$. Figure 21 shows the flow net, wall slope and curvature variations as well as the centerline Mach number distribution for this contour.

In Appendix II, five axisymmetric nozzle coordinate tables with exit Mach number range of 10 to 27 at various specific heat ratios are given. These coordinates were computed by the NACA using the method derived in Reference 27.

3.2.5.3 Computational accuracy. To derive a general criterion for predicting the computational accuracy of the perfect fluid coordinates using the step-by-step procedure formulated here is almost impossible. The accuracy of flow net computation depends, generally, on the following:

(a) Number of divisions N of the source flow front and the exit characteristic line.

(b) Limits on iterations and/or number of iterations permitted per point.

(c) Number of J lines.

In computing the transition wall coordinates, the accuracy in assuming linear variation in a unit quadrilateral depends on the flow net size N. Further, all the computations are limited by the number of digits which the computer can handle.

It is, however, possible to arrive at some qualitative information regarding the computing accuracy by varying the flow net size N, and fixing all the other parameters. Thus it is possible to determine the variation of the exit Mach number from the area ratio with N.

In particular, four contours, at $M_1 = 8.0$ and $\theta_A = 10^o$, at N = 5, 10, 15 and 20 were computed.

For each value of N the exit Mach number can be found from isentropic flow relations. Therefore, the deviation from the design value for various values of N can be determined as shown in Figure 22.

3.3 Turbulent Boundary Layer Growth

3.3.1 General Discussion

The method generally used to calculate the physical coordinates of a supersonic wind tunnel nozzle is by adding the so-called boundary layer displacement thicknesses to the perfect fluid coordinates so that the mass flow in each cross section of the nozzle is compensated. This method of computing these so-called real fluid coordinates may be equally valid for a hypersonic nozzle.

In supersonic nozzles, the existence of turbulent boundary layers is usually assumed. The growth of turbulent boundary layer may be estimated by integration of Karman's momentum-integral relation

$$\frac{d\theta}{dx} + \frac{\theta}{M_\infty}\left(\frac{dM_\infty}{dx}\right)\left(\frac{H + 2 - M_\infty^2}{1 + \frac{\gamma-1}{2} M_\infty^2}\right) + \frac{\theta}{r}\frac{dr}{dx} = \frac{c_f}{2} \qquad (66)$$

The last term on the left hand side of (66) vanishes in the two-dimensional case. Integration of Equation (66) either numerically or by quadrature may be possible once the relationships of $c_f/2$, H, and the turbulent boundary layer velocity profiles with the other variables are established.

Due to complex non-linear behavior in the mechanism of turbulence, these relationships cannot be treated by rigorous mathematical analysis. In general, they may only be determined empirically for a thermally insulated flat plate with zero pressure gradient in a limited Reynolds number and Mach number range.

It is known that the influences of pressure gradients, velocity profiles, and heat transfer, as well as the history of boundary layer build-up may cause considerable deviation in the skin friction law and shape factor values determined for a flat plate. However, it is generally agreed that the use of flat plate data in a region of small favorable pressure gradient such as in the supersonic nozzle may be quite valid provided that the turbulent boundary layer velocity profiles are known. Therefore, this allows integration of (66).

Usually, the initial momentum thickness may be assumed to be zero or an arbitrarily small quantity at the throat for the purpose of starting the integration. Sibulkin has demonstrated[28] that such an assumption will not cause appreciable change in the momentum thickness at the exit of the nozzle.

A method for approximation of turbulent boundary layer development in compressible flow was formulated by Tucker[29]. This method assumes thermally insulated walls and that the skin friction behaves according to Falkner's[30] low-speed flat-plate relation, except that the fluid properties are evaluated at the arithmetic mean of the wall and the free-stream temperature.

For supersonic nozzles of Mach numbers less than 4, the heat transfer rate through

the walls is small and the boundary layers are thinner than in hypersonic nozzles of the same length. Even if the estimated boundary layer growth is off by a factor of 2 in the lower Mach number range, the potential flow region will not change to a great extent. Therefore, Tucker's method of approximating the boundary layer growth is satisfactory.

In hypersonic nozzles, the boundary layer growth is sensitive to heat transfer through the walls. The measured displacement thicknesses in several hypersonic nozzles indicate that these changes may exceed more than 10% of the exit height or diameter of the nozzles. Erroneous estimates of the boundary layer growth in hypersonic nozzles may change the perfect fluid flow completely. Thus it is imperative that the boundary layer parameters and the skin friction law be evaluated by taking account of the wall heat transfer.

Several methods have been derived recently for estimating the turbulent boundary layer development in compressible adiabatic flow. Two of these methods, by Bartz and by Persh and Lee, are suitable for engineering applications; these will be discussed in the next sections.

3.3.2 Method of Bartz

In Reference 31, Bartz adopted Tucker's approach to extend the Blasius incompressible skin friction law to account for compressible adiabatic flow by evaluating the fluid properties at a temperature which is the arithmetic mean between the free-stream and the wall temperatures:

$$\frac{c_f}{2} = 0.0228\,\sigma\left(\frac{\mu_0}{\rho_\infty u_\infty \delta}\right)^{\frac{1}{4}} \tag{67}$$

where

$$\sigma = \left(\frac{1}{2}\frac{T_w}{T_\infty} + \frac{1}{2}\right)^{-c}\left(\frac{T_0}{T_\infty}\right)^{-d} \tag{68}$$

σ accounts for changes of density, viscosity, and heat transfer with temperatures across the boundary layer.

Assuming one-dimensional isentropic flow, the free-stream Mach number along the wall and the radius of the axisymmetric nozzle may be expressed in terms of the area ratio

$$\frac{A}{A^*} = \left(\frac{r}{r^*}\right)^2 \tag{69}$$

Hence Equation (66) becomes

$$\left(\frac{d\theta}{dx}\right)^{5/4} + \frac{5}{8}\theta^{5/4}\left[\frac{M_\infty^2 - 2H - 3}{1 - M_\infty^2}\right]\frac{d}{dx}\left(\ln\frac{A}{A^*}\right) =$$

$$= \frac{5}{4}(0.0228)\,\sigma\left[\left(\frac{\mu_0}{\rho^* u^*}\right)\left(\frac{\theta}{\delta}\right)\left(\frac{A}{A^*}\right)\right]^{\frac{1}{4}} \tag{70}$$

The shape factor H and θ/δ are evaluated according to the following equations:

$$\frac{u}{u_\infty} = \left(\frac{y}{\delta}\right)^{1/7} \tag{71a}$$

$$\frac{\rho_\infty}{\rho} = \frac{T}{T_\infty} = \frac{T_w}{T_\infty} + \left(\frac{T_0}{T_\infty} - \frac{T_w}{T_\infty}\right)\left(\frac{y}{\delta}\right)^{1/7} -$$

$$- \left(\frac{\gamma-1}{2}M_\infty^2\right)\left(\frac{\Delta}{\delta}\right)^{2/7}\left(\frac{y}{\Delta}\right)^{2/7} \tag{71b}$$

$$\frac{t_0 - T_w}{T_0 - T_w} = \left(\frac{y}{\Delta}\right)^{1/7} \tag{71c}$$

$$\frac{\theta}{\delta} = \int_0^1 \frac{\rho u}{\rho_\infty u_\infty}\left(1 - \frac{u}{u_\infty}\right)d\left(\frac{y}{\delta}\right) \tag{71d}$$

$$\frac{\delta^*}{\delta} = \int_0^1 \left(1 - \frac{\rho u}{\rho_\infty u_\infty}\right)d\left(\frac{y}{\delta}\right) \tag{71e}$$

For flow on a flat plate of Prandtl number equal to unity, $\Delta = \delta$. Equation (71b) is the same as Crocco's temperature distribution:

$$\frac{\rho_\infty}{\rho} = \frac{T}{T_\infty} = \frac{T_W}{T_\infty} + \left(\frac{T_0}{T_\infty} - \frac{T_W}{T_\infty}\right)\frac{u}{u_\infty} - \left(\frac{\gamma-1}{2} M_\infty^2\right)\left(\frac{u}{u_\infty}\right)^2 \quad (72)$$

The boundary parameters, H and θ/δ are functions of M_∞ T_W/T_0, γ and Δ/δ and these values can be prescribed along the nozzle wall. The procedures for calculating (71a) through (71e) reduce to evaluating two definite integrals. Values of these integrals over a wide range of parameters are tabulated in Reference 31.

All the parameters in Equation (70) are in terms of x. Therefore the growth of the momentum thickness along the wall, starting with zero or an arbitrarily small quantity at the throat, can be calculated by numerical integration of (70). The $\delta^*(x)$ values can also be obtained from the known H(x) values.

The advantage in this method is its simplicity. It is noted that Equation (70) may be integrated by simple quadrature if it is written as

$$\frac{d\bar{\theta}}{dx} + P(x)\bar{\theta} = Q(x) \quad (73)$$

where $\bar{\theta} = \theta^{5/4}(x)$

$$P(x) = \frac{5}{8}\left(\frac{M_\infty^2 - 2H - 3}{1 - M_\infty^2}\right)\frac{d}{dx}\left(\ln \frac{A}{A^*}\right)$$

$$Q(x) = \frac{5}{4}(0.0228) \times \times \sigma\left[\left(\frac{\mu_0}{\rho^* u^*}\right)\left(\frac{\theta}{\delta}\right)\left(\frac{A}{A^*}\right)\right]^{\frac{1}{4}} \quad (73a)$$

The solution of (73) is

$$\bar{\theta}(x) = e^{-\int_0^x P.\,dx}\left[\int_0^x e^{\int_0^x P.\,dx} Q.\,dx + \bar{\theta}_i\right] \quad (74)$$

$\bar{\theta}_i$ is the initial momentum thickness at the throat, that, is, where x = o.

It is seen from (74) that the momentum thickness at any station may be explicitly determined once $\bar{\theta}_i$ is given.

3.3.3 Method of Persh and Lee

Another method formulated by Persh and Lee[32] is of interest. Persh has extended Donaldson's turbulent boundary layer skin friction law[33] by relating the exponent n of the power law velocity profile with the Reynolds number based on momentum thickness Re_θ. The relationhsip of Re_θ and n is obtained by equating Donaldson's incompressible skin friction equation with the Karman-Schoenherr incompressible skin friction law as illustrated in Reference 32. Thus the local skin friction coefficients for compressible turbulent boundary layer with wall heat transfer are as follows:

$$c_f = 2(20n)^{\frac{1-n}{1+n}}\left(\frac{\theta/\delta}{Re_\theta}\right)^{\frac{2}{n+1}}\left(\frac{T_\infty}{T_L}\right)^{\frac{n-2\omega-1}{n+1}} \quad (75a)$$

$$\frac{T_L}{T_\infty} = 1 + rf\,\frac{\gamma-1}{2}M_\infty^2\left[1 - \left(\frac{u_L}{u_\infty}\right)^2\right] + \frac{T_W - T_a}{T_\infty}\left[1 - \frac{u_L}{u_\infty}\right] \quad (75b)$$

$$\frac{u_L}{u_\infty} = \left[\frac{20n(\theta/\delta)}{Re_\theta}\right]^{\frac{1}{n+1}}\left[\frac{T_L}{T_\infty}\right]^{\frac{1-n}{n+1}} \quad (75c)$$

To solve for c_f in Equation (75a) with Re_θ given, one must first obtain T_∞/T_L from the simultaneous relation of T_L/T_∞ and u_L/u_∞ in Equations (75b) and (75c). The quantity θ/δ and the other boundary layer parameters are calculated in a manner similar to the Bartz method, in Equations (71a) through (71e) except:

(a) The exponent n in power law velocity profile is made variable.

(b) The temperature boundary layer profile has the same thickness as the velocity profile.

(c) Recovery factor is accounted for in the temperature profile.

Crocco's temperature distribution thus becomes

$$\frac{\rho_\infty}{\rho} = \frac{T}{T_\infty} = 1 + rf\left(\frac{\gamma-1}{2}\right)M_\infty^2\left[1 - \left(\frac{u}{u_\infty}\right)^2\right] + \frac{T_w - T_s}{T_\infty}\left[1 - \frac{u}{u_\infty}\right] \quad (76)$$

For starting the numerical integration of Equation (66), θ_1 may be assumed to be zero either at the throat or a short distance upstream of the throat. It should be noted that the numerical integration must be carried out stepwise since the local skin friction coefficients depend on the momentum thicknesses.

A table of boundary layer parameters δ^*/δ, θ/δ and H with varying n and wall heat transfer rates for the Mach number range of 0 through 20 have been computed and are tabulated in Reference 34.

3.3.4 Concluding Remarks

The reliability of using the aforesaid methods for calculating the boundary layer growth in hypersonic flow is questionable owing to the uncertain assumptions used in these methods. These assumptions were necessary at the time to establish the methods, due to lack of experimental data. However, these methods are valid for use of hypersonic wind tunnel nozzles when the pressure gradients along the nozzle wall are moderate and favorable.

Perhaps better results may be achieved if the boundary layer growth is calculated starting from the exit of the nozzle and moving towards the throat. This will be a more realistic approach since we are interested mainly in obtaining the design exit Mach number for a particular wind tunnel nozzle. The estimation of δ_1^* is relatively simple since there are a number of experimental surveys of δ_1^*'s on various hypersonic nozzles listed in Table I. Most of these data are reduced from References 35 through 38; the recent ones (BRL, AEDC, NOL and JPL) are obtained through private communications since these data have not yet been published.

By plotting $\delta_1^* R_e^{1/5}/x^{4/5}$ vs M_1 at various heat transfer rates, we may fit a design curve as shown in Figure 23. The data for certain two-dimensional nozzles are badly scattered. However, these data were taken along the centerline of the contoured walls where the δ_1^*'s are thicker than the average boundary layer thickness, as illustrated earlier in Figure 1. Thus, the design curve in Figure 23 is purposely chosen to be slightly lower than the data suggested.

Using the design curve, δ_1^* for any nozzle may be easily calculated once the supply conditions and the length x of the nozzle are given. Knowing δ_1^* we may obtain θ_1 from the shape factor at the exit of the nozzle. The shape factor may be calculated from prescribed conditions of the nozzle. Integration of Equation (66) using the methods discussed may be performed with θ_1 as initial momentum thickness.

It is obvious that the probability of the nozzle conforming to the design exit Mach

number is greater if calculation of the boundary layer growth is according to the realistic approach. It should also be pointed out that improvement of the design curve on Figure 23 can be made if more data are gathered.

3.4 Nozzle Cut-off Point

In hypersonic nozzles the length to exit half height (or radius in axisymmetric case) ratios are much larger than in the supersonic case due to the low Mach angle. Moreover, the great length combined with the generally high supply temperature results in thicker δ^* growth. Shortening the nozzle by omitting a section near the exit will not only reduce this excessive boundary layer growth, but will also optimize the size of the usable test region.

The usable test region lies inside of the actual boundary layer, δ. The tabulated data in References 29 and 34 show that this layer is approximately $1.5\delta^*$ for a Mach number range of 6 through 12. Hence the maximum usable test section height is located at a point given by the following relation:

$$\frac{d(r + \delta^* - \delta)}{dz} \approx \frac{d(r - 0.5\delta^*)}{dz} = 0 \qquad (77)$$

Downstream of this point the test region actually begins to decrease in height.

A more conservative approach to test section height optimization is to terminate the nozzle at a distance $2(\delta_1 - \delta_1^*)\cot\alpha_1 = \delta_1^*\cot\alpha_1$ upstream of the theoretical exit. This is approximately the point where the right-running characteristic wave, which meets in a common point with the exit characteristic wave and the inner surface of δ, originates from the perfect fluid wall. The measurements on existing hypersonic wind tunnels indicate that δ_1^*/r_1 can be as great as 1/4. Therefore the cut-off length is approximately $M_1 r_1/4$. Figure 24 shows the cut-off length for a hypersonic nozzle.

3.5 Focusing Effect Due to the Wall Errors

It is well known that the wall ordinate errors in a supersonic axisymmetric nozzle can cause the Mach waves to become compression shocks which will focus on the centerline and generate downstream to the test region. Hence care must be exercised in the design and fabrication of the nozzle.

The exact criterion for determining the allowable wall errors is unknown. However, by some simple assumptions, i.e., considering a two-dimensional uniform and parallel flow field in a straight wall channel, an approximate formula for allowable errors in wall curvature may be derived.

Figure 25 shows that the ordinate error Δr to the first order may be expressed

$$\Delta r = \frac{\Delta z^2 . \sin^2\alpha}{r} = \frac{1}{r}\frac{\Delta z^2}{M^2} \qquad (78)$$

where Δz is the interval along the z-axis, r is the ordinate, and M is the flow Mach number. The curvature error to the first order may be written as

$$\frac{1}{\rho} = \frac{2\Delta r}{\Delta z^2} \qquad (79)$$

by substitution $$\frac{\rho}{r} = \frac{M^2}{2} \qquad (80)$$

It is seen from (80) that to prevent focusing effect ρ/r must be made much larger than $M^2/2$ along the nozzle wall.

A theoretical treatment of radial focusing in supersonic flows in ducts has been reported recently by J.J. Mahoney[39].

4. PERFORMANCE AND CONTROL

4.1 Wind Tunnel Parameters

4.1.1 Effuser

The important parameters that govern the performance of an effuser are P_0, T_0, M_1, γ and A_1. From these parameters, the weight flow rate (w_1) and the Reynolds number per inch (R_e) in the test region can be obtained.

Figure 26 consists of a number of continuous graphs that relate the effuser parameters to yield the weight flow rate for air:

$$w_1 = g\left(\frac{\gamma}{R}\right)^{\frac{1}{2}} \frac{P_0}{(T_0)^{\frac{1}{2}}} \frac{A_1 M_1}{(1 + 0.2M_1^2)^3} \qquad (81)$$

e.g. given $P_0 = 800$ lb/in^2, $T_0 = 1000^0$R, $M_1 = 8$ and $A_1 = 600$ in^2, the line with arrows in Figure 26 indicates $w_1 \cong 42$ lb/sec.

This technique may also be used to relate the effuser parameters with R_e:

$$R_e = \left(\frac{\gamma}{R}\right)^{\frac{1}{2}} \frac{P_0}{T_0^{\frac{1}{2}}} \frac{M_1}{(1 + 0.2M_1^2)^3 \mu} \qquad (82)$$

where μ is a function of M_1 and T_0 may be calculated from Sutherland's formula.

4.1.2 Run Time for Blowdown Tunnels

If the pressure ratio P_0/P_e is constant or greater than the required running ratio during a run, the steady flow duration is

$$\tau = \frac{\Delta W}{w_1}$$

or by substitution of (1) and (81)

$$\tau = \left(\frac{g}{R}\right)\left(\frac{V_s}{T_s}\right)\left(\frac{T_0^{\frac{1}{2}}}{A_1 \lambda}\right)\left(\frac{P_{si}}{P_0}\right)\left[1 - \left(\frac{P_0}{P_{si}}\right)^{\frac{1}{n}}\right] \qquad (83)$$

where $$f = g\left(\frac{\gamma}{R}\right)^{\frac{1}{2}} \frac{M_1}{(1 + 0.2M_1^2)^3} \qquad (84)$$

Equation (83) assumes an isentropic process. In actual run time calculation, the thermodynamic process is polytropic i.e., n in the exponent of the P_0/P_{si} term lies between 1 and 1.4 for air.

4.2 Starting and Running Pressure Ratios

4.2.1 Empty Test Section Data

Starting and running pressure ratio data for supersonic wind tunnels of varying sizes and types are available. For empty closed test sections, the data seem to indicate that most of the starting ratios are about 100% of the pitot pressure recovery and the running ratios can be as low as 50% of the pitot pressure recovery. For free-jet operation, the required ratios are perhaps 50% higher than the closed test-section data.

Very little of this information is available on operation in the hypersonic range. Table II contains many of the existing starting and running ratio data on various free-jet wind tunnels for a wide range of Mach numbers. The majority of data are for empty test-section runs and in most cases the area ratios between the second throat and the test section are recorded. These data are plotted on Figure 27. It is interesting to note that Hermann's theory[40], as indicated in Figure 27, seems to match the starting ratio data fairly well.

In general, the starting and running ratios for testing with models are in the order of 20% to 50% higher than the empty cases. The variations are functions of model size and angle of attack, diffuser configuration, second throat opening, etc. With fixed diffusers, the ratios are usually much higher.

4.2.2 *Special Starting Techniques*

The starting problems involved in high speed wind tunnels are:

(a) Starting pressure ratio

(b) Model load

(c) Model blockage.

These problems vary with tunnel configurations and range of operations. To date, theoretical and experimental treatments of the starting problems are confined to particular tunnels, therefore no conclusive generalizations exist.

In supersonic tunnels these problems are less severe than those in hypersonic tunnels due to relatively lower pressure ratios and model loads.

The starting pressure ratio can usually only be estimated for tunnels while empty, such as shown in Figure 27. The data for empty test section starting cannot be extrapolated to test sections with model conditions as discussed earlier. Perhaps the main reason for optimizing the tunnel starting is to reduce starting pressure ratio and model starting load as well as to maximize the model size.

A special technique developed by the General Electric Research Laboratory for starting a hypersonic nozzle with a large blunt nose model is of interest. This technique utilizes injection of flow along one side of the nozzle during starting. In doing so, the initial main stream flow is forced to separate along one side but remains stabilized, thus resulting in weaker shock interaction with the boundary layer near the model due to asymmetric flow. The weaker interaction causes less severe viscous feedback, which retards chocking downstream in the diffuser. With this technique General Electric was able to start a model of 1 inch in diameter in their 3.6 inch diameter Mach 22 hypersonic helium tunnel, whereas 3/8 inch diameter was the largest size model they had previously started. This technique is described in Reference 41.

Reports from others employing the same technique indicate that lower starting ratios and reduction of the model loads were accomplished. With further research, this procedure can be developed as a standard technique.

There are other available techniques which have not been published. However, successful results were indicated. For example, if a tunnel is limited by pressure ratio and has high stagnation temperature, the flow may be established for the tunnel with large models by injection of water into the stilling chamber during starting.

Another technique to reduce model starting and stopping loads is to shield the model with protectors which can be quickly opened and closed to protect the model. The simplest type of protector is a pair of flat plates which partially enclose the model during starting and stopping of the tunnel. Protectors may be constructed to fully enclose the model, such as those illustrated in Figure 28. The original purpose of the device shown in Figure 28 was to cool the model by injecting cold air through the protector from an outside source while enclosing the model. With an initially cooled model, a step function in stagnation temperature is provided; thus transient heat transfer experiments on the model can be successfully performed.

4.3 Stagnation Pressure and Temperature Controls

4.3.1 *General Discussion*

For continuously operating wind tunnels the stagnation pressure and temperature controls are less problematical, since stabilization can always be accomplished as there is a longer time period allowed for this. The controls for the intermittent tunnels then are more of interest.

In supersonic intermittent tunnels, the supply usually does not require heating; therefore, the control problem simplifies to control of P_0 alone. In almost all existing hypersonic intermittent tunnels storage heaters are generally used. The blowdown cycles in these were designed to be compatible with the tunnel run duration so that only small temperature variations occur during the cycle. Therefore, control of T_0 in these facilities was not attempted.

However, control of T_0 may be incorporated in the overall control system. For example, the T_0 control can be achieved by by-passing an amount of cold air to a thermal mixer. A schematic diagram for the P_0 and T_0 control system is shown in Figure 29.

4.3.2 Stagnation Pressure Control

In conventional hypersonic wind tunnels, the accuracy and stability of P_0 are, in general, of more interest than T_0, since the high stagnation temperature is used mainly to prevent gas liquefaction in the test region. Small variation in stagnation temperature during the run changes the tunnel Reynolds number at a lower order than the changes due to the stagnation pressure

The location of the P_0 control valve in an intermittent hypersonic tunnel circuit deserves careful consideration. It is undesirable to locate a hot control valve downstream of the storage heater because of the high heat transfer rate that complicates the construction of the valve. Thus, a cold control valve downstream of the storage tank should be considered as shown in Figure 29. The total void volume of the heater, thermal mixer, and piping causes process lag in the servo control loop.

An approximate analysis of the process may be derived as follows:

1) The change of weight in the storage tank may be expressed as

$$\frac{dW_s}{d\tau} = \frac{V_s}{R}\frac{(P_{si})^{\frac{n_1-1}{n_1}}}{T_{si}} \cdot \left(\frac{1}{n_1}\right) \cdot P_s^{\frac{1-n_1}{n_1}} \frac{dP_s}{d\tau} \quad (85)$$

2) The change of weight in the total void volume V_0 is

$$\frac{dW_0}{d\tau} = \frac{V_0}{R}\frac{(P_{0i})^{\frac{n_2-1}{n_2}}}{T_{0i}} \cdot \left(\frac{1}{n_2}\right) \cdot P_0^{\frac{1-n_2}{n_2}} \frac{dP_s}{d\tau} \quad (86)$$

3) The storage tank pressure change assuming sonic flow through the control valve is

$$P_s^{\frac{1-3n_1}{2n_1}} \cdot \frac{dP_s}{d\tau} = -(\gamma R)^{\frac{1}{2}} n_1 \left[\frac{2}{2(n_1+1)}\right]^{\frac{n_1+1}{2(n_1-1)}} \times \times \cdot \frac{A_s T_{si}}{V_s}(P_{si})^{\frac{1-n_1}{2n_1}} \quad (87)$$

4) The stilling chamber pressure change assuming sonic flow through nozzle throat is

$$-\left(\frac{dW_0}{d\tau} + \frac{dW_s}{d\tau}\right) = \left(\frac{\gamma}{R}\right)^{\frac{1}{2}}\left(\frac{2}{n_3+1}\right)^{\frac{n_3+1}{2(n_3-1)}} \times$$

$$\times \frac{(P_{0i})^{\frac{n_2-1}{2n_2}}}{(T_{0i})^{\frac{1}{2}}} A^* P_0^{\frac{n_2+1}{2n_2}} \qquad (88)$$

The constants n_1, n_2 and n_3 are involved in the thermodynamic processes. It is reasonable to assume $n_1 = n_3 = 1.4$ and $n_2 = 1$. Rearranging Equations (85) through (88):

$$P_s^{\beta_1} \cdot \frac{dP_s}{d\tau} = C_1 A_s \qquad (89a)$$

$$C_2 P_s^{\beta_2} \cdot \frac{dP_s}{d\tau} + C_3 \frac{dP_0}{d\tau} = C_4 P_0 \qquad (89b)$$

The electro hydraulic controller provides the third equation

$$A_s = f(P_c, \dot{A}_s, \ddot{A}_s, \ldots \overset{n}{A}_s) \qquad (89c)$$

where $P_c = P_{desired} - P_0$. $P_{desired}$ can be programmed to match the tunnel starting and running characteristics.

Equations (89a), (89b) and (89c) are non-linear simultaneous differential equations. Solutions may be obtained by simulation in an electronic differential analyzer. However, for approximation of the time constant in the thermodynamic process, (89a) and (89b) may be linearized by letting $n_1 = n_3 = 1$. The resulting transfer function is

$$\frac{P_0(s)}{A_s(s)} = \frac{P_s C_1 C_2 / C_4}{1 - C_3/C_4 s} \qquad (90)$$

where the loop gain is $K_A = P_s C_1 C_2 / C_4$ and the time constant is $\tau_c = C_3/C_4$ or

$$K_A = \frac{P_s}{A^*}\left(\frac{T_{0i}}{T_{si}}\right)^{\frac{1}{2}} \qquad (91)$$

$$\tau_c = \frac{V_0}{A^* a_{0i}} \qquad (92)$$

Equations (91) and (92) will give certain clues for designing the electro hydraulic controller. A lead-lag compensation network is necessary to overcome the process lag. The order of magnitude in the total loop gain may be approximated from Equation (91).

5. NOZZLE DESIGN AND FABRICATION

5.1 Wall Heating

Transfer of heat from the boundary layer to the relatively cool inside surface of the nozzle wall can be said to take place according to the following relationship:

$$g = h_g A(T_a - T_u) \qquad (93)$$

The rate of heat transfer per unit area is the best index of the heating intensity and thus will determine the degree of difficulty in cooling the nozzle. This index is equal to the product of the film coefficient and the temperature difference, $h_g(T_a - T_u)$. Values for this index may be in the order of 10^6 to 10^7 B.t.u./hr/ft^2 for hypersonic nozzles.

Probably the largest source of error in determining the nozzle wall temperatures and stresses is from the film coefficient on the gas side. While much work, both theoretical and experimental, has been performed, there is considerable spread in the results. The theoretical work naturally contains many assumptions, and the experimental work is hampered by the difficulty inherent in measuring temperatures with precision. A

comparison of various film coefficient formulas[42-45] is shown in Figure 30 for a turbulent boundary layer, along a typical nozzle wall. Significant variations can be produced in any of the above equations by using properties of air taken from different sources. Recent experimental investigation of film coefficients[46] presents additional results which are somewhat lower than those shown in Figure 30.

For large nozzles operating with continuum flow it is reasonable to expect that a turbulent boundary layer will exist at the throat. Greenfield's formula[42] is frequently used for determining the turbulent film coefficient. Rapid determination of the coefficient using this formula can be obtained by means of the continuous graphs, as in Figure 31.

Under certain circumstances the boundary layer at the throat will be laminar and the heat load will be an order of magnitude lower than with a turbulent boundary layer. One such nozzle is reported by Ohio State University[8].

Attainment of good flow quality is not possible if a transition from laminar to turbulent boundary layer occurs downstream of the throat, since transition produces shock waves, which will reflect downstream to the test region. Consequently, unless the entire length of the nozzle boundary layer is laminar, it must be made turbulent by tripping upstream of the throat.

5.2 Throat Configurations

Figure 30, discussed previously, shows one region of the nozzle - the throat, subjected to unusually high film coefficients. It is here that the major design problem is encountered.

With concerted effort the following factors can be minimized:

(a) Combined Stresses

i) Transient

ii) Steady-state

(b) Deflections in the aerodynamic surface

i) Transient

ii) Steady-state

iii) Permanent

(c) Disturbance of the boundary layer

Depending on the requirements and operating conditions of a specific tunnel, some of the above factors need not be minimized. In the design of a nozzle for a continuous tunnel only slight consideration need be given to the transient stresses and deflections. These can be held to acceptably low values by proper tunnel start-up and shut-down procedures. Conversely, an intermittent tunnel can frequently be designed to minimize only the transient conditions of stresses and deflections if the operating duration is held short enough to avoid steady-state problems.

Disturbance of the boundary layer is a design factor only when cooling is accomplished by the addition of a cool liquid or gas into the airstream. This type of cooling, coolant injection, is referred to by various names, such as sweat cooling or transpiration cooling, film cooling or boundary layer cooling. If the nozzle is cooled by heat conduction through the airstream walls, this factor need not be minimized in the design.

Minimization of the design factors must be performed with full knowledge of their effects on:

(a) Fabrication

(b) Useful Life

(c) Reliability

(d) Tunnel Operation

(e) Initial and Operation Cost.

Two broad concepts can be considered for designing a nozzle, especially its throat region.

The first concept is to make the entire airstream surface or the throat region an adiabatic surface.

The second and most conventional concept is to cool the nozzle, thus preventing the airstream surface and wall from heating up to the recovery temperature of the working gas.

The first concept is not feasible at present. Without considerable research and development in high temperature materials, the desired strength, creep, oxidation resistance, and fabrication accuracy of the airstream wall is unobtainable. Also, no method is available for calculating what effect out-of-roundness has on the flow quality.

The second concept has been used extensively although the methods of cooling have taken numerous forms. The two principal classes of cooling used are:

1) Coolant injected into the hot airstream

2) Conduction of heat away from the airstream surface to a suitable heat sink.

Coolant injection, whether gas transpiration cooling (sweat cooling), Figure 32(a); boundary layer cooling (film cooling), Figure 32(b); or a combination of these two types, Figure 32(c), has been under investigation as a means of cooling rockets and high speed vehicles. High cooling efficiency[47, 48] makes this method attractive for airborne applications. Efforts to adapt coolant injection to hypersonic nozzles have been successful so far as cooling is concerned[10, 11].

The simplest heat sink suitable for steady-state operation is obtained by attaching tubing carrying water to the external side of the airstream-wall. Generally, the tubing for axisymmetric nozzles is wrapped circumferentially and soldered or brazed to form the heat conduction path. Such a configuration is ideal for low heat fluxes because it is inexpensive.

In order to decrease the thermal resistance of the tubing wall and that of the material holding the tubing to the airstream wall, 'integral passage cooling' has been tried. It is best used for two-dimensional nozzles (Fig. 8) rather than for axisymmetric nozzles (Fig. 33).

Thin ribs act as cooling fins while thick ribs behave like thermal barriers causing hot spots on the airstream surface opposite the ribs. A rapid method for determining rib thickness for a given wall temperature is presented in Reference 49.

The major difficulty in using integral passage cooling for axisymmetric nozzles is the thermal stress in the airstream wall produced by the high degree of restraint. If the supporting wall is thick in comparison with the airstream wall, the restraint is, at very worst, triaxial. In this case thermal stress in the airstream wall is approximately given by:

$$\sigma = \frac{\alpha E(T_2 - T_1)}{(1 - 2\nu)} \qquad (95)$$

By comparison, the thermal stress in a two-dimensional nozzle wall, integral-passage-cooled, is approximately:

$$\sigma = \alpha E(T_2 - T_1) \qquad (96)$$

Thus, for most materials, the thermal stress for an axisymmetric integral-passage nozzle may be 2.5 to 3.0 times that of a similarly cooled two-dimensional nozzle.

The problem of thermal stress in axisymmetrical nozzles, whether tube-cooled or integral-passage-cooled, led to annulus passage cooling (Fig. 34). Annulus passage cooling, whereby water passes over a floating

liner which directs the air flow, has been successfully applied on a Mach 9 nozzle.

The airstream wall experiences biaxial thermal stresses proportional to about one-half of the temperature drop across the wall. A more detailed solution of this thermal stress problem is given in Reference 50.

The handling of the liner during fabrication and under certain unavoidable operating loads, principally longitudinal, makes it necessary that not too thin a wall be used at the throat section. A pure electroformed nickel liner has heat flux limitations. Higher film coefficients and stagnation temperatures can be accommodated by bonding a ceramic thermal barrier on the inside surface of the nickel (Fig.34). At present the best all-metallic annulus passage liner has a beryllium-copper throat (Fig.35).

Another method of cooling is by using water spray in the throat region so that the wall temperature can be kept sufficiently high. Successful results are reported in Reference 15.

In addition to the aforementioned thermal stresses, the nozzle airstream wall will be subjected to forces which produce stresses that must be superimposed on the thermal stresses. Pressure differential across the airstream wall and seal friction on the liner of an annulus passage nozzle are typical forces which produce additive stresses. In general, the stress resulting from the difference in pressure between the airstream and the cooling medium is much lower than the thermal stress. For annulus passage cooling, the liner must be strong enough to transmit the longitudinal force developed during tunnel starting and this strength is usually sufficient for the seal friction loads.

A bar graph (Fig.36) shows the capabilities of various throat configurations. The ordinates, gas film heat transfer coefficients, are approximate allowable values based on a stagnation temperature of 2000°F and usual mechanical loading.

5.3 Cooling System

When the airstream surface is prevented from heating to the adiabatic wall temperature by conduction back to a heat sink, the temperature difference between the wall and the adjacent water must be low.

Because of its availability and excellent cooling effectiveness water is generally used as the coolant. Fortunately, even heat fluxes of 5,000,000 B.t.u./hr/ft^2 can be transmitted by forced convection produced with high velocity water. Velocities of 125 ft/sec have been used.

Such high velocities are required only in the throat region. Gradual deceleration of the water downstream of the throat region can result in tolerably small pressure losses.

Prevention of cavitation in the throat cooling passages is of utmost importance if a long service life is to be realized from a forced convection cooled nozzle. Sufficient pressurization is used for this purpose. For open cooling systems, i.e., non-return systems, this does add to the circulating pump horsepower required. In a closed system, the power is consumed by pipe friction only while the static pressure to avert cavitation is produced by raising the system pressure level with a pressurization tank. For this reason, closed pressurized cooling systems are more economical to operate.

Closed recirculating coolant systems are desirable when passage sealing represents a problem. The higher throat heat fluxes mean higher wall temperatures on the water side which will form scale unless the coolant is suitably treated. Distilled, de-oxygenized water should be used for cooling. A closed system which recirculates its water is filled once initially and after that refilled only during periodic maintenance checks.

A considerable margin of safety exists when using forced convection cooling. Before the wall temperature could rise disastrously following a failure of the

circulating pump or a leak in the pressurization system, the heat would be transferred by nucleate boiling for some time. This additional time margin allows the interlock which shuts down the tunnel in the event of a coolant system failure to be set more liberally.

Nucleate boiling can transmit the high throat heat fluxes in a hypersonic nozzle just as it does in a rocket nozzle (Refs. 51 and 52). While the temperature driving potential ($T_a - T_w$ in a rocket nozzle is considerably higher than in a hypersonic nozzle, the lower stagnation pressure results in lower heat transfer film coefficients. The net result is that the heat flux is of the same magnitude in rocket nozzle throats as in the latest hypersonic wind tunnel nozzle throats.

The principal drawbacks to using nucleate boiling to cool the throat of hypersonic nozzles are:

(a) Unknown caviation danger

(b) Higher wall stresses because of the greater temperature drop between the wall and the water

(c) Lower margin of safety in the event of a circulating pump failure.

Rapid stabilization of flow is required for an intermittent type tunnel. For this case it is considered advantageous to use hot water in the cooling passages to pre-heat the nozzle wall to the anticipated mean steady state temperature.

5.4 Fabrication

All the previously mentioned axisymmetric nozzle configurations have common fabricating problems. Basic among these is the difficulty in obtaining an exact airstream contour and a satisfactory surface finish. The smallness of the throat diameter in comparison with the nozzle length and the restricted choice of materials magnifies the fabrication problem.

Two approaches are possible. The airstream wall can be formed either by direct internal machining or by placing the wall around a mandrel which is subsequently removed. The latter approach covers such techniques as casting, spinning, spraying, and electro-depositing.

Direct machining to produce one-piece nozzles is limited to the low hypersonic Mach numbers and the smaller size nozzles. At the lower hypersonic Mach numbers, the throat diameter is large enough to permit internal machining from both ends. Stock is available from which to machine the smaller size nozzles, but definite limitations are encountered as the nozzle size increases. Rough casting to size offers one method for castable materials to be supplied in large dimensions to the machine shop.

Direct machining to produce an axisymmetric hypersonic nozzle is limited neither to Mach number nor to size if joints are deemed permissible in the airstream wall. Making a nozzle by joining sections together has been tried successfully by Brooklyn Polytechnic Institute[15]. Not only will the shorter sections be machinable, but virtually stock of any diameter can be obtained through rolling up cones from the selected plate material.

Use of a mandrel on which to form the wall is feasible for fabricating one-piece nozzles of almost any dimensions. External machining and polishing the mandrel can be done to high accuracy.

Placing the wall on the mandrel through electrodepositing a metal reproduces the contour and surface down to microscopic levels.

Nickel is favored at present for electrodepositing or electroforming. Electroformed nickel has good mechanical strength and good thermal conductivity[53]. Strengths of 100,000 - 135,000 lb/in^2 are obtainable and the thermal conductivity is 36-41 B.t.u./$hr/ft^2/^oF$.

When the nozzle wall is cooled by conduction of heat back to a heat sink, only beryllium-copper appears to have a better combination of strength, thermal conductivity, modulus of elasticity, and coefficient of thermal expansion[54].

Typical steps in fabricating the nozzle wall by electroforming on a mandrel are:

(a) Jig bore and polish a template of the desired contour

(b) Machine the mandrel with a copying lathe from the template

(c) Hand polish the mandrel (Fig.37)

(d) Place mandrel in the electroforming bath

(e) Electroform enough nickel on the mandrel to allow for machining to the required external dimensions; about two to three weeks is required to deposit 3/8 inch nickel

(f) Remove mandrel-nickel unit from bath, place in lathe and machine external nickel surface to final dimensions

(g) Remove the mandrel from inside the nickel shell, leaving the completed nozzle wall (Fig.38).

ACKNOWLEDGMENTS

The author wishes to thank the personnel of the Sandberg-Serrell Corporation for their assistance in preparing this AGARDograph. He is particularly indebted to Mr. Bradford C. Houser for writing the section on nozzle design and fabrication, and to Mr. James T. Kenney for the valuable suggestions he made while reviewing the manuscript. He is also grateful to the NASA (formerly NACA) for supplying the tables of nozzle coordinates in Appendix II, and to various laboratories and installations for information on the development of hypersonic facilities.

REFERENCES

1. Ruptash, J. — *Supersonic Wind Tunnels - Theory, Design and Performance.* University of Toronto, UTIA Review No.5, June 1953.

2. Ferri, A. Bogdonoff, S.M. — *Design and Operation of Intermittent Supersonic Wind Tunnels.* AGARDograph 1, May 1954.

3. Kenney, J.T. Webb, L.M. — *A Summary of the Techniques of Variable Mach Number Supersonic Wind Tunnel Nozzle Design.* AGARDograph 3, October 1954.

4. Smolderen, J.J. — *Condensation Effects and Air Drying Systems for Supersonic Wind Tunnels.* AGARDograph 17, July 1956.

5. Fejer, A.A. Clark, J. — *Compressors for High Speed Wind Tunnels.* AGARDograph 14, January 1956.

6. Stever, H. Guyford and Rathburn, K.C. — *Theoretical and Experimental Investigation of Condensation of Air in Hypersonic Wind Tunnels.* NACA TN 2559, November 1951.

7. Wegener, P.P. Mack, L.M. — *Condensation in Supersonic and Hypersonic Wind Tunnels.* Advances in Applied Mechanics, Vol.V., Academic Press Inc., New York, N.Y., 1958, pp.307-440.

8. Thomas, R.E. et alii — *Configuration Details and Initial Performance of a Hypersonic Wind Tunnel for the Range of Mach Number 8 to 14.* Technical Report No.2, The Ohio State Research Foundation, October 1957.

9. Bloom, M.H. — *A High Temperature-Pressure Air Heater (suitable for Intermittent Hypersonic Wind Tunnel Operation).* WADC TN 55-695, November 1955.

10. Hermann, R. et alii — *Research on the Design of Hypersonic Nozzles and Diffusers at High Temperatures, Part I: Design and Construction Problems of a Hypersonic Facility and Preliminary Investigation of Liquid Film Cooling.* WADC 55-507; also RAL Report 127, March 1955.

11. Hermann, R. et alii — *Research on the Design of Hypersonic Nozzles and Diffusers at High Temperatures, Part II: Design and Construction of a Gas-Fired Storage Heater and Investigation of Evaporation Film Cooling on Typical Hypersonic Nozzle Throat Sections.* (unpublished).

12. Dabora, E.K. — *Regenerative Heat Exchanger with Heat-Loss Consideration.* AFOSR TN 57-613, ASTIA Document No.AD136603, Univ. of Michigan 2284-14-T, August 1957.

13. Dabora, E.K. et alii — *Description and Experimental Results of Two Regenerative Heat Exchangers.* TN 58-226, ASTIA AD 154-128, Univ. of Michigan 2284-18-T February 1958.

14. Ferri, A. et alii — *A Theoretical Analysis of a New Type of Heater Suitable for Intermittent Wind Tunnel Operation.* PIBAL Report No.201, July 1952.

15. Ferri, A. Libby, P.A. — *The Hypersonic Facility of the Polytechnic Institute of Brooklyn and its Application to Problems of Hypersonic Flight.* WADC TR 57-369, ASTIA Document No. AD130809, August 1957.

16. Keenan, J.H. et alii — *An Investigation of Ejector Design by Analysis and Experiment.* Journal of Applied Mechanics 17, 1950.

17. Fabri, J. Siestrunck, R. — *Supersonic Air Ejectors.* Advances in Applied Mechanics, Vol.V, Academic Press Inc., Publishers, New York, N.Y., 1958.

18. Ferri, A. — *Elements of Aerodynamics of Supersonic Flows.* The Macmillan Company, New York, 1949.

19. Schaaf, S.A. — *An Axially Symmetric Nozzle with Boundary Layer Correction.* Tech. Rep. HE-150-58, June 1949.

20. Sauer, R. — *General Characteristics of the Flow Through Nozzles at Near Critical Speeds.* NACA TM 1147, June 1947.

21. Foelsch, K. — *The Analytical Design of an Axially Symmetric Laval Nozzle for a Parallel and Uniform Jet.* Journal of the Aeronautical Sciences, Vol.16, No.3, March 1949.

22. Sauer, R. — *Method of Characteristics for Three-Dimensional Axially Symmetrical Supersonic Flows.* NACA TM No.1133 January 1947.

23. Evvard, J.C. Marcus, L.R. — *Achievement of Continuous Wall Curvature in Design of Two-Dimensional Symmetrical Supersonic Nozzles.* NACA TN 2616, January 1952.

24. Tsien, H.S. — *On the Design of the Contraction Cone for a Wind Tunnel.* Journal of the Aeronautical Sciences, Vol.10, No.2, Feb. 1943.

25. Smith, R.H. Wang, C.T. — *Contracting Cones Giving Uniform Throat Speeds.* Journal of The Aeronautical Sciences, Vol.11, No.4, October 1944.

26. Cronvich, L.L. — *A Numerical-Graphical Method of Characteristics for Axially Symmetric Isentropic Flow.* Journal of The Aeronautical Sciences, Vol.15, No.3, March 1948.

27. Beckwith, I.E. et alii — *The Aerodynamic Design of High Mach Number Nozzles Utilizing Axisymmetric Flow with Application to a Nozzle of Square Test Section.* NACA TN 2711, June 1952.

28. Sibulkin, M. — *On the Calculation of Turbulent-Boundary-Layer Growth in Supersonic Nozzles.* Jet Propulsion Laboratory Memo No.20-116, November 1955.

29. Tucker, M. — *Approximate Calculation of Turbulent Boundary-Layer Development in Compressible Flow.* NACA TN 2337, April 1951.

30. Falkner, V.M. — *A New Law for Calculating Drag.* Aircraft Eng., Vol.XV, No.169, March 1943.

31. Bartz, D.R. — *An Approximate Solution of Compressible Turbulent Boundary-Layer Development and Convective Heat Transfer in Convergent-Divergent Nozzles.* Transactions of ASME, November 1955.

32. Persh, J.; Lee, R. — *A Method for Calculating Turbulent Boundary Layer Development in Supersonic and Hypersonic Nozzles Including the Effects of Heat Transfer.* NAVORD Report 4200, June 1956.

33. Donaldson, C. Du P. — *Heat Transfer and Skin Friction for Turbulent Boundary Layers on Heated or Cooled Surfaces at High Speeds.* NACA RM L52H04, October 1952.

34. Persh, J.; Lee, R. — *Tabulation of Compressible Turbulent Boundary Layer Parameters.* NAVORD Report 4282, May 1956.

35. Sibulkin, M. — *Boundary Layer Corrections for the Hypersonic Wind Tunnel (Sidewall Divergence and Test Section Dimensions).* JPL Internal Memorandum, HWT 21 T31, February 1956.

36. Lobb, R.K. et alii — *Experimental Investigation of Turbulent Boundary Layers in Hypersonic Flow.* Journal of Aeronautical Sciences, Vol.22, No.1, January 1955.

37. Hill, F.K. — *Boundary-Layer Measurements in Hypersonic Flow.* Journal of The Aeronautical Sciences, Vol.23, No.1, January 1956.

38. Barnett, R.M. — *Performance of 3/8 Scale Model Hypersonic Wind Tunnel: Initial Test Program.* JPL Internal Memorandum HWT 21 T40 (unpublished).

39. Mahoney, J.J. — *Radial Focusing in Supersonic Flows in Ducts.* Note ARL/A160 Aeronautical Research Laboratories, Department of Supply, Commonwealth of Australia, 1957.

40. Hermann, R. — *Diffuser Efficiency of Free-Jet Supersonic Wind Tunnels at Variable Test Chamber Pressure.* Journal of The Aeronautical Sciences, Vol.19, No.6, June 1952.

41. Johnson, R.H. — *Asymmetric Starting for Hypersonic Wind Tunnels.* Journal of The Aeronautical Sciences, Vol.25, No.5, May 1958.

42. Greenfield, S. — *Determination of Rocket-Motor Heat Transfer Coefficients by the Transient Method.* Journal of The Aeronautical Sciences, Vol.18, No.8, August 1951.

43. Sibulkin, M. — *Heat Transfer to an Incompressible Turbulent Boundary Layer and Estimation of Heat Transfer Coefficients at Supersonic Nozzle Throats.* Journal of The Aeronautical Sciences, Vol.23, No.2, February 1956.

44. Bartz, D.R. — *A Simple Equation for Rapid Estimation of Rocket Nozzle Convective Heat Transfer Coefficients.* Jet Propulsion, January 1957.

45. McAdams, W.H. — *Heat Transmission.* Third Edition, McGraw-Hill Book Company, P.219, 1954.

46. Kolozzi, J.S. — *An Investigation of Heat Transfer Through the Turbulent Boundary Layer in an Axially Symmetric Convergent-Divergent Nozzle.* (M.S. Thesis to appear as an Ohio State University Interim Report) June 1958.

47. Zucrow, M.
Graham, A.R. — *Some Considerations of Film Cooling for Rocket Motors.* Jet Propulsion, June 1957.

48. Eckert, E.R.G. — *Transpiration and Film Cooling.* Heat Transfer Symposium, University of Michigan, 1952.

49. Bartas, J.G. — *Gas Side Wall Temperatures in Rib-Backed Liquid-Cooled Combustion Chambers.* Jet Propulsion, July 1957.

50. Baltrukonis, J.H. — *Comparison of Approximate Solutions of the Thermoelastic Problem of the Thick-Walled Tube.* Preprint No.836, Institute of The Aeronautical Sciences National Summer Meeting, July 1958.

51. Forster, H.K.
Zuber, N. — *Dynamics of Vapor Bubbles and Boiling Heat Transfer.* Journal of American Institute of Chemical Engineers, Vol.1, No.4, December 1955.

52. Bartz, D.R. — *Factors Which Influence the Suitability of Liquid Propellants as Rocket Motor Regenerative Coolants.* Jet Propulsion, January 1958.

53. Brenner, A.
Jenning, C.W. — *Physical Properties of Electrodeposited Metals - #1 Nickel.* American Electroplater's Society Research Report Serial No.20, 1952.

54. — *Beryllium Copper - Wrought Alloys with Unique Properties.* The Beryllium Corporation, 1956.

55. — *Handbook of Supersonic Aerodynamics.* NAVORD Report (Vol.5) August 1953.

TABLE I

Survey of Boundary Layer Displacement Thickness

Tunnel	M_1	P_0 (atm)	T_0	$\frac{T_w}{T_\infty}$	x_1	δ_1^*	$\frac{\delta_1^* R_{e_1}^{1/5}}{x_1^{4/5}}$
NOL HWT	5.0	3.1	325($^\circ$K)	5.4	50(cm)	.71(cm)	.30
	"	5.0	400	4.3	"	.61	.26
	"	7.8	510	3.5	"	.58	.25
	"	8.6	560	3.3	"	.57	.24
	6.8	15	470	6.3	"	1.09	.49
	"	28	590	5.2	"	.94	.44
	"	21	590	5.2	"	1.03	.45
	"	21	640	4.6	"	.93	.40
	7.7	24	645	5.9	"	1.31	.55
NOL HWT (old measurement)	7.0	10	590	5.9	60	1.0	.33
JPL 20"SWT	3.0	1.2	554($^\circ$R)		90(in)	.46(in)	.15
	3.7	2.0	576		90	.65	.22
	4.1	3.5	585		89	.68	.24
	4.5	4.1	578		88	.84	.30
JPL 12" SWT	3.0	4.2	570		45	.28	.20
GALCIT Leg 1	5.7	6.4	685		20	.27	.30
Langley 11" HWT	6.9	25	1210		56	.72	.35
NOL 8" HWT	8.1	50	1400		44	.45	.26
Johns Hopkins	8.99	28.2	1360	7.6	9.6	.23	.40
2" dia HWT	9.04	35.0	1360	8.0	9.6	.22	.39
	9.07	41.8	1360	8.3	9.6	.22	.41
	9.10	52.0	1360	8.7	9.6	.22	.42
BRL 5.6" Dia.Model HWT	9.05	31.6	1560	6.1	39	.67	.37
JPL 7" Model HWT	8.25	18.0	1460	5.5	47.6	1.07	.46
AEDC 50" Dia. 'B'	8.03	41.5	1345	5.3	270	2.85	.39
Minor	7.13	40.8	1350	4.2	195	1.75	.32
	6.03	40.1	1355	3.1	118	0.72	.22

BRL Ballistic Research Laboratory
JPL Jet Propulsion Laboratory
NOL Naval Ordnance Laboratory
GALCIT Guggenheim Aeronautical Laboratory California Institute of Technology
AEDC Arnold Engineering and Development Center

TABLE II

Survey of Pressure Ratio

Symbol	*Tunnel location*	*Size (ins)*	*Diffuser configuration*	*Supply pressure (lb/in^2)*	*Nozzle to scoop area ratio*	*Second throat to nozzle area ratio*	*Remarks*
▼	Ohio State Univ.	12 x 12	Var. Geom. Conv.-Div.	-	-	1.8	Starting empty
▼	" " "	12 x 12	" "	-	-	1.47	Starting w/model
▼	" " "	12 x 12	" "	-	-	1.56	Starting empty
⊗	" " "	3 conical	Fixed-Conv.- Straight Div.	1800	-	.45	Running-wedge center body
⊕	" " "	3 conical	Fixed-Conv.- Straight-Div.	1000	-	.21	Running-w/o center body
◗	Johns Hopkins	2 conical	- -	800	-	.50	Starting empty
◗	Langley-NACA	- -	None	-	-	-	Starting w/o diffuser-atmos. exhaust
○	Peenemuende-Kochel	16 x 16	Conv.-Div.	-	.64	-	- -
△	Goettingen-AVA	4.33 x 5.9	Con.-Sudden Expansion	-	.73	-	- -
□	Aachen-AIA	3.94 x 3.94		-	.70	-	Humid air
▷	Boeing	12 conical	Fixed-Conv.-	-	-	-	Starting & running
◁	Rosemount	6 x 6	Fixed-Conv.- Div.	-	.54	-	Starting & running

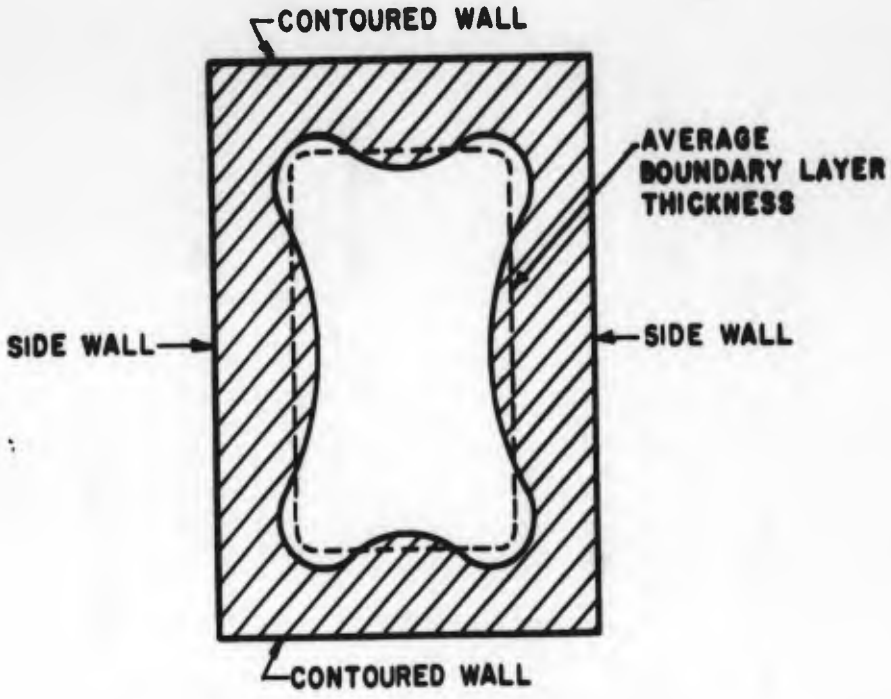

(a) TWO DIMENSIONAL TEST SECTION

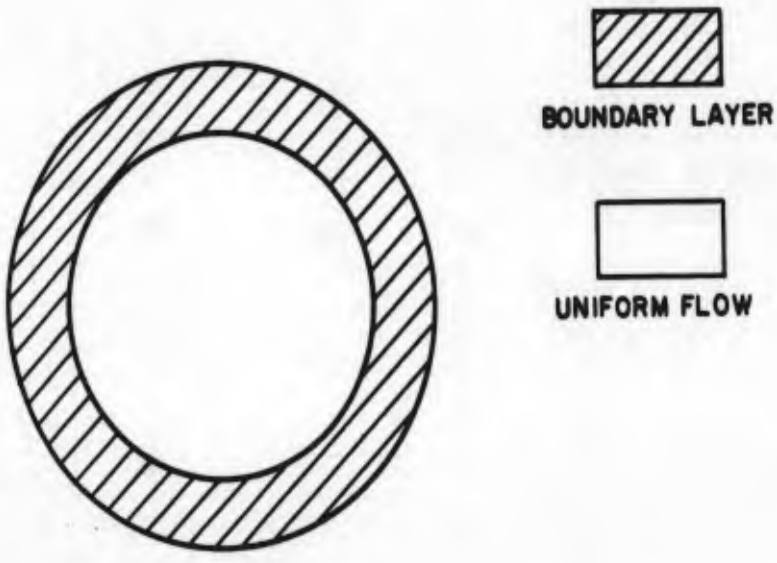

(b) AXISYMMETRIC TEST SECTION

Fig. 1 Boundary-layers in two-dimensional and axisymmetric nozzle test sections

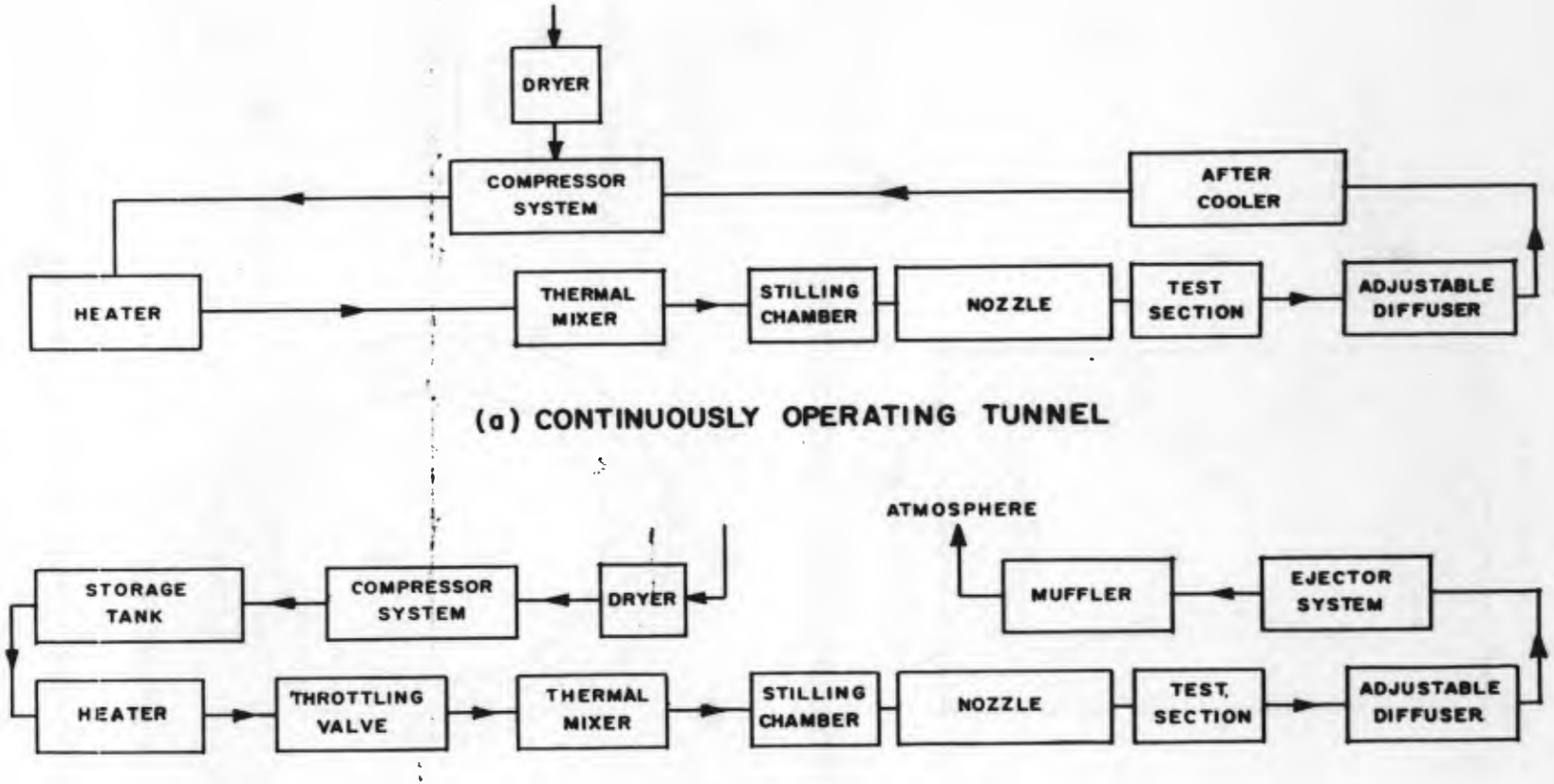

Fig.2 Arrangement of hypersonic wind tunnel circuits

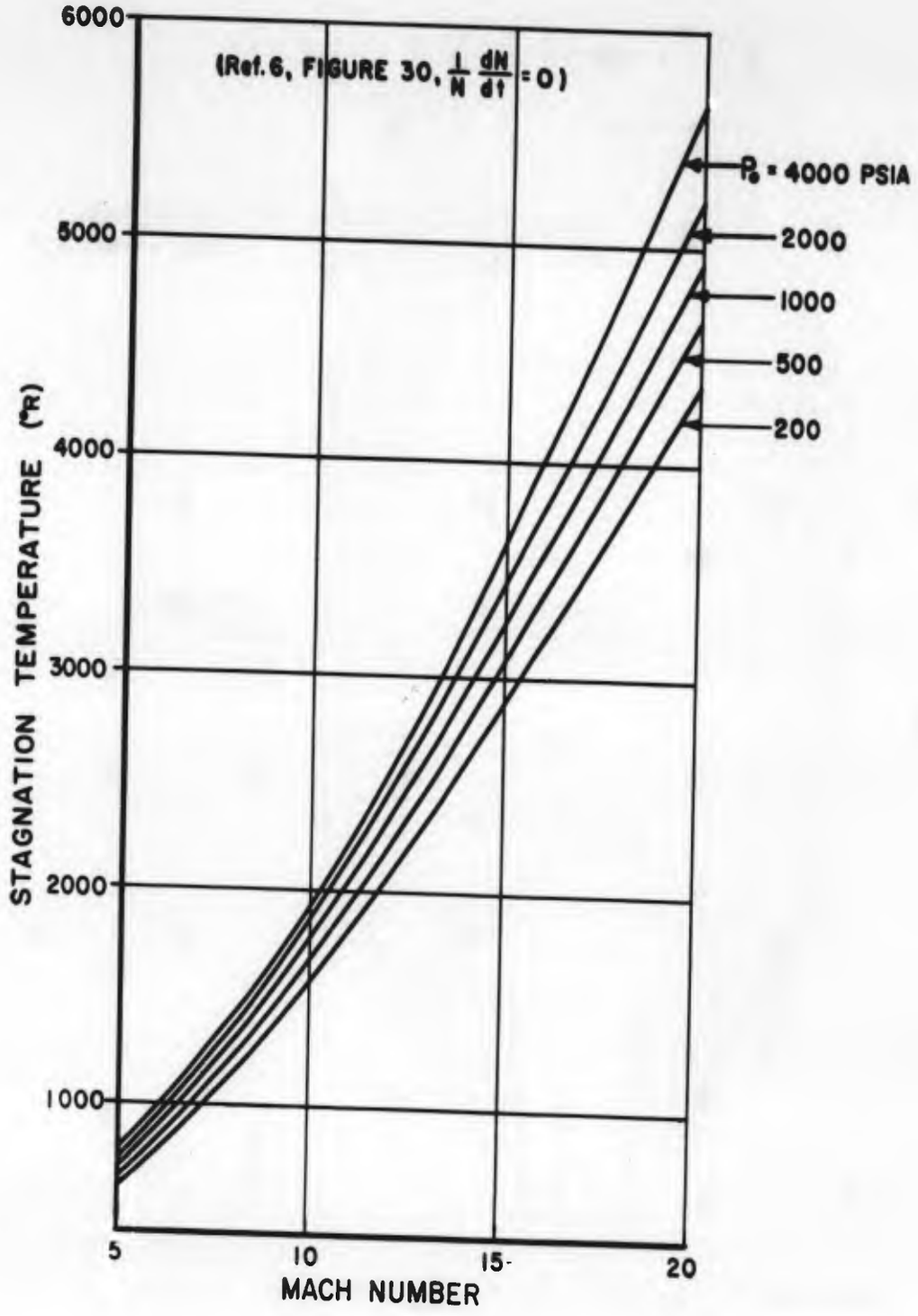

Fig. 3 Stagnation temperature requirements for liquefaction - free flow at high Mach numbers

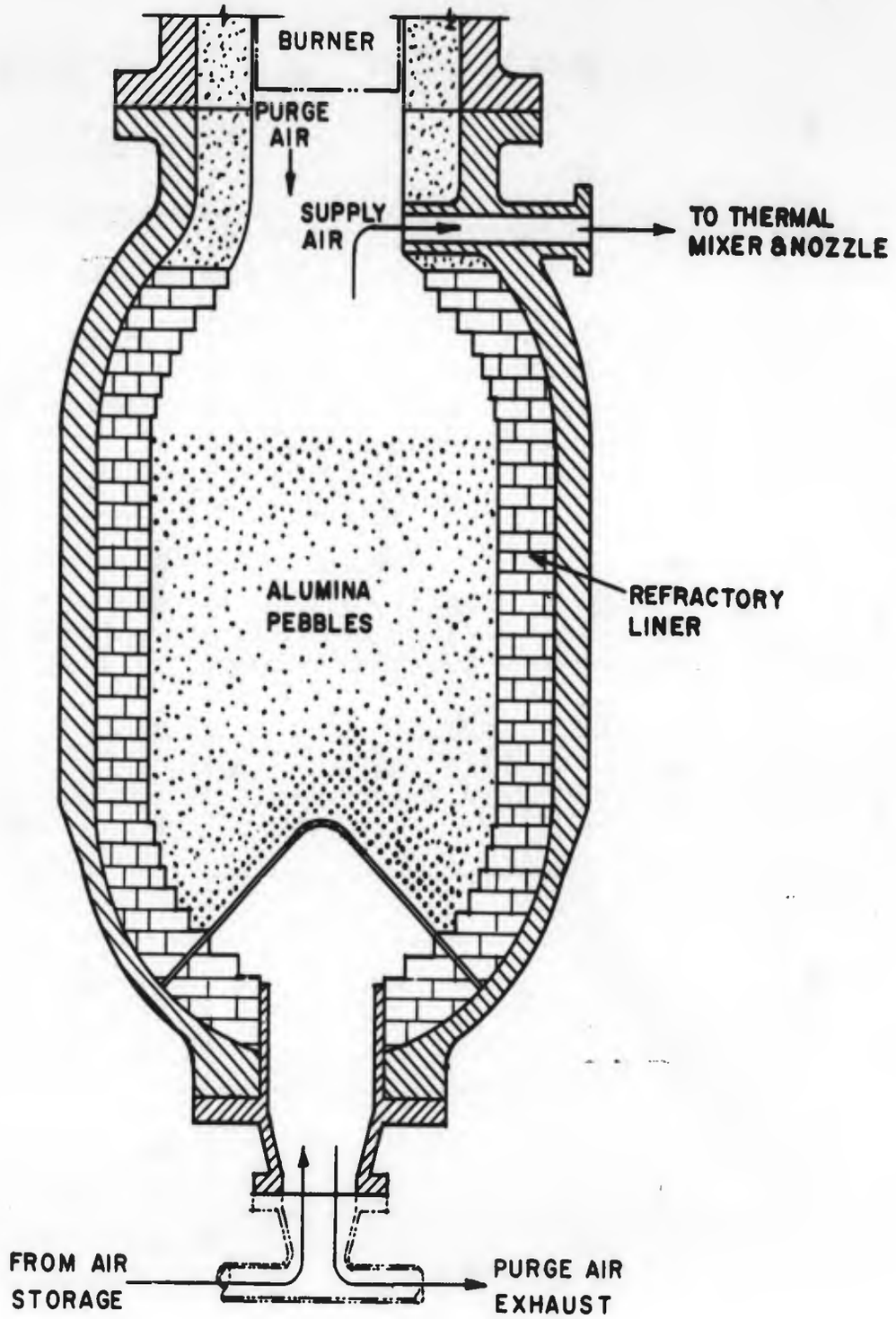

Fig.4 Gas-fired or oil-fired pebble bed heater

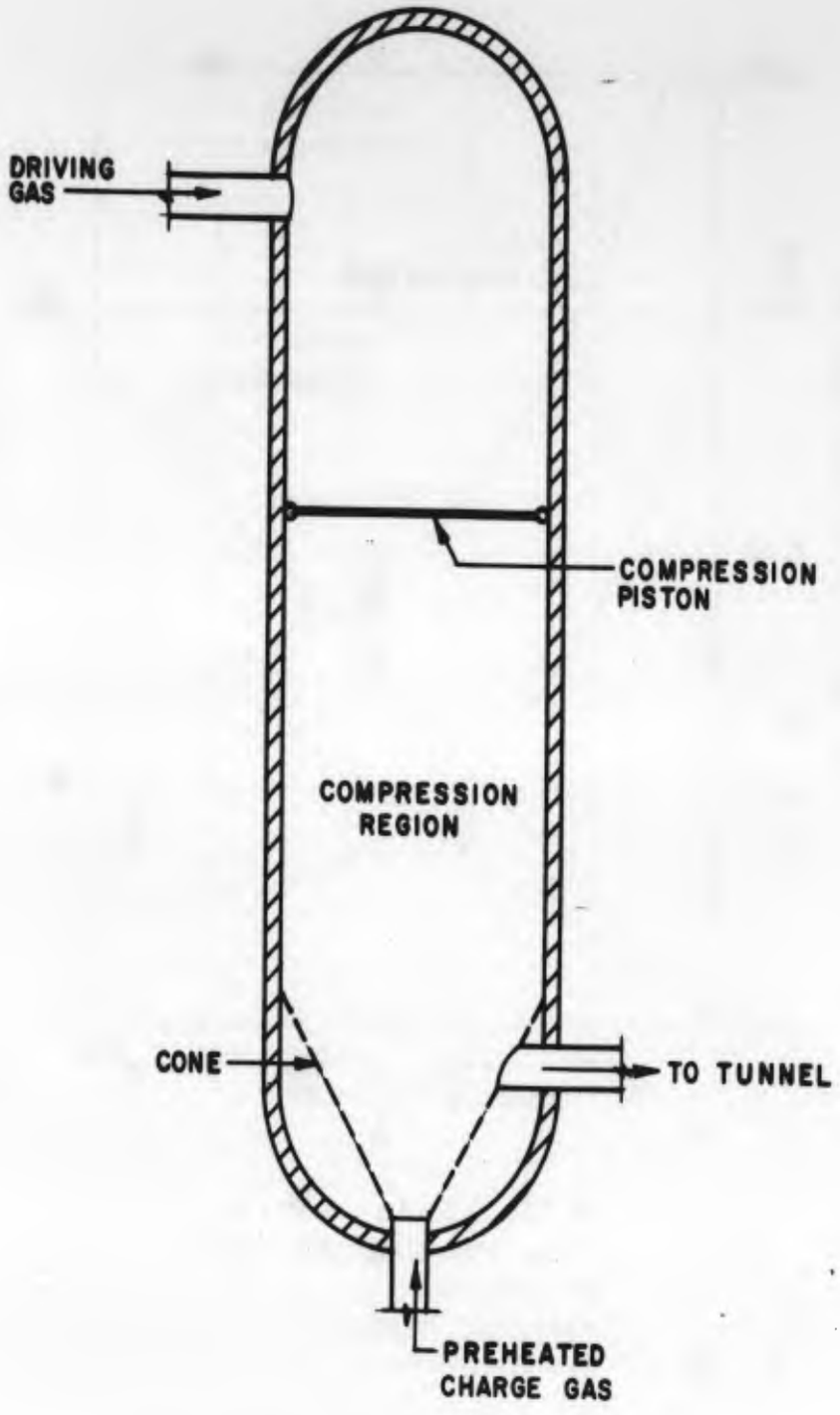

Fig.5 Compression heater

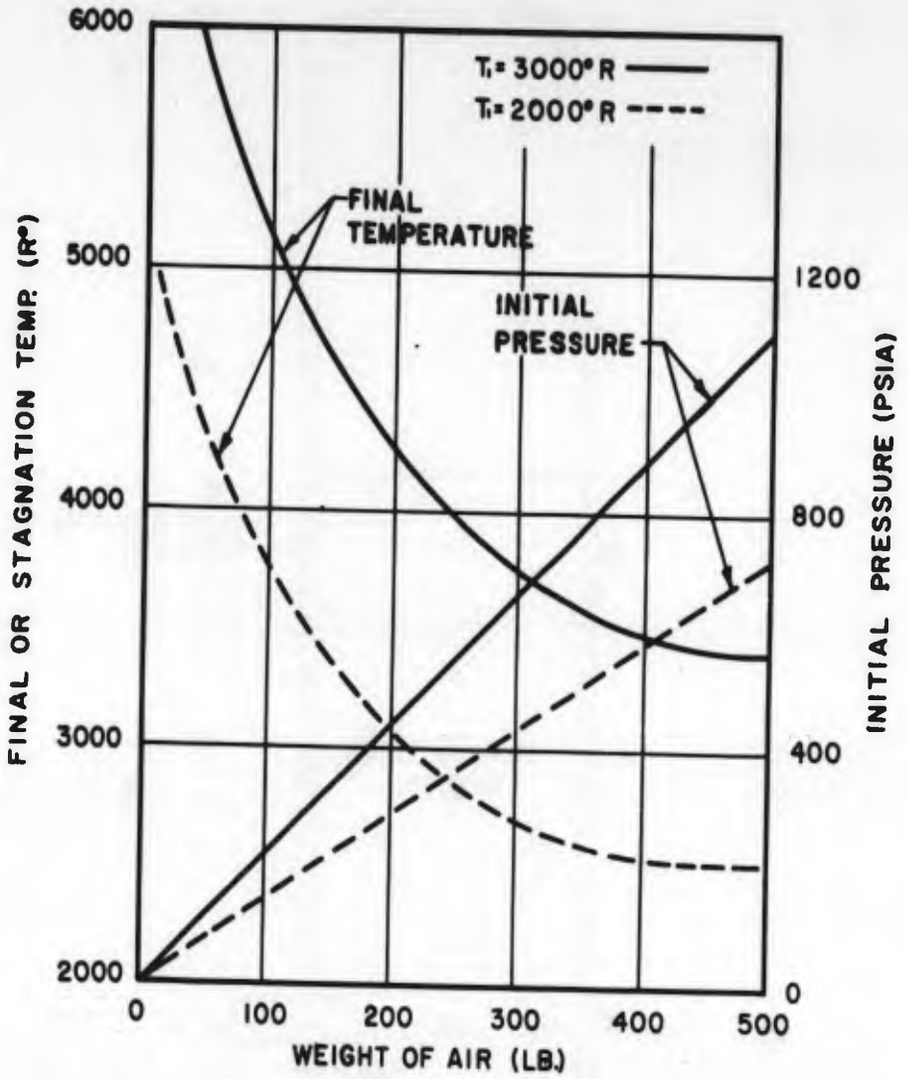

INITIAL VOLUME 500 FT.^{3}
FINAL PRESSURE 2000 PSIA
γ VARIABLE
T_i = INITIAL TEMP.

Fig. 6 Ideal performance for compression heater

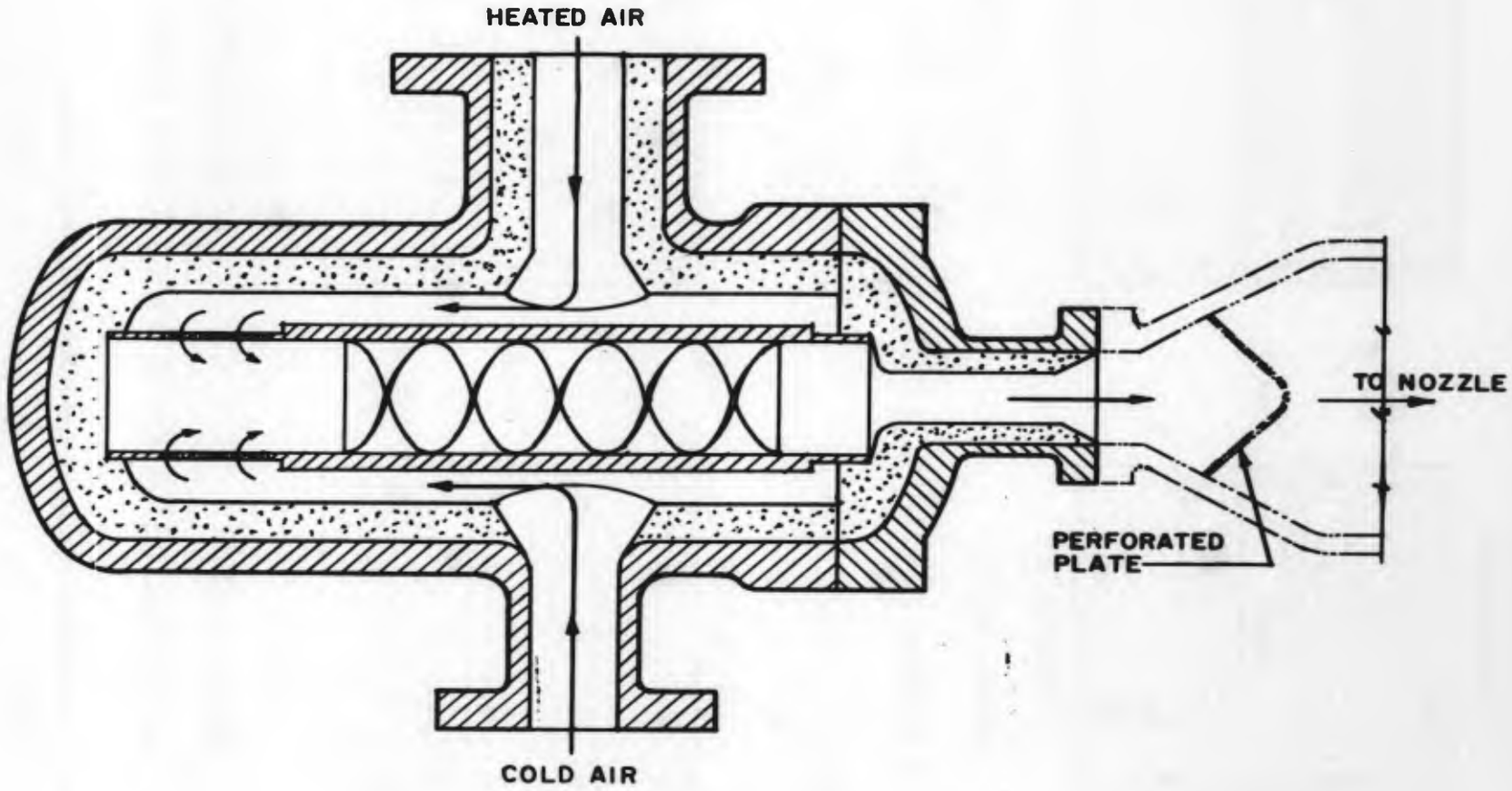

Fig.7 Typical thermal mixer design

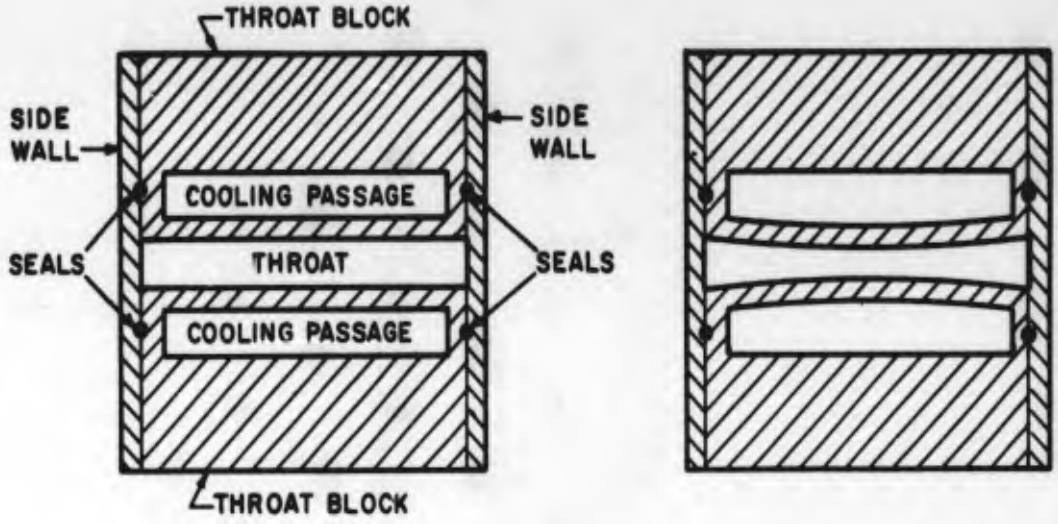

(a) THERMAL DISTORTION OF NON-RIBBED THROAT BLOCK

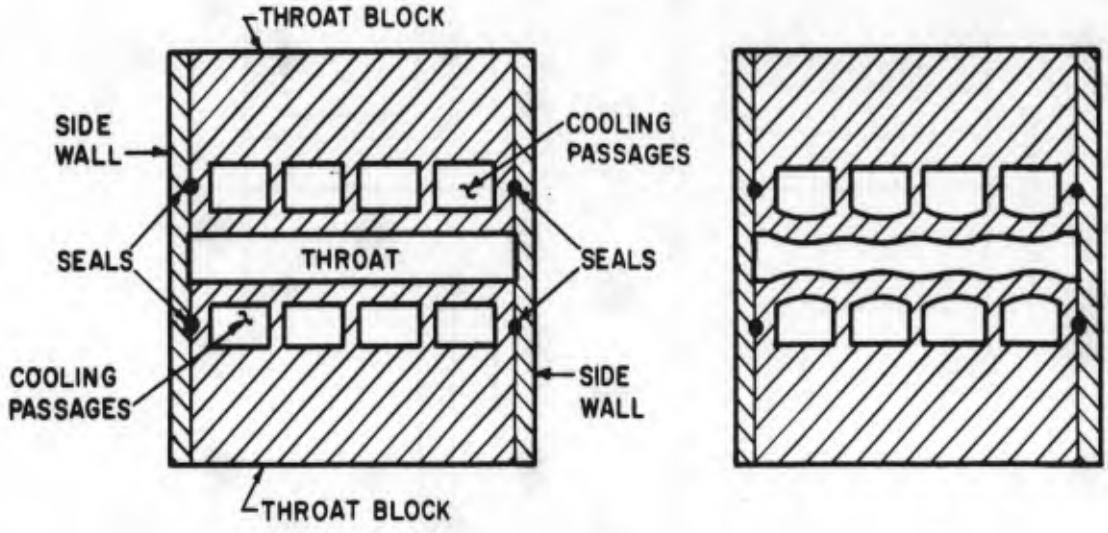

(b) THERMAL DISTORTION OF RIBBED THROAT BLOCK

Fig.8 Thermal distortion in two-dimensional nozzle throat sections

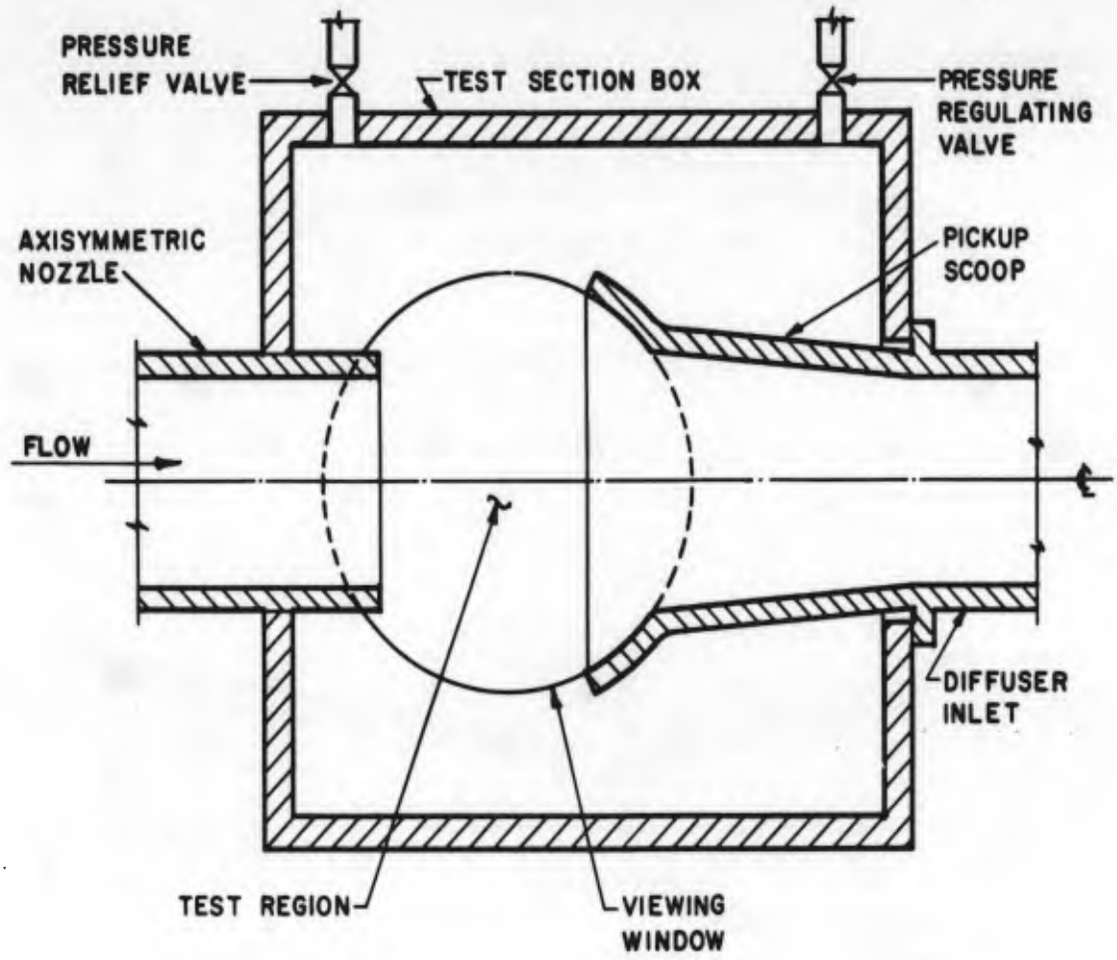

Fig.9 Typical free-jet test section

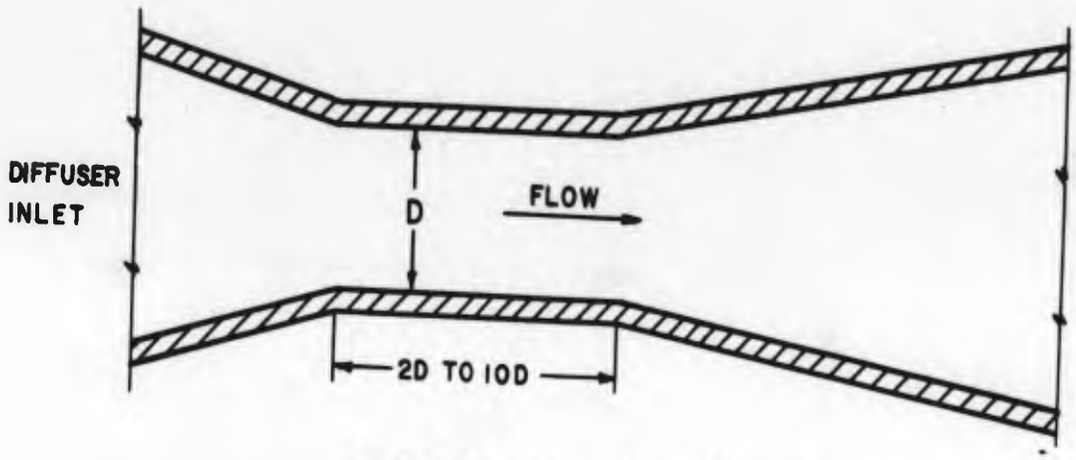

(a) FIXED CONICAL DIFFUSER

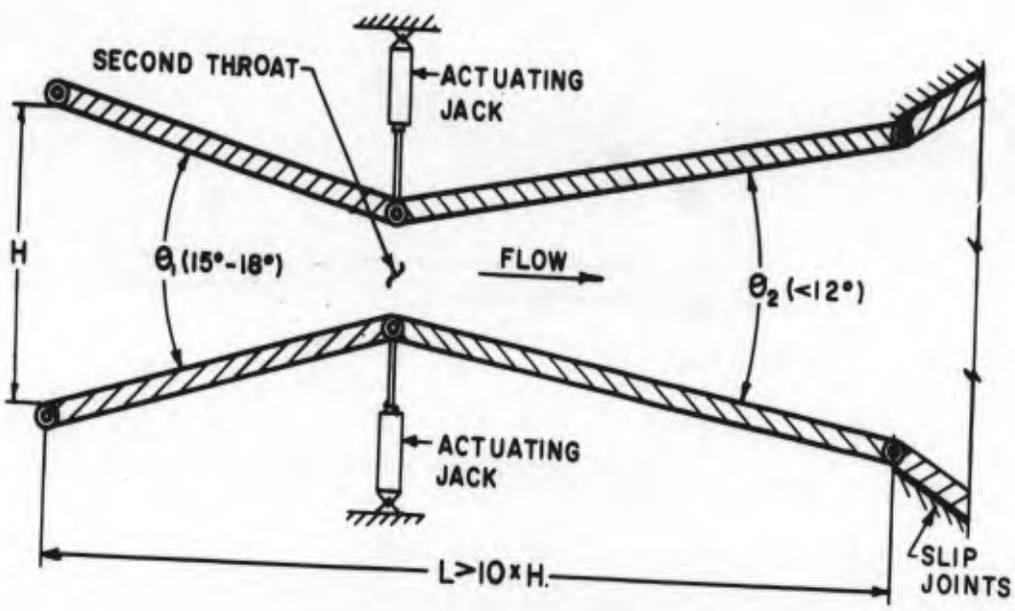

(b) TWO DIMENSIONAL VARIABLE DIFFUSER

Fig.10 Supersonic diffusers

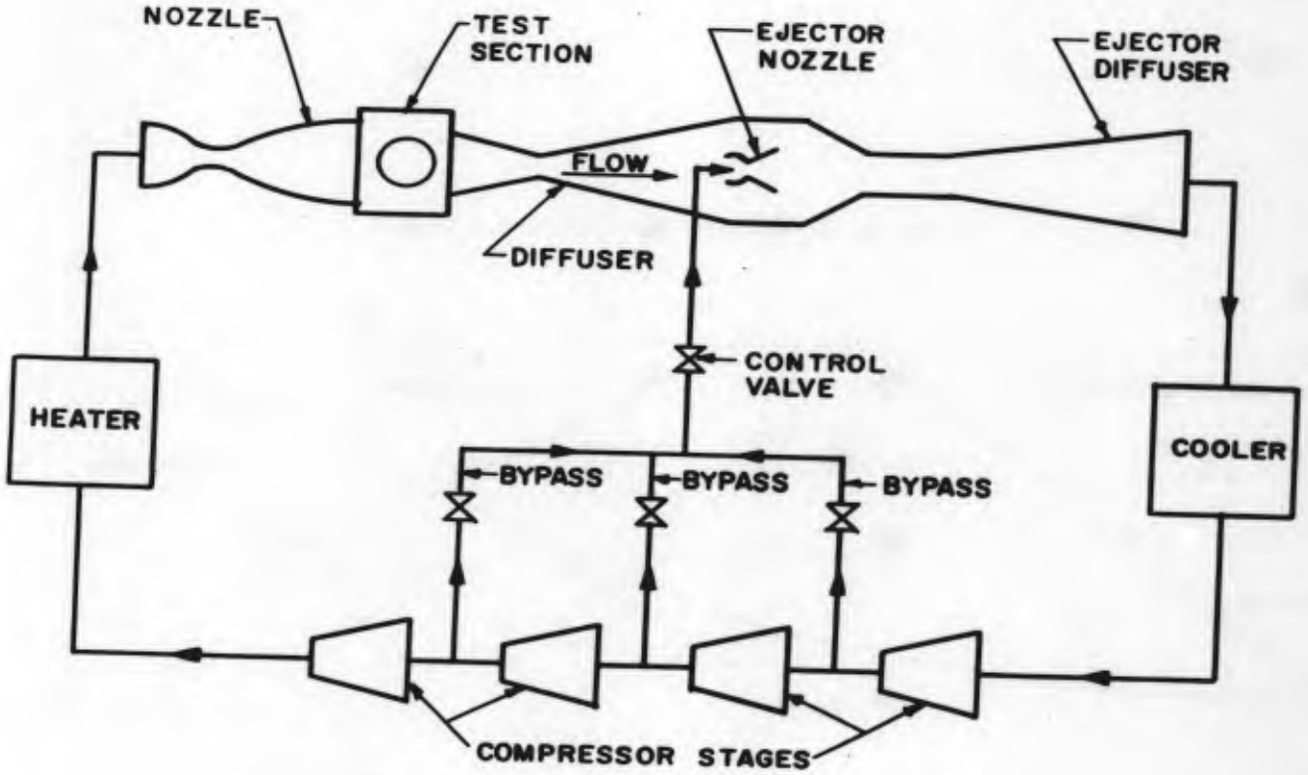

Fig.11 Ejector by-pass arrangement in a continuous circuit

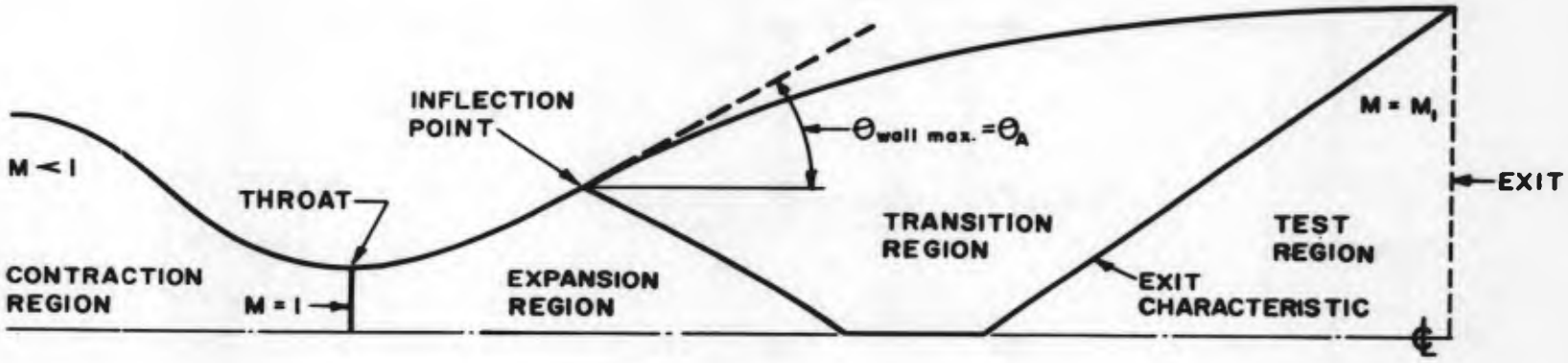

Fig. 12 Definition of nozzle flow regions

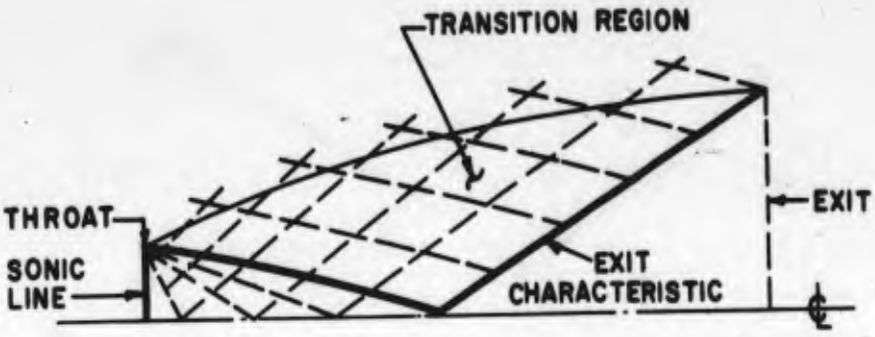

(a) NOZZLE WITH CORNER EXPANSION AT THROAT

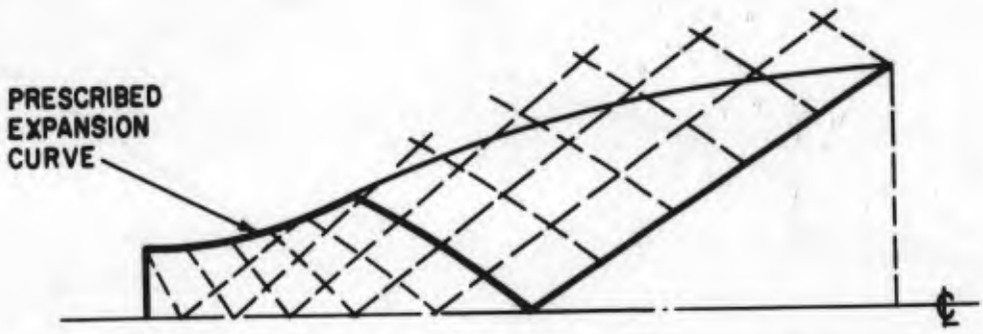

(b) NOZZLE WITH PRESCRIBED EXPANSION CURVE

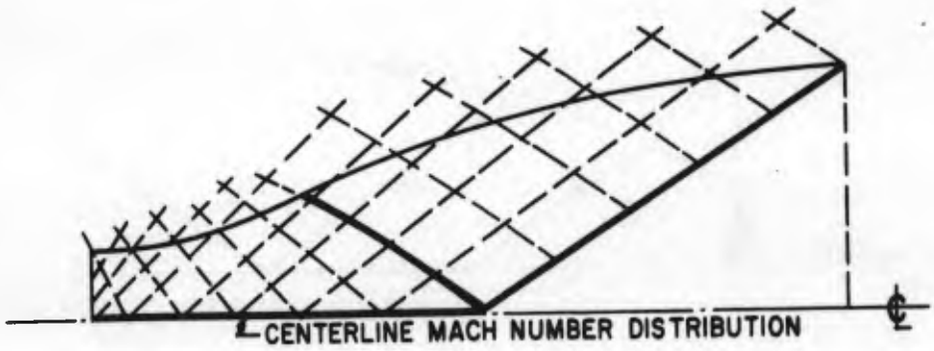

(c) NOZZLE WITH CENTERLINE MACH NUMBER DISTRIBUTION

Fig. 13 Computation of nozzle contours starting from the throat

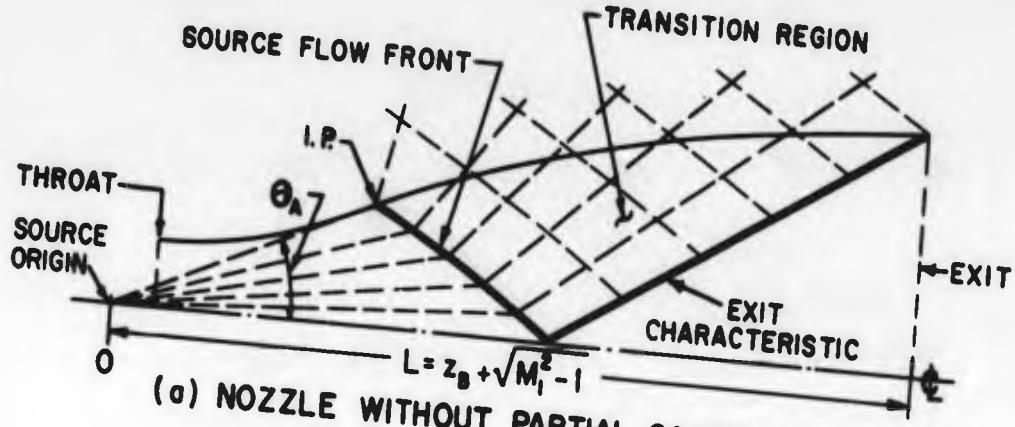

(a) NOZZLE WITHOUT PARTIAL CANCELLATION REGION

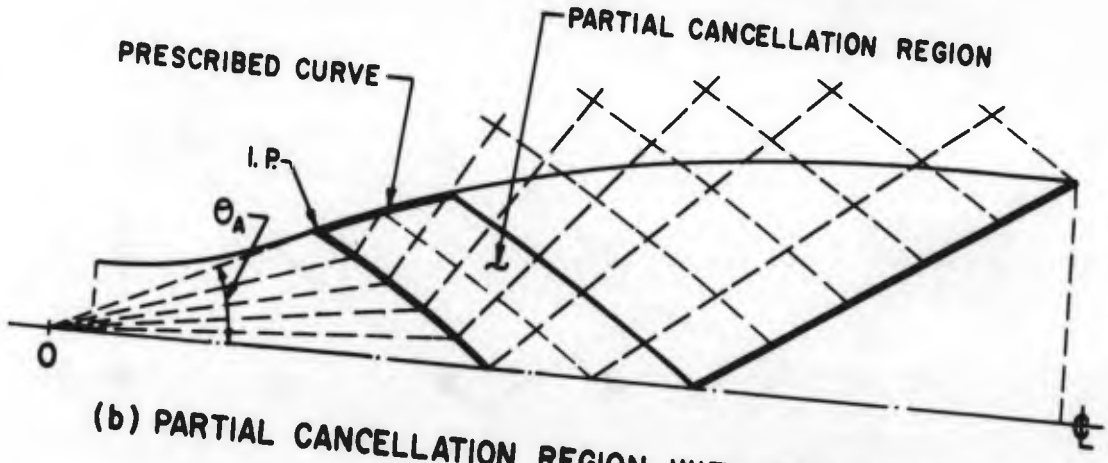

(b) PARTIAL CANCELLATION REGION WITH PRESCRIBED CURVE

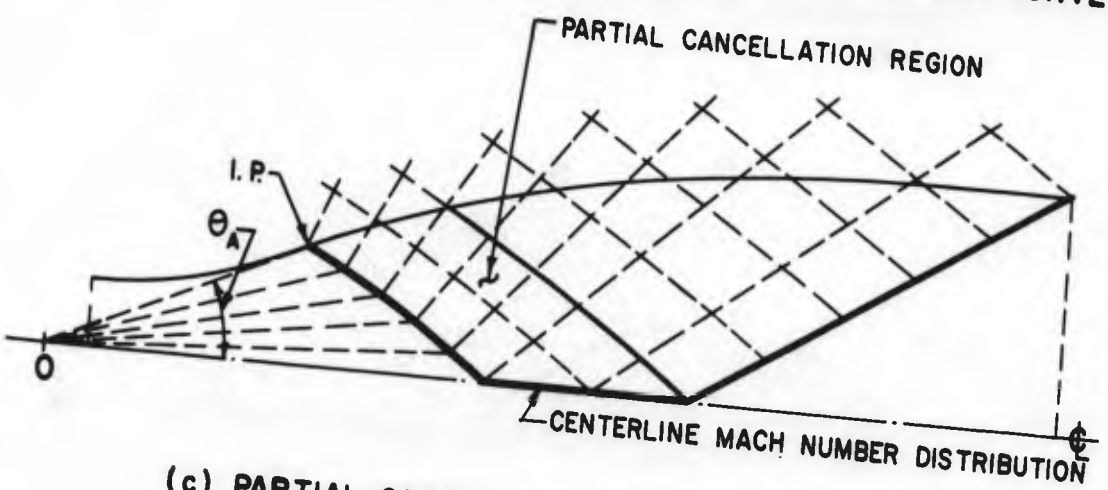

(c) PARTIAL CANCELLATION REGION WITH CENTERLINE MACH NUMBER DISTRIBUTION

Fig. 14 Computation of nozzle contours assuming source flow

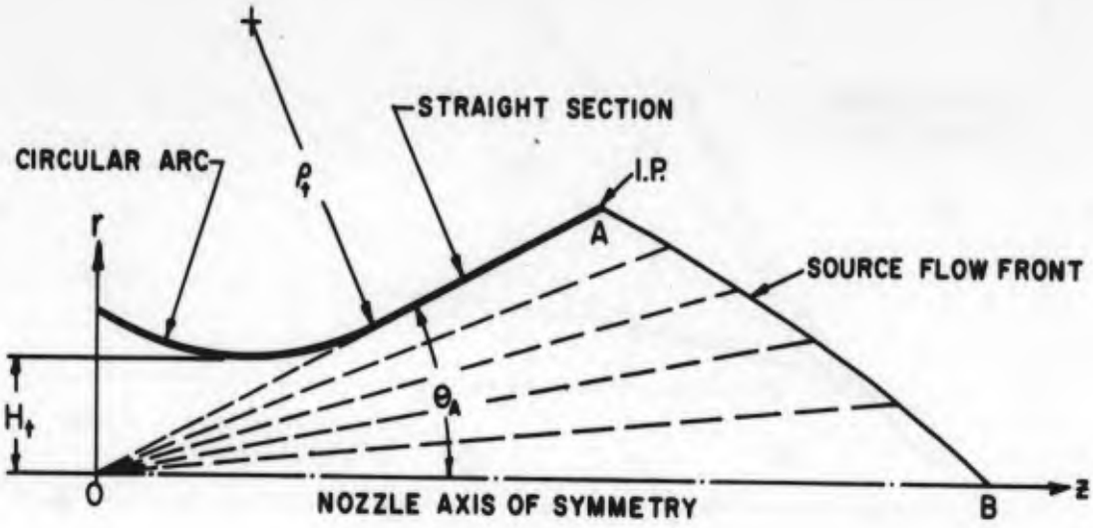

(a) EXPANSION CURVE WITH CIRCULAR ARC AT THROAT

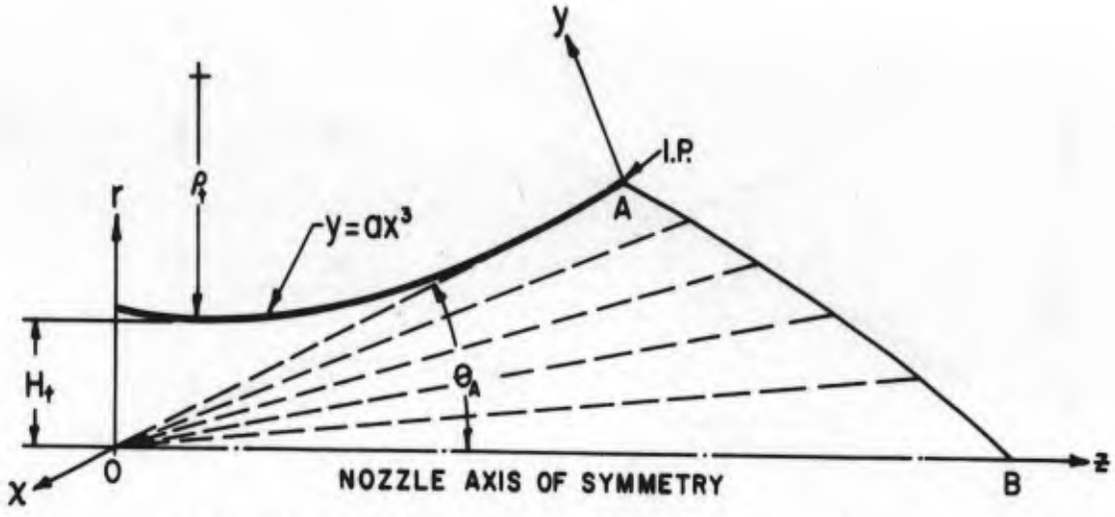

(b) EXPANSION CURVE WITH CUBIC PARABOLA

Fig. 15 Typical expansion region curves

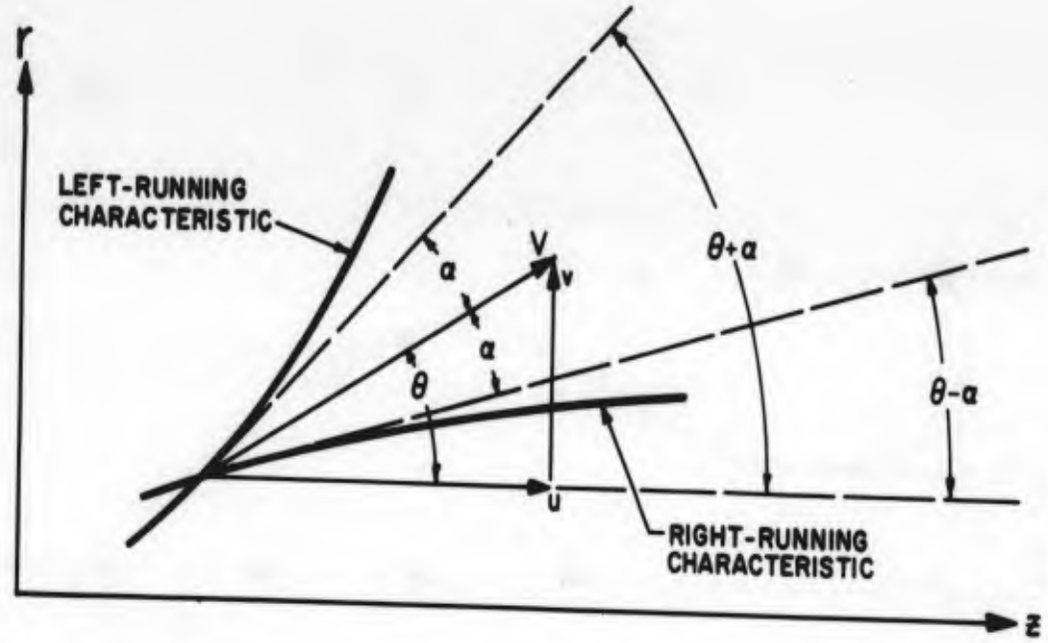

(a) RELATION BETWEEN STREAMLINES AND CHARACTERISTICS

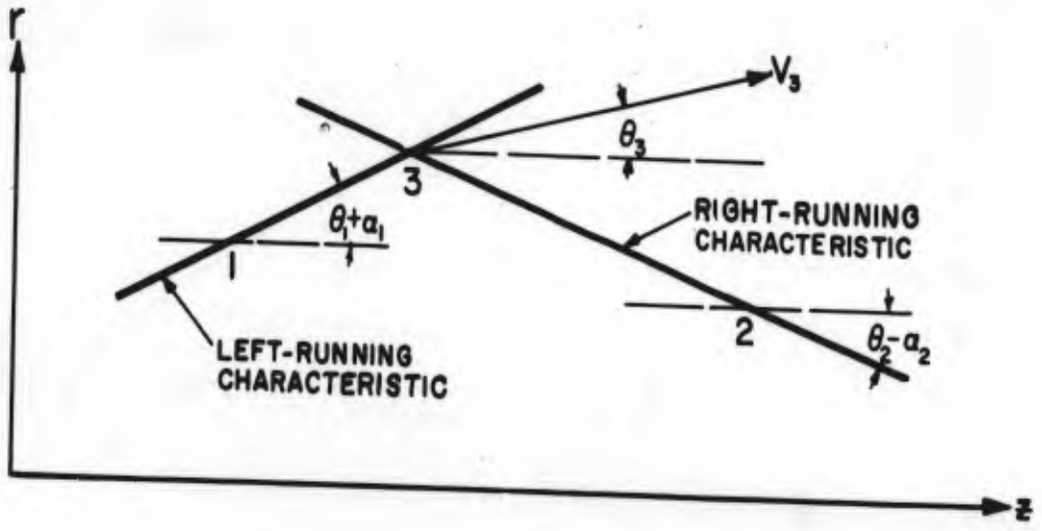

(b) UNIT PROCESS IN FLOW NET COMPUTATION

Fig.16 Numerical procedure of method of characteristics for axisymmetric flow

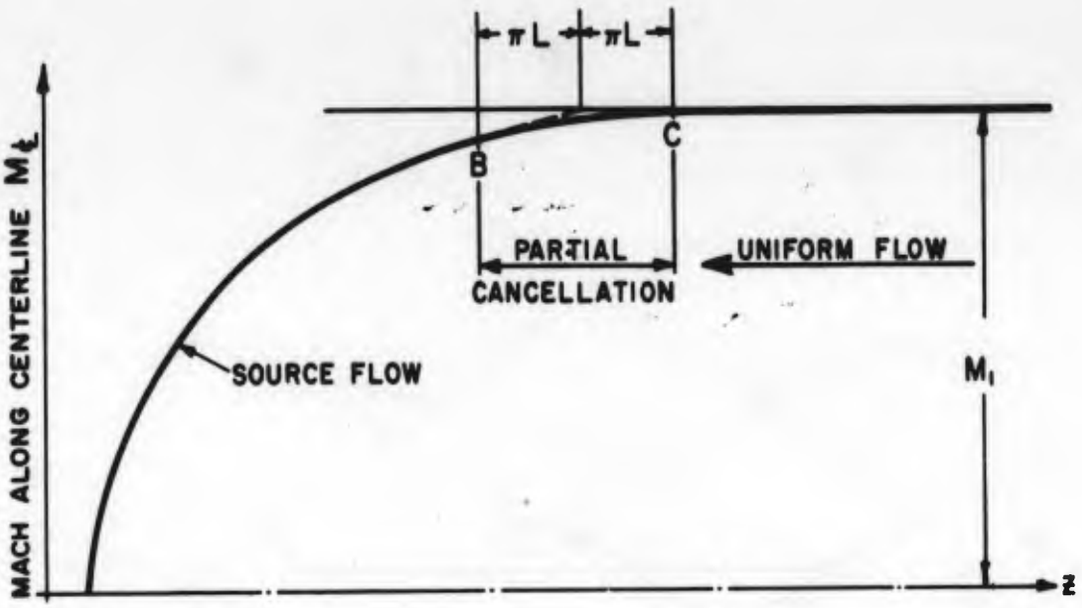

(a) CENTERLINE MACH NUMBER DISTRIBUTION

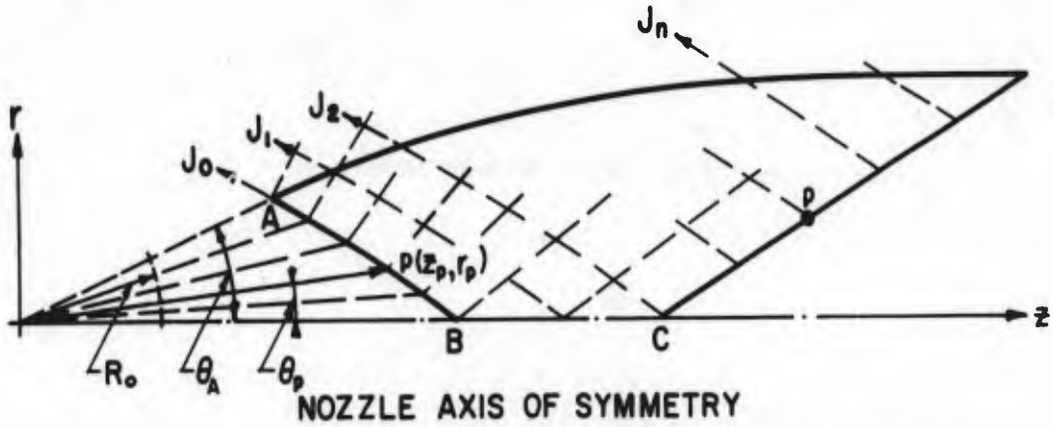

(b) SOURCE FLOW FRONT AND TRANSITION REGION

Fig. 17 Flow net construction in transition region

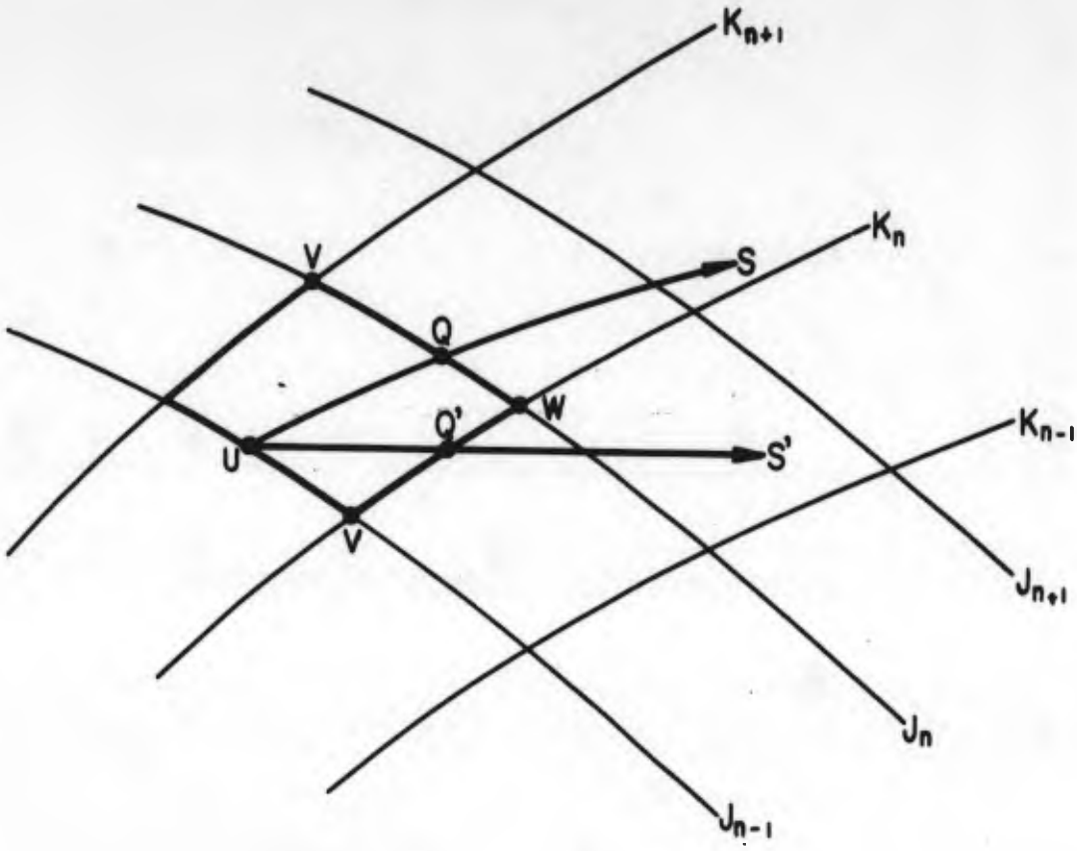

Fig.18 Wall coordinates computation

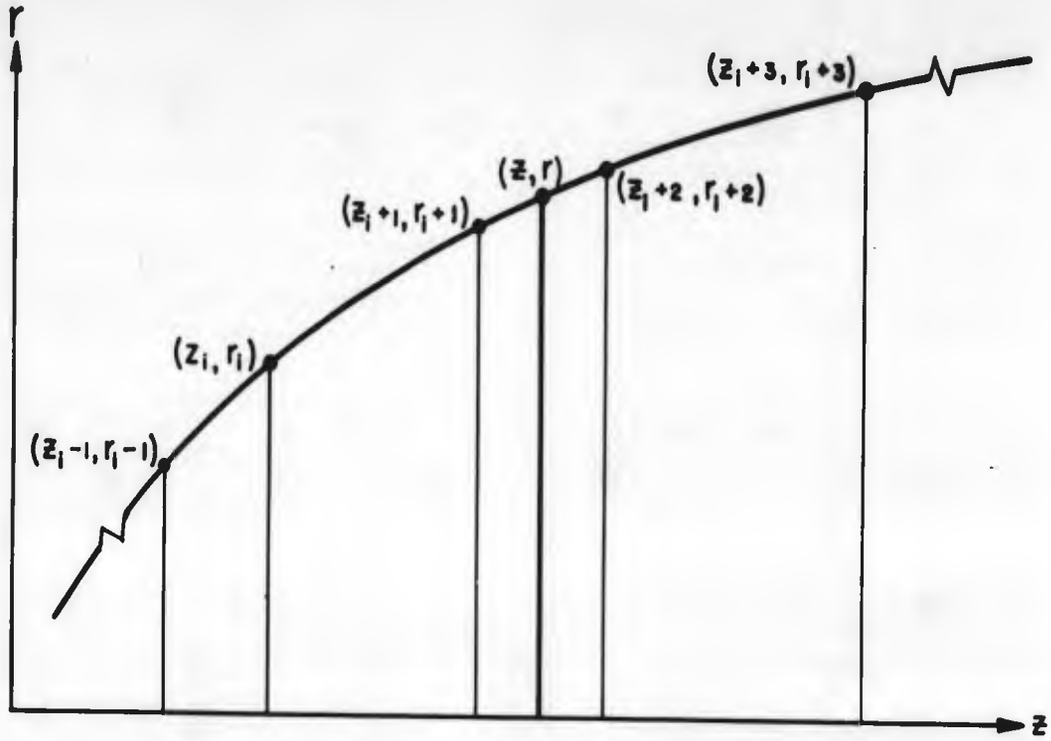

Fig.19 Wall coordinates in equal axial increments

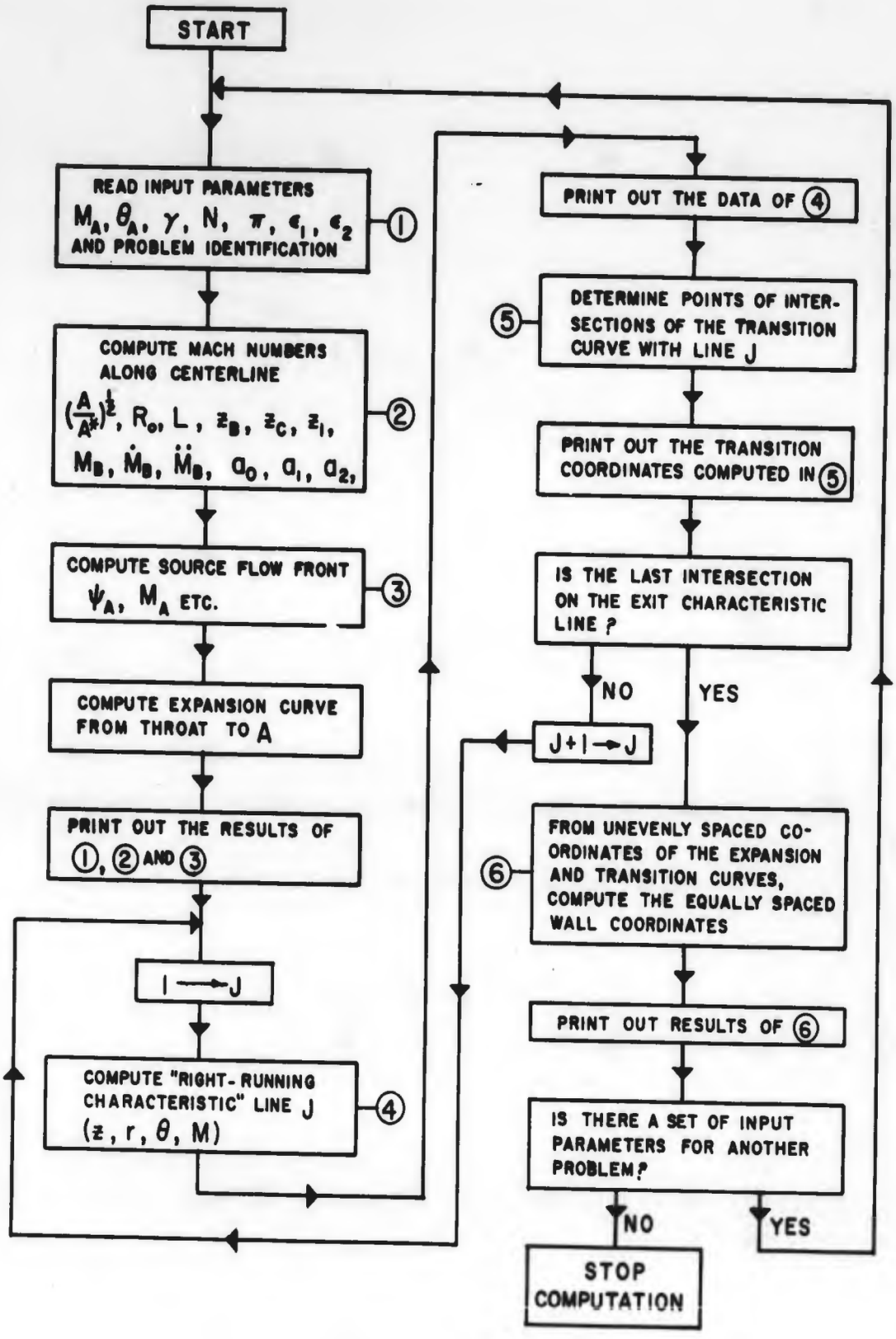

Fig. 20 Computer routine for nozzle coordinates

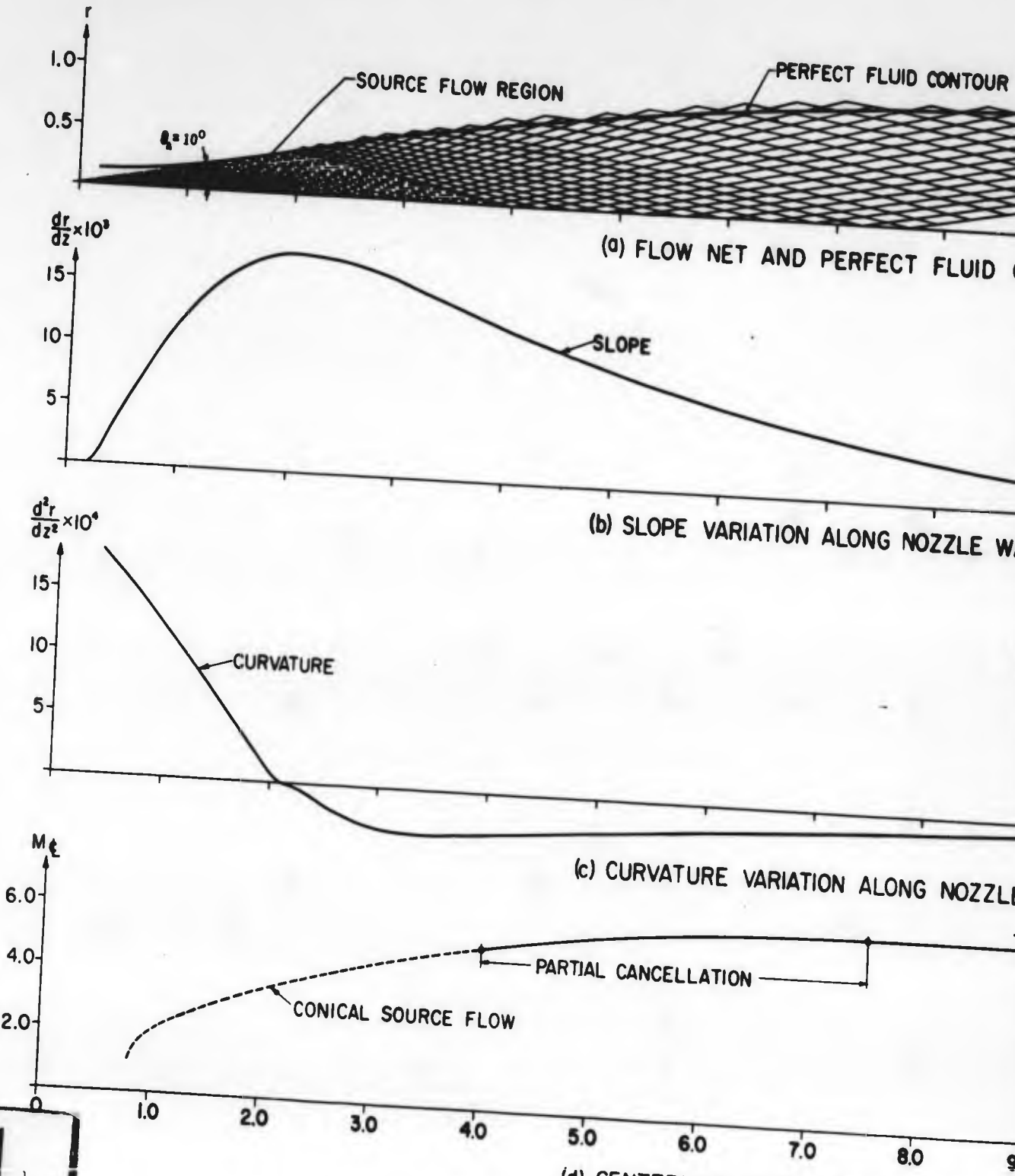

Fig. 21 Wall contour geometry for a nozzle with $M_1 = 6.0$, $\theta_A =$

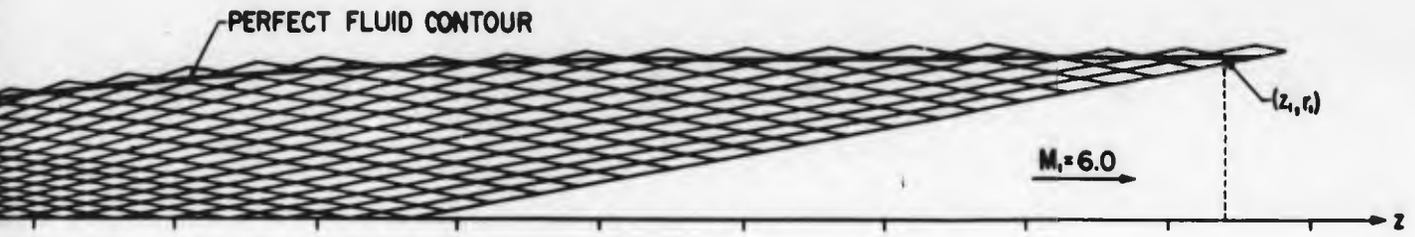

(a) FLOW NET AND PERFECT FLUID CONTOUR

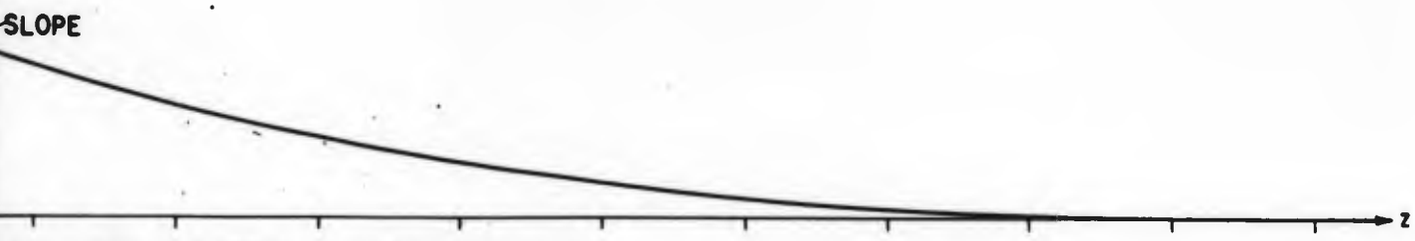

(b) SLOPE VARIATION ALONG NOZZLE WALL

(c) CURVATURE VARIATION ALONG NOZZLE WALL

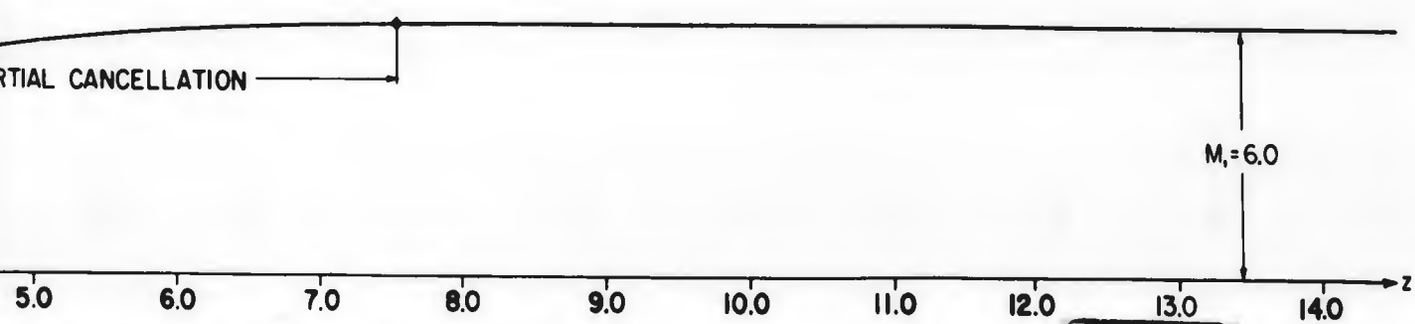

(d) CENTERLINE MACH NUMBER DISTRIBUTION

.ll contour geometry for a nozzle with $M_1 = 6.0$, $\theta_A = 10^0$, $\gamma = 1.4$

2

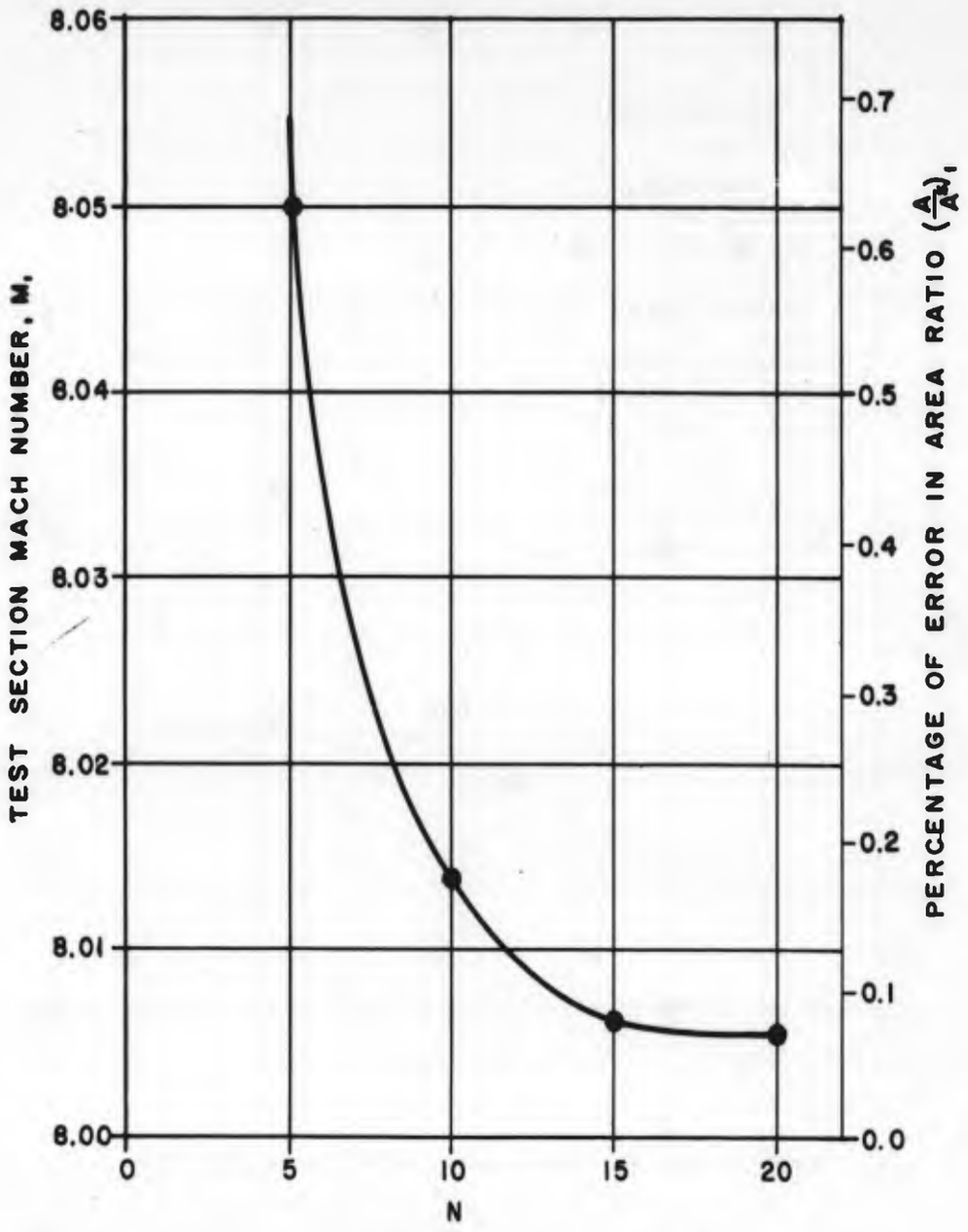

Fig. 22 Grid size effect at $M_1 = 8.0$, $\theta_A = 10^0$, $\gamma = 1.4$

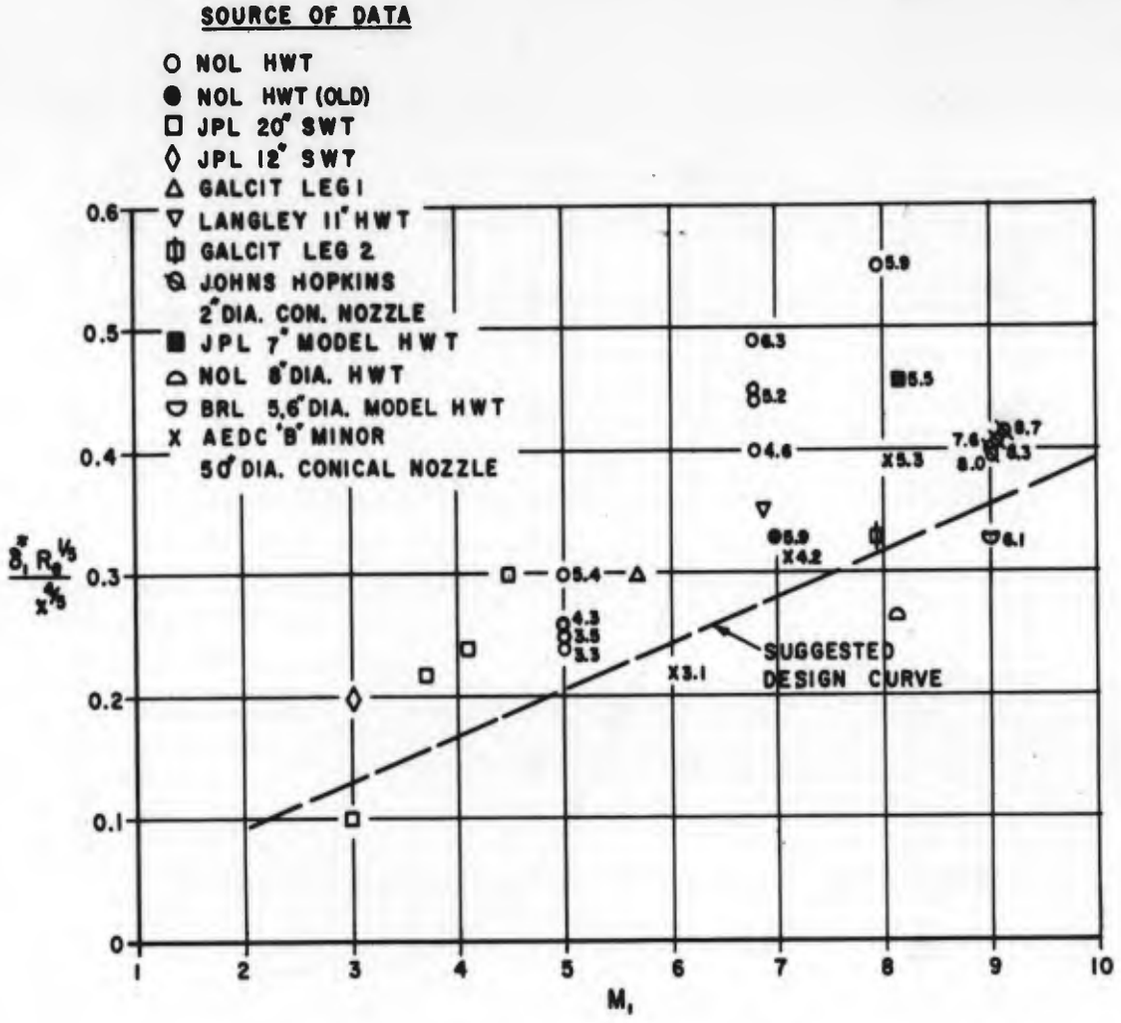

Fig. 23 Survey of boundary-layer displacement thickness data

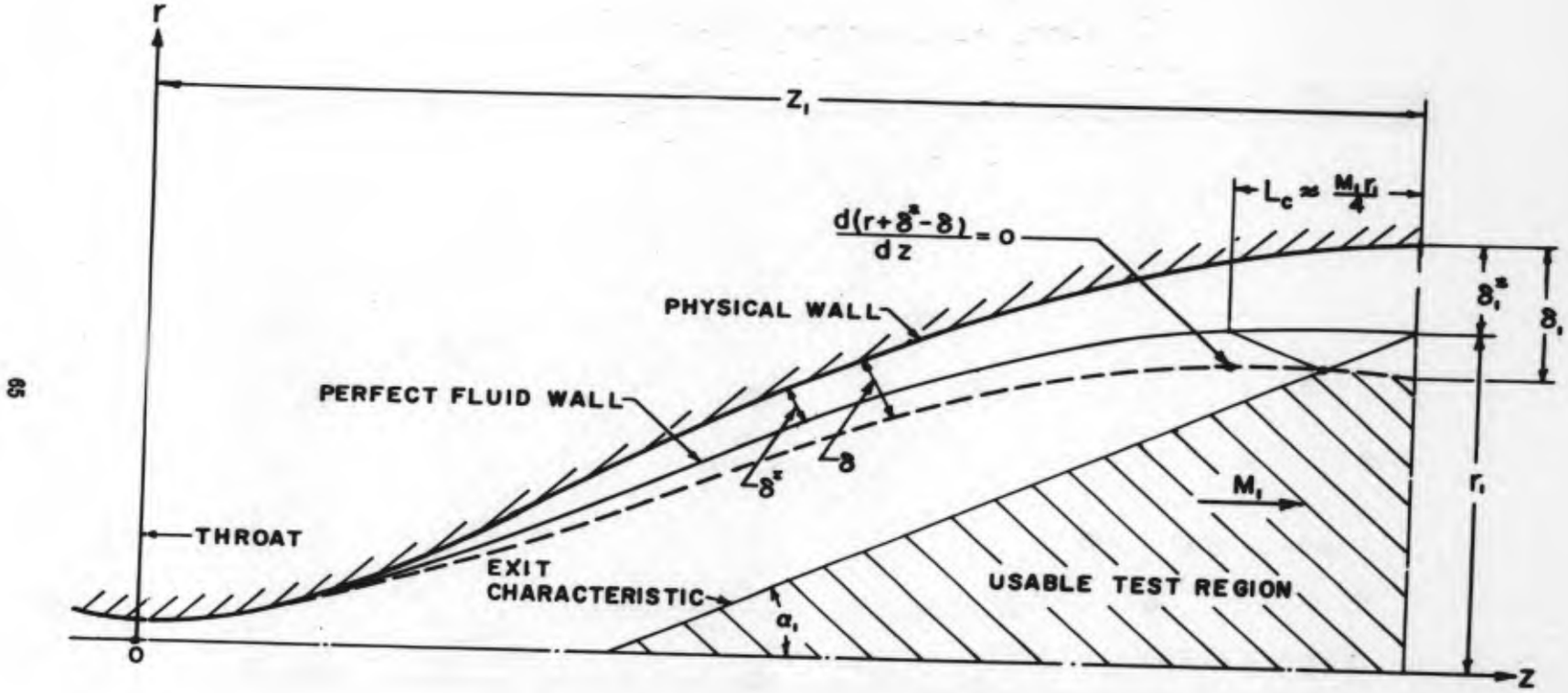

Fig. 24 Cut-off point of a typical hypersonic nozzle

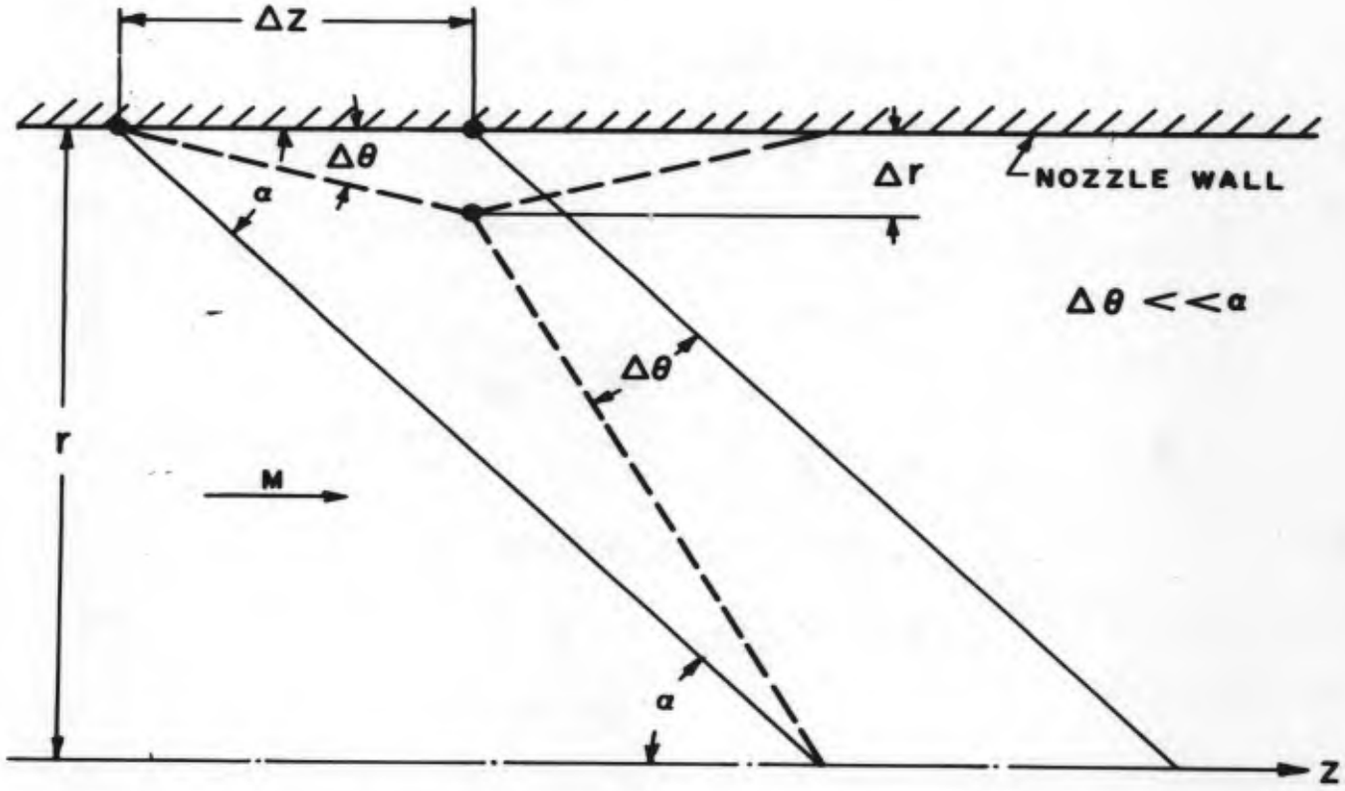

Fig. 25 Focusing effect due to wall errors

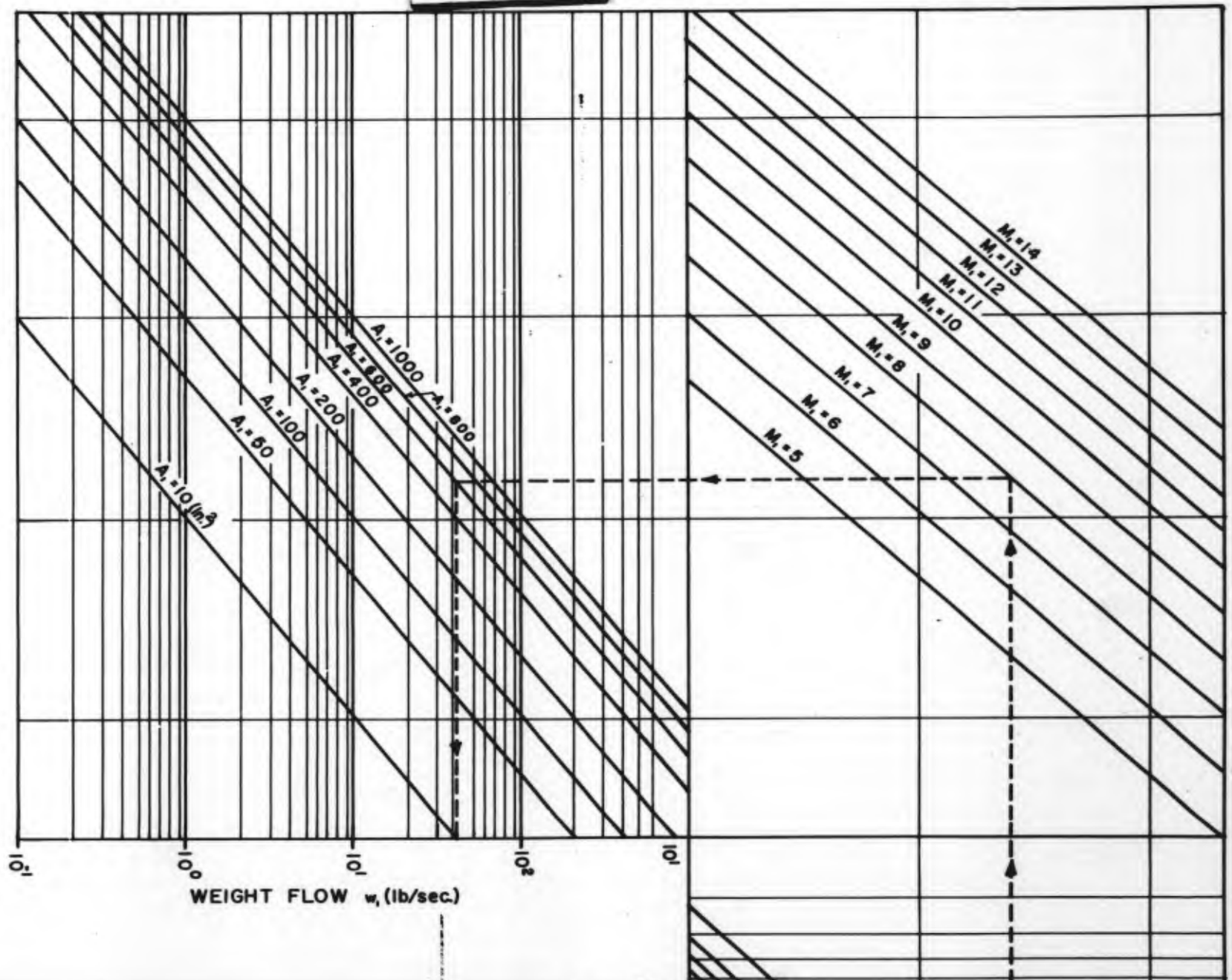
A₁=1000
A₁=800
A₁=400
A₁=200
A₁=100
A₁=50
A₁=10 (in.²)
M₁=14
M₁=13
M₁=12
M₁=11
M₁=10
M₁=9
M₁=8
M₁=7
M₁=6
M₁=5
10⁻¹
10⁰
10¹
10²
10³
WEIGHT FLOW w₁ (lb/sec.)

$$w_i = g\left(\frac{\gamma}{R}\right)^{\frac{1}{2}} \frac{P_o}{T_o^{\frac{1}{2}}} \frac{A_i M_i}{(1+0.2\,M^2)^3}$$

$$\begin{cases} g = 32.2\ \text{FT./SEC.}^2 \\ \gamma = 1.4\ \text{(FOR AIR)} \\ R = 1716\ \text{FT.}^2/\text{R}^\circ\text{-SEC.}^2 \end{cases}$$

2

Fig. 26 Weight flow for hypersonic nozzles

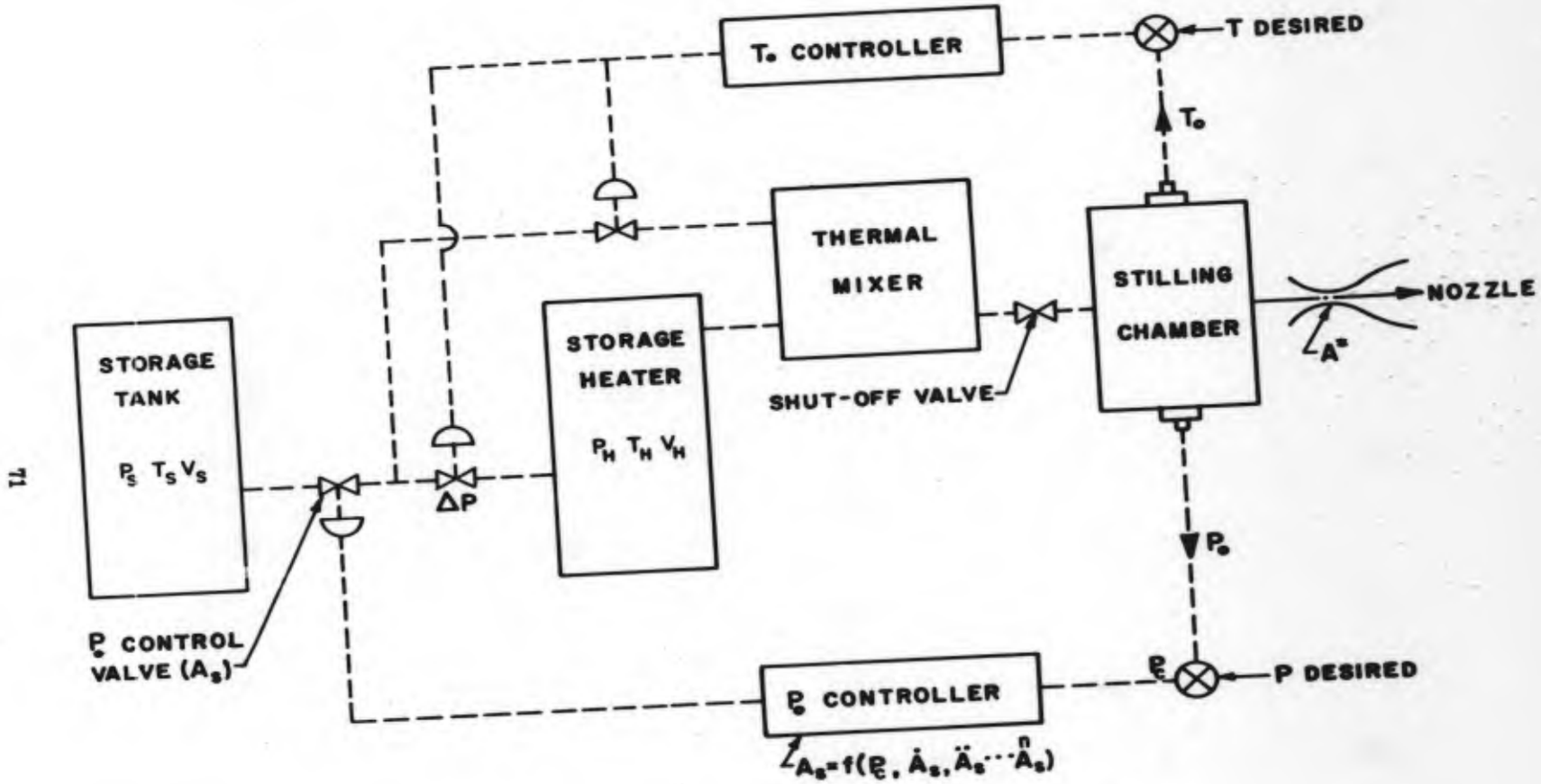

Fig. 29 Stagnation temperature and pressure control system

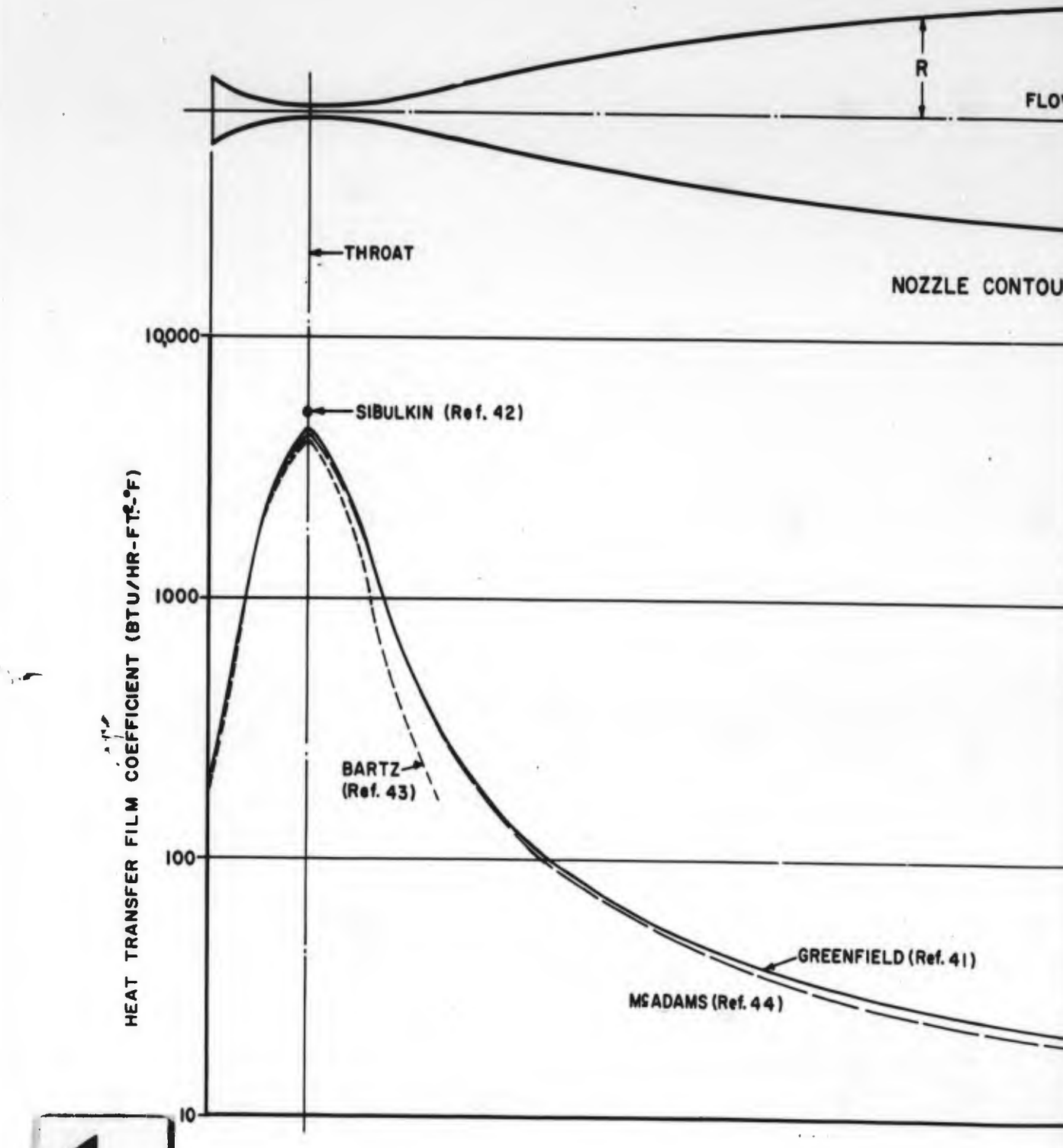

Fig. 30 Comparison of various heat transfer fi

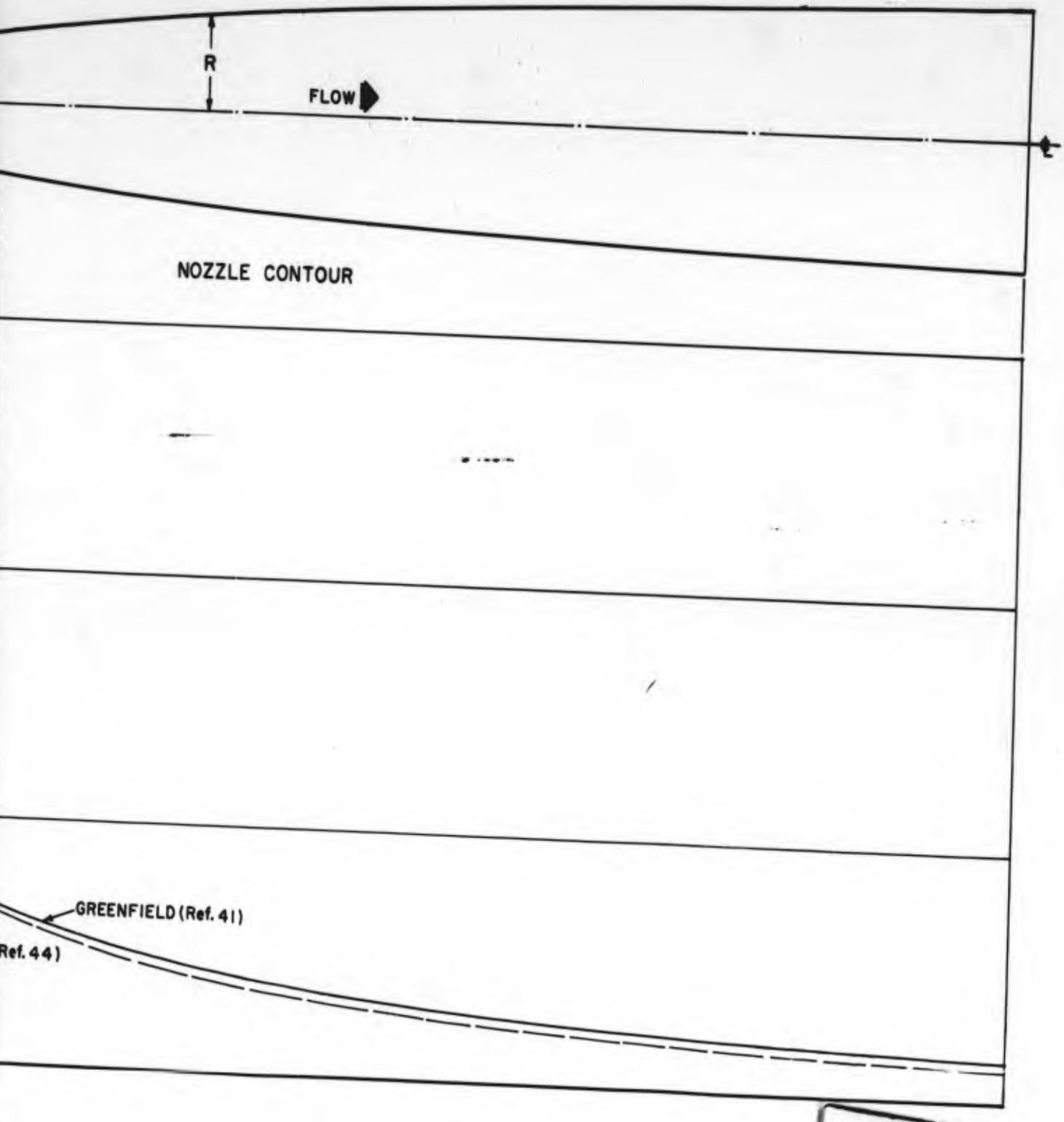

Comparison of various heat transfer film coefficient theories

2

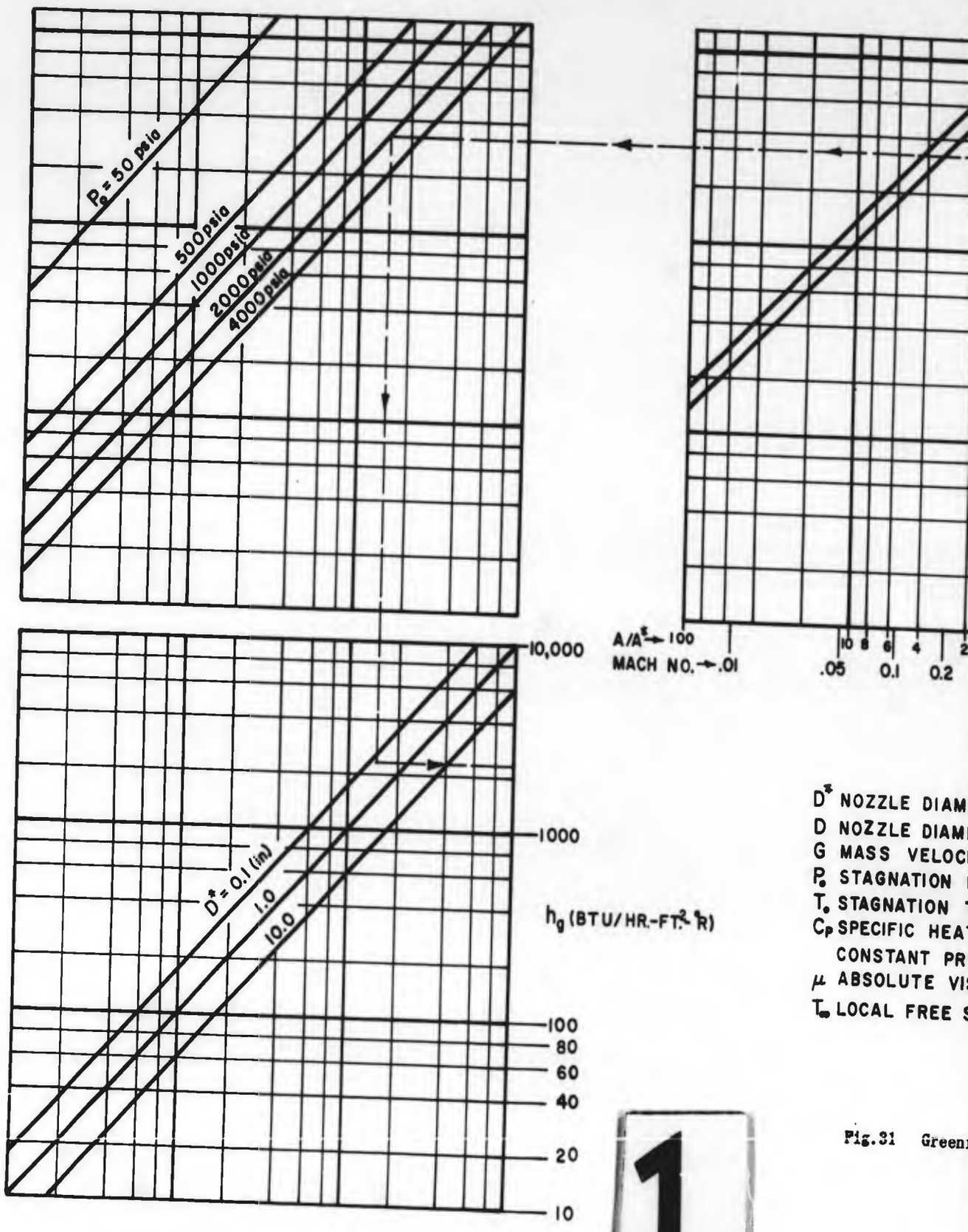

D^* NOZZLE DIAM
D NOZZLE DIAM
G MASS VELOC
P_o STAGNATION
T_o STAGNATION
C_p SPECIFIC HEA
CONSTANT PR
μ ABSOLUTE VI
T_∞ LOCAL FREE S

Fig.31 Green

1

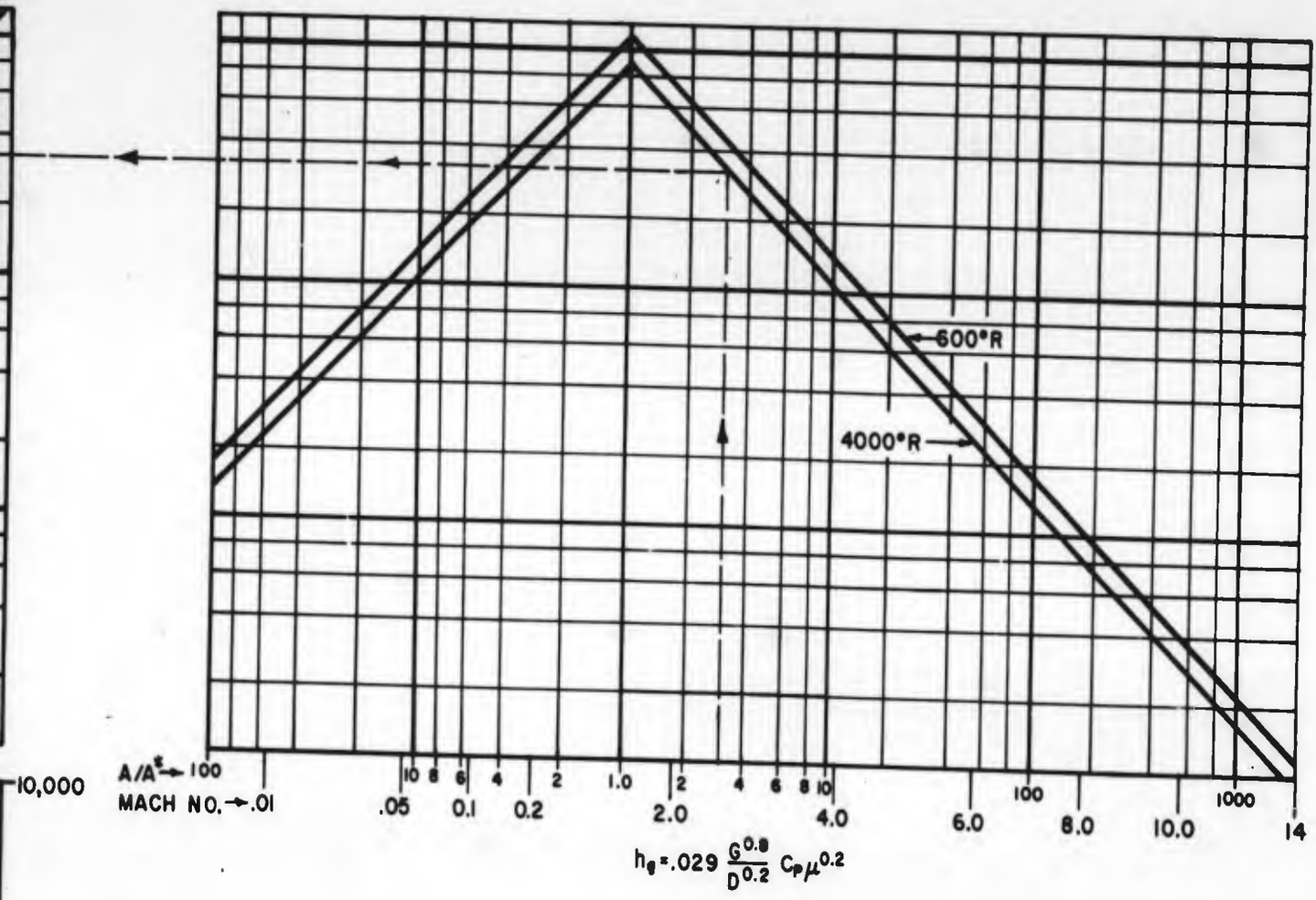

10,000

1000

h_g (BTU/HR.-FT.^{2}-°R)

100
80
60
40

20

10

D^* NOZZLE DIAMETER AT THROAT
D NOZZLE DIAMETER
G MASS VELOCITY
P_o STAGNATION PRESSURE
T_o STAGNATION TEMPERATURE
C_p SPECIFIC HEAT AT CONSTANT PRESSURE
μ ABSOLUTE VISCOSITY
} EVALUATED AT RECOVERY TEMPERATURE, $T_{rf} = T_\infty + 0.89(T_o - T_\infty)$ · PROPERTY VALUES TAKEN FROM REF. 55
T_∞ LOCAL FREE STREAM TEMPERATURE

Fig. 31 Greenfield's heat transfer film coefficient

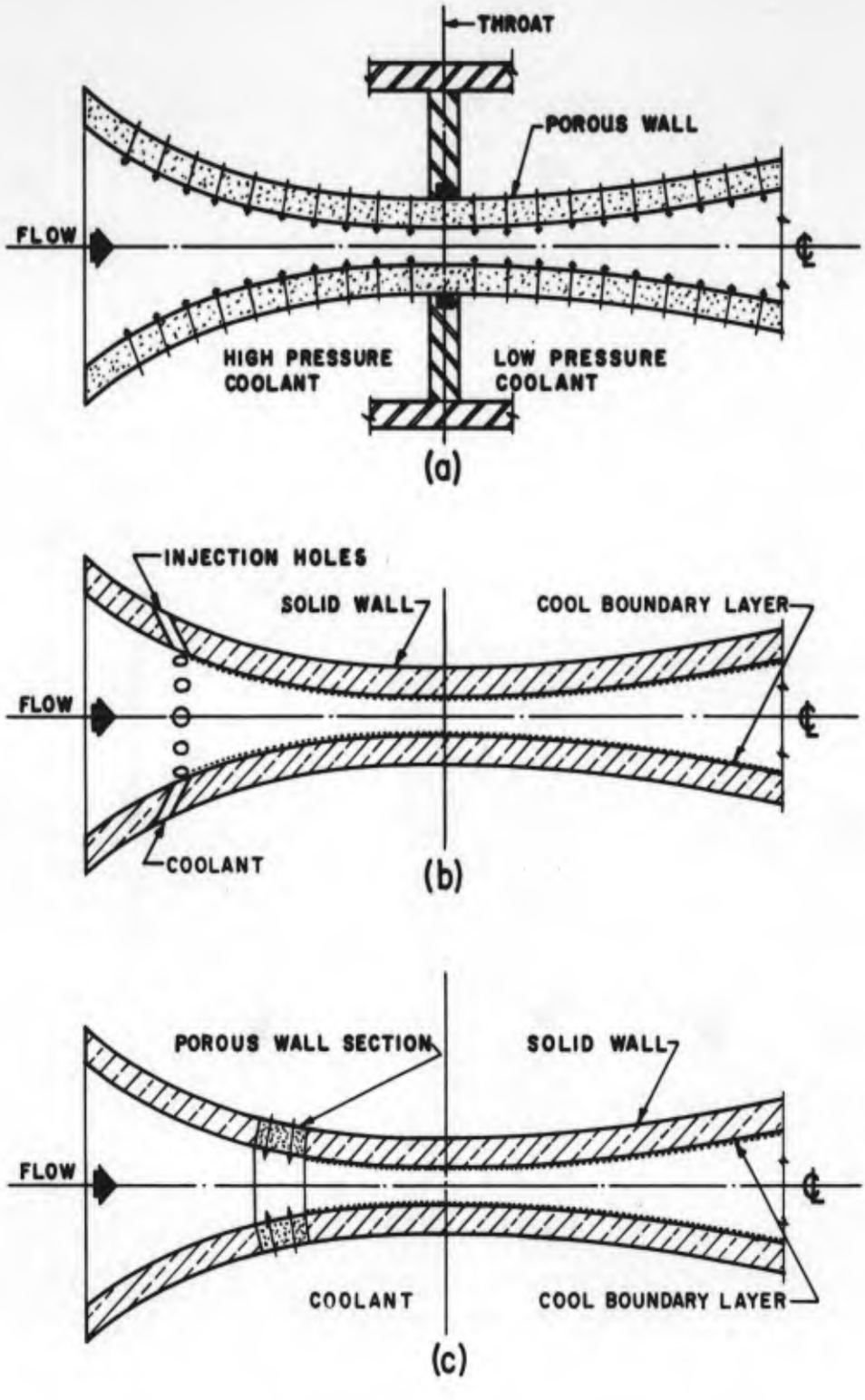

Fig.32 Cooling methods for axisymmetric nozzle throats

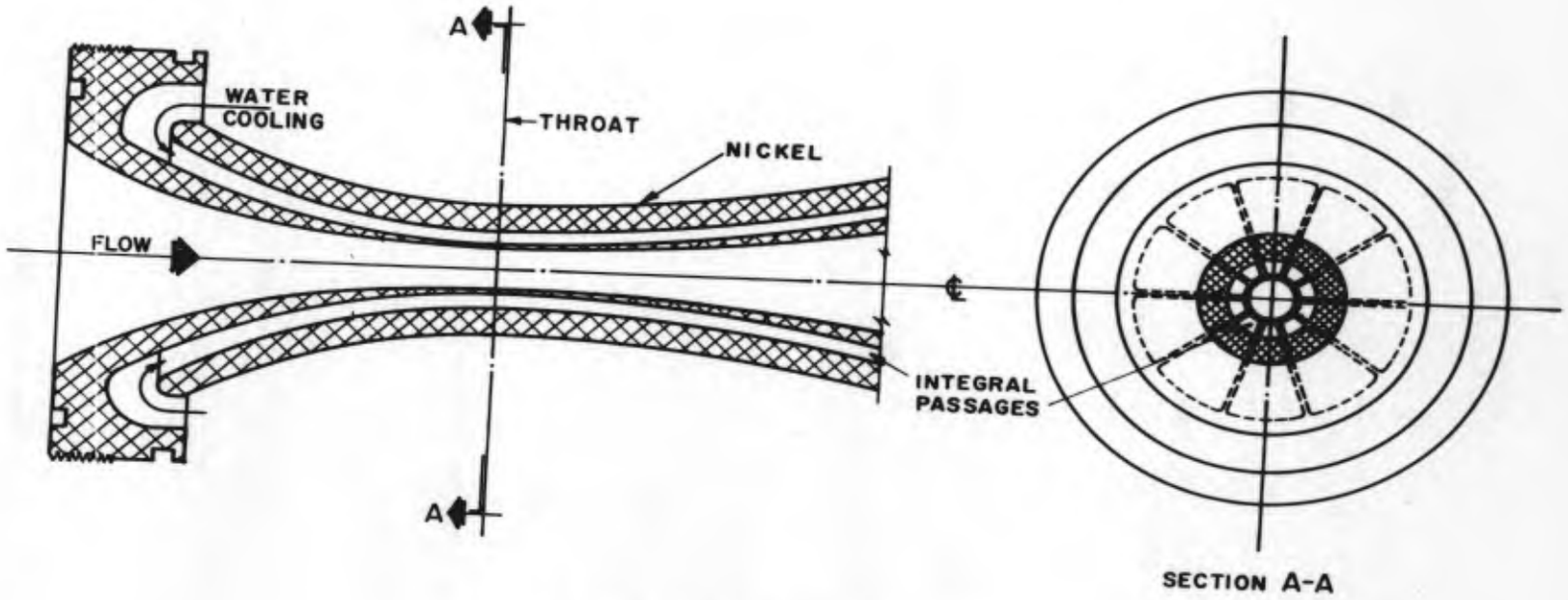

Fig.33 Integral-passage cooling

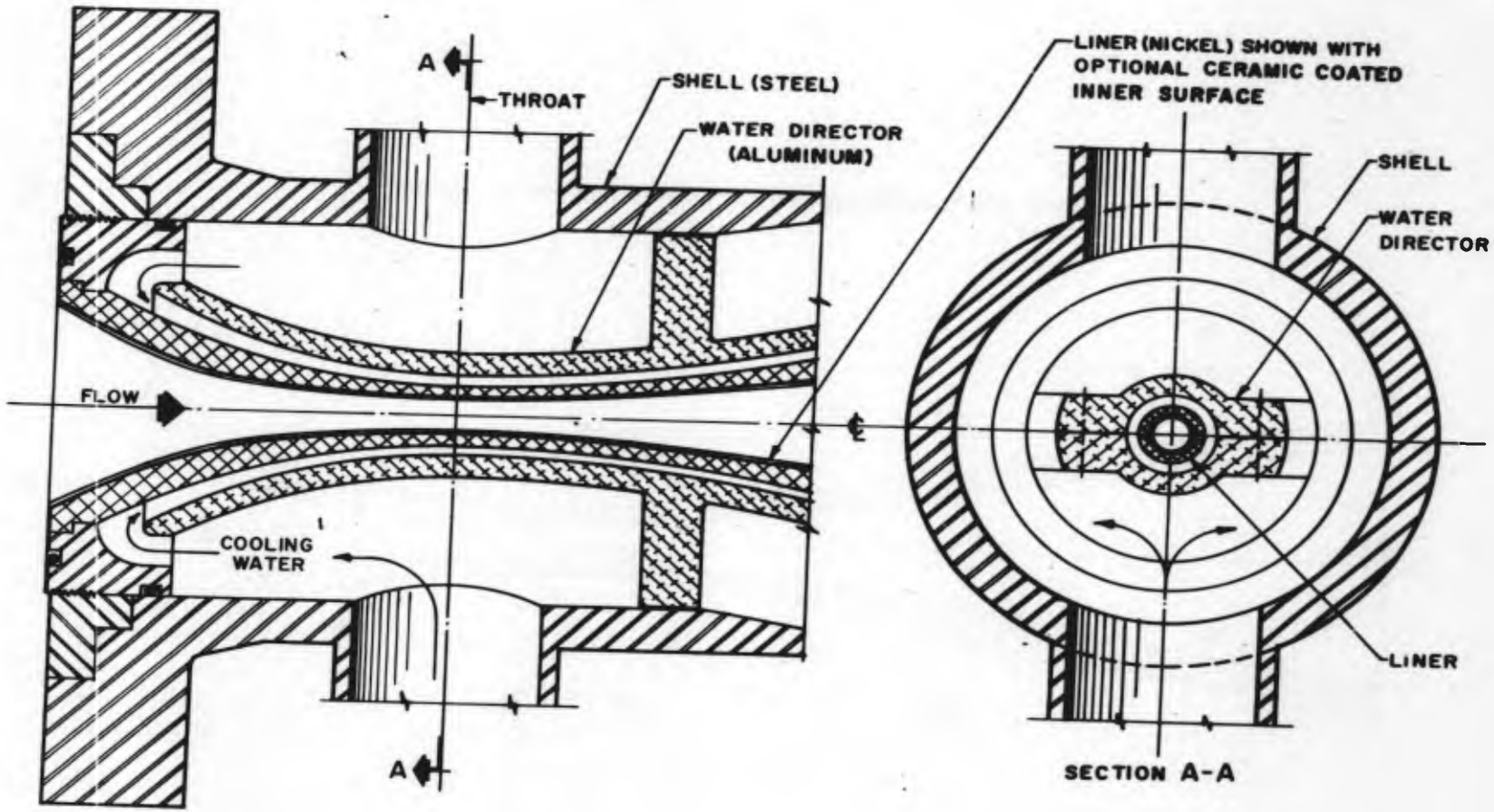

Fig. 34 Annulus-passage cooling

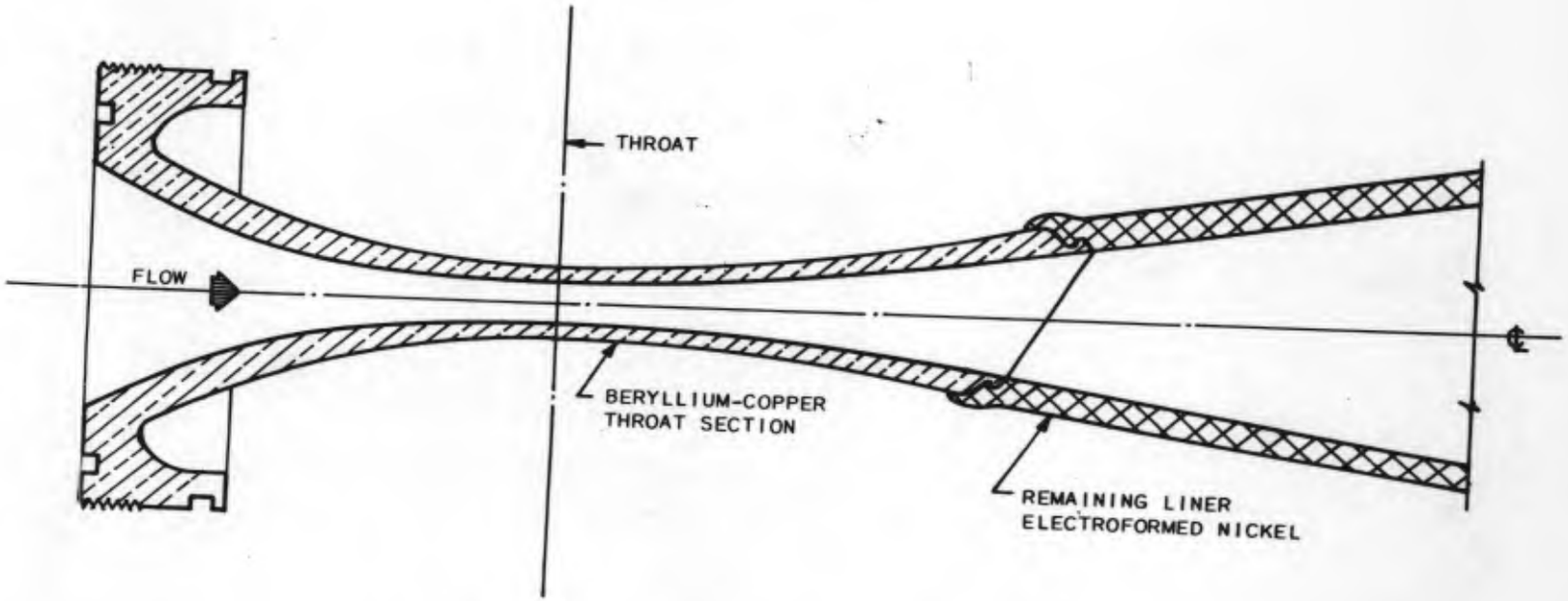

Fig.35 A beryllium-copper throat and nickel liner nozzle

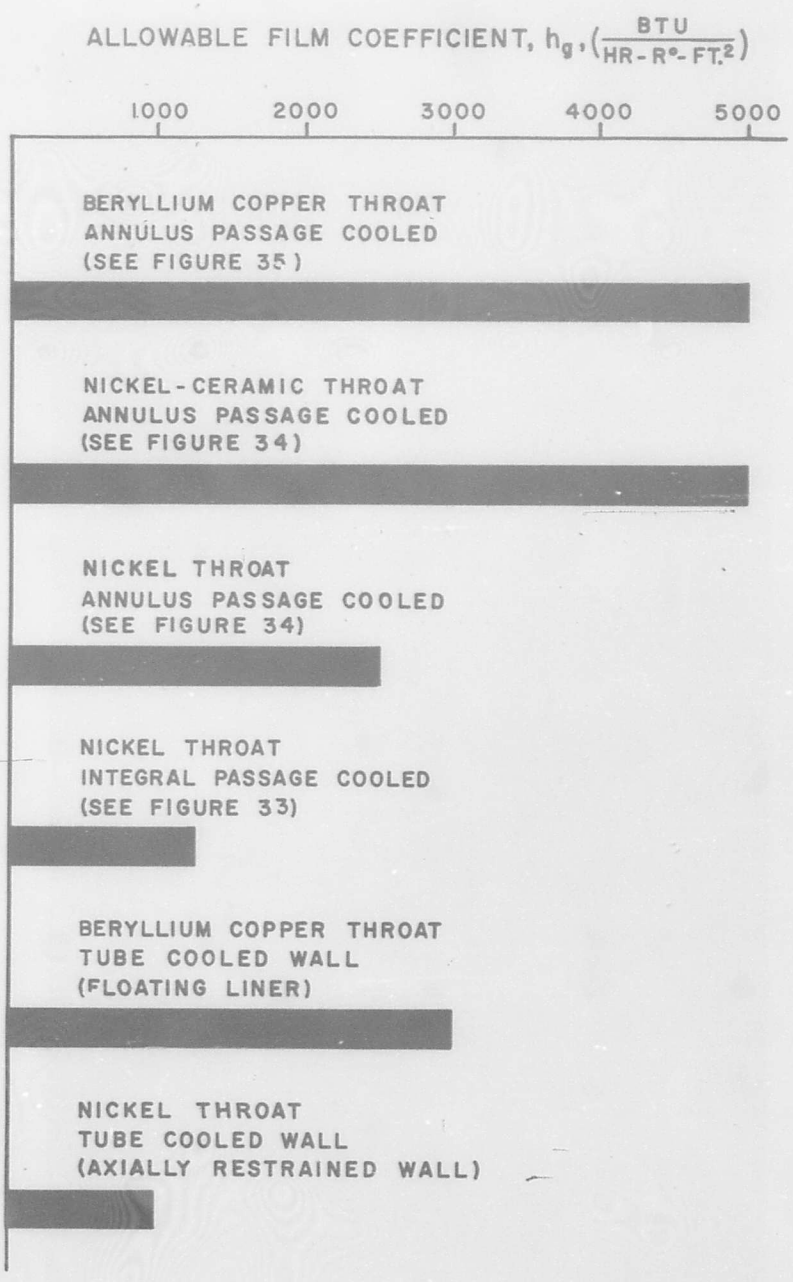

Fig.36 Capabilities of various throat configurations

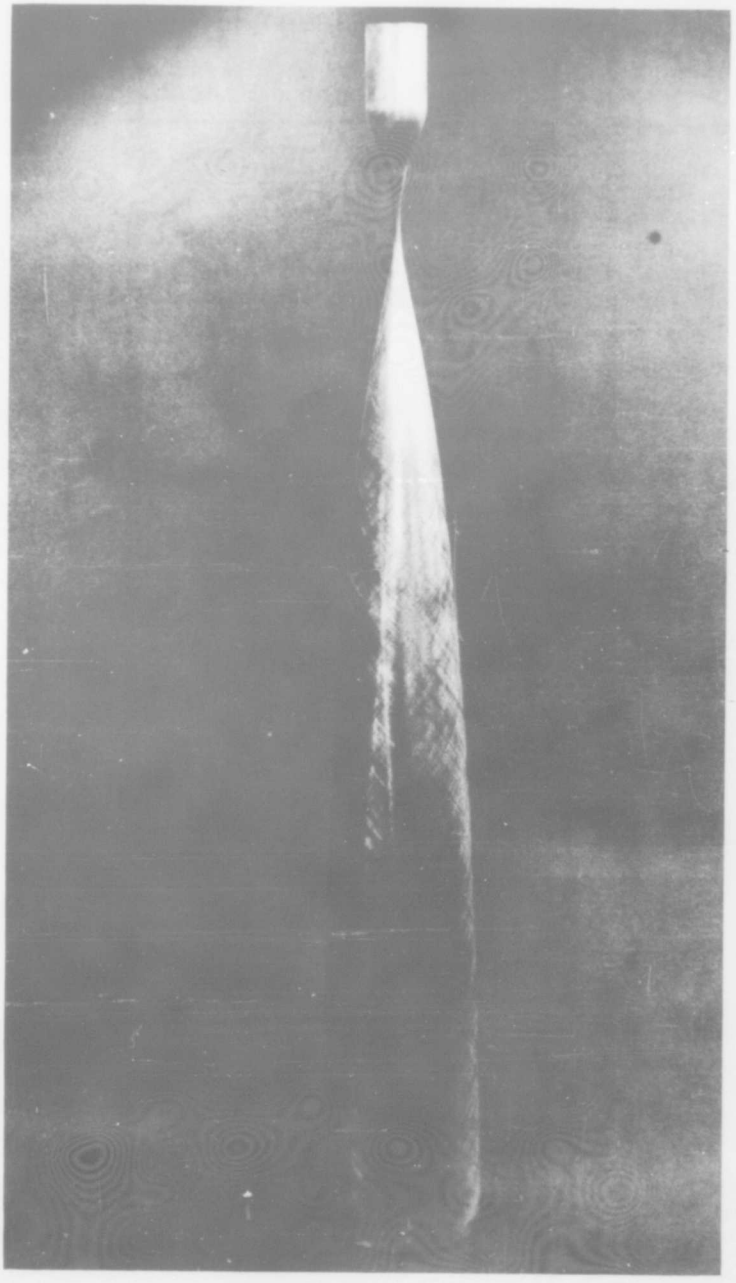

Fig. 37 Typical axisymmetric nozzle mandrel (Sandberg-Serrell Corp.)

Fig. 38 An electroformed nozzle liner (Sandberg-Serrell Corp.)

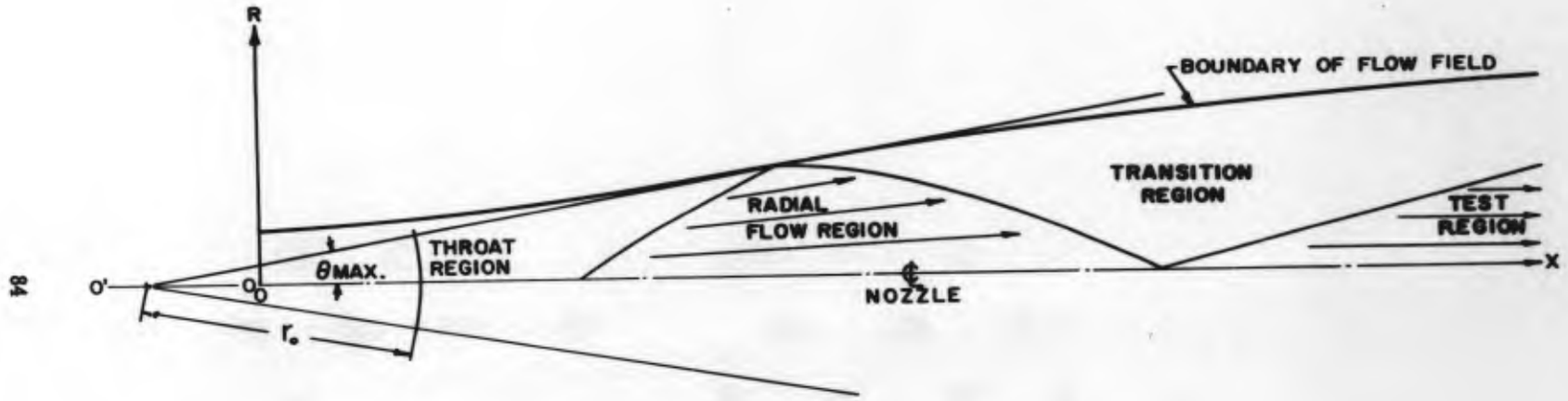

Fig.39 Nozzle coordinate system for Appendix II

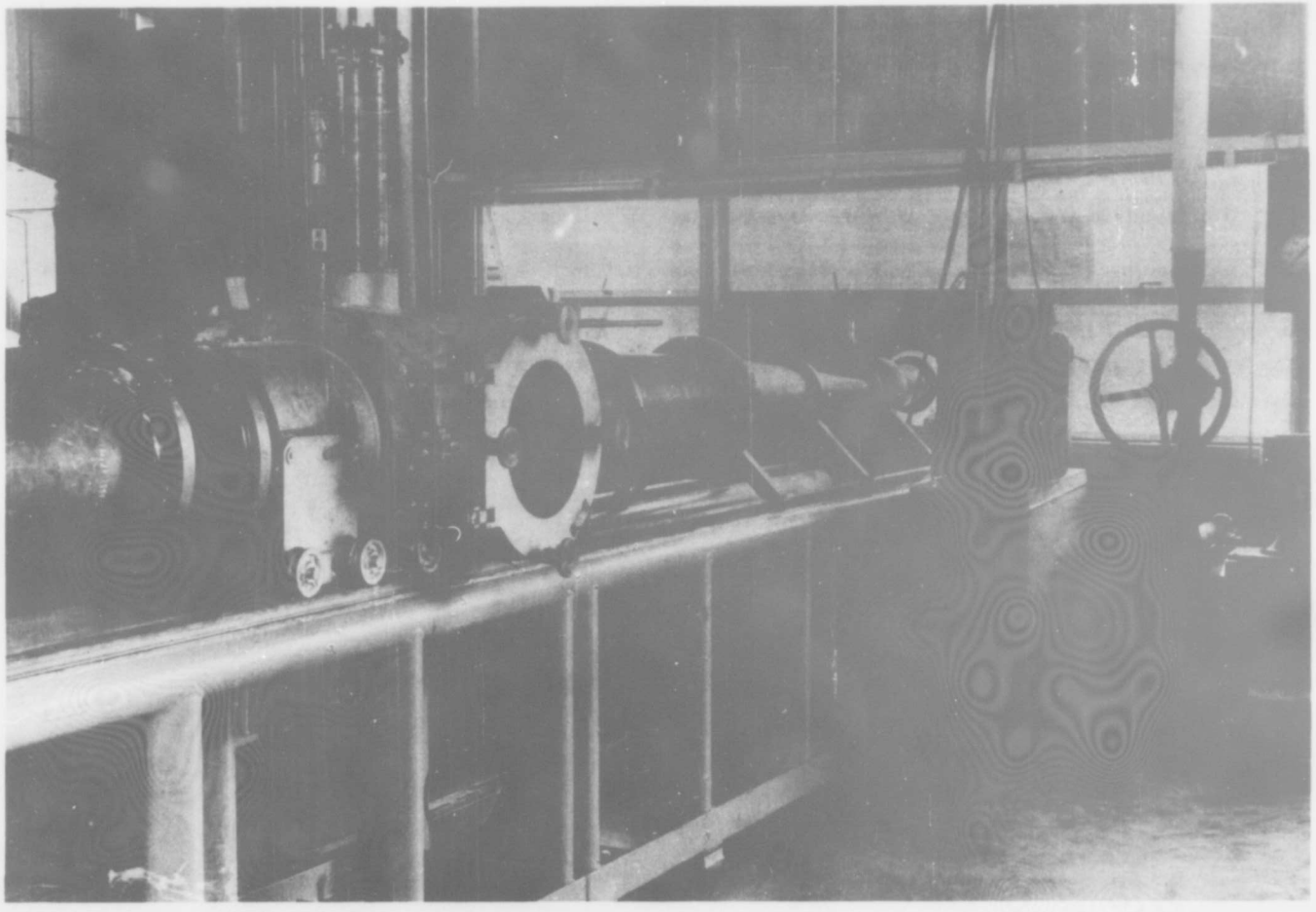

Fig.40 Axisymmetric hypersonic nozzle with free-jet test section
(Courtesy of Boeing Airplane Company)

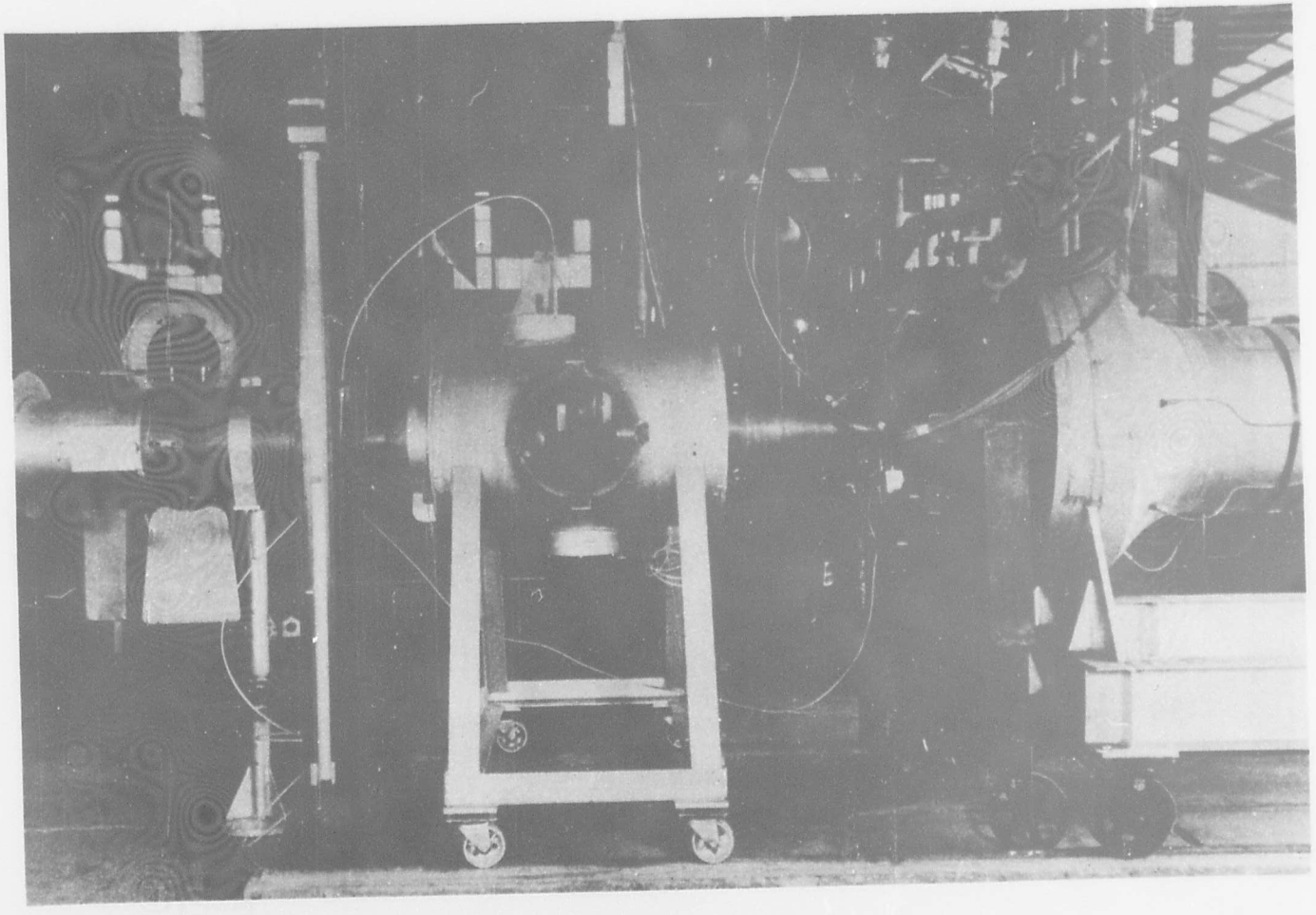

Fig.41 Hypersonic wind tunnel and continuously operated electric heater
(Courtesy of Ohio State University)

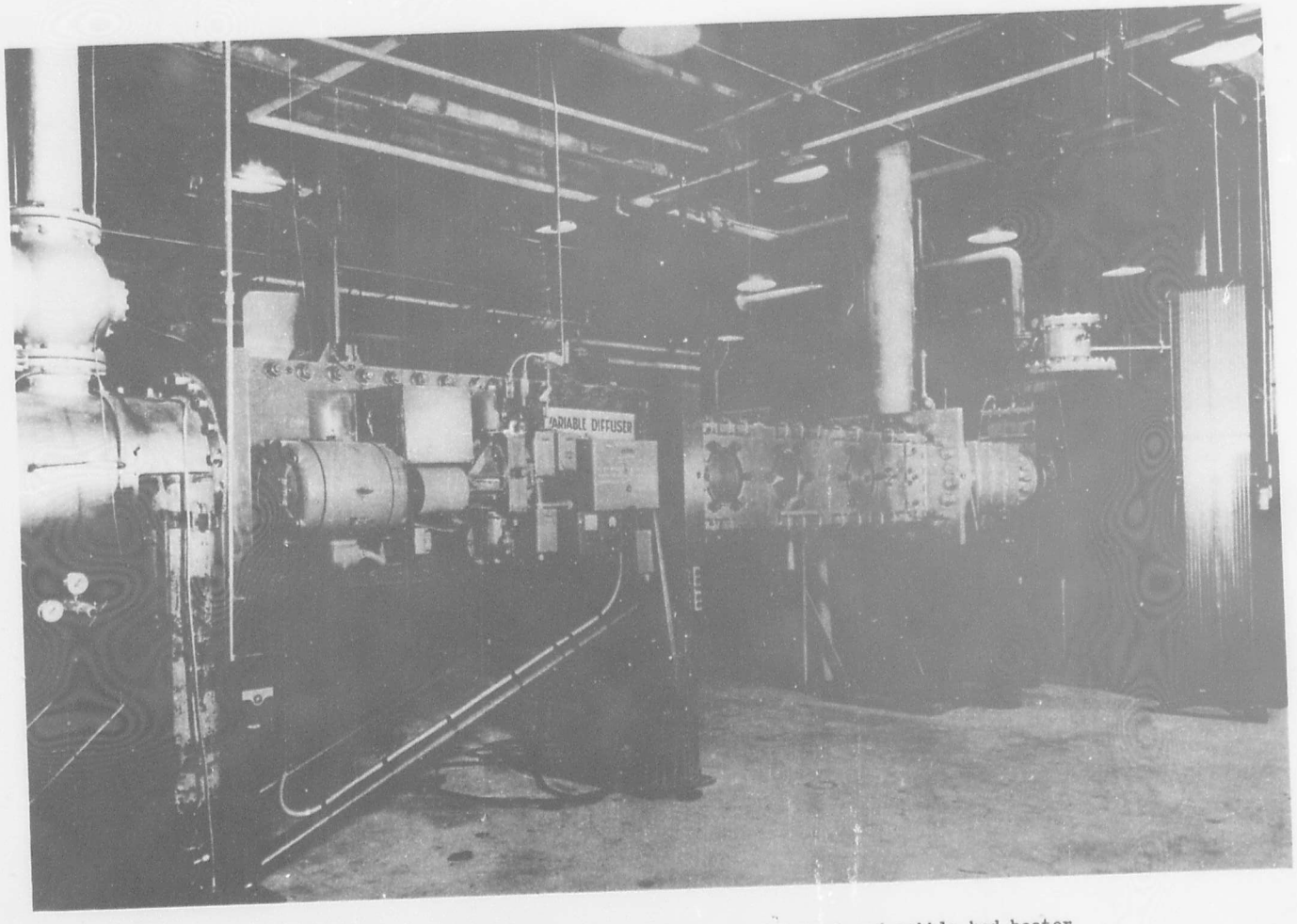

Fig. 42 12" x 12" two-dimensional hypersonic wind tunnel and pebble bed heater
(Courtesy of Rosemount Aeronautical Laboratory, University of Minnesota)

APPENDIX I

LISTING OF A FAMILY OF PERFECT FLUID CONTOURS

APPENDIX I

Listing of a Family of Perfect Fluid Contours

Contour No.	M_1	θ_A	γ	*Contour No.*	M_1	θ_A	γ
1	5.0	6.0	7/5	24	11.0	10.0	7/5
2	5.0	10.0	↓	25	12.0	6.0	↓
3	5.5	6.0		26	12.0	10.0	
4	5.5	10.0		27	9.0	↓	6/5
5	6.0	6.0		28	9.0		5/3
6	6.0	10.0		29	10.0		6/5
7	6.5	6.0		30	10.0		5/3
8	6.5	10.0		31	11.0		6/5
9	7.0	6.0		32	11.0		5/3
10	7.0	10.0		33	12.0		6/5
11	7.5	6.0		34	12.0		5/3
12	7.5	10.0		35	14.0		6/5
13	8.0	6.0		36	14.0		7/5
14	8.0	10.0		37	14.0		5/3
15	8.5	6.0		38	16.0		6/5
16	8.5	10.0		39	16.0		7/5
17	9.0	6.0		40	16.0		5/3
18	9.0	10.0		41	18.0		6/5
19	9.5	6.0		42	18.0		7/5
20	9.5	10.0		43	18.0		5/3
21	10.0	6.0		44	20.0		6/5
22	10.0	10.0		45	20.0		7/5
23	11.0	6.0	↓	46	20.0	↓	5/3

M_1	θ_A	γ	Z_1	π	a
5.00	6.00	1.4000	16.620537	0.150	0.001667
$(A/A^*)_1^{1/2}$	$1/\rho_1$	$\dot{M}_B$	$\ddot{M}_B$	a_0	
5.000000	0.045102	0.315456	-0.031886	0.012715	
a_1	a_2	M_A	Z_A	r_A	
-0.000953	-0.000052	3.496088	4.942485	0.519476	

CONTOUR # 1

z	r	M	z	r	M
0.366281	0.200000		4.266281	0.448931	
0.466281	0.200224		4.366281	0.459240	
0.566281	0.200890		4.466281	0.469609	
0.666281	0.201988		4.566281	0.480026	
0.766281	0.203510		4.666281	0.490482	
0.866281	0.205446		4.766281	0.500965	
0.966281	0.207787		4.866281	0.511467	
1.066281	0.210523		4.966281	0.521977	
1.166281	0.213645		5.066281	0.532487	
1.266281	0.217144		5.093245	0.535320	3.5604
1.366281	0.221009		5.151183	0.541407	3.5848
1.466281	0.225232		5.250708	0.551859	3.6260
1.566281	0.229803		5.371037	0.564484	3.6746
1.666281	0.234713		5.416416	0.569240	3.6926
1.766281	0.239951		5.591989	0.587599	3.7605
1.866281	0.245508		5.602514	0.588696	3.7644
1.966281	0.251374		5.779115	0.607044	3.8293
2.066281	0.257540		5.845881	0.613940	3.8528
2.166281	0.263996		5.979916	0.627696	3.8990
2.266281	0.270731		6.101495	0.640056	3.9390
2.366281	0.277737		6.196147	0.649588	3.9694
2.466281	0.285003		6.369446	0.666804	4.0222
2.566281	0.292520		6.429172	0.672661	4.0400
2.666281	0.300277		6.649720	0.693899	4.1018
2.766281	0.308265		6.679689	0.696736	4.1100
2.866281	0.316473		6.942234	0.721030	4.1775
2.966281	0.324892		6.947483	0.721506	4.1788
3.066281	0.333512		7.231158	0.746538	4.2455
3.166281	0.342322		7.246902	0.747890	4.2490
3.266281	0.351313		7.528363	0.771345	4.3096
3.366281	0.360474		7.563602	0.774187	4.3168
3.466281	0.369796		7.835934	0.795433	4.3706
3.566281	0.379268		7.892265	0.799669	4.3812
3.666281	0.388880		8.232706	0.824110	4.4426
3.766281	0.398622		8.244265	0.824905	4.4446
3.866281	0.408485		8.585156	0.847349	4.5010
3.966281	0.418457		8.664087	0.852270	4.5135
4.066281	0.428529		8.949403	0.869213	4.5566
4.166281	0.438690		9.094684	0.877338	4.5775

z	r	M
9.325398	0.889563	4.6094
9.535318	0.899977	4.6370
9.713067	0.908280	4.6595
9.985418	0.920114	4.6921
10.112264	0.925267	4.7068
10.444509	0.937726	4.7429
10.522734	0.940444	4.7512
10.912119	0.952827	4.7895
10.944011	0.953757	4.7925
11.387683	0.965472	4.8317
11.817240	0.974742	4.8654
11.870564	0.975758	4.8692
12.267020	0.982469	4.8965
12.360395	0.983839	4.9021
12.721138	0.988451	4.9233
12.856448	0.989914	4.9301
13.175914	0.992857	4.9457
13.357893	0.994233	4.9531
13.627714	0.995921	4.9637
13.863798	0.997086	4.9710
14.073340	0.997908	4.9774
14.373180	0.998789	4.9842
14.510413	0.999091	4.9872
14.885034	0.999668	4.9928
14.937691	0.999723	4.9936
15.355235	1.000013	4.9974
15.398376	1.000030	4.9976
15.764387	1.000120	4.9992
15.912458	1.000135	4.9994
16.167550	1.000147	4.9998
16.426814	1.000150	4.9999
16.567675	1.000150	4.9999
16.941208	1.000150	5.0000
16.967172	1.000150	5.0000

M_1	β_A	γ	z_1	τ	a
5.00	10.00	1.4000	12.231212	0.150	0.019994
$(A/A^*)_1^{1/2}$	$1/\rho_1$	$\dot{M}_B$	$\ddot{M}_B$	a_0	
5.000000	0.196451	0.553135	-0.101463	0.038377	
a_1	a_2	M_A	z_A	r_A	
-0.003505	-0.000316	2.940218	2.259923	0.398485	

CONTOUR #2

z	r	M	z	r	M
0.553926	0.200000		4.337972	0.718846	4.0889
0.653926	0.200967		4.610947	0.749959	4.1734
0.753926	0.203803		4.629351	0.751964	4.1787
0.853926	0.208413		4.937112	0.783864	4.2643
0.953926	0.214693		4.988707	0.788913	4.2779
1.053926	0.222541		5.261265	0.814240	4.3461
1.153926	0.231849		5.381454	0.824703	4.3745
1.253926	0.242507		5.601889	0.842828	4.4241
1.353926	0.254402		5.788531	0.857131	4.4637
1.453926	0.267418		5.959115	0.869399	4.4984
1.553926	0.281438		6.209218	0.886063	4.5460
1.653926	0.296343		6.332972	0.893745	4.5687
1.753926	0.312010		6.642879	0.911441	4.6216
1.853926	0.328317		6.723332	0.915684	4.6349
1.953926	0.345138		7.088880	0.933264	4.6907
2.053926	0.362348		7.129800	0.935062	4.6968
2.153926	0.379820		7.546569	0.951587	4.7534
2.253926	0.397428		7.551553	0.951765	4.7540
2.348106	0.414033	3.0200	7.986992	0.965723	4.8062
2.403836	0.423852	3.0691	8.014937	0.966511	4.8092
2.441818	0.430540	3.1018	8.436697	0.977006	4.8532
2.543042	0.448340	3.1858	8.493505	0.978221	4.8584
2.560559	0.451414	3.1998	8.894765	0.985629	4.8940
2.654079	0.467776	3.2724	8.981360	0.986965	4.9005
2.730857	0.481125	3.3288	9.354274	0.991793	4.9278
2.778074	0.489288	3.3625	9.477345	0.993073	4.9352
2.915435	0.512773	3.4544	9.807846	0.995856	4.9544
2.918132	0.513230	3.4562	9.980117	0.996960	4.9621
3.076763	0.539741	3.5524	10.248769	0.998285	4.9739
3.114637	0.545960	3.5737	10.488154	0.999115	4.9814
3.256001	0.568757	3.6506	10.672254	0.999569	4.9870
3.328757	0.580222	3.6872	10.999802	1.000075	4.9933
3.455791	0.599778	3.7489	11.076525	1.000147	4.9947
3.557965	0.615072	3.7950	11.463221	1.000353	4.9985
3.673700	0.631916	3.8452	11.513389	1.000365	4.9986
3.802420	0.650053	3.8975	11.837058	1.000403	4.9998
3.905400	0.664108	3.9377	12.027658	1.000408	4.9999
4.062441	0.684775	3.9951	12.204425	1.000409	4.9999
4.249029	0.708147	4.0599	12.542050	1.000409	5.0000

M_1	θ_1	γ	Z_1	π	a
5.50	6.00	1.4000	17.206287	0.150	0.001569
$(A/A^*)_1^{1/2}$		$1/\rho_1$	$\dot{M}_B$	$\ddot{M}_B$	a_0
6.071981		0.043758	0.334885	-0.032885	0.012576
a_1		a_2	M_A	Z_A	r_A
-0.000908		-0.000048	3.808675	4.699941	0.493983

CONTOUR # 3

z	r	M	z	r	M
-0.016875	0.164691		3.883124	0.409006	
0.083125	0.164908		3.983124	0.419233	
0.183125	0.165555		4.083124	0.429530	
0.283125	0.166621		4.183124	0.439885	
0.383125	0.168099		4.283124	0.450290	
0.483125	0.169980		4.383124	0.460735	
0.583125	0.172255		4.483124	0.471211	
0.683125	0.174916		4.583124	0.481708	
0.783125	0.177952		4.683124	0.492216	
0.883125	0.181356		4.783124	0.502726	
0.983125	0.185119		4.855001	0.510279	3.8800
1.083125	0.189231		4.921608	0.517276	3.9101
1.183125	0.193684		5.017443	0.527340	3.9528
1.283125	0.198469		5.156029	0.541878	4.0129
1.383125	0.203575		5.189138	0.545347	4.0271
1.483124	0.208996		5.371954	0.564455	4.1028
1.583124	0.214720		5.403697	0.567762	4.1155
1.683124	0.220740		5.568165	0.584824	4.1800
1.783124	0.227046		5.665012	0.594802	4.2162
1.883124	0.233628		5.780299	0.606599	4.2585
1.983124	0.240478		5.940311	0.622796	4.3141
2.083124	0.247587		6.010480	0.629826	4.3380
2.183124	0.254944		6.229654	0.651451	4.4083
2.283124	0.262541		6.260250	0.654427	4.4179
2.383124	0.270368		6.530204	0.680170	4.4972
2.483124	0.278416		6.532988	0.680430	4.4980
2.583124	0.286676		6.819508	0.706645	4.5750
2.683124	0.295138		6.850232	0.709385	4.5827
2.783124	0.303793		7.126238	0.733342	4.6503
2.883124	0.312631		7.181260	0.737976	4.6630
2.983124	0.321642		7.446829	0.759658	4.7225
3.083124	0.330819		7.525993	0.765901	4.7392
3.183124	0.340150		7.880790	0.792641	4.8115
3.283124	0.349627		7.884178	0.792886	4.8121
3.383124	0.359239		8.256174	0.818745	4.8812
3.483124	0.368978		8.329016	0.823554	4.8942
3.583124	0.378834		8.641748	0.843270	4.9471
3.683124	0.388797		8.790413	0.852120	4.9712
3.783124	0.398857		9.040871	0.866290	5.0099

z	r	M
9.264024	0.878147	5.0428
9.453517	0.887662	5.0696
9.749143	0.901519	5.1093
9.879609	0.907260	5.1261
10.245180	0.922176	5.1708
10.318994	0.924982	5.1794
10.751615	0.940109	5.2273
10.771355	0.940746	5.2294
11.236176	0.954494	5.2759
11.267658	0.955339	5.2788
11.712274	0.966194	5.3186
11.792889	0.967950	5.3252
12.200865	0.975909	5.3575
12.326849	0.978064	5.3664
12.698151	0.983655	5.3919
12.868790	0.985860	5.4021
13.199766	0.989544	5.4214
13.417792	0.991572	5.4322
13.701030	0.993781	5.4458
13.972816	0.995491	5.4564
14.197406	0.996634	5.4649
14.532707	0.997950	5.4748
14.685056	0.998409	5.4791
15.096238	0.999308	5.4876
15.161351	0.999409	5.4889
15.625294	0.999903	5.4950
15.662136	0.999927	5.4953
16.077643	1.000106	5.4982
16.229321	1.000136	5.4987
16.520810	1.000167	5.4996
16.797076	1.000177	5.4998
16.958356	1.000178	5.4999
17.364949	1.000179	5.4999
17.393923	1.000179	5.5000

M_1	θ_2	γ	z_1	τ	a
5.50	10.00	1.4000	12.816961	0.150	0.018826
$(A/A^*)_1^{1/2}$	$1/\rho_1$	$\dot{M}_3$	$\ddot{M}_3$	a_0	
6.071981	0.190629	0.589499	-0.105684	0.037002	
a_1	a_2	M_A	z_A	r_A	
-0.003192	-0.000279	3.188422	2.094056	0.369238	

CONTOUR # 4

z	r	M	z	r	M
0.335952	0.164691		4.275814	0.702617	4.4695
0.435952	0.165629		4.304884	0.705997	4.4793
0.535952	0.168385		4.619770	0.740874	4.5800
0.635952	0.172867		4.671081	0.746259	4.5955
0.735952	0.178979		4.953001	0.774445	4.6763
0.835952	0.186624		5.084408	0.786786	4.7119
0.935952	0.195702		5.304689	0.806397	4.7685
1.035952	0.206108		5.515025	0.823905	4.8195
1.135952	0.217738		5.675092	0.836463	4.8566
1.235952	0.230484		5.962048	0.857403	4.9189
1.335952	0.244234		6.064397	0.864397	4.9403
1.435952	0.258877		6.424715	0.887161	5.0105
1.535952	0.274298		6.472665	0.889975	5.0195
1.635952	0.290382		6.899762	0.913000	5.0941
1.735952	0.307013		6.902282	0.913125	5.0945
1.835952	0.324072		7.345342	0.933307	5.1637
1.935952	0.341440		7.393521	0.935288	5.1706
2.035952	0.358997		7.808234	0.950758	5.2281
2.135952	0.376626		7.898313	0.953751	5.2394
2.181641	0.384681	3.2743	8.286477	0.965282	5.2867
2.244004	0.395668	3.3339	8.415826	0.968645	5.3008
2.274994	0.401125	3.3628	8.781357	0.976976	5.3394
2.376206	0.418922	3.4539	8.945107	0.980169	5.3546
2.408155	0.424526	3.4814	9.285800	0.985849	5.3851
2.488021	0.438489	3.5483	9.484970	0.988605	5.4002
2.587457	0.455754	3.6270	9.791384	0.992118	5.4227
2.613997	0.460334	3.6474	10.033997	0.994331	5.4372
2.757512	0.484843	3.7507	10.289177	0.996181	5.4520
2.782629	0.489082	3.7675	10.590533	0.997817	5.4654
2.921782	0.512242	3.8578	10.771090	0.998549	5.4733
2.994081	0.524045	3.9012	11.152695	0.999612	5.4848
3.108929	0.542442	3.9677	11.231577	0.999759	5.4872
3.222126	0.560131	4.0283	11.668989	1.000277	5.4951
3.318612	0.574848	4.0780	11.718380	1.000308	5.4955
3.466976	0.596818	4.1490	12.086002	1.000448	5.4987
3.547547	0.608409	4.1861	12.285718	1.000473	5.4993
3.728995	0.633642	4.2635	12.488995	1.000484	5.4998
3.900105	0.656347	4.3329	12.853563	1.000487	5.4999
4.008176	0.670154	4.3737	12.885871	1.000487	5.5000

M_1	θ_A	γ	z_1	τ	a
6.00	6.00	1.4000	17.790203	0.150	0.001533
$(A/A^*)_1^{V2}$	$1/\rho_1$	$\dot{M}_B$	$\ddot{M}_B$	a_0	
7.292446	0.043246	0.355973	-0.034307	0.012462	
a_1	a_2	M_A	z_A	r_A	
-0.000865	-0.000045	4.107800	4.474786	0.470318	

CONTOUR # 5

z	r	M
-0.297862	0.137128	
-0.197862	0.137343	
-0.097862	0.137982	
0.002138	0.139036	
0.102138	0.140498	
0.202138	0.142358	
0.302138	0.144608	
0.402138	0.147239	
0.502138	0.150243	
0.602138	0.153611	
0.702138	0.157334	
0.802138	0.161404	
0.902138	0.165812	
1.002138	0.170548	
1.102138	0.175605	
1.202138	0.180973	
1.302138	0.186643	
1.402138	0.192606	
1.502138	0.198854	
1.602138	0.205378	
1.702138	0.212167	
1.802138	0.219215	
1.902138	0.226510	
2.002138	0.234045	
2.102138	0.241810	
2.202138	0.249795	
2.302137	0.257993	
2.402137	0.266393	
2.502137	0.274987	
2.602137	0.283765	
2.702137	0.292718	
2.802137	0.301837	
2.902137	0.311112	
3.002137	0.320535	
3.102137	0.330095	
3.202137	0.339784	
3.302137	0.349592	
3.402137	0.359511	
3.502137	0.369530	
3.602137	0.379640	
3.702137	0.389832	
3.802137	0.400097	
3.902137	0.410425	
4.002137	0.420806	
4.102137	0.431232	
4.202137	0.441693	
4.302137	0.452180	
4.402137	0.462683	
4.502137	0.473193	
4.602137	0.483703	
4.632657	0.486910	4.1862
4.707613	0.494784	4.2228
4.798538	0.504331	4.2664
4.954829	0.520723	4.3395
4.974609	0.522795	4.3486
5.162959	0.542473	4.4325
5.216926	0.548089	4.4556
5.366552	0.563590	4.5183
5.494479	0.576741	4.5694
5.588310	0.586315	4.6061
5.787780	0.606424	4.6797
5.830718	0.610705	4.6952
6.095489	0.636664	4.7850
6.096851	0.636796	4.7854
6.382804	0.663878	4.8740
6.421627	0.667473	4.8852
6.691738	0.691891	4.9614
6.762016	0.698072	4.9800
7.019176	0.720060	5.0459
7.117885	0.728235	5.0698
7.360617	0.747704	5.1267
7.489214	0.757654	5.1552
7.828712	0.782711	5.2274
7.875767	0.786047	5.2369
8.277817	0.813212	5.3146
8.313127	0.815484	5.3212
8.695441	0.838950	5.3886
8.812111	0.845701	5.4082

z	r	M
9.128475	0.863073	5.4591
9.325077	0.873193	5.4891
9.576911	0.885426	5.5261
9.851280	0.897844	5.5642
10.040672	0.905877	5.5895
10.390102	0.919593	5.6335
10.519580	0.924318	5.6493
10.940959	0.938431	5.6973
11.013261	0.940661	5.7053
11.503254	0.954394	5.7555
11.521016	0.954847	5.7573
12.041554	0.966847	5.8049
12.076045	0.967556	5.8078
12.576435	0.976737	5.8482
12.658810	0.978055	5.8541
13.120921	0.984534	5.8863
13.250820	0.986086	5.8942
13.669626	0.990371	5.9188
13.851005	0.991905	5.9277
14.216768	0.994480	5.9452
14.458127	0.995830	5.9544
14.756817	0.997168	5.9656
15.070808	0.998229	5.9745
15.285287	0.998777	5.9804
15.687570	0.999498	5.9881
15.799386	0.999637	5.9902
16.298514	1.000031	5.9960
16.306938	1.000035	5.9960
16.784349	1.000176	5.9988
16.927552	1.000192	5.9991
17.260528	1.000212	5.9998
17.548668	1.000215	5.9999
17.731767	1.000216	5.9999
18.169857	1.000216	6.0000
18.201995	1.000216	6.0000

M_1	β_A	γ	Z_1	π	a
6.00	10.00	1.4000	13.400877	0.150	0.018586
$(A/A^*)_1^{1/2}$	$1/\rho_1$	$\dot{M}_B$	$\ddot{M}_B$	a_0	
7.292446	0.189408	0.629310	-0.111484	0.035819	
a_1	a_2	M_A	Z_A	r_A	
-0.002920	-0.000248	3.420597	1.945217	0.342994	

CONTOUR # 6

z	r	M	z	r	M
0.175782	0.137128		4.196678	0.684867	4.8339
0.275782	0.138061		4.271725	0.693461	4.8606
0.375782	0.140800		4.608101	0.729885	4.9736
0.475782	0.145254		4.619319	0.731041	4.9771
0.575782	0.151331		4.965291	0.764996	5.0813
0.675782	0.158934		5.061945	0.773896	5.1087
0.775782	0.167963		5.343170	0.798425	5.1844
0.875782	0.178316		5.524355	0.813183	5.2303
0.975782	0.189890		5.742075	0.829889	5.2830
1.075782	0.202577		6.005598	0.848673	5.3427
1.175782	0.216269		6.162247	0.859123	5.3767
1.275782	0.230856		6.504854	0.880227	5.4462
1.375782	0.246224		6.603785	0.885887	5.4655
1.475782	0.262260		7.021336	0.907786	5.5412
1.575782	0.278848		7.066548	0.909968	5.5491
1.675782	0.295872		7.550052	0.931187	5.6271
1.775782	0.313214		7.554192	0.931352	5.6277
1.875782	0.330757		8.053250	0.949406	5.6992
1.975782	0.348383		8.102090	0.950977	5.7055
2.031369	0.358184	3.5126	8.573654	0.964534	5.7647
2.099566	0.370199	3.5835	8.664722	0.966821	5.7749
2.123454	0.374405	3.6077	9.113230	0.976688	5.8237
2.223594	0.392014	3.7057	9.241012	0.979086	5.8358
2.269463	0.400055	3.7485	9.663679	0.985865	5.8746
2.334992	0.411505	3.8081	9.829612	0.988064	5.8874
2.456069	0.432501	3.9116	10.215080	0.992294	5.9164
2.461544	0.433445	3.9162	10.428895	0.994149	5.9294
2.606793	0.458233	4.0292	10.756790	0.996406	5.9488
2.660050	0.467191	4.0676	11.036957	0.997835	5.9614
2.774838	0.486225	4.1475	11.279281	0.998757	5.9720
2.881965	0.503625	4.2164	11.651608	0.999711	5.9833
2.967830	0.517300	4.2696	11.776171	0.999925	5.9870
3.122130	0.541241	4.3579	12.245926	1.000405	5.9953
3.185178	0.550782	4.3925	12.270427	1.000418	5.9955
3.380818	0.579491	4.4923	12.692322	1.000554	5.9989
3.422877	0.585483	4.5129	12.891056	1.000573	5.9994
3.658543	0.617904	4.6198	13.123464	1.000582	5.9999
3.796788	0.636025	4.6792	13.512221	1.000584	5.9999
3.955377	0.656021	4.7426	13.548710	1.000584	6.0000

M_1	θ_A	γ	z_1	π	a
6.50	6.00	1.4000	18.372720	0.150	0.001535
$(A/A^*)_1^{1/2}$	$1/\rho_1$	$\dot{M}_B$	$\ddot{M}_B$	a_0	
8.668005	0.043283	0.378363	-0.036037	0.012360	
a_1	a_2	M_A	z_A	r_A	
-0.000823	-0.000042	4.394589	4.265020	0.448271	

CONTOUR # 7

z	r	M
-0.503539	0.115367	
-0.403539	0.115582	
-0.303539	0.116221	
-0.203539	0.117277	
-0.103539	0.118739	
-0.003539	0.120601	
0.096461	0.122853	
0.196461	0.125486	
0.296461	0.128492	
0.396461	0.131863	
0.496461	0.135589	
0.596461	0.139662	
0.696461	0.144073	
0.796461	0.148813	
0.896461	0.153873	
0.996461	0.159245	
1.096461	0.164919	
1.196461	0.170886	
1.296461	0.177138	
1.396461	0.183666	
1.496461	0.190460	
1.596461	0.197512	
1.696461	0.204812	
1.796461	0.212351	
1.896461	0.220120	
1.996461	0.228111	
2.096461	0.236313	
2.196461	0.244718	
2.296461	0.253316	
2.396461	0.262098	
2.496461	0.271056	
2.596461	0.280179	
2.696461	0.289458	
2.796461	0.298884	
2.896461	0.308449	
2.996461	0.318141	
3.096461	0.327953	
3.196461	0.337875	
3.296461	0.347897	
3.396461	0.358010	
3.496461	0.368205	
3.596461	0.378472	
3.696461	0.388802	
3.796461	0.399185	
3.896461	0.409613	
3.996461	0.420075	
4.096461	0.430563	
4.196461	0.441066	
4.296461	0.451576	
4.396461	0.462086	
4.424497	0.465032	4.4802
4.507445	0.473745	4.5239
4.592539	0.482679	4.5680
4.765910	0.500859	4.6553
4.771643	0.501459	4.6581
4.964084	0.521558	4.7503
5.040893	0.529543	4.7855
5.173572	0.543270	4.8451
5.333169	0.559641	4.9131
5.403420	0.566790	4.9424
5.642967	0.590847	5.0365
5.656501	0.592191	5.0417
5.934379	0.619326	5.1415
5.970260	0.622766	5.1536
6.237534	0.647873	5.2410
6.315024	0.654978	5.2646
6.564159	0.677258	5.3385
6.677136	0.687073	5.3699
6.910042	0.706724	5.4327
7.056545	0.718679	5.4698
7.395204	0.745115	5.5521
7.452987	0.749459	5.5653
7.866738	0.779168	5.6563
7.900627	0.781493	5.6634
8.297986	0.807578	5.7429
8.423560	0.815372	5.7668
8.746557	0.834461	5.8255
8.963115	0.846500	5.8630

z	r	M
9.212499	0.859631	5.9043
9.518345	0.874696	5.9524
9.695827	0.882926	5.9791
10.088484	0.899854	6.0351
10.196482	0.904206	6.0500
10.672867	0.921927	6.1115
10.714257	0.923354	6.1167
11.248779	0.940279	6.1791
11.270616	0.940911	6.1814
11.799201	0.954913	6.2369
11.880929	0.956857	6.2447
12.363803	0.967225	6.2898
12.503477	0.969876	6.3016
12.944621	0.977306	6.3378
13.137405	0.980121	6.3518
13.535990	0.985178	6.3799
13.781641	0.987813	6.3948
14.131384	0.990991	6.4154
14.434886	0.993247	6.4303
14.723817	0.995006	6.4441
15.095647	0.996779	6.4581
15.306751	0.997566	6.4658
15.762267	0.998819	6.4783
15.875002	0.999045	6.4813
16.425696	0.999799	6.4912
16.432969	0.999805	6.4913
16.958777	1.000121	6.4967
17.105923	1.000164	6.4974
17.477005	1.000226	6.4992
17.780011	1.000243	6.4996
17.985394	1.000248	6.4999
18.454374	1.000249	6.4999
18.489689	1.000249	6.5000

M_1	θ_n	γ	Z_1	π	a
6.50	10.00	1.4000	13.983394	0.150	0.018938
$(A/A^*)_1^{1/2}$	$1/\rho_1$	$\dot{M}_p$	$\ddot{M}_p$	a_0	
8.668005	0.191194	0.671970	-0.118526	0.034771	
a_1	a_2	M_A	Z_A	r_A	
-0.002681	-0.000221	3.638421	1.810892	0.319309	

CONTOUR # 8

z	r	M
0.057992	0.115367	
0.157992	0.116308	
0.257992	0.119072	
0.357992	0.123566	
0.457992	0.129694	
0.557992	0.137359	
0.657992	0.146459	
0.757992	0.156891	
0.857992	0.168547	
0.957992	0.181319	
1.057992	0.195095	
1.157992	0.209764	
1.257992	0.225210	
1.357992	0.241317	
1.457992	0.257967	
1.557992	0.275041	
1.657992	0.292420	
1.757992	0.309984	
1.857992	0.327614	
1.895033	0.334145	3.7364
1.968320	0.347056	3.8194
1.985197	0.350027	3.8380
2.083495	0.367312	3.9427
2.142580	0.377666	4.0027
2.193544	0.386567	4.0530
2.319372	0.408381	4.1697
2.335014	0.411072	4.1833
2.465094	0.433240	4.2927
2.546334	0.446866	4.3558
2.635292	0.461570	4.4225
2.777174	0.484513	4.5206
2.832303	0.493250	4.5572
3.027886	0.523412	4.6770
3.055380	0.527545	4.6932
3.298831	0.562996	4.8259
3.299911	0.563148	4.8264
3.590697	0.602790	4.9669
3.693036	0.616066	5.0136
3.903653	0.642327	5.1030
4.115155	0.667299	5.1877
4.238136	0.681199	5.2339
4.563018	0.715827	5.3489
4.594690	0.719044	5.3595
4.974217	0.755552	5.4794
5.033753	0.760942	5.4971
5.376941	0.790361	5.5941
5.526404	0.802313	5.6338
5.803059	0.823143	5.7038
6.040444	0.839731	5.7600
6.252888	0.853619	5.8081
6.574967	0.873043	5.8762
6.726574	0.881531	5.9070
7.129131	0.902175	5.9829
7.223985	0.906649	6.0001
7.702046	0.927122	6.0802
7.744578	0.928778	6.0870
8.287104	0.947770	6.1673
8.292691	0.947945	6.1681
8.848968	0.963528	6.2403
8.899562	0.964765	6.2461
9.432706	0.976179	6.3059
9.522090	0.977809	6.3146
10.028773	0.985704	6.3625
10.158759	0.987373	6.3729
10.625742	0.992340	6.4090
10.807742	0.993863	6.4203
11.211211	0.996544	6.4448
11.466889	0.997794	6.4565
11.774080	0.998914	6.4702
12.133706	0.999786	6.4813
12.307027	1.000067	6.4865
12.805429	1.000526	6.4952
12.808586	1.000528	6.4953
13.283613	1.000664	6.4990
13.479199	1.000679	6.4994
13.741974	1.000687	6.4999
14.153552	1.000688	6.4999
14.194507	1.000688	6.5000

M_1	θ_A	γ	Z_1	π	a
7.00	6.00	1.4000	18.954144	0.150	0.001565
$(A/A^*)_1^{1/2}$		$1/\rho_1$	$\dot{M}_B$	$\ddot{M}_B$	a_0
10.205040		0.043706	0.401822	-0.038010	0.012263
a_1		a_2	M_A	Z_A	r_A
-0.000785		-0.000040	4.669944	4.069045	0.427674

CONTOUR # 9

z	r	M	z	r	M
-0.653368	0.097991		3.246632	0.342124	
-0.553368	0.098208		3.346632	0.352348	
-0.453368	0.098853		3.446632	0.362641	
-0.353368	0.099919		3.546632	0.372994	
-0.253368	0.101395		3.646632	0.383397	
-0.153368	0.103274		3.746632	0.393840	
-0.053368	0.105547		3.846632	0.404315	
0.046632	0.108204		3.946632	0.414811	
0.146632	0.111237		4.046632	0.425318	
0.246632	0.114638		4.146632	0.435829	
0.346632	0.118396		4.229143	0.444500	4.7628
0.446632	0.122504		4.319699	0.454012	4.8142
0.546632	0.126953		4.398293	0.462263	4.8582
0.646632	0.131732		4.579220	0.481233	4.9563
0.746632	0.136834		4.588011	0.482153	4.9609
0.846632	0.142249		4.774578	0.501630	5.0570
0.946632	0.147968		4.874546	0.512013	5.1061
1.046632	0.153982		4.988665	0.523805	5.1610
1.146632	0.160282		5.180188	0.543411	5.2481
1.246632	0.166859		5.225229	0.547983	5.2682
1.346632	0.173703		5.487379	0.574237	5.3777
1.446632	0.180805		5.505099	0.575988	5.3847
1.546632	0.188156		5.776944	0.602415	5.4883
1.646632	0.195746		5.849272	0.609304	5.5140
1.746632	0.203567		6.094288	0.632149	5.5986
1.846632	0.211609		6.212693	0.642911	5.6368
1.946632	0.219863		6.436775	0.662756	5.7068
2.046632	0.228318		6.595226	0.676371	5.7532
2.146632	0.236967		6.799095	0.693370	5.8110
2.246632	0.245799		6.996905	0.709306	5.8637
2.346632	0.254805		7.313928	0.733703	5.9447
2.446632	0.263976		7.417491	0.741371	5.9696
2.546632	0.273301		7.851443	0.771916	6.0695
2.646632	0.282772		7.857169	0.772302	6.0707
2.746632	0.292380		8.316469	0.801881	6.1668
2.846632	0.302114		8.408166	0.807461	6.1851
2.946632	0.311965		8.795114	0.829859	6.2585
3.046632	0.321923		8.983500	0.840103	6.2925
3.146632	0.331980		9.293174	0.856037	6.3459

z	r	M
9.576491	0.869656	6.3923
9.810682	0.880244	6.4290
10.186317	0.896010	6.4846
10.347581	0.902330	6.5076
10.812275	0.919116	6.5698
10.903655	0.922171	6.5816
11.453640	0.938975	6.6480
11.478412	0.939668	6.6508
12.070945	0.954754	6.7149
12.109249	0.955630	6.7187
12.679282	0.967392	6.7734
12.778484	0.969196	6.7820
13.305805	0.977687	6.8264
13.460632	0.979839	6.8379
13.943853	0.985660	6.8726
14.154483	0.987793	6.8856
14.585647	0.991476	6.9115
14.858555	0.993368	6.9250
15.222932	0.995426	6.9425
15.571134	0.996947	6.9556
15.848060	0.997886	6.9657
16.290296	0.998971	6.9776
16.455180	0.999262	6.9819
17.014003	0.999913	6.9915
17.041405	0.999933	6.9919
17.607352	1.000202	6.9973
17.740141	1.000230	6.9978
18.157030	1.000280	6.9994
18.467367	1.000291	6.9997
18.696887	1.000293	6.9999
19.194824	1.000294	6.9999
19.233539	1.000294	7.0000

M_1	β_1	γ	z_1	π	a
7.00	10.00	1.4000	14.564819	0.150	0.019723
$(A/A^*)_1^{1/2}$	$1/\rho_1$	$\dot{M}_B$	$\ddot{M}_B$	a_0	
10.205040	0.195114	0.717112	-0.126630	0.033823	
a_1	a_2	M_A	z_A	r_A	
-0.002472	-0.000197	3.843225	1.689112	0.297836	

CONTOUR #10

z	r	M
-0.028575	0.097991	
0.071425	0.098951	
0.171425	0.101769	
0.271425	0.106349	
0.371425	0.112591	
0.471425	0.120393	
0.571425	0.129648	
0.671425	0.140248	
0.771425	0.152083	
0.871425	0.165038	
0.971425	0.178997	
1.071425	0.193843	
1.171425	0.209455	
1.271425	0.225712	
1.371425	0.242491	
1.471425	0.259668	
1.571425	0.277119	
1.671425	0.294717	
1.770841	0.312247	3.9470
1.848530	0.325934	4.0428
1.858635	0.327713	4.0549
1.954516	0.344573	4.1662
2.025997	0.357094	4.2450
2.062511	0.363468	4.2841
2.186613	0.384985	4.4091
2.223005	0.391239	4.4434
2.331699	0.409734	4.5422
2.440391	0.427920	4.6333
2.502633	0.438180	4.6836
2.678807	0.466560	4.8145
2.702050	0.470229	4.8311
2.929014	0.505085	4.9803
2.938701	0.506533	4.9863
3.178256	0.541321	5.1262
3.220660	0.547273	5.1492
3.525046	0.588238	5.3054
3.589232	0.596491	5.3366
3.852726	0.629034	5.4552
4.031760	0.649949	5.5311
4.203964	0.669194	5.5996
4.503001	0.700678	5.7113
4.579397	0.708339	5.7383
4.979820	0.746125	5.8711
5.000550	0.747975	5.8776
5.406107	0.782224	5.9979
5.521982	0.791344	6.0301
5.858206	0.816254	6.1192
6.067458	0.830630	6.1709
6.336517	0.847918	6.2347
6.636001	0.865657	6.3007
6.841246	0.876942	6.3442
7.226696	0.896339	6.4198
7.372275	0.903077	6.4473
7.838576	0.922659	6.5284
7.929034	0.926114	6.5436
8.470592	0.944673	6.6267
8.510112	0.945887	6.6325
9.112581	0.962293	6.7134
9.121446	0.962506	6.7144
9.739901	0.975475	6.7861
9.789465	0.976359	6.7911
10.381212	0.985388	6.8488
10.473551	0.986548	6.8564
11.023563	0.992273	6.9003
11.171693	0.993483	6.9098
11.652750	0.996609	6.9399
11.881494	0.997698	6.9507
12.255962	0.999029	6.9679
12.600163	0.999837	6.9787
12.824847	1.000190	6.9856
13.324550	1.000629	6.9945
13.357884	1.000644	6.9951
13.860970	1.000774	6.9990
14.051370	1.000787	6.9994
14.345706	1.000795	6.9999
14.778808	1.000795	6.9999
14.824470	1.000795	7.0000

M_1	θ_n	γ	Z_1	π	a
7.50	6.00	1.4000	19.534700	0.150	0.001616
$(A/A^*)_1^{1/2}$	$1/\rho_1$	$\dot{M}_B$	$\ddot{M}_B$	a_0	
11.909720	0.044415	0.426195	-0.040185	0.012168	
a_1	a_2	M_A	Z_A	r_A	
-0.000748	-0.000037	4.934618	3.885539	0.408386	

CONTOUR #11

Z	r	M
-0.761502	0.083965	
-0.661502	0.084186	
-0.561502	0.084841	
-0.461502	0.085924	
-0.361502	0.087423	
-0.261502	0.089331	
-0.161502	0.091638	
-0.061502	0.094336	
0.038498	0.097414	
0.138498	0.100864	
0.238498	0.104678	
0.338498	0.108844	
0.438498	0.113355	
0.538498	0.118200	
0.638498	0.123372	
0.738498	0.128859	
0.838498	0.134653	
0.938498	0.140745	
1.038498	0.147124	
1.138498	0.153782	
1.238498	0.160708	
1.338498	0.167894	
1.438498	0.175330	
1.538498	0.183005	
1.638498	0.190912	
1.738498	0.199039	
1.838498	0.207377	
1.938498	0.215917	
2.038498	0.224648	
2.138498	0.233562	
2.238498	0.242648	
2.338498	0.251896	
2.438498	0.261297	
2.538498	0.270841	
2.638498	0.280519	
2.738498	0.290319	
2.838498	0.300233	
2.938498	0.310251	
3.038498	0.320362	
3.138498	0.330558	
3.238498	0.340827	
3.338498	0.351160	
3.438498	0.361548	
3.538498	0.371980	
3.638498	0.382446	
3.738497	0.392937	
3.838497	0.403442	
3.938497	0.413953	
4.038497	0.424462	
4.045452	0.425193	5.0346
4.143214	0.435461	5.0946
4.214836	0.442980	5.1376
4.396568	0.462033	5.2438
4.420121	0.464498	5.2571
4.593823	0.482624	5.3530
4.717011	0.495406	5.4178
4.811355	0.505143	5.4664
5.034789	0.527971	5.5749
5.053395	0.529855	5.5837
5.323127	0.556819	5.7038
5.373536	0.561779	5.7247
5.623051	0.585919	5.8255
5.733368	0.596363	5.8671
5.953039	0.616706	5.9472
6.114214	0.631238	6.0021
6.309671	0.648396	6.0664
6.515974	0.665949	6.1302
6.686681	0.680035	6.1812
6.938778	0.700114	6.2519
7.229669	0.722220	6.3300
7.382422	0.733380	6.3686
7.797598	0.762180	6.4688
7.847137	0.765469	6.4802
8.333354	0.796144	6.5864
8.387335	0.799372	6.5976
8.841193	0.825167	6.6876
8.997326	0.833493	6.7170
9.370550	0.852314	6.7842

z	r	M
9.627060	0.864384	6.8278
9.921497	0.877403	6.8759
10.275675	0.891925	6.9303
10.493991	0.900276	6.9627
10.942391	0.916064	7.0249
11.087791	0.920799	7.0444
11.626414	0.936801	7.1116
11.702340	0.938865	7.1207
12.326909	0.954190	7.1903
12.336509	0.954403	7.1914
12.988220	0.967380	7.2558
13.042365	0.968329	7.2606
13.660187	0.977905	7.3140
13.772256	0.979399	7.3225
14.344677	0.986000	7.3647
14.515315	0.987645	7.3754
15.032610	0.991843	7.4070
15.269889	0.993394	7.4188
15.714344	0.995752	7.4405
16.034027	0.997049	7.4525
16.381088	0.998136	7.4653
16.805547	0.999082	7.4765
17.026306	0.999433	7.4822
17.582106	0.999999	7.4914
17.647152	1.000039	7.4925
18.245036	1.000268	7.4977
18.361324	1.000287	7.4981
18.825335	1.000328	7.4996
19.141593	1.000335	7.4998
19.395981	1.000336	7.4999.
19.922061	1.000337	7.5000
19.964229	1.000336	7.5000

M_1	θ_1	γ	z_1	π	a
7.50	10.00	1.4000	15.145375	0.150	0.020859
$(A/A^*)_1^{V2}$	$1/\rho_1$	$\dot{M}_B$	$\ddot{M}_B$	a_0	
11.909720	0.200653	0.764506	-0.135702	0.032955	
a_1	a_2	M_A	z_A	r_A	
-0.002289	-0.000176	4.036109	1.578281	0.278293	

CONTOUR #12

z	r	M
-0.091988	0.083965	
0.008012	0.084952	
0.108012	0.087847	
0.208012	0.092548	
0.308012	0.098949	
0.408012	0.106942	
0.508012	0.116415	
0.608012	0.127251	
0.708012	0.139333	
0.808012	0.152541	
0.908012	0.166751	
1.008012	0.181837	
1.108012	0.197673	
1.208012	0.214129	
1.308012	0.231075	
1.408012	0.248380	
1.508012	0.265911	
1.608012	0.283536	
1.657340	0.292234	4.1454
1.738788	0.306583	4.2547
1.742452	0.307228	4.2595
1.835513	0.323592	4.3770
1.918484	0.338122	4.4763
1.940921	0.342038	4.5024
2.062536	0.363127	4.6355
2.118998	0.372818	4.6929
2.206013	0.387606	4.7784
2.341324	0.410197	4.9009
2.376469	0.415977	4.9315
2.576729	0.448164	5.0917
2.586133	0.449643	5.0986
2.805780	0.483333	5.2539
2.854018	0.490510	5.2855
3.058651	0.520080	5.4134
3.145647	0.532222	5.4638
3.461240	0.574198	5.6359
3.485715	0.577322	5.6485
3.802362	0.616109	5.7998
3.946963	0.632846	5.8647
4.169067	0.657429	5.9580
4.439996	0.685650	6.0648
4.562101	0.697760	6.1103
4.962628	0.735004	6.2499
4.982242	0.736732	6.2564
5.430717	0.774026	6.3959
5.511811	0.780321	6.4195
5.907605	0.809239	6.5293
6.087432	0.821413	6.5758
6.413247	0.842042	6.6565
6.688800	0.858114	6.7198
6.947914	0.872143	6.7770
7.314930	0.890320	6.8520
7.511541	0.899277	6.8906
7.964764	0.918002	6.9726
8.103497	0.923216	6.9968
8.637159	0.941208	7.0817
8.722275	0.943782	7.0948
9.330842	0.960059	7.1794
9.364617	0.960855	7.1839
10.034834	0.974594	7.2642
10.044126	0.974757	7.2652
10.721006	0.984933	7.3335
10.775000	0.985601	7.3381
11.408585	0.992107	7.3904
11.521765	0.993018	7.3979
12.081535	0.996611	7.4341
12.281793	0.997550	7.4438
12.725249	0.999111	7.4649
13.052002	0.999865	7.4756
13.330166	1.000298	7.4844
13.828856	1.000726	7.4936
13.894571	1.000756	7.4948
14.425293	1.000885	7.4990
14.608615	1.000896	7.4993
14.935668	1.000905	7.4999
15.389057	1.000905	7.4999
15.439681	1.000905	7.5000

M_1	β_1	γ	z_1	π	a
8.00	6.00	1.4000	20.114553	0.150	0.001685
$(A/A^*)_1^{1/2}$	$1/\rho_1$	$\dot{M}_B$	$\ddot{M}_B$	a_0	
13.788015	0.045345	0.451374	-0.042538	0.012071	
a_1	a_2	M_A	z_A	r_A	
-0.000713	-0.000035	5.189259	3.713375	0.390291	

CONTOUR #13

z	r	M
-0.838312	0.072527	
-0.738312	0.072752	
-0.638312	0.073421	
-0.538312	0.074526	
-0.438312	0.076055	
-0.338312	0.078001	
-0.238312	0.080354	
-0.138312	0.083104	
-0.038312	0.086241	
0.061688	0.089757	
0.161688	0.093641	
0.261688	0.097884	
0.361688	0.102476	
0.461688	0.107408	
0.561688	0.112669	
0.661688	0.118251	
0.761688	0.124143	
0.861688	0.130335	
0.961688	0.136817	
1.061688	0.143580	
1.161688	0.150614	
1.261688	0.157908	
1.361688	0.165453	
1.461688	0.173238	
1.561688	0.181255	
1.661688	0.189491	
1.761688	0.197938	
1.861688	0.206586	
1.961688	0.215423	
2.061688	0.224441	
2.161688	0.233629	
2.261688	0.242976	
2.361688	0.252472	
2.461688	0.262108	
2.561687	0.271873	
2.661687	0.281757	
2.761687	0.291749	
2.861687	0.301839	
2.961687	0.312017	
3.061687	0.322273	
3.161687	0.332596	
3.261687	0.342975	
3.361687	0.353402	
3.461687	0.363865	
3.561687	0.374354	
3.661687	0.384859	
3.761687	0.395369	
3.861687	0.405879	
3.872437	0.407009	5.2964
3.976996	0.417990	5.3654
4.041327	0.424744	5.4070
4.223044	0.443794	5.5211
4.261404	0.447807	5.5443
4.421287	0.464484	5.6390
4.567542	0.479646	5.7213
4.641233	0.487244	5.7619
4.887523	0.512369	5.8895
4.896310	0.513257	5.8937
5.163644	0.539927	6.0203
5.247764	0.548174	6.0574
5.472584	0.569828	6.1536
5.622107	0.583905	6.2132
5.813759	0.601543	6.2870
6.019243	0.619936	6.3609
6.182939	0.634193	6.4177
6.439118	0.655798	6.5013
6.573103	0.666752	6.5434
6.881981	0.691105	6.6346
7.142803	0.710706	6.7082
7.347673	0.725495	6.7626
7.739867	0.752351	6.8618
7.836456	0.758677	6.8850
8.348650	0.790391	7.0019
8.361546	0.791150	7.0047
8.884838	0.820413	7.1130
9.005122	0.826719	7.1366
9.444725	0.848495	7.2191
9.670627	0.858926	7.2590

z	r	M
10.028414	0.874441	7.3198
10.357140	0.887645	7.3723
10.635862	0.898082	7.4152
11.063814	0.912817	7.4767
11.266832	0.919277	7.5049
11.789785	0.934441	7.5724
11.920692	0.937911	7.5888
12.534142	0.952569	7.6594
12.596173	0.953906	7.6663
13.290789	0.967226	7.7369
13.295777	0.967311	7.7374
14.007969	0.977998	7.8006
14.072924	0.978834	7.8057
14.738704	0.986234	7.8560
14.864796	0.987401	7.8640
15.472536	0.992125	7.9019
15.669541	0.993351	7.9119
16.198407	0.996015	7.9381
16.484989	0.997109	7.9490
16.906294	0.998344	7.9646
17.308687	0.999171	7.9752
17.588954	0.999579	7.9824
18.137966	1.000077	7.9912
18.243635	1.000135	7.9929
18.872657	1.000334	7.9980
18.970171	1.000346	7.9982
19.482843	1.000381	7.9997
19.803406	1.000385	7.9998
20.083614	1.000387	7.9999
20.636818	1.000386	8.0000
20.682639	1.000386	8.0000

M_1	θ_2	γ	z_1	π	a
8.00	10.00	1.4000	15.725227	0.150	0.022305
$(A/A^*)_1^{1/2}$	$1/\rho_1$	$\dot{M}_B$	$\ddot{M}_B$	a_0	
13.788015	0.207494	0.814011	-0.145701	0.032153	
a_1	a_2	M_A	z_A	r_A	
+0.002130	-0.000156	4.218000	1.477079	0.260449	

CONTOUR #14

z	r	M
-0.138126	0.072527	
-0.038126	0.073547	
0.061874	0.076536	
0.161874	0.081386	
0.261874	0.087983	
0.361874	0.096210	
0.461874	0.105946	
0.561874	0.117069	
0.661874	0.129450	
0.761874	0.142961	
0.861874	0.157468	
0.961874	0.172837	
1.061874	0.188931	
1.161874	0.205611	
1.261874	0.222738	
1.361874	0.240171	
1.461874	0.257768	
1.553308	0.273891	4.3326
1.635509	0.288373	4.4526
1.637904	0.288794	4.4560
1.725500	0.304197	4.5761
1.819009	0.320569	4.6976
1.827922	0.322124	4.7088
1.946461	0.342685	4.8494
2.022100	0.355654	4.9327
2.087524	0.366761	5.0021
2.248373	0.393568	5.1591
2.256437	0.394892	5.1667
2.455927	0.426973	5.3388
2.498523	0.433652	5.3727
2.686049	0.462323	5.5149
2.773237	0.475245	5.5761
2.941263	0.499425	5.6884
3.073383	0.517778	5.7701
3.382480	0.558532	5.9492
3.399098	0.560639	5.9581
3.752334	0.603519	6.1370
3.861140	0.616012	6.1887
4.133300	0.645882	6.3095
4.374456	0.670768	6.4098
4.542714	0.687295	6.4757
4.920415	0.722050	6.6142
4.981489	0.727374	6.6355
5.450777	0.765769	6.7883
5.496475	0.769275	6.8023
5.951276	0.802104	6.9343
6.101004	0.812112	6.9747
6.483104	0.835999	7.0735
6.734063	0.850444	7.1336
7.046615	0.867145	7.2056
7.394561	0.884147	7.2795
7.641781	0.895260	7.3301
8.081378	0.913178	7.4127
8.267962	0.920099	7.4465
8.793270	0.937575	7.5333
8.923529	0.941464	7.5541
9.528853	0.957452	7.6413
9.604979	0.959225	7.6519
10.286433	0.973009	7.7365
10.317461	0.973549	7.7402
11.048038	0.984348	7.8165
11.063926	0.984543	7.8179
11.780716	0.991848	7.8791
11.858785	0.992472	7.8845
12.497559	0.996554	7.9273
12.668609	0.997353	7.9360
13.182067	0.999160	7.9614
13.490044	0.999870	7.9718
13.823292	1.000393	7.9829
14.319172	1.000819	7.9924
14.419156	1.000865	7.9943
14.977270	1.000996	7.9989
15.151767	1.001007	7.9992
15.512633	1.001017	7.9999
15.985143	1.001017	7.9999
16.040979	1.001017	8.0000

M_1	β_A	γ	Z_1	τ	a
8.50	6.00	1.4000	20.693828	0.150	0.001768
$(A/A^*)_1^{1/2}$	$1/\rho_1$	$\dot{M}_B$	$\ddot{M}_B$	a_0	
15.845697	0.046454	0.477282	-0.045052	0.011972	
a_1	a_2	M_A	Z_A	r_A	
-0.000679	-0.000033	5.434435	3.551582	0.373286	

CONTOUR #15

z	r	M
-0.891429	0.063109	
-0.791429	0.063339	
-0.691429	0.064025	
-0.591429	0.065155	
-0.491429	0.066721	
-0.391429	0.068712	
-0.291429	0.071119	
-0.191429	0.073931	
-0.091429	0.077138	
0.008571	0.080731	
0.108571	0.084700	
0.208571	0.089033	
0.308571	0.093722	
0.408571	0.098756	
0.508571	0.104124	
0.608571	0.109816	
0.708571	0.115823	
0.808571	0.122134	
0.908571	0.128737	
1.008571	0.135624	
1.108571	0.142783	
1.208571	0.150204	
1.308571	0.157877	
1.408571	0.165791	
1.508571	0.173935	
1.608571	0.182299	
1.708571	0.190872	
1.808571	0.199644	
1.908571	0.208604	
2.008571	0.217741	
2.108571	0.227044	
2.208571	0.236504	
2.308571	0.246109	
2.408571	0.255848	
2.508571	0.265711	
2.608571	0.275687	
2.708571	0.285764	
2.808571	0.295934	
2.908571	0.306183	
3.008571	0.316503	
3.108571	0.326881	
3.208571	0.337307	
3.308571	0.347770	
3.408571	0.358260	
3.508571	0.368765	
3.608571	0.379276	
3.708571	0.389786	
3.709251	0.389857	5.5487
3.820191	0.401509	5.6273
3.877045	0.407477	5.6668
4.058042	0.426452	5.7888
4.111110	0.432001	5.8232
4.256478	0.447158	5.9153
4.425493	0.464666	6.0169
4.477933	0.470066	6.0477
4.727214	0.495479	6.1855
4.764165	0.499205	6.2046
5.008736	0.523541	6.3276
5.127314	0.535124	6.3830
5.325411	0.554127	6.4728
5.515105	0.571895	6.5527
5.676412	0.586657	6.6183
5.927471	0.608981	6.7136
6.056636	0.620151	6.7609
6.364590	0.645912	6.8659
6.627963	0.666978	6.9517
6.826311	0.682264	7.0121
7.232558	0.712043	7.1301
7.312891	0.717693	7.1521
7.824845	0.751910	7.2856
7.865628	0.754505	7.2957
8.362669	0.784645	7.4129
8.524245	0.793861	7.4490
8.926214	0.815612	7.5346
9.207897	0.829877	7.5913
9.515717	0.844583	7.6507
9.915448	0.862358	7.7233
10.131328	0.871356	7.7610

z	r	M
10.645949	0.891192	7.8452
10.773038	0.895749	7.8653
11.398444	0.916331	7.9575
11.440587	0.917610	7.9635
12.133377	0.936817	8.0550
12.171520	0.937776	8.0597
12.849902	0.953279	8.1397
12.964165	0.955603	8.1519
13.587212	0.966952	8.2167
13.775747	0.969956	8.2343
14.349241	0.977975	8.2862
14.604896	0.981031	8.3064
15.125893	0.986363	8.3464
15.449819	0.989111	8.3675
15.905342	0.992318	8.3963
16.308386	0.994574	8.4170
16.675040	0.996207	8.4353
17.178070	0.997887	8.4545
17.423652	0.998500	8.4636
18.056029	0.999588	8.4801
18.143218	0.999689	8.4823
18.831102	1.000208	8.4931
18.939052	1.000251	8.4940
19.490540	1.000384	8.4982
19.824556	1.000412	8.4990
20.129961	1.000423	8.4998
20.710812	1.000426	8.4999
20.760213	1.000426	8.5000

M_1	β_1	γ	z_1	τ	a
8.50	10.00	1.4000	16.304503	0.150	0.024044
$(A/A^*)_1^{1/2}$	$1/\rho_1$	$\dot{M}_B$	$\ddot{M}_B$	a_0	
15.845697	0.215431	0.865548	-0.156618	0.031407	
a_1	a_2	M_A	z_A	r_A	
-0.001992	-0.000138	4.389702	1.384396	0.244106	

CONTOUR # 16

z	r	M
-0.171294	0.063109	
-0.071294	0.064167	
0.028706	0.067266	
0.128706	0.072287	
0.228706	0.079109	
0.328706	0.087604	
0.428706	0.097642	
0.528706	0.109089	
0.628706	0.121807	
0.728706	0.135656	
0.828706	0.150492	
0.928706	0.166168	
1.028706	0.182537	
1.128706	0.199448	
1.228706	0.216750	
1.328706	0.234291	
1.428706	0.251920	
1.457709	0.257034	4.5094
1.536829	0.270975	4.6348
1.544882	0.272392	4.6471
1.623618	0.286236	4.7642
1.722704	0.303584	4.9037
1.726684	0.304278	4.9090
1.837771	0.323548	5.0517
1.931562	0.339617	5.1633
1.975741	0.347111	5.2139
2.141900	0.374808	5.3890
2.160883	0.377919	5.4075
2.339761	0.406658	5.5736
2.415398	0.418488	5.6382
2.569748	0.442026	5.7636
2.695922	0.460666	5.8585
2.826157	0.479344	5.9516
3.003519	0.503884	6.0684
3.279444	0.540087	6.2386
3.338440	0.547527	6.2722
3.702446	0.591232	6.4670
3.774484	0.599445	6.5032
4.096525	0.634532	6.6542
4.306665	0.656040	6.7463
4.521155	0.676931	6.8348
4.874601	0.709156	6.9710
4.977384	0.718032	7.0085
5.466284	0.757457	7.1752
5.476329	0.758219	7.1784
5.989231	0.794854	7.3341
6.108579	0.802744	7.3677
6.546108	0.829798	7.4857
6.772214	0.842665	7.5422
7.137356	0.861959	7.6298
7.466052	0.877837	7.7025
7.762994	0.891038	7.7657
8.188914	0.908203	7.8488
8.422387	0.916770	7.8928
8.939430	0.933788	7.9814
9.113822	0.938944	8.0103
9.716135	0.954699	8.1003
9.833509	0.957410	8.1172
10.517178	0.971129	8.2051
10.587589	0.972346	8.2139
11.340555	0.983374	8.2953
11.362105	0.983637	8.2976
12.139705	0.991500	8.3665
12.183261	0.991848	8.3696
12.900592	0.996442	8.4195
13.042452	0.997107	8.4270
13.626277	0.999181	8.4571
13.914791	0.999853	8.4674
14.304273	1.000476	8.4809
14.795985	1.000906	8.4909
14.931852	1.000971	8.4936
15.517256	1.001110	8.4988
15.681319	1.001120	8.4991
16.077070	1.001131	8.4999
16.567578	1.001132	8.4999
16.628888	1.001132	8.5000

M_1	θ_1	γ	z_1	τ	a
9.00	6.00	1.4000	21.272624	0.150	0.001865
$(A/A^*)_1^{1/2}$	$1/\rho_1$	$\dot{M}_B$	$\ddot{M}_B$	a_0	
18.088372	0.047713	0.503866	-0.047717	0.011870	
a_1	a_2	M_A	z_A	r_A	
-0.000647	-0.000032	5.670656	3.399309	0.357281	

CONTOUR #17

z	r	M
-0.926530	0.055284	
-0.826530	0.055521	
-0.726530	0.056225	
-0.626530	0.057385	
-0.526530	0.058991	
-0.426530	0.061034	
-0.326530	0.063501	
-0.226530	0.066384	
-0.126530	0.069670	
-0.026530	0.073351	
0.073470	0.077414	
0.173470	0.081850	
0.273470	0.086647	
0.373470	0.091795	
0.473470	0.097283	
0.573470	0.103100	
0.673470	0.109235	
0.773470	0.115678	
0.873470	0.122417	
0.973470	0.129442	
1.073470	0.136741	
1.173470	0.144303	
1.273470	0.152117	
1.373470	0.160173	
1.473470	0.168458	
1.573470	0.176962	
1.673470	0.185673	
1.773470	0.194581	
1.873470	0.203674	
1.973470	0.212941	
2.073470	0.222370	
2.173470	0.231950	
2.273470	0.241670	
2.373470	0.251519	
2.473470	0.261484	
2.573470	0.271556	
2.673470	0.281722	
2.773470	0.291970	
2.873470	0.302291	
2.973470	0.312671	
3.073470	0.323100	
3.173470	0.333567	
3.273470	0.344059	
3.373470	0.354566	
3.473470	0.365077	
3.555146	0.373660	5.7919
3.672047	0.385938	5.8808
3.721343	0.391112	5.9175
3.901026	0.409949	6.0472
3.968580	0.417011	6.0940
4.098970	0.430601	6.1824
4.290295	0.450405	6.3051
4.321121	0.453576	6.3244
4.572433	0.479182	6.4723
4.637903	0.485769	6.5083
4.858265	0.507644	6.6259
5.011771	0.522589	6.7019
5.181513	0.538811	6.7833
5.412020	0.560302	6.8859
5.541051	0.572050	6.9413
5.838627	0.598352	7.0604
5.930974	0.606287	7.0960
6.291893	0.636263	7.2256
6.524811	0.654743	7.3054
6.771746	0.673607	7.3844
7.154610	0.701402	7.5009
7.278479	0.710025	7.5365
7.812515	0.745206	7.6820
7.815971	0.745424	7.6829
8.374833	0.778896	7.8204
8.504741	0.786209	7.8507
8.965113	0.810780	7.9529
9.220919	0.823548	8.0065
9.583627	0.840619	8.0792
9.963317	0.857238	8.1508
10.230595	0.868198	8.1993
10.730959	0.887158	8.2842
10.906011	0.893325	8.3129

z	r	M
11.522736	0.913253	8.4070
11.609612	0.915838	8.4198
12.337718	0.935534	8.5192
12.340653	0.935606	8.5196
13.097695	0.952536	8.6116
13.173750	0.954048	8.6200
13.877323	0.966573	8.6954
14.030590	0.968956	8.7101
14.683996	0.977867	8.7709
14.906770	0.980458	8.7890
15.506453	0.986427	8.8363
15.800377	0.988845	8.8558
16.331417	0.992465	8.8902
16.709052	0.994504	8.9099
17.144750	0.996371	8.9321
17.630020	0.997919	8.9509
17.933757	0.998641	8.9624
18.560135	0.999656	8.9788
18.689808	0.999796	8.9821
19.410316	1.000286	8.9933
19.495886	1.000316	8.9940
20.099544	1.000445	8.9983
20.434230	1.000468	8.9991
20.767569	1.000477	8.9998
21.373341	1.000479	8.9999
21.426639	1.000479	9.0000

M_1	θ_2	γ	Z_1	π	a
9.00	10.00	1.4000	16.883298	0.150	0.026072
$(A/A^*)_1^{1/2}$		$1/\rho_1$	$\dot{M}_B$	$\ddot{M}_B$	a_0
18.088372		0.224333	0.919078	-0.168466	0.030712
a_1		a_2	M_A	Z_A	r_A
-0.001873		-0.000121	4.551914	1.299291	0.229100

CONTOUR #18

z	r	M	z	r	M
-0.194672	0.055284		4.497358	0.666659	7.1876
-0.094672	0.056385		4.825653	0.696349	7.3204
0.005328	0.059607		4.969894	0.708704	7.3757
0.105328	0.064819		5.451380	0.747143	7.5474
0.205328	0.071890		5.477398	0.749100	7.5563
0.305328	0.080682		6.021453	0.787491	7.7287
0.405328	0.091051		6.110759	0.793338	7.7550
0.505328	0.102853		6.602231	0.823440	7.8932
0.605328	0.115936		6.803901	0.834805	7.9457
0.705328	0.130148		7.220086	0.856586	8.0496
0.805328	0.145330		7.530105	0.871416	8.1209
0.905328	0.161325		7.875104	0.886611	8.1973
1.005328	0.177970		8.288066	0.903100	8.2810
1.105328	0.195101		8.566659	0.913233	8.3355
1.205328	0.212555		9.076380	0.929868	8.4261
1.305328	0.230165		9.292965	0.936222	8.4633
1.369659	0.241509	4.6764	9.893426	0.951816	8.5563
1.445636	0.254897	4.8070	10.050012	0.955411	8.5798
1.458899	0.257231	4.8290	10.737246	0.969132	8.6713
1.529124	0.269578	4.9421	10.844972	0.970987	8.6852
1.624553	0.286291	5.0875	11.605689	0.982105	8.7705
1.640730	0.289112	5.1108	11.662977	0.982805	8.7767
1.735940	0.305623	5.2430	12.485309	0.991065	8.8523
1.846735	0.324593	5.3852	12.495936	0.991151	8.8531
1.870289	0.328585	5.4143	13.290488	0.996279	8.9107
2.032780	0.355701	5.5992	13.404061	0.996817	8.9169
2.078281	0.363147	5.6468	14.057860	0.999177	8.9522
2.228159	0.387194	5.7964	14.326972	0.999816	8.9622
2.336292	0.404073	5.8954	14.773235	1.000551	8.9785
2.456938	0.422433	6.0005	15.260029	1.000991	8.9891
2.621687	0.446709	6.1331	15.433014	1.001079	8.9927
2.713514	0.459842	6.2031	16.045803	1.001228	8.9985
2.935750	0.490491	6.3591	16.198003	1.001239	8.9989
3.177315	0.522054	6.5176	16.629683	1.001252	8.9999
3.278854	0.534801	6.5789	17.137092	1.001253	8.9999
3.652535	0.579222	6.7901	17.204221	1.001253	9.0000
3.687352	0.583167	6.8086			
4.058632	0.623361	6.9923			
4.237029	0.641489	7.0746			

M_1	β_1	γ	Z_1	π	a
9.50	6.00	1.4000	21.851016	0.150	0.001975
$(A/A^*)_1^{1/2}$	$1/\rho_1$	$\dot{M}_B$	$\ddot{M}_B$	a_0	
20.521483	0.049099	0.531086	-0.050528	0.011765	
a_1	a_2	M_A	Z_A	r_A	
-0.000617	-0.000030	5.898381	3.255800	0.342198	

CONTOUR #19

z	r	M
-0.947876	0.048729	
-0.847876	0.048973	
-0.747876	0.049697	
-0.647876	0.050890	
-0.547876	0.052541	
-0.447876	0.054640	
-0.347876	0.057174	
-0.247876	0.060134	
-0.147876	0.063507	
-0.047876	0.067283	
0.052124	0.071450	
0.152124	0.075997	
0.252124	0.080913	
0.352124	0.086186	
0.452124	0.091804	
0.552124	0.097757	
0.652124	0.104032	
0.752124	0.110618	
0.852124	0.117504	
0.952124	0.124677	
1.052124	0.132126	
1.152124	0.139840	
1.252124	0.147806	
1.352124	0.156013	
1.452124	0.164449	
1.552124	0.173102	
1.652124	0.181960	
1.752124	0.191011	
1.852124	0.200244	
1.952124	0.209646	
2.052124	0.219205	
2.152124	0.228910	
2.252124	0.238748	
2.352124	0.248707	
2.452124	0.258776	
2.552124	0.268942	
2.652124	0.279193	
2.752124	0.289518	
2.852124	0.299903	
2.952124	0.310337	
3.052124	0.320808	
3.152124	0.331304	
3.252124	0.341812	
3.352124	0.352323	
3.409445	0.358347	6.0264
3.531895	0.371207	6.1261
3.573641	0.375589	6.1594
3.751518	0.394236	6.2968
3.833233	0.402776	6.3573
3.948376	0.414773	6.4405
4.161440	0.436811	6.5862
4.170493	0.437741	6.5922
4.422922	0.463450	6.7503
4.517091	0.472906	6.8052
4.712069	0.492218	6.9155
4.900771	0.510534	7.0144
5.040783	0.523869	7.0854
5.312548	0.549099	7.2131
5.407621	0.557714	7.2561
5.752467	0.588030	7.4016
5.806015	0.592604	7.4234
6.220969	0.626846	7.5801
6.421078	0.642606	7.6520
6.718066	0.665115	7.7517
7.074905	0.690795	7.8655
7.244094	0.702464	7.9163
7.763081	0.736300	8.0641
7.799522	0.738567	8.0740
8.385338	0.773155	8.2242
8.481502	0.778504	8.2475
9.001591	0.805921	8.3677
9.229306	0.817139	8.4173
9.648401	0.836598	8.5047
10.005736	0.852017	8.5746
10.326053	0.864961	8.6349
10.809714	0.883010	8.7200
11.034574	0.890808	8.7581
11.640129	0.910056	8.8537

z	r	M
11.773686	0.913965	8.8740
12.493905	0.933163	8.9759
12.542576	0.934292	8.9822
13.339585	0.951688	9.0821
13.375332	0.952386	9.0862
14.161170	0.966099	9.1729
14.276919	0.967861	9.1843
15.012229	0.977676	9.2546
15.199754	0.979808	9.2702
15.880309	0.986423	9.3253
16.141694	0.988518	9.3431
16.750623	0.992562	9.3835
17.100188	0.994392	9.4022
17.607436	0.996499	9.4286
18.072234	0.997928	9.4469
18.436637	0.998761	9.4609
19.054362	0.999713	9.4773
19.228793	0.999892	9.4818
19.981438	1.000361	9.4934
20.042753	1.000381	9.4938
20.699924	1.000507	9.4985
21.033885	1.000527	9.4991
21.395945	1.000535	9.4999
22.025810	1.000537	9.4999
22.083184	1.000536	9.5000

M_1	θ_B	γ	z_1	π	a
9.50	10.00	1.4000	17.461690	0.150	0.028394
$(A/A^*)_1^{1/2}$	$1/\rho_1$	$\dot{M}_B$	$\ddot{M}_B$	a_0	
20.521483	0.234109	0.974596	-0.181279	0.030065	
a_1	a_2	M_A	z_A	r_A	
-0.001773	-0.000105	4.705257	1.220955	0.215287	

CONTOUR #20

z	r	M	z	r	M
-0.210624	0.048729		4.773777	0.683630	7.6625
-0.110624	0.049878		4.958962	0.699379	7.7368
-0.010624	0.053233		5.422091	0.736068	7.9097
0.089376	0.058654		5.483994	0.740688	7.9317
0.189376	0.065996		6.047905	0.780012	8.1181
0.289376	0.075108		6.107775	0.783899	8.1365
0.389376	0.085833		6.651439	0.816926	8.2959
0.489376	0.098013		6.829370	0.826869	8.3441
0.589376	0.111481		7.294755	0.851029	8.4650
0.689376	0.126070		7.586937	0.864891	8.5348
0.789376	0.141608		7.978030	0.881984	8.6248
0.889376	0.157920		8.379118	0.897876	8.7091
0.989376	0.174828		8.700666	0.909491	8.7744
1.089376	0.192155		9.204375	0.925821	8.8673
1.189376	0.209720		9.460824	0.933302	8.9130
1.288385	0.227178	4.8343	10.061010	0.948811	9.0093
1.361213	0.240013	4.9698	10.254288	0.953233	9.0393
1.379229	0.243183	5.0021	10.946921	0.967025	9.1349
1.441360	0.254107	5.1102	11.089345	0.969476	9.1540
1.533009	0.270163	5.2613	11.859815	0.980746	9.2436
1.560546	0.274963	5.3041	11.950323	0.981855	9.2538
1.640472	0.288822	5.4238	12.796834	0.990384	9.3345
1.767058	0.310483	5.5990	12.817270	0.990549	9.3364
1.770760	0.311111	5.6039	13.666923	0.996066	9.4006
1.928924	0.337537	5.7980	13.753692	0.996484	9.4056
2.000089	0.349170	5.8781	14.476571	0.999151	9.4464
2.120951	0.368542	6.0076	14.726836	0.999761	9.4563
2.260801	0.390338	6.1449	15.230053	1.000622	9.4757
2.347550	0.403518	6.2258	15.711531	1.001078	9.4868
2.550204	0.433317	6.4001	15.922669	1.001193	9.4916
2.603328	0.440899	6.4433	16.563084	1.001356	9.4983
2.869807	0.477553	6.6425	16.702044	1.001367	9.4986
3.076133	0.504418	6.7862	17.170760	1.001383	9.4999
3.220133	0.522426	6.8785	17.693920	1.001384	9.4999
3.599763	0.567159	7.1049	17.767306	1.001384	9.5000
3.602470	0.567464	7.1064			
4.019509	0.612349	7.3238			
4.165693	0.627110	7.3948			
4.471239	0.656463	7.5341			

M_1	θ_A	γ	z_1	π	a
10.00	6.00	1.4000	22.429066	0.150	0.002098
$(A/A^*)_1^{1/2}$	$1/\rho_1$	$\dot{M}_B$	$\ddot{M}_B$	a_0	
23.150321	0.050599	0.558916	-0.053480	0.011658	
a_1	a_2	M_A	z_A	r_A	
-0.000589	-0.000028	6.118029	3.120385	0.327966	

CONTOUR # 21

z	r	M	z	r	M
-0.958685	0.043196		2.941315	0.309157	
-0.858685	0.043447		3.041315	0.319656	
-0.758685	0.044193		3.141315	0.330166	
-0.658685	0.045421		3.241315	0.340677	
-0.558685	0.047120		3.271560	0.343855	6.2528
-0.458685	0.049279		3.399143	0.357254	6.3639
-0.358685	0.051886		3.433425	0.360852	6.3930
-0.258685	0.054929		3.609067	0.379265	6.5379
-0.158685	0.058395		3.704550	0.389242	6.6133
-0.058685	0.062274		3.804326	0.399634	6.6902
0.041315	0.066552		4.025617	0.422515	6.8512
0.141315	0.071219		4.038427	0.423831	6.8600
0.241315	0.076261		4.278521	0.448264	7.0197
0.341315	0.081667		4.401346	0.460576	7.0956
0.441315	0.087425		4.570050	0.477251	7.1966
0.541315	0.093522		4.793988	0.498927	7.3208
0.641315	0.099946		4.903163	0.509292	7.3792
0.741315	0.106684		5.216426	0.538261	7.5345
0.841315	0.113725		5.276206	0.543655	7.5630
0.941315	0.121056		5.668784	0.577997	7.7374
1.041315	0.128664		5.681965	0.579117	7.7430
1.141315	0.136537		6.151653	0.617649	7.9295
1.241315	0.144663		6.317000	0.630584	7.9918
1.341315	0.153028		6.665140	0.656780	8.1143
1.441315	0.161621		6.993752	0.680241	8.2239
1.541315	0.170429		7.209633	0.695004	8.2918
1.641315	0.179438		7.707635	0.727175	8.4398
1.741315	0.188637		7.785664	0.731982	8.4618
1.841315	0.198013		8.394152	0.767426	8.6242
1.941315	0.207552		8.454890	0.770767	8.6396
2.041315	0.217243		9.035627	0.801039	8.7792
2.141315	0.227073		9.233442	0.810667	8.8239
2.241315	0.237028		9.710051	0.832527	8.9271
2.341315	0.247096		10.043089	0.846713	8.9947
2.441315	0.257264		10.417732	0.861653	9.0678
2.541315	0.267519		10.882669	0.878765	9.1525
2.641315	0.277849		11.158741	0.888205	9.2009
2.741315	0.288241		11.751049	0.906757	9.2976
2.841315	0.298681		11.932798	0.911998	9.3262

z	r	M
12.647040	0.930689	9.4302
12.739047	0.932881	9.4431
13.569262	0.950624	9.5503
13.575575	0.950745	9.5511
14.438748	0.965536	9.6491
14.515271	0.966680	9.6568
15.333915	0.977407	9.7373
15.484308	0.979084	9.7502
16.247399	0.986356	9.8136
16.474230	0.988135	9.8294
17.162956	0.992609	9.8762
17.482275	0.994241	9.8937
18.063141	0.996594	9.9246
18.505187	0.997913	9.9424
18.932360	0.998860	9.9591
19.539191	0.999759	9.9755
19.760380	0.999977	9.9813
20.544796	1.000430	9.9934
20.580137	1.000440	9.9936
21.292039	1.000567	9.9985
21.624011	1.000583	9.9992
22.015484	1.000591	9.9999
22.668717	1.000592	9.9999
22.730253	1.000592	10.0000

M_1	β_1	γ	z_1	τ	α
10.00	10.00	1.4000	18.039741	0.150	0.031021
$(A/A^*)_1^{1/2}$	$1/\rho_1$	$\dot{M}_0$	$\ddot{M}_0$	a_0	
23.150321	0.244701	1.032121	-0.195104	0.029463	
a_1	a_2	M_A	z_A	r_A	
-0.001690	-0.000090	4.850276	1.148685	0.202544	

CONTOUR # 2 2

z	r	M	z	r	M
-0.220926	0.043196		4.719333	0.671009	7.9974
-0.120926	0.044395		4.944496	0.690039	8.0921
-0.020926	0.047894		5.389155	0.725027	8.2656
0.079074	0.053539		5.485912	0.732201	8.3016
0.179074	0.061171		6.068509	0.772407	8.5022
0.279074	0.070624		6.100076	0.774441	8.5123
0.379074	0.081726		6.693623	0.810247	8.6936
0.479074	0.094301		6.849131	0.818874	8.7374
0.579074	0.108168		7.361236	0.845278	8.8758
0.679074	0.123142		7.637154	0.858279	8.9443
0.779074	0.139033		8.071602	0.877146	9.0480
0.879074	0.155650		8.462646	0.892545	9.1334
0.979074	0.172798		8.824210	0.905535	9.2095
1.079074	0.190281		9.324054	0.921658	9.3051
1.179074	0.207903		9.617141	0.930174	9.3592
1.213221	0.213925	4.9837	10.219521	0.945690	9.4594
1.282924	0.226210	5.1237	10.446045	0.950862	9.4956
1.305242	0.230137	5.1670	11.146855	0.964809	9.5961
1.359730	0.239717	5.2592	11.320363	0.967799	9.6201
1.447544	0.255106	5.4256	12.103591	0.979291	9.7146
1.485573	0.261734	5.4893	12.223701	0.980772	9.7286
1.550914	0.273062	5.5947	13.086738	0.989542	9.8141
1.676548	0.294578	5.7822	13.135026	0.989937	9.8188
1.691988	0.297193	5.8036	14.029377	0.995792	9.8891
1.830123	0.320273	5.9359	14.092007	0.996100	9.8929
1.925887	0.335915	6.1016	14.881946	0.999091	9.9397
2.018064	0.350679	6.2076	15.115026	0.999679	9.9494
2.188571	0.377222	6.3869	15.674451	1.000679	9.9723
2.241574	0.385266	6.4398	16.151125	1.001155	9.9841
2.481178	0.420442	6.6598	16.400727	1.001302	9.9902
2.495717	0.422513	6.6724	17.069272	1.001484	9.9979
2.805453	0.465028	6.9187	17.194069	1.001495	9.9983
2.976111	0.487185	7.0449	17.700641	1.001515	9.9998
3.162090	0.510370	7.1710	18.238690	1.001517	9.9999
3.511263	0.551348	7.3910	18.318625	1.001517	10.0000
3.552405	0.555966	7.4152			
3.979020	0.601471	7.6488			
4.093005	0.612917	7.7070			
4.442688	0.646323	7.8744			

M_1	θ_A	γ	Z_1	π	a
11.00	6.00	1.4000	23.584330	0.150	0.002380
$(A/A^*)_1^{1/2}$	$1/\rho_0$	$\dot{M}_B$	$\ddot{M}_B$	a_0	
29.015668	0.053898	0.616330	-0.059806	0.011437	
a_1	a_2	M_A	Z_A	r_A	
-0.000537	-0.000025	6.534604	2.871488	0.301805	

CONTOUR #23

z	r	M	z	r	M
-0.957935	0.034464		2.942065	0.309224	
-0.857935	0.034731		3.017089	0.317109	6.6824
-0.757935	0.035525		3.153752	0.331462	6.9176
-0.657935	0.036831		3.173519	0.333536	6.9367
-0.557935	0.038636		3.343740	0.351380	6.9961
-0.457935	0.040927		3.465341	0.364081	7.1048
-0.357935	0.043692		3.534565	0.371287	7.1651
-0.257935	0.046915		3.752313	0.393802	7.3440
-0.157935	0.050585		3.808369	0.399549	7.3872
-0.057935	0.054686		4.004308	0.419449	7.5336
0.042065	0.059206		4.183681	0.437372	7.6578
0.142065	0.064131		4.298076	0.448639	7.7343
0.242065	0.069448		4.591923	0.476941	7.9159
0.342065	0.075141		4.637115	0.481208	7.9428
0.442065	0.081198		5.019332	0.516345	8.1531
0.542065	0.087604		5.033307	0.517596	8.1603
0.642065	0.094346		5.435926	0.552654	8.3586
0.742065	0.101409		5.508334	0.558752	8.3918
0.842065	0.108779		6.017230	0.599865	8.6135
0.942065	0.116443		6.108547	0.606926	8.6514
1.042065	0.124386		6.561114	0.640555	8.8257
1.142065	0.132594		6.827984	0.659342	8.9229
1.242065	0.141052		7.140156	0.680377	9.0298
1.342065	0.149746		7.590261	0.708988	9.1753
1.442065	0.158663		7.755077	0.718972	9.2257
1.542065	0.167787		8.392447	0.755244	9.4095
1.642065	0.177104		8.406660	0.756011	9.4134
1.742065	0.186601		9.096341	0.791218	9.5922
1.842065	0.196261		9.230140	0.797596	9.6248
1.942065	0.206071		9.823900	0.824253	9.7630
2.042065	0.216017		10.103878	0.835913	9.8239
2.142065	0.226084		10.589684	0.854848	9.9255
2.242065	0.236257		11.012516	0.870042	10.0079
2.342065	0.246522		11.393867	0.882770	10.0794
2.442065	0.256864		11.954846	0.899903	10.1770
2.542065	0.267269		12.236170	0.907811	10.2243
2.642065	0.277721		12.929472	0.925482	10.3316
2.742065	0.288208		13.115607	0.929799	10.3595
2.842065	0.298713		13.934840	0.946835	10.4716

z	r	M
14.029952	0.948610	10.4843
14.969228	0.964093	10.5969
14.974911	0.964175	10.5976
15.957437	0.976669	10.6996
16.029573	0.977449	10.7061
16.961217	0.986062	10.7877
17.114422	0.987226	10.7990
17.966965	0.992590	10.8599
18.220730	0.993840	10.8745
18.953770	0.996708	10.9155
19.344724	0.997826	10.9319
19.902870	0.999016	10.9548
20.482050	0.999828	10.9710
20.802175	1.000128	10.9797
21.627836	1.000559	10.9928
21.649316	1.000565	10.9931
22.452903	1.000691	10.9986
22.777101	1.000704	10.9992
23.229663	1.000711	10.9999
23.927288	1.000712	10.9999
23.997652	1.000712	11.0000

M_1	θ_A	γ	z_1	π	a
11.00	10.00	1.4000	19.195004	0.150	0.037266
$(A/A^*)_1^{1/2}$	$1/\rho_1$	$\dot{M}_B$	$\ddot{M}_B$	a_0	
29.015668	0.268200	1.153368	-0.226046	0.028394	
a_1	a_2	M_A	z_A	r_A	
-0.001573	-0.000062	5.117252	1.019983	0.179850	

CONTOUR #24

z	r	M
-0.229625	0.034464	
-0.129625	0.035776	
-0.029625	0.039593	
0.070375	0.045728	
0.170375	0.053989	
0.270375	0.064175	
0.370375	0.076076	
0.470375	0.089477	
0.570375	0.104159	
0.670375	0.119894	
0.770375	0.136453	
0.870375	0.153603	
0.970375	0.171108	
1.070375	0.188737	
1.078929	0.190246	5.2586
1.142567	0.201464	5.4070
1.172176	0.206675	5.4736
1.212825	0.213821	5.5619
1.292971	0.227875	5.7274
1.349354	0.237700	5.8368
1.387950	0.244391	5.9088
1.503482	0.264222	6.1088
1.554071	0.272765	6.1896
1.646798	0.288277	6.3307
1.788025	0.311326	6.5269
1.824661	0.317191	6.5752
2.039371	0.350621	6.8340
2.052730	0.352647	6.8489
2.286812	0.387143	7.0944
2.349862	0.396112	7.1548
2.680650	0.441065	7.4501
2.779629	0.453863	7.5324
3.047338	0.487084	7.7353
3.334035	0.520520	7.9365
3.450847	0.533546	8.0125
3.893585	0.580049	8.2796
3.943886	0.585055	8.3079
4.378030	0.626161	8.5363
4.603368	0.646066	8.6461
4.904729	0.671283	8.7847
5.312934	0.703050	8.9584
5.475514	0.714976	9.0242
6.070763	0.755447	9.2466
6.092097	0.756807	9.2542
6.756635	0.796372	9.4737
6.872358	0.802720	9.5090
7.469221	0.833178	9.6830
7.718505	0.844803	9.7497
8.230181	0.866824	9.8812
8.608122	0.881580	9.9699
9.039115	0.896957	10.0675
9.539407	0.913000	10.1701
9.894166	0.923271	10.2405
10.510347	0.939112	10.3504
10.790745	0.945523	10.3988
11.518455	0.960062	10.5105
11.740789	0.963924	10.5436
12.561072	0.976108	10.6500
12.726816	0.978189	10.6709
13.634843	0.987638	10.7680
13.726028	0.988410	10.7775
14.710370	0.995051	10.8616
14.735480	0.995180	10.8633
15.650814	0.998868	10.9230
15.857174	0.999433	10.9327
16.524404	1.000751	10.9634
16.995312	1.001287	10.9771
17.321202	1.001515	10.9864
18.048207	1.001751	10.9967
18.142736	1.001762	10.9971
18.727459	1.001796	10.9997
19.292724	1.001800	10.9999
19.386925	1.001800	11.0000

M_1	β_A	γ	z_1	τ	a
12.00	6.00	1.4000	24.738711	0.150	0.002714
$(A/A^*)_1^{1/2}$	$1/\rho_1$	$\dot{M}_B$	$\ddot{M}_B$	a_0	
35.724148	0.057551	0.676026	-0.066703	0.011212	
a_1	a_2	M_A	z_A	r_A	
-0.000491	-0.000023	6.923116	2.648450	0.278363	

CONTOUR #25

z	r	M	z	r	M
-0.937888	0.027992		2.932169	0.308172	7.2445
-0.837888	0.028278		2.938248	0.308810	7.2512
-0.737888	0.029123		3.102113	0.325988	7.4243
-0.637888	0.030515		3.247698	0.341188	7.5707
-0.537888	0.032437		3.287224	0.345301	7.6094
-0.437888	0.034874		3.499557	0.367259	7.8056
-0.337888	0.037811		3.597406	0.377276	7.8900
-0.237888	0.041232		3.748276	0.392574	8.0159
-0.137888	0.045123		3.982486	0.415914	8.1967
-0.037888	0.049467		4.041326	0.421692	8.2406
0.062112	0.054250		4.382533	0.454460	8.4748
0.162112	0.059454		4.403546	0.456435	8.4882
0.262112	0.065066		4.769562	0.490010	8.7115
0.362112	0.071068		4.861058	0.498156	8.7635
0.462112	0.077445		5.194152	0.526974	8.9442
0.562112	0.084181		5.355739	0.540483	9.0257
0.662112	0.091260		5.887564	0.582830	9.2790
0.762112	0.098666		5.900332	0.583808	9.2847
0.862112	0.106382		6.458857	0.624876	9.5194
0.962112	0.114394		6.658375	0.638756	9.5985
1.062112	0.122683		7.069480	0.666116	9.7513
1.162112	0.131235		7.465315	0.690935	9.8898
1.262112	0.140033		7.720353	0.706167	9.9742
1.362112	0.149060		8.317931	0.739656	10.1600
1.462112	0.158301		8.412443	0.744678	10.1880
1.562112	0.167738		9.147091	0.781338	10.3923
1.662112	0.177355		9.212739	0.784412	10.4094
1.762112	0.187136		9.925086	0.815825	10.5870
1.862112	0.197064		10.147530	0.824916	10.6388
1.962112	0.207123		10.746393	0.847817	10.7726
2.062112	0.217296		11.122503	0.861067	10.8507
2.162112	0.227566		11.611296	0.877058	10.9484
2.262112	0.237917		12.136191	0.892762	11.0455
2.362112	0.248333		12.519555	0.903318	11.1139
2.462112	0.258796		13.187101	0.919977	11.2236
2.562112	0.269290		13.470083	0.926404	11.2685
2.662112	0.279799		14.273545	0.942758	11.3849
2.762112	0.290311		14.460438	0.946172	11.4112
2.787025	0.293023	7.0832	15.393529	0.961227	11.5294

z	r	M
15.485640	0.962537	11.5407
16.544588	0.975589	11.6566
16.554069	0.975689	11.6576
17.647318	0.985577	11.7584
17.723127	0.986141	11.7643
18.742944	0.992433	11.8411
18.926516	0.993318	11.8522
19.816394	0.996736	11.9046
20.150719	0.997671	11.9194
20.845501	0.999125	11.9494
21.390754	0.999871	11.9654
21.816003	1.000261	11.9776
22.640985	1.000677	11.9912
22.725331	1.000699	11.9926
23.583990	1.000821	11.9986
23.895545	1.000833	11.9991
24.412173	1.000840	11.9999
25.151127	1.000841	11.9999
25.231026	1.000841	12.0000

M_1	θ_1	γ	z_1	π	a
12.00	10.00	1.4000	20.349385	0.150	0.044992
$(A/A^*)_1^{1/2}$	$1/\rho_2$	$\dot{M}_3$	$\ddot{M}_3$	a_3	
35.724148	0.294696	1.283347	-0.261935	0.027508	
a_1	a_2	M_4	z_4	r_4	
-0.001518	-0.000034	5.356174	0.909146	0.160307	

CONTOUR #26

z	r	M
-0.228110	0.027992	
-0.128110	0.029431	
-0.028110	0.033601	
0.071890	0.040278	
0.171890	0.049226	
0.271890	0.060198	
0.371890	0.072940	
0.471890	0.087187	
0.571890	0.102669	
0.671890	0.119110	
0.771890	0.136229	
0.871890	0.153740	
0.962850	0.169778	5.5045
1.020765	0.179989	5.6602
1.056033	0.186196	5.7516
1.084797	0.191253	5.3235
1.157544	0.204016	5.9968
1.228793	0.216433	6.1560
1.244131	0.219093	6.1889
1.349227	0.237171	6.3989
1.430160	0.250872	6.5474
1.481228	0.259409	6.6366
1.646754	0.286470	6.9005
1.662227	0.288948	6.9232
1.849247	0.318224	7.1817
1.926696	0.329974	7.2799
2.087946	0.353755	7.4719
2.225621	0.373345	7.6209
2.559878	0.418340	7.9546
2.588284	0.422005	7.9811
2.933406	0.464722	8.2725
3.157202	0.490717	8.4469
3.346620	0.511751	8.5831
3.790369	0.557844	8.8773
3.801720	0.558966	8.8843
4.302775	0.606059	9.1731
4.478975	0.621509	9.2669
4.850063	0.652340	9.4529
5.224173	0.681222	9.6260
5.445670	0.697347	9.7233
6.024309	0.736367	9.9575
6.091678	0.740627	9.9835
6.790495	0.781753	10.2325
6.875381	0.786374	10.2604
7.543026	0.820223	10.4700
7.776124	0.831027	10.5371
8.349462	0.855580	10.6955
8.726506	0.870239	10.7905
9.209676	0.887436	10.9078
9.724560	0.903928	11.0212
10.121886	0.915445	11.1056
10.768091	0.932111	11.2292
11.081387	0.939319	11.2871
11.854338	0.954910	11.4144
12.102935	0.959288	11.4541
12.980366	0.972561	11.5764
13.168428	0.974980	11.6019
14.142579	0.985435	11.7145
14.253867	0.986414	11.7270
15.328600	0.993998	11.8269
15.336521	0.994041	11.8275
16.359683	0.998468	11.9011
16.555361	0.999056	11.9115
17.318928	1.000743	11.9511
17.794417	1.001370	11.9674
18.191585	1.001704	11.9806
18.981490	1.002020	11.9947
19.045734	1.002031	11.9952
19.710662	1.002089	11.9994
20.300899	1.002096	11.9999
20.410827	1.002096	12.0000

M_1	θ_A	γ	z_1	π	a
9.00	10.00	1.2000	16.149242	0.100	0.018934
$(A/A^*)_1^{1/2}$	$1/\rho_1$	$\dot{M}_B$	$\ddot{M}_B$	a_0	
111.278850	0.191173	0.456178	-0.088960	0.036660	
a_1	a_2	M_A	z_A	r_A	
-0.003287	-0.000428	6.207626	1.207709	0.212952	

CONTOUR #27

z	r	M	z	r	M
-0.545389	0.008986		4.936604	0.699376	8.0535
-0.445389	0.009928		5.469220	0.742635	8.1667
-0.345389	0.012691		5.513723	0.746024	8.1757
-0.245389	0.017184		6.141050	0.790457	8.2917
-0.145389	0.023313		6.148544	0.790950	8.2930
-0.045389	0.030977		6.821193	0.832029	8.4015
0.054611	0.040076		6.858572	0.834126	8.4070
0.154611	0.050506		7.556171	0.870079	8.5048
0.254611	0.062161		7.599631	0.872119	8.5103
0.354611	0.074932		8.347826	0.903993	8.6012
0.454611	0.088708		8.370689	0.904870	8.6037
0.554611	0.103376		9.169904	0.932377	8.6874
0.654611	0.118821		9.197032	0.933203	8.6901
0.754611	0.134927		9.995443	0.954739	8.7613
0.854611	0.151576		10.102681	0.957226	8.7706
0.954611	0.166650		10.846678	0.972179	8.8262
1.054611	0.186028		11.059649	0.975735	8.8416
1.154611	0.203592		11.721895	0.984996	8.8818
1.254611	0.221222		12.054232	0.988668	8.9014
1.315446	0.231942	6.3432	12.618722	0.993610	8.9279
1.385769	0.244303	6.4255	13.068566	0.996485	8.9434
1.445243	0.254725	6.4917	13.534018	0.998618	8.9635
1.591028	0.280038	6.6365	14.037792	1.000121	8.9794
1.617903	0.284659	6.6617	14.462902	1.000871	8.9871
1.824801	0.319586	6.8318	14.909994	1.001294	8.9949
1.853123	0.324274	6.8535	15.399584	1.001478	8.9979
2.088559	0.362267	7.0133	15.684076	1.001514	8.9996
2.150171	0.371921	7.0521	16.338665	1.001527	8.9999
2.384055	0.407460	7.1836	16.410707	1.001527	9.0000
2.596972	0.438325	7.2933			
2.713015	0.454573	7.3474			
3.077263	0.503026	7.5031			
3.095134	0.505307	7.5102			
3.479815	0.552376	7.6499			
3.633013	0.570068	7.7009			
3.922266	0.601946	7.7907			
4.209639	0.631727	7.8724			
4.407002	0.651144	7.9252			
4.822350	0.689434	8.0270			

M_1	θ_A	γ	z_1	τ	a
9.00	10.00	1.6667	17.617354	0.200	0.071989
$(A/A^*)_1^{1/2}$	$1/\rho_1$	$\dot{M}_B$	$\ddot{M}_B$	a_0	
6.999450	0.372769	1.457829	-0.227406	0.030545	
a_1	a_2	M_A	z_A	r_A	
-0.002252	0.000021	3.011685	1.403479	0.247471	

CONTOUR #28

z	r	M	z	r	M
0.504409	0.142868		5.995973	0.790458	7.1064
0.604409	0.144676		6.368178	0.813479	7.2612
0.704409	0.149864		6.619890	0.827897	7.3602
0.804409	0.158066		7.284675	0.861949	7.6012
0.904409	0.168893		7.294557	0.862413	7.6045
1.004409	0.181938		8.007928	0.893029	7.8320
1.104409	0.196777		8.278766	0.903226	7.9104
1.204409	0.212973		8.783830	0.920371	8.0499
1.304409	0.230077		9.320455	0.936117	8.1829
1.404409	0.247635		9.606674	0.943551	8.2509
1.464399	0.258214	3.1384	10.414945	0.961351	8.4205
1.528720	0.269552	3.2696	10.466648	0.962335	8.4310
1.560494	0.275146	3.3330	11.350093	0.976733	8.5866
1.597595	0.281673	3.4053	11.554326	0.979436	8.6172
1.671994	0.294754	3.5463	12.238501	0.987034	8.7159
1.742436	0.307092	3.6750	12.733896	0.991251	8.7746
1.753548	0.309033	3.6949	13.112304	0.993835	8.8180
1.844082	0.324790	3.8506	13.946594	0.997894	8.8930
1.946829	0.342492	4.0183	13.952973	0.997917	8.8935
1.952550	0.343471	4.0272	14.746553	1.000091	8.9450
2.065073	0.362553	4.1971	15.181154	1.000768	8.9636
2.193478	0.383884	4.3780	15.485951	1.001081	8.9764
2.204023	0.385612	4.3925	16.173885	1.001448	8.9925
2.368096	0.412030	4.6023	16.429140	1.001503	8.9950
2.467266	0.427534	4.7197	16.821859	1.001545	8.9987
2.562700	0.442118	4.8288	17.447318	1.001559	8.9999
2.775143	0.473406	5.0528	17.681051	1.001559	8.9999
2.790832	0.475651	5.0687	18.066712	1.001559	9.0000
3.051147	0.511645	5.3140			
3.118776	0.520607	5.3735			
3.338807	0.548726	5.5585			
3.499691	0.568305	5.6831			
3.917534	0.615592	5.9871			
3.986898	0.622969	6.0348			
4.375988	0.662115	6.2800			
4.711192	0.692960	6.4772			
4.873804	0.707033	6.5661			
5.413389	0.749978	6.8420			
5.506765	0.756849	6.8867			

M_1	β_A	γ	z_1	π	a
10.00	10.00	1.2000	17.255404	0.100	0.024715
$(A/A^*)_1^{1/2}$	$1/\rho_1$	$\dot{M}_B$	$\ddot{M}_B$	a_0	
177.827930	0.218416	0.504061	-0.099922	0.034602	
a_1	a_2	M_A	z_A	r_A	
-0.002759	-0.000365	6.738980	1.044357	0.184148	

CONTOUR # 29

z	r	M	z	r	M
-0.490078	0.005623		5.521948	0.728024	9.0333
-0.390078	0.006696		6.201548	0.775136	9.1692
-0.290078	0.009836		6.239976	0.777603	9.1762
-0.190078	0.014922		6.942677	0.819411	9.2980
-0.090078	0.021827		7.013362	0.823273	9.3090
0.009922	0.030422		7.748213	0.860116	9.4193
0.109922	0.040572		7.823285	0.863544	9.4294
0.209922	0.052139		8.620609	0.896544	9.5325
0.309922	0.064982		8.668586	0.898333	9.5381
0.409922	0.078954		9.547560	0.927632	9.6355
0.509922	0.093908		9.561136	0.928033	9.6370
0.609922	0.109694		10.456866	0.951490	9.7213
0.709922	0.126160		10.568825	0.954009	9.7315
0.809922	0.143149		11.396560	0.970157	9.7966
0.909922	0.160507		11.637610	0.974060	9.8149
1.009922	0.178077		12.364755	0.983930	9.8612
1.109922	0.195709		12.751189	0.988073	9.8850
1.143833	0.201683	6.8900	13.356624	0.993228	9.9149
1.217284	0.214591	6.9933	13.889358	0.996532	9.9402
1.265575	0.223050	7.0575	14.374529	0.998689	9.9567
1.419447	0.249732	7.2390	14.973573	1.000427	9.9764
1.431991	0.251885	7.2529	15.406717	1.001164	9.9846
1.652353	0.288970	7.4656	15.940046	1.001655	9.9944
1.665389	0.291120	7.4773	16.446398	1.001834	9.9975
1.917962	0.331665	7.6763	16.787935	1.001875	9.9996
1.965549	0.339074	7.7109	17.493051	1.001887	9.9999
2.218595	0.377238	7.8742	17.580351	1.001887	10.0000
2.431586	0.407812	7.9991			
2.556467	0.425110	8.0651			
2.933887	0.474691	8.2467			
2.956914	0.477589	8.2569			
3.354582	0.525538	8.4181			
3.528437	0.545286	8.4823			
3.820592	0.576928	8.5826			
4.145264	0.609941	8.6842			
4.334959	0.628238	8.7400			
4.804417	0.670611	8.8657			
4.900955	0.678828	8.8902			
5.503677	0.726666	9.0293			

M_1	θ_2	γ	z_1	π	a
10.00	10.00	1.6667	18.824077	0.200	0.080592
$(A/A^*)_1^{1/2}$		$1/\rho_1$	$\dot{M}_B$	$\ddot{M}_B$	a_0
8.142166		0.394413	1.640748	-0.267894	0.029958
a_1		a_2	M_A	z_A	r_A
-0.002221		0.000038	3.135991	1.257208	0.221680

CONTOUR #30

z	r	M	z	r	M
0.407478	0.122817		5.883920	0.766111	7.7004
0.507478	0.124726		6.188790	0.785395	7.8419
0.607478	0.130190		6.531493	0.805538	7.9920
0.707478	0.138796		7.177093	0.839473	8.2527
0.807478	0.150105		7.224588	0.841771	8.2709
0.907478	0.163658		7.983938	0.875332	8.5402
1.007478	0.178976		8.234652	0.885140	8.6212
1.107478	0.195566		8.804814	0.905360	8.7968
1.207478	0.212921		9.360066	0.922469	8.9508
1.307478	0.230544		9.682339	0.931322	9.0364
1.313039	0.231525	3.2671	10.549067	0.951656	9.2409
1.371911	0.241904	3.4029	10.607746	0.952857	9.2542
1.408395	0.248328	3.4852	11.567812	0.969833	9.4457
1.434859	0.252984	3.5435	11.792694	0.973106	9.4843
1.502635	0.264905	3.6891	12.543095	0.982382	9.6082
1.576666	0.277884	3.8428	13.086055	0.987635	9.6831
1.584732	0.279293	3.8590	13.511781	0.990998	9.7398
1.658431	0.292138	4.0035	14.421551	0.996280	9.8374
1.750655	0.308088	4.1758	14.451655	0.996414	9.8405
1.789766	0.314792	4.2453	15.343603	0.999465	9.9120
1.856517	0.326147	4.3608	15.786535	1.000396	9.9370
1.980415	0.346900	4.5621	16.174860	1.000963	9.9563
2.026502	0.354491	4.6323	16.943311	1.001580	9.9844
2.127361	0.370857	4.7811	17.171320	1.001668	9.9882
2.297092	0.397593	5.0129	17.657515	1.001774	9.9962
2.303229	0.398540	5.0210	18.335216	1.001814	9.9996
2.511624	0.429880	5.2764	18.563396	1.001815	9.9997
2.603608	0.443203	5.3807	18.997532	1.001816	10.0000
2.755134	0.464488	5.5456			
2.947276	0.490333	5.7394			
3.030683	0.501160	5.8200			
3.330841	0.538302	6.0850			
3.691118	0.579368	6.3822			
3.753033	0.586063	6.4288			
4.219178	0.633432	6.7593			
4.442059	0.654283	6.9072			
4.728497	0.679539	7.0829			
5.277318	0.723510	7.3961			
5.281875	0.723852	7.3985			

M_1	θ_2	γ	z_1	π	a
11.00	10.00	1.2000	18.360439	0.100	0.032283
$(A/A^*)_1^{1/2}$	$1/\rho_1$	$\dot{M}_B$	$\ddot{M}_B$	a_0	
274.138380	0.249625	0.555017	-0.112125	0.032803	
a_1	a_2	M_A	z_A	r_A	
-0.002336	-0.000313	7.239797	0.906569	0.159852	

CONTOUR # 31

z	r	M	z	r	M
-0.436023	0.003648		6.326004	0.764827	10.0510
-0.336023	0.004871		7.051496	0.806990	10.1858
-0.236023	0.008437		7.160342	0.812797	10.2040
-0.136023	0.014185		7.924946	0.850201	10.3263
-0.036023	0.021951		8.036914	0.855188	10.3424
0.063977	0.031559		8.875844	0.889038	10.4577
0.163977	0.042833		8.954439	0.891895	10.4673
0.263977	0.055587		9.905953	0.922744	10.5789
0.363977	0.069633		9.911449	0.922902	10.5794
0.463977	0.084777		10.902994	0.948206	10.6779
0.563977	0.100821		11.014526	0.950651	10.6886
0.663977	0.117566		11.929704	0.968072	10.7641
0.763977	0.134809		12.194654	0.972256	10.7853
0.863977	0.152345		12.989596	0.982800	10.8384
0.963977	0.169975		13.427425	0.987388	10.8667
0.997787	0.175932	7.4059	14.079498	0.992820	10.9002
1.073178	0.189178	7.5326	14.690754	0.996540	10.9307
1.110992	0.195800	7.5924	15.195236	0.998746	10.9487
1.269615	0.223276	7.8136	15.891987	1.000741	10.9728
1.270672	0.223457	7.8149	16.330186	1.001476	10.9815
1.498358	0.261674	8.0720	16.954264	1.002049	10.9936
1.500768	0.262070	8.0744	17.476571	1.002229	10.9970
1.765967	0.304436	8.3160	17.875565	1.002278	10.9996
1.798484	0.309470	8.3432	18.626667	1.002289	10.9999
2.069177	0.350026	8.5428	18.731603	1.002289	11.0000
2.279735	0.379983	8.6828			
2.413155	0.398285	8.7625			
2.800712	0.448618	8.9717			
2.828569	0.452080	8.9854			
3.236345	0.500592	9.1691			
3.430276	0.522288	9.2482			
3.722575	0.553447	9.3589			
4.084131	0.589576	9.4829			
4.263156	0.606533	9.5406			
4.786787	0.652890	9.6933			
4.862128	0.659174	9.7141			
5.523737	0.710653	9.8795			
5.535221	0.711488	9.8821			
6.252361	0.760205	10.0367			

M_1	θ_A	γ	Z_1	π	a
11.00	10.00	1.6667	20.029569	0.200	0.092875
$(A/A^*)_1^{1/2}$	$1/\rho_1$	$\dot{M}_B$	$\ddot{M}_B$	a_0	
9.345986	0.423403	1.838404	-0.319055	0.029673	
a_1	a_2	M_A	Z_A	r_A	
-0.002279	0.000059	3.228819	1.129102	0.199091	

CONTOUR # 3 2

z	r	M
0.337552	0.106998	
0.437552	0.109042	
0.537552	0.114870	
0.637552	0.124004	
0.737552	0.135932	
0.837552	0.150119	
0.937552	0.166008	
1.037552	0.183024	
1.137552	0.200580	
1.180017	0.208070	3.3631
1.233641	0.217525	3.5023
1.272274	0.224327	3.6004
1.290899	0.227605	3.6466
1.352334	0.238413	3.7954
1.419138	0.250138	3.9522
1.440143	0.253812	4.0000
1.492529	0.262952	4.1163
1.574592	0.277192	4.2909
1.636468	0.287828	4.4163
1.668212	0.293248	4.4790
1.776791	0.311589	4.6819
1.864530	0.326135	4.8355
1.905509	0.332840	4.9051
2.059435	0.357507	5.1489
2.126907	0.368040	5.2482
2.244375	0.385974	5.4149
2.425553	0.412635	5.6523
2.464673	0.418230	5.7016
2.720106	0.453451	5.9996
2.762546	0.459080	6.0459
3.005574	0.490191	6.2989
3.140441	0.506649	6.4277
3.559790	0.554480	6.8040
3.715883	0.571082	6.9357
4.023826	0.602117	7.1725
4.527739	0.648398	7.5328
4.532320	0.648794	7.5359
5.091856	0.694381	7.8851
5.430755	0.719384	8.0814
5.699275	0.737929	8.2270
6.357039	0.779112	8.5578
6.424351	0.783002	8.5894
7.067141	0.817522	8.8736
7.500829	0.838258	9.0498
7.847480	0.853484	9.1836
8.660521	0.884990	9.4697
8.697491	0.886288	9.4821
9.615903	0.915330	9.7628
9.893883	0.922946	9.8390
10.593182	0.939994	10.0222
11.198806	0.952494	10.1623
11.617022	0.960010	10.2552
12.569049	0.974124	10.4387
12.669849	0.975388	10.4574
13.729683	0.986436	10.6255
13.993542	0.988584	10.6601
14.770702	0.993742	10.7586
15.464421	0.997029	10.8281
15.768561	0.998128	10.8577
16.704473	1.000468	10.9257
16.969994	1.000885	10.9388
17.568799	1.001537	10.9676
18.363819	1.001935	10.9895
18.495924	1.001965	10.9911
19.104133	1.002042	10.9981
19.812707	1.002058	10.9999
20.028905	1.002058	10.9999
20.512177	1.002058	11.0000

M_1	θ_A	γ	z_1	π	α
12.00	10.00	1.2000	19.464629	0.100	0.042083
$(A/A^*)_1^{1/2}$	$1/\rho_1$	$\dot{M}_1$	$\ddot{M}_1$	a_0	
409.507100	0.285007	0.608941	-0.125610	0.031209	
a_1	a_2	M_A	z_A	r_A	
-0.001997	-0.000267	7.712475	0.789752	0.139255	

CONTOUR # 33

z	r	M	z	r	M
-0.386164	0.002442		7.299788	0.802660	11.0921
-0.286164	0.003834		8.086984	0.840327	11.2262
-0.186164	0.007876		8.240962	0.847036	11.2495
-0.086164	0.014356		9.114054	0.881475	11.3767
0.013836	0.023056		9.228815	0.885554	11.3915
0.113836	0.033745		10.231874	0.917338	11.5157
0.213836	0.046187		10.261737	0.918178	11.5190
0.313836	0.060135		11.334604	0.944894	11.6310
0.413836	0.075339		11.439904	0.947153	11.6417
0.513836	0.091541		12.446877	0.965934	11.7289
0.613836	0.108479		12.730635	0.970326	11.7527
0.713836	0.125888		13.597261	0.981614	11.8133
0.813836	0.143501		14.082558	0.986613	11.8461
0.872991	0.153929	7.8933	14.782193	0.992360	11.8838
0.949309	0.167335	8.0455	15.472199	0.996511	11.9198
0.977559	0.172280	8.0984	15.996992	0.998789	11.9395
1.126943	0.198154	8.3442	16.792686	1.001062	11.9684
1.140888	0.200540	8.3643	17.234162	1.001805	11.9777
1.348785	0.235362	8.6377	17.952840	1.002474	11.9925
1.366804	0.238313	8.6585	18.484945	1.002660	11.9963
1.629927	0.280105	8.9340	18.947788	1.002720	11.9995
1.646700	0.282689	8.9501	19.740376	1.002732	11.9999
1.933653	0.325427	9.1909	19.865515	1.002732	12.0000
2.139659	0.354500	9.3456			
2.281417	0.373774	9.4408			
2.676542	0.424549	9.6789			
2.708686	0.428497	9.6965			
3.124334	0.477340	9.9038			
3.337517	0.500858	9.9995			
3.627827	0.531353	10.1202			
4.025545	0.570462	10.2693			
4.191544	0.585924	10.3276			
4.769032	0.636142	10.5104			
4.820351	0.640344	10.5258			
5.519604	0.693869	10.7147			
5.563290	0.696985	10.7253			
6.294060	0.745636	10.8945			
6.406749	0.752562	10.9179			
7.148296	0.794750	11.0651			

M_1	θ_B	γ	z_1	τ	a
12.00	10.00	1.6667	21.234141	0.200	0.109583
$(A/A^*)_1^{1/2}$	$1/\rho_1$	$\dot{M}_B$	$\ddot{M}_B$	a_0	
10.607763	0.459914	2.053012	-0.384102	0.029788	
a_1	a_2	M_A	z_A	r_A	
-0.002440	0.000083	3.292069	1.015460	0.179053	

CONTOUR # 34

z	r	M
0.286749	0.094271	
0.386749	0.096484	
0.486749	0.102764	
0.586749	0.112540	
0.686749	0.125204	
0.786749	0.140114	
0.886749	0.156606	
0.986749	0.173993	
1.061692	0.187206	3.4286
1.110338	0.195784	3.5700
1.148905	0.202575	3.6797
1.162214	0.204917	3.7167
1.217698	0.214682	3.8676
1.277757	0.225231	4.0261
1.305967	0.230170	4.0984
1.343366	0.236703	4.1920
1.416017	0.249344	4.3671
1.490495	0.262187	4.5386
1.498159	0.263500	4.5558
1.592228	0.279507	4.7571
1.702933	0.298003	4.9795
1.705957	0.298502	4.9852
1.834393	0.319419	5.2209
1.955207	0.338540	5.4266
1.993339	0.344458	5.4894
2.184624	0.373334	5.7813
2.240646	0.381524	5.8606
2.412123	0.405880	6.0936
2.564409	0.426626	6.2853
2.675288	0.441226	6.4188
2.928511	0.473087	6.7030
2.967888	0.477859	6.7452
3.337064	0.520460	7.1078
3.722317	0.561097	7.4596
3.788137	0.567679	7.5145
4.289254	0.614766	7.9079
4.587458	0.640406	8.1259
4.838913	0.660782	8.2963
5.440356	0.705375	8.6754
5.557492	0.713420	8.7445
6.096852	0.748112	9.0423
6.625908	0.778640	9.3118
6.805848	0.788292	9.3985
7.592585	0.826663	9.7489
7.789755	0.835349	9.8297
8.456652	0.862308	10.0890
9.043877	0.883163	10.2962
9.395682	0.894473	10.4147
10.385877	0.922101	10.7145
10.405295	0.922583	10.7201
11.477063	0.946190	10.9988
11.803923	0.952256	11.0734
12.593230	0.965010	11.2465
13.295087	0.974279	11.3792
13.732747	0.979168	11.4590
14.850544	0.988965	11.6305
14.870002	0.989103	11.6334
15.977897	0.995501	11.7690
16.455112	0.997429	11.8146
17.029941	0.999205	11.8679
18.008067	1.001099	11.9341
18.099514	1.001214	11.9381
18.905351	1.001917	11.9732
19.728155	1.002196	11.9924
19.765845	1.002202	11.9927
20.496207	1.002261	11.9990
21.236658	1.002268	11.9999
21.439478	1.002268	11.9999
21.972047	1.002268	12.0000

M_1	θ_2	γ	z_1	π	a
14.00	10.00	1.2000	20.686152	0.050	0.051818
$(A/A^*)_1^{1/2}$	$1/\rho_1$	$\dot{M}_B$	$\ddot{M}_B$	a_0	
843.802940	0.316260	0.600814	-0.102714	0.122849	
a_1	a_2	M_A	z_A	r_A	
-0.021578	-0.002252	8.890079	0.705950	0.124478	

CONTOUR # 35

z	r	M	z	r	M
-0.353763	0.001185		10.318295	0.893327	13.3065
-0.253763	0.002726		10.732905	0.905387	13.3637
-0.153763	0.007181		11.361958	0.921938	13.4379
-0.053763	0.014290		12.348460	0.943993	13.5499
0.046237	0.023779		12.452687	0.946052	13.5598
0.146237	0.035361		13.569241	0.965394	13.6630
0.246237	0.048739		14.107867	0.972966	13.7111
0.346237	0.063606		14.727534	0.980421	13.7559
0.446237	0.079647		15.923535	0.991433	13.8391
0.546237	0.096541		15.975706	0.991314	13.8427
0.646237	0.113961		17.137949	0.998628	13.9023
0.746237	0.131576		17.854198	1.001285	13.9378
0.815193	0.143675	9.1671	18.385243	1.002624	13.9543
0.905253	0.159266	9.3544	19.591593	1.004182	13.9905
1.044212	0.182747	9.6110	19.650745	1.004208	13.9909
1.154277	0.200831	9.7813	20.923715	1.004480	13.9999
1.406045	0.240422	10.1212	20.927407	1.004480	14.0000
1.457959	0.248296	10.1821			
1.822919	0.301040	10.5564			
1.852712	0.305152	10.5835			
2.257160	0.358456	10.9088			
2.364544	0.371843	10.9849			
2.768201	0.419653	11.2442			
2.935961	0.438406	11.3394			
3.364466	0.483677	11.5631			
3.562368	0.503372	11.6546			
4.054996	0.549453	11.8665			
4.241029	0.565808	11.9374			
4.849292	0.615768	12.1550			
4.970615	0.625106	12.1934			
5.750021	0.680802	12.4267			
5.757439	0.681296	12.4288			
6.570093	0.732031	12.6338			
6.790883	0.744646	12.6871			
7.438357	0.779099	12.8243			
7.958507	0.804167	12.9300			
8.355318	0.821842	13.0005			
9.269657	0.858265	13.1563			
9.320971	0.860134	13.1639			

M_1	θ_A	γ	Z_1	π	a
14.00	10.00	1.4000	21.178679	0.075	0.039088
$(A/A^*)_1^{1/2}$	$1/\rho_1$	$\dot{M}_B$	$\ddot{M}_B$	a_0	
51.820684	0.274679	1.208108	-0.174717	0.105416	
a_1	a_2	M_A	Z_A	r_A	
-0.011697	-0.000908	6.402831	0.914520	0.161254	

CONTOUR # 36

Z	r	M
-0.305613	0.019297	
-0.205613	0.020640	
-0.105613	0.024544	
-0.005613	0.030813	
0.094387	0.039244	
0.194387	0.049626	
0.294387	0.061738	
0.394387	0.075355	
0.494387	0.090244	
0.594387	0.106167	
0.694387	0.122882	
0.794387	0.140144	
0.894387	0.157705	
0.982270	0.173200	6.6087
1.072675	0.189071	6.8625
1.146640	0.201886	7.0455
1.217232	0.213943	7.2086
1.432619	0.249526	7.6387
1.441280	0.250915	7.6547
1.775658	0.302272	8.1901
1.823263	0.309228	8.2593
2.180572	0.358941	8.7175
2.277733	0.371720	8.8305
2.652044	0.418386	9.2228
2.794351	0.435104	9.3582
3.194993	0.479535	9.7072
3.368124	0.497589	9.8442
3.814366	0.541338	10.1715
3.996122	0.558061	10.2926
4.515015	0.602755	10.6161
4.676525	0.615781	10.7077
5.301602	0.662758	11.0412
5.408306	0.670246	11.0930
6.178462	0.720341	11.4464
6.190474	0.721068	11.4514
7.018037	0.767728	11.7800
7.150212	0.774561	11.8302
7.893492	0.810229	12.0850
8.218777	0.824413	12.1920
8.816618	0.848451	12.3686
9.385393	0.869035	12.5300
9.786569	0.882304	12.6317
10.649030	0.907681	12.8419
10.802029	0.911747	12.8750
11.857271	0.936698	13.0948
12.005330	0.939770	13.1246
12.950636	0.957242	13.2911
13.442890	0.964918	13.3748
14.084528	0.973612	13.4684
14.939228	0.983082	13.5887
15.255546	0.986011	13.6257
16.451569	0.994687	13.7611
16.459017	0.994729	13.7617
17.686275	1.000147	13.8677
17.976089	1.000982	13.8919
18.938949	1.002857	13.9462
19.350261	1.003279	13.9687
20.207843	1.003706	13.9902
20.484004	1.003749	13.9969
21.466849	1.003785	14.0000

M_1	β_1	γ	z_1	τ	a
14.00	10.00	1.6667	21.671206	0.100	0.046762
$(A/A^*)_1^{1/2}$	$1/\rho_1$	$\dot{M}_B$	$\ddot{M}_B$	a_0	
13.294786	0.300436	1.925446	-0.183094	0.100314	
a_1	a_2	M_A	z_A	r_A	
-0.009662	-0.000318	4.494650	1.162637	0.205004	

CONTOUR # 37

z	r	M
0.047109	0.075217	
0.147109	0.076683	
0.247109	0.080930	
0.347109	0.087723	
0.447109	0.096816	
0.547109	0.107953	
0.647109	0.120868	
0.747109	0.135287	
0.847109	0.150926	
0.947109	0.167498	
1.047109	0.184710	
1.147109	0.202266	
1.211287	0.213583	4.6411
1.264499	0.222966	4.7988
1.327802	0.234093	4.9778
1.401177	0.246870	5.1714
1.409511	0.248311	5.1927
1.520523	0.267284	5.4540
1.675026	0.292851	5.7823
1.690368	0.295329	5.8122
1.875374	0.324413	6.1557
2.031898	0.347844	6.4169
2.264922	0.380878	6.7810
2.426826	0.402624	7.0089
2.720663	0.439810	7.3953
2.878251	0.458629	7.5849
3.235937	0.498771	7.9865
3.388765	0.514902	8.1454
3.807484	0.556366	8.5515
3.960802	0.570601	8.6905
4.433410	0.611707	9.0898
4.596552	0.624971	9.2195
5.112444	0.664191	9.6017
5.297858	0.677323	9.7317
5.843652	0.713391	10.0878
6.066133	0.727037	10.2258
6.626115	0.758990	10.5484
6.902190	0.773548	10.7002
7.458943	0.800761	10.9838
7.806076	0.816362	11.1530
8.341140	0.838546	11.3940
8.776756	0.855050	11.5822
9.271518	0.872240	11.7788
9.811771	0.889267	11.9852
10.248805	0.901800	12.1379
10.906695	0.918760	12.3593
11.271196	0.927224	12.4707
12.054188	0.943386	12.7015
12.336886	0.948572	12.7764
13.243001	0.963140	13.0085
13.443368	0.965951	13.0541
14.455073	0.978171	13.2769
14.587887	0.979536	13.3023
15.733126	0.989336	13.5146
15.767541	0.989576	13.5200
16.977714	0.996396	13.7023
17.022361	0.996587	13.7089
18.214619	1.000441	13.8468
18.255157	1.000530	13.8513
19.368608	1.002221	13.9410
19.472108	1.002307	13.9458
20.333552	1.002743	13.9852
20.742413	1.002812	13.9919
21.177270	1.002841	13.9989
21.975271	1.002847	14.0000

M_1	θ_A	γ	Z_1	π	a
16.00	10.00	1.2000	22.790855	0.050	0.083064
$(A/A^*)_1^{V2}$	$1/\rho_1$	$\dot{M}_B$	$\ddot{M}_B$	a_0	
1594.170000	0.400415	0.689452	-0.119984	0.113270	
a_1	a_2	M_A	Z_A	r_A	
-0.017224	-0.001865	9.723957	0.555830	0.098008	

CONTOUR #38

z	r	M
-0.281164	0.000627	
-0.181164	0.002564	
-0.081164	0.008104	
0.018836	0.016820	
0.118836	0.028260	
0.218836	0.041949	
0.318836	0.057392	
0.418836	0.074079	
0.518836	0.091489	
0.618836	0.109098	
0.648242	0.114249	10.0396
0.738261	0.129807	10.2889
0.857396	0.149876	10.5775
0.972595	0.168706	10.8082
1.218924	0.207068	11.2305
1.265328	0.214026	11.2988
1.624963	0.265327	11.7554
1.677810	0.272496	11.8138
2.061526	0.322113	12.1871
2.213681	0.340659	12.3158
2.584611	0.383542	12.5987
2.820104	0.409165	12.7554
3.205140	0.448696	12.9905
3.491848	0.476365	13.1436
3.934899	0.516486	13.3636
4.225914	0.541217	13.4901
4.786341	0.585637	13.7187
5.020754	0.603030	13.8025
5.772587	0.654702	14.0562
5.875756	0.661315	14.0867
6.784473	0.715348	14.3420
6.908098	0.722117	14.3753
7.744913	0.764809	14.5716
8.206606	0.786103	14.6754
8.764461	0.809895	14.7842
9.679780	0.844747	14.9553
9.843392	0.850447	14.9816
10.964631	0.885822	15.1558
11.339085	0.896218	15.2120
12.137187	0.916294	15.3137
13.187014	0.938695	15.4425
13.368038	0.942114	15.4611
14.631565	0.962938	15.5863
15.213379	0.970759	15.6421
15.944412	0.979195	15.6985
17.303616	0.991217	15.7996
17.375140	0.991720	15.8048
18.685127	0.999158	15.8765
19.551301	1.002292	15.9222
20.107587	1.003670	15.9408
21.552410	1.005543	15.9876
21.555969	1.005545	15.9878
23.007414	1.005879	15.9996
23.056409	1.005880	16.0000

M_1	β_1	γ	z_1	τ	a
16.00	10.00	1.4000	23.333494	0.075	0.054102
$(A/A^*)_1^{1/2}$	$1/\rho_1$	$\dot{M}_1$	$\ddot{M}_1$	a_0	
71.725543	0.323155	1.400095	-0.208714	0.097731	
a_1	a_2	M_A	z_A	r_A	
-0.009381	-0.000735	6.838789	0.763379	0.134604	

CONTOUR #39

z	r	M	z	r	M
-0.273723	0.013942		11.396045	0.902939	14.6025
-0.173723	0.015515		12.579494	0.929939	14.8693
-0.073723	0.020061		12.793020	0.934204	14.9159
0.026277	0.027307		13.810523	0.952339	15.1093
0.126277	0.036965		14.420539	0.961542	15.2212
0.226277	0.048736		15.090847	0.970350	15.3265
0.326277	0.062308		16.120015	0.981468	15.4826
0.426277	0.077360		16.416382	0.984156	15.5200
0.526277	0.093562		17.780392	0.994023	15.6869
0.626277	0.110578		17.841669	0.994370	15.6942
0.726277	.0.128065		19.175193	1.000326	15.8195
0.820577	0.144691	7.0567	19.585370	1.001552	15.8569
0.896702	0.158067	7.3256	20.602043	1.003644	15.9210
0.986218	0.173562	7.6032	21.161431	1.004288	15.9554
1.021624	0.179604	7.7053	22.050330	1.004802	15.9826
1.222645	0.212905	8.2055	22.447655	1.004887	15.9945
1.267175	0.220027	8.3023	23.507614	1.004943	15.9999
1.605517	0.271371	8.9577	23.526622	1.004943	16.0000
1.610102	0.272034	8.9655			
2.022147	0.328618	9.5940			
2.072219	0.335096	9.6627			
2.509226	0.388584	10.1984			
2.611828	0.400374	10.3116			
3.077615	0.450816	10.7796			
3.219009	0.465169	10.9076			
3.733778	0.514223	11.3379			
3.890605	0.528212	11.4562			
4.484110	0.577706	11.8738			
4.624686	0.589660	11.9632			
5.334769	0.640160	12.3872			
5.419913	0.645916	12.4331			
6.274960	0.699522	12.8691			
6.291694	0.700495	12.8773			
7.184773	0.748919	13.2685			
7.360736	0.757651	13.3422			
8.152578	0.794107	13.6399			
8.544832	0.810512	13.7812			
9.177830	0.834914	13.9853			
9.846047	0.858101	14.1920			
10.259443	0.871212	14.3059			
11.263674	0.899562	14.5715			

M_1	θ_n	γ	z_1	π	a
16.00	10.00	1.6667	23.876134	0.100	0.057850
$(A/A^*)_1^{1/2}$	$1/\rho_1$	$\dot{M}_B$	$\ddot{M}_B$	a_0	
16.185564	0.334162	2.228553	-0.221001	0.093604	
a_1	a_2	M_A	z_A	r_A	
-0.008034	-0.000245	4.708385	1.012161	0.178471	

CONTOUR # 4 0

z	r	M
0.009220	0.061783	
0.109220	0.063409	
0.209220	0.068099	
0.309220	0.075560	
0.409220	0.085485	
0.509220	0.097552	
0.609220	0.111425	
0.709220	0.126759	
0.809220	0.143201	
0.909220	0.160387	
1.009220	0.177953	
1.054290	0.185901	4.8581
1.099903	0.193945	5.0185
1.153489	0.203376	5.1991
1.221864	0.215312	5.4150
1.245127	0.219335	5.4832
1.314775	0.231263	5.6797
1.445504	0.253115	6.0147
1.532276	0.267157	6.2170
1.623215	0.281484	6.4186
1.842818	0.314556	6.8613
1.875362	0.319268	6.9212
2.277120	0.374042	7.6072
2.277602	0.374104	7.6079
2.741993	0.430481	8.2748
2.784058	0.435260	8.3311
3.272653	0.487500	8.9281
3.358018	0.496026	9.0253
3.872314	0.544243	9.5664
3.996954	0.555144	9.6884
4.543999	0.599939	10.1884
4.699444	0.611797	10.3205
5.290396	0.653883	10.7928
5.464441	0.665411	10.9220
6.113692	0.705423	11.3778
6.291044	0.715565	11.4933
7.015432	0.753961	11.9415
7.178335	0.761948	12.0348
7.996239	0.798954	12.4815
8.125276	0.804333	12.5465
9.055542	0.839925	12.9950
9.130674	0.842560	13.0283
10.191070	0.876471	13.4789
10.193133	0.876531	13.4797
11.309306	0.906156	13.8975
11.398703	0.908282	13.9298
12.478742	0.931493	14.2837
12.670209	0.935138	14.3443
13.699319	0.952615	14.6374
13.993324	0.956973	14.7184
14.968109	0.969647	14.9575
15.348563	0.973884	15.0479
16.281425	0.982784	15.2418
16.788851	0.986785	15.3440
17.635871	0.992301	15.4884
18.256581	0.995490	15.5911
19.026612	0.998567	15.6941
19.676636	1.000488	15.7785
20.447504	1.002082	15.8533
20.971737	1.002802	15.9029
21.890862	1.003522	15.9585
22.093056	1.003603	15.9705
23.050555	1.003785	15.9960
23.346244	1.003796	15.9974
23.918983	1.003804	16.0000
24.786819	1.003804	16.0000

M_1	β_1	γ	z_1	π	a
18.00	10.00	1.2000	24.894510	0.050	0.130666
$(A/A^*)_1^{1/2}$	$1/\rho_1$	$\dot{M}_B$	$\ddot{M}_B$	a_0	
2810.843700	0.502211	0.782201	-0.138785	0.104996	
a_1	a_2	M_A	z_A	r_A	
-0.013908	-0.001563	10.482792	0.442347	0.077998	

CONTOUR #41

z	r	M	z	r	M
-0.224992	0.000356		14.262258	0.938534	17.3546
-0.124992	0.002764		15.670540	0.960737	17.5032
-0.024992	0.009556		16.290134	0.968744	17.5665
0.075008	0.020046		17.135399	0.978150	17.6357
0.175008	0.033499		18.655888	0.991148	17.7556
0.275008	0.049141		18.748125	0.991776	17.7627
0.375008	0.066166		20.202691	0.999829	17.8472
0.475008	0.083750		21.226310	1.003468	17.9044
0.520019	0.091650	10.8336	21.799047	1.004876	17.9250
0.608272	0.106880	11.1533	23.421407	1.007068	17.9814
0.708724	0.123756	11.4671	23.505016	1.007110	17.9842
0.827226	0.143035	11.7692	25.058699	1.007490	17.9989
1.066013	0.179877	12.2798	25.171891	1.007492	18.0000
1.107249	0.185992	12.3549			
1.458719	0.235508	12.8980			
1.532710	0.245379	12.9961			
1.893641	0.291206	13.4140			
2.088253	0.314419	13.6071			
2.423768	0.352318	13.9065			
2.725330	0.384295	14.1382			
3.062672	0.417993	14.3758			
3.437961	0.453168	14.6042			
3.825069	0.487159	14.8230			
4.222942	0.519904	15.0179			
4.726586	0.558501	15.2492			
5.078493	0.583727	15.3895			
5.783844	0.630490	15.6547			
6.004345	0.644118	15.7267			
6.999667	0.700622	16.0348			
7.014100	0.701381	16.0391			
8.047590	0.752082	16.3044			
8.437083	0.769328	16.4003			
9.165376	0.799170	16.5545			
10.066897	0.832097	16.7376			
10.353773	0.841691	16.7875			
11.596542	0.879030	16.9953			
11.918291	0.887591	17.0474			
12.894304	0.911162	17.1807			
13.996593	0.933713	17.3256			

M_1	β_1	γ	z_1	τ	a
18.00	10.00	1.4000	25.487237	0.075	0.073958
$(A/A^*)_1^{1/2}$	$1/\rho_1$	$\dot{M}_B$	$\ddot{M}_B$	a_0	
95.704122	0.377831	1.602269	-0.246961	0.090984	
a_1	a_2	M_A	z_A	r_A	
-0.007635	-0.000596	7.215347	0.644542	0.113650	

CONTOUR # 4 2

z	r	M
-0.242481	0.010449	
-0.142481	0.012280	
-0.042481	0.017533	
0.057519	0.025830	
0.157519	0.036772	
0.257519	0.049938	
0.357519	0.064893	
0.457519	0.081186	
0.557519	0.098357	
0.657519	0.115939	
0.692961	0.122189	7.4423
0.756884	0.133431	7.7212
0.857083	0.150766	8.1040
0.863681	0.151892	8.1274
1.040863	0.181362	8.6692
1.130751	0.195712	8.9095
1.289421	0.220114	9.2906
1.471695	0.246785	9.6733
1.735900	0.283125	10.1639
1.886689	0.302756	10.4118
2.269742	0.349503	10.9697
2.384007	0.362641	11.1205
2.882766	0.416364	11.7054
2.971889	0.425372	11.8017
3.570447	0.482038	12.3777
3.658517	0.489831	12.4567
4.330284	0.545478	12.9947
4.451882	0.554854	13.0862
5.160506	0.605946	13.5634
5.359710	0.619256	13.6903
6.060373	0.662940	14.0899
6.389193	0.681844	14.2680
7.029361	0.716074	14.5786
7.546895	0.741442	14.8180
8.066753	0.765038	15.0331
8.837992	0.796905	15.3381
9.171804	0.809601	15.4559
10.265604	0.847155	15.8253
10.343460	0.849595	15.8487
11.571786	0.884664	16.2035
11.830684	0.891236	16.2756
12.861100	0.914954	16.5282
13.526285	0.928285	16.6852
14.212383	0.940557	16.8262
15.337442	0.957744	17.0492
15.621996	0.961537	17.0975
17.081655	0.978001	17.3370
17.235631	0.979448	17.3616
18.585767	0.990165	17.5411
19.164237	0.993707	17.6156
20.136415	0.998444	17.7152
21.129229	1.001864	17.8138
21.726783	1.003313	17.8560
22.915602	1.005121	17.9376
23.346057	1.005468	17.9535
24.366621	1.005891	17.9905
24.982418	1.005955	17.9955
25.546021	1.005974	17.9999
26.623302	1.005974	17.9999
26.681742	1.005974	18.0000

M_1	β_A	γ	z_1	π	a
18.00	10.00	1.6667	26.079963	0.100	0.071437
$(A/A^*)_1^{1/2}$	$1/\rho_1$	$\dot{M}_B$	$\ddot{M}_B$	a_0	
19.266190	0.371336	2.546185	-0.265215	0.087702	
a_1	a_2	M_A	z_A	r_A	
-0.006811	-0.000184	4.880203	0.889885	0.156911	

CONTOUR # 4 3

z	r	M
-0.012653	0.051904	
0.087347	0.053705	
0.187347	0.058875	
0.287347	0.067050	
0.387347	0.077845	
0.487347	0.090855	
0.587347	0.105661	
0.687347	0.121828	
0.787347	0.138912	
0.887347	0.156463	
0.926621	0.163389	5.0320
0.965997	0.170335	5.1937
1.011618	0.178372	5.3739
1.068833	0.188388	5.5869
1.114890	0.196360	5.7462
1.146132	0.201718	5.8503
1.255023	0.220077	6.1821
1.396289	0.242998	6.5708
1.408791	0.244975	6.6035
1.605740	0.275151	7.0741
1.737396	0.294288	7.3560
2.035338	0.334919	7.9460
2.140356	0.348423	8.1322
2.548977	0.397539	8.8014
2.610362	0.404471	8.8931
3.140435	0.460369	9.6243
3.151863	0.461498	9.6389
3.769589	0.518689	10.3679
3.805822	0.521813	10.4076
4.466815	0.575178	11.0809
4.544356	0.580996	11.1542
5.246912	0.630225	11.7763
5.355396	0.637281	11.8653
6.112960	0.683160	12.4519
6.237936	0.690173	12.5415
7.067309	0.733354	13.1053
7.191262	0.739318	13.1831
8.111356	0.780227	13.7334
8.214204	0.784439	13.7902
9.245176	0.823257	14.3333
9.305494	0.825339	14.3625
10.463826	0.861895	14.8996
10.466993	0.861986	14.9010
11.685541	0.893985	15.3981
11.772958	0.896048	15.4325
12.970255	0.921646	15.8601
13.154868	0.925158	15.9237
14.315286	0.944923	16.2845
14.600175	0.949184	16.3702
15.717653	0.963924	16.6703
16.088736	0.968150	16.7667
17.173213	0.978823	17.0148
17.684491	0.983029	17.1280
18.678287	0.989872	17.3164
19.329279	0.993468	17.4361
20.227606	0.997417	17.5721
20.943634	0.999802	17.6774
21.814780	1.001918	17.7765
22.437354	1.002967	17.8455
23.431473	1.004002	17.9215
23.740281	1.004187	17.9446
24.838500	1.004515	17.9888
25.066540	1.004535	17.9915
25.794380	1.004564	17.9997
26.707177	1.004565	17.9999
26.714983	1.004565	18.0000

M_1	θ_1	γ	z_1	τ	a
20.00	10.00	1.2000	26.997433	0.050	0.201864
$(A/A^*)_1^{1/2}$	$1/\rho_1$	$\dot{M}_0$	$\ddot{M}_0$	a_0	
4686.092200	0.624215	0.879008	-0.159195	0.097760	
a_1	a_2	M_A	z_A	r_A	
-0.011340	-0.001322	11.176053	0.355476	0.062680	

CONTOUR # 44

z	r	M	z	r	M
-0.181430	0.000213		16.686984	0.958761	19.4138
-0.081430	0.003174		17.339286	0.966901	19.4843
0.018570	0.011381		18.301514	0.977274	19.5675
0.118570	0.023743		19.981412	0.991218	19.7073
0.218570	0.039089		20.095269	0.991974	19.7165
0.318570	0.056183		21.691654	1.000634	19.8143
0.418570	0.073774		22.879361	1.004808	19.8843
0.420539	0.074119	11.5585	23.460676	1.006234	19.9066
0.505837	0.088817	11.9564	25.259247	1.008774	19.9734
0.589173	0.102784	12.2872	25.439788	1.008874	19.9799
0.709533	0.122281	12.6716	27.078461	1.009306	19.9978
0.939363	0.157424	13.2758	27.277051	1.009311	20.0000
0.976082	0.162812	13.3572			
1.317684	0.210367	13.9903			
1.410719	0.222579	14.1360			
1.748231	0.264686	14.5947			
1.982515	0.292055	14.8640			
2.281690	0.325103	15.1723			
2.646713	0.362864	15.4923			
2.934396	0.390858	15.7231			
3.396791	0.433004	16.0401			
3.724110	0.460912	16.2484			
4.228849	0.501205	16.5239			
4.669868	0.533941	16.7495			
5.141473	0.566664	16.9570			
5.791828	0.608341	17.2268			
6.134239	0.628791	17.3492			
7.111290	0.682261	17.6798			
7.207879	0.687164	17.7080			
8.345823	0.740637	18.0244			
8.651935	0.753685	18.1062			
9.557879	0.789451	18.3129			
10.433244	0.820214	18.5044			
10.852161	0.833707	18.5823			
12.214455	0.872835	18.8258			
12.472692	0.879443	18.8705			
13.633887	0.906463	19.0393			
14.779055	0.929016	19.1994			
15.136156	0.935264	19.2407			

M_1	θ_1	γ	z_1	τ	a
20.00	10.00	1.4000	27.640229	0.075	0.099779
$(A/A^*)_1^{\nu 2}$	$1/\rho_1$	$\dot{M}_3$	$\ddot{M}_3$	a_0	
124.005400	0.438859	1.815225	-0.290011	0.085054	
a_1	a_2	M_A	z_A	r_A	
-0.006313	-0.000481	7.542847	0.549628	0.096914	

CONTOUR # 45

z	r	M	z	r	M
-0.214046	0.008064		12.347598	0.882712	17.9527
-0.114046	0.010180		13.441553	0.907217	18.2391
-0.014046	0.016201		14.201848	0.922077	18.4308
0.085954	0.025609		14.919458	0.934617	18.5881
0.185954	0.037855		16.190405	0.953646	18.8566
0.285954	0.052359		16.465172	0.957247	18.9063
0.385954	0.068519		18.067760	0.975166	19.1870
0.485954	0.085714		18.281972	0.977166	19.2234
0.585954	0.103321		19.723699	0.988601	19.4283
0.590779	0.104172	7.7764	20.414430	0.992874	19.5233
0.644489	0.113626	8.0615	21.434204	0.997946	19.6359
0.734426	0.129220	8.4801	22.602339	1.002132	19.7608
0.751410	0.132116	8.5499	23.191869	1.003654	19.8067
0.889095	0.155052	9.0591	24.609669	1.006024	19.9139
1.016516	0.175368	9.4669	24.984852	1.006376	19.9304
1.117057	0.190799	9.7546	26.242206	1.007022	19.9843
1.352647	0.225134	10.3368	26.800608	1.007105	19.9911
1.559254	0.253330	10.7843	27.533779	1.007144	19.9999
1.767988	0.280251	11.1805	28.624166	1.007145	19.9999
2.100276	0.320271	11.7347	28.735903	1.007145	20.0000
2.272147	0.339746	11.9927			
2.731319	0.388330	12.6005			
2.874994	0.402577	12.7750			
3.447437	0.455605	13.3900			
3.586419	0.467625	13.5287			
4.245751	0.520899	14.1129			
4.416162	0.533705	14.2545			
5.124545	0.583400	14.7783			
5.373683	0.599588	14.9522			
6.082889	0.642530	15.3934			
6.467873	0.664016	15.6206			
7.120477	0.697863	15.9641			
7.706888	0.725740	16.2580			
8.236407	0.749037	16.4946			
9.097345	0.783526	16.8617			
9.430168	0.795796	16.9880			
10.643584	0.836200	17.4283			
10.700526	0.837932	17.4466			
12.035209	0.875003	17.8595			

M_1	θ_1	γ	Z_1	π	a
20.00	10.00	1.6667	28.283025	0.100	0.087861
$(A/A^*)_1^{1/2}$		$1/\rho_1$	$\dot{M}_B$	$\ddot{M}_B$	a_0
22.525322		0.411816	2.879743	-0.316990	0.082555
a_1		a_2	M_A	Z_A	r_A
-0.005901		-0.000132	5.017868	0.788756	0.139079

CONTOUR # 46

z	r	M	z	r	M
-0.025065	0.044394		9.455920	0.808771	15.6499
0.074935	0.046384		10.633880	0.845633	16.2432
0.174935	0.052068		10.704848	0.847659	16.2760
0.274935	0.060992		12.022316	0.881888	16.8587
0.374935	0.072677		12.028730	0.882039	16.8613
0.474935	0.086617		13.423810	0.911841	17.4022
0.574935	0.102288		13.499787	0.913292	17.4307
0.674935	0.119147		14.888631	0.937124	17.9003
0.774935	0.136642		15.053609	0.939622	17.9542
0.821017	0.144768	5.1709	16.419998	0.957976	18.3545
0.855281	0.150814	5.3329	16.663591	0.960820	18.4236
0.894410	0.157712	5.5117	18.013490	0.974554	18.7621
0.942497	0.166149	5.7200	18.405056	0.977916	18.8571
1.004112	0.176827	5.9685	19.664950	0.987090	19.1214
1.006704	0.177273	5.9785	20.222263	0.990388	19.2346
1.096397	0.192504	6.2997	21.369205	0.995903	19.4296
1.225591	0.213724	6.7177	22.034396	0.998375	19.5393
1.277216	0.221933	6.8704	23.119333	1.001423	19.6819
1.400158	0.240921	7.2135	23.741287	1.002674	19.7616
1.611737	0.271839	7.7362	24.906563	1.004226	19.8706
1.818758	0.300135	8.2078	25.251838	1.004511	19.9022
2.010950	0.324889	8.5958	26.523663	1.005086	19.9736
2.333072	0.363524	9.1941	26.719153	1.005121	19.9780
2.480460	0.380125	9.4420	27.595136	1.005199	19.9974
2.935508	0.427816	10.1463	28.541880	1.005208	19.9999
3.025588	0.436658	10.2746	28.576230	1.005208	20.0000
3.622838	0.491223	11.0577			
3.651544	0.493673	11.0928			
4.363628	0.550418	11.8944			
4.392650	0.552569	11.9246			
5.165994	0.606112	12.6785			
5.243796	0.611104	12.7487			
6.062168	0.660029	13.4432			
6.176808	0.666372	13.5332			
7.055496	0.711524	14.1856			
7.190545	0.717933	14.2782			
8.148238	0.759986	14.9023			
8.283948	0.765474	14.9838			
9.341352	0.804857	15.5896			

CONTOUR #6

PERFECT FLUID COORDINATES IN EQUAL z INCREMENTS

z	r	First Difference	Second Difference
0.175782	0.137128	0.	0.
0.275782	0.138061	0.000933	0.
0.375782	0.140800	0.002739	0.001806
0.475782	0.145254	0.004455	0.001716
0.575782	0.151331	0.006077	0.001622
0.675782	0.158934	0.007602	0.001526
0.775782	0.167963	0.009029	0.001426
0.875782	0.178316	0.010354	0.001325
0.975782	0.189890	0.011574	0.001220
1.075782	0.202577	0.012687	0.001114
1.175782	0.216269	0.013692	0.001005
1.275782	0.230856	0.014586	0.000894
1.375782	0.246224	0.015368	0.000782
1.475782	0.262260	0.016036	0.000668
1.575782	0.278848	0.016588	0.000552
1.675782	0.295872	0.017024	0.000436
1.775782	0.313214	0.017343	0.000319
1.875782	0.330757	0.017543	0.000200
1.975782	0.348383	0.017626	0.000083
2.075782	0.366010	0.017627	0.000001
2.175782	0.383613	0.017603	-0.000024
2.275782	0.401161	0.017548	-0.000055
2.375782	0.418604	0.017444	-0.000104
2.475782	0.435895	0.017291	-0.000153
2.575782	0.452983	0.017087	-0.000204
2.675782	0.469822	0.016840	-0.000247
2.775782	0.486380	0.016558	-0.000282
2.875782	0.502630	0.016251	-0.000307
2.975782	0.518554	0.015923	-0.000327
3.075782	0.534137	0.015583	-0.000340
3.175782	0.549369	0.015233	-0.000350
3.275782	0.564248	0.014878	-0.000354
3.375782	0.578769	0.014521	-0.000357
3.475782	0.592932	0.014163	-0.000359
3.575782	0.606740	0.013809	-0.000354
3.675782	0.620200	0.013459	-0.000350
3.775782	0.633314	0.013114	-0.000345
3.875782	0.646090	0.012776	-0.000338
3.975782	0.658533	0.012443	-0.000333
4.075782	0.670649	0.012116	-0.000328
4.175782	0.682443	0.011794	-0.000322
4.275782	0.693920	0.011477	-0.000316
4.375782	0.705092	0.011172	-0.000306
4.475782	0.715961	0.010869	-0.000302
4.575782	0.726532	0.010571	-0.000299
4.675782	0.736809	0.010277	-0.000293

CONTOUR #6

z	r	First Difference	Second Difference
4.775782	0.746807	0.009997	-0.000280
4.875782	0.756527	0.009721	-0.000277
4.975782	0.765974	0.009446	-0.000274
5.075782	0.775150	0.009176	-0.000270
5.175782	0.784067	0.008917	-0.000259
5.275782	0.792729	0.008662	-0.000255
5.375782	0.801141	0.008411	-0.000251
5.475782	0.809305	0.008164	-0.000247
5.575782	0.817229	0.007924	-0.000240
5.675782	0.824918	0.007689	-0.000235
5.775782	0.832378	0.007459	-0.000230
5.875782	0.839612	0.007234	-0.000225
5.975782	0.846624	0.007012	-0.000222
6.075782	0.853419	0.006795	-0.000218
6.175781	0.860002	0.006583	-0.000212
6.275781	0.866379	0.006378	-0.000205
6.375781	0.872554	0.006174	-0.000203
6.475781	0.878528	0.005974	-0.000200
6.575781	0.884304	0.005776	-0.000198
6.675781	0.889891	0.005587	-0.000189
6.775781	0.895294	0.005403	-0.000184
6.875781	0.900513	0.005219	-0.000183
6.975781	0.905551	0.005038	-0.000182
7.075781	0.910409	0.004858	-0.000180
7.175781	0.915099	0.004690	-0.000169
7.275781	0.919623	0.004524	-0.000165
7.375781	0.923983	0.004359	-0.000165
7.475781	0.928178	0.004195	-0.000164
7.575781	0.932209	0.004031	-0.000164
7.675781	0.936088	0.003879	-0.000152
7.775781	0.939820	0.003732	-0.000147
7.875781	0.943405	0.003585	-0.000147
7.975781	0.946843	0.003438	-0.000146
8.075781	0.950135	0.003292	-0.000146
8.175781	0.953288	0.003153	-0.000140
8.275781	0.956308	0.003021	-0.000132
8.375780	0.959198	0.002889	-0.000131
8.475780	0.961957	0.002760	-0.000130
8.575780	0.964588	0.002631	-0.000129
8.675780	0.967092	0.002504	-0.000127
8.775780	0.969479	0.002387	-0.000117
8.875780	0.971750	0.002271	-0.000116
8.975780	0.973907	0.002157	-0.000114
9.075780	0.975951	0.002044	-0.000113
9.175780	0.977883	0.001932	-0.000112
9.275780	0.979710	0.001827	-0.000106

CONTOUR #6

s	r	First Difference	Second Difference
9.375780	0.981437	0.001727	-0.000100
9.475779	0.983065	0.001628	-0.000099
9.575779	0.984597	0.001532	-0.000097
9.675779	0.986033	0.001437	-0.000095
9.775779	0.987377	0.001344	-0.000093
9.875779	0.988634	0.001257	-0.000087
9.975779	0.989808	0.001174	-0.000083
10.075779	0.990902	0.001093	-0.000081
10.175779	0.991916	0.001015	-0.000079
10.275779	0.992854	0.000937	-0.000077
10.375779	0.993718	0.000864	-0.000073
10.475778	0.994513	0.000795	-0.000069
10.575778	0.995243	0.000730	-0.000066
10.675778	0.995910	0.000667	-0.000063
10.775778	0.996516	0.000606	-0.000060
10.875778	0.997065	0.000548	-0.000058
10.975778	0.997559	0.000494	-0.000054
11.075778	0.998001	0.000443	-0.000051
11.175778	0.998396	0.000394	-0.000048
11.275778	0.998745	0.000349	-0.000045
11.375778	0.999054	0.000309	-0.000041
11.475778	0.999324	0.000270	-0.000039
11.575777	0.999557	0.000233	-0.000037
11.675777	0.999756	0.000199	-0.000034
11.775777	0.999924	0.000168	-0.000031
11.875777	1.000067	0.000143	-0.000025
11.975777	1.000187	0.000120	-0.000023
12.075777	1.000285	0.000098	-0.000022
12.175777	1.000362	0.000078	-0.000020
12.275777	1.000421	0.000059	-0.000019
12.375777	1.000467	0.000046	-0.000013
12.475777	1.000504	0.000036	-0.000010
12.575776	1.000532	0.000028	-0.000009
12.675776	1.000552	0.000020	-0.000008
12.775776	1.000564	0.000013	-0.000007
12.875776	1.000572	0.000008	-0.000005
12.975776	1.000578	0.000005	-0.000003
13.075776	1.000581	0.000003	-0.000002
13.175776	1.000583	0.000002	-0.000002
13.275776	1.000584	0.000001	-0.000001
13.375776	1.000584	0.000000	-0.000001
13.475776	1.000584	-0.000000	-0.000000
13.548710	1.000584	-0.000000	0.000000

APPENDIX II

DIMENSIONLESS COORDINATES OF FLOW FIELD

APPENDIX II

The tables of nozzle coordinates in this Appendix are provided by the NACA.

The Mach numbers and ratios of specific heats for these coordinates are

M	γ
10.0	5/3
18.0	5/3
27.1	5/3
10.0	7/5
12.0	7/5

Description of the computational method may be found in Reference 27. Figure 39 shows the coordinate system used.

Dimensionless Coordinates of Flow Field

for Mach 10 Nozzle

$\gamma = 5/3$, $\theta_{max} = 10^{\circ}$

x/r_o	R/r_o
0.0000	0.1743
0.0673	0.1771
0.1600	0.1812
0.2358	0.1871
0.3089	0.1942
0.3820	0.2025
0.4564	0.2121
0.5326	0.2229
0.6111	0.2347
0.6921	0.2474
0.7759	0.2610
0.8627	0.2755
0.9526	0.2907
1.0458	0.3067
1.1425	0.3235
1.2428	0.3410
1.3469	0.3592
1.4549	0.3782
1.5668	0.3979
1.6828	0.4184
1.8029	0.4395
1.9264	0.4612
2.1338	0.4970
2.3695	0.5365
2.6373	0.5794
2.9415	0.6255
3.2886	0.6755
3.6812	0.7275
4.1320	0.7836
4.6465	0.8419
5.2343	0.9023
5.9122	0.9652
6.6927	1.0293
7.5949	1.0940
8.6389	1.1579
9.8511	1.2197
11.2621	1.2777
12.8914	1.3280
14.7825	1.3700
16.9269	1.3989
19.2871	1.4144
21.5545	1.4185

r_o = distance from point source to sonic sphere in radial flow

Dimensionless Coordinates of Flow Field

for Mach 18 Nozzle

$\gamma = 5/3$, $\theta_{max} = 12^{\circ}$

x/r_o	R/r_o	x/r_o	R/r_o
0.0000	0.2091	7.9156	1.5432
0.0642	0.2128	9.1364	1.6912
0.1682	0.2189	10.7084	1.8559
0.2398	0.2262	12.3266	2.0231
0.3078	0.2347	14.4314	2.2117
0.3755	0.2445	16.9456	2.4113
0.4439	0.2554	20.1190	2.6305
0.5138	0.2674	23.9784	2.8579
0.5854	0.2804	28.7809	3.0941
0.6592	0.2943	34.7754	3.3312
0.7353	0.3091	42.3632	3.5610
0.8140	0.3247	51.8741	3.7640
0.8954	0.3411	63.6494	3.9194
0.9798	0.3584	77.5568	4.0073
1.0674	0.3765	90.9731	4.0285
1.1582	0.3954		
1.2526	0.4152		
1.3506	0.4358		
1.4525	0.4574		
1.5582	0.4797		
1.6680	0.5030		
1.7823	0.52733		
1.9008	0.5524		
2.0236	0.5785		
2.1514	0.6057		
2.2830	0.6335		
2.5499	0.6891		
2.8570	0.7516		
3.2094	0.8200		
3.6159	0.8960		
4.0914	0.9821		
4.6335	1.0728		
5.2718	1.1756		
6.0127	1.2865		
6.8860	1.4095		

r_o = distance from point source to sonic sphere in radial flow

Following are the non-dimensional ordinates for a Mach number of 27 axisymmetric nozzle for use with helium as calculated by the characteristics method. The ordinates are made non-dimensional with respect to the <u>throat radius</u>. The ordinates do <u>not</u> include a correction for the boundary layer. This nozzle has not been constructed and it is not known how good the flow will be for this nozzle.

M = 27.112983

$\gamma = 5/3$

$\frac{x}{y_o}$	$\frac{y}{y_o}$	$\frac{x}{y_o}$	$\frac{y}{y_o}$
0.01180	1.00000	20.69288	5.47324
.02667	1.00000	24.59023	6.25347
.04304	1.00001	28.82146	7.05123
.06057	1.00012	33.63856	7.87267
.07916	1.00017	39.05761	8.71044
.11907	1.00041	44.77941	9.55194
.16232	1.00079	50.99901	10.39820
.20856	1.00133	57.68930	11.24514
.25821	1.00203	64.93383	12.09512
.31152	1.00295	72.53907	12.94214
.37292	1.00422	80.70016	13.78335
.63661	1.01221	89.36522	14.62070
.78595	1.01855	98.47014	15.45262
.90202	1.02434	108.1828	16.27398
1.00413	1.03009	118.3027	17.08596
1.09895	1.03593	128.7716	17.88923
1.27632	1.04823	140.0699	18.67716
1.44779	1.06175	151.5685	19.45863
1.61764	1.07670	163.9566	20.21856
1.79135	1.09361	176.4056	20.97271
1.97265	1.11290	189.6318	21.70261
2.17849	1.13686	203.0491	22.42508
3.06475	1.26366	217.4121	23.12061
3.61598	1.36082	233.1475	23.78141
4.07186	1.45101	248.7594	24.44009
4.50204	1.54379	264.2852	25.09788
4.93343	1.64393	279.7106	25.75379
5.84430	1.87664	295.7865	26.38592
6.19099	1.96902	314.3718	26.93600
6.30605	2.00162	332.8140	27.48587
6.40403	2.02932	351.1358	28.03583
6.54803	2.07080	369.3423	28.58568
6.56756	2.08254	387.4399	29.13525
7.43577	2.32535	406.4804	29.64825
9.03423	2.77551	428.8279	30.03777
11.13536	3.34081	451.0114	30.42981
13.68614	3.98642	473.0272	30.82394
17.04654	4.71363	494.9003	31.22031

Dimensionless Coordinates of Flow Field

for Mach 10 Nozzle

$\gamma = 7/5$, $\theta_{max} = 16^{\circ}$

x/r_o	R/r_o
0.0000	0.2783
0.0457	0.2790
0.0957	0.2799
0.1457	0.2839
0.2557	0.2935
0.3757	0.3084
0.4357	0.3176
0.4957	0.3279
0.5657	0.3412
0.6457	0.3577
0.7257	0.3754
0.8157	0.3965
0.8957	0.4161
0.9957	0.4415
1.0457	0.4544
1.0957	0.4675
1.2457	0.5077
1.2957	0.5213
1.3957	0.5488
1.5457	0.5905
1.8957	0.6891
2.4839	0.8569
3.2159	1.0667
4.4405	1.4025
5.0919	1.5694
6.9957	2.0161
7.9957	2.2293
8.9957	2.4298
10.4957	2.7088
13.9957	3.2801
16.9957	3.6975
20.9957	4.1737
25.4957	4.6235
29.4957	4.9602
33.4957	5.2484
37.4957	5.4956
41.4957	5.7063
44.4957	5.8434
47.4957	5.9642
52.4957	6.1330
56.4957	6.2420
60.4957	6.3305
64.4957	6.4005
66.4957	6.4294
69.9957	6.4711
72.9957	6.4981
76.4957	6.5207
79.4957	6.5338
82.4957	6.5420
88.6176	6.5478

r_o = distance from point source to sonic sphere in radial flow

Dimensionless Coordinates of Flow Field

for Mach 12 Nozzle

$\gamma = 7/5$, $\theta_{max} = 16^{\circ}$

x/r_o	R/r_o	x/r_o	R/r_o
0.0000	0.2783	31.4957	5.930
0.0457	0.2790	35.4957	6.341
0.0957	0.2799	39.4957	6.713
0.1457	0.2839	43.4957	7.044
0.2557	0.2935	47.4957	7.340
0.3757	0.3084	51.4957	7.621
0.4357	0.3176	55.4957	7.877
0.4957	0.3279	59.4957	8.110
0.5657	0.3412	63.4957	8.326
0.6457	0.3577	67.4957	8.521
0.7257	0.3754	71.4957	8.698
0.8157	0.3965	75.4957	8.860
0.8957	0.4161	79.4957	9.012
0.9957	0.4415	83.4957	9.148
1.0457	0.4544	87.4957	9.270
1.0957	0.4675	91.4957	9.382
1.2457	0.5077	95.4957	9.484
1.2957	0.5213	99.4957	9.577
1.3957	0.5488	103.4957	9.654
1.5457	0.5905	107.4957	9.726
1.8957	0.6891	113.4957	9.820
2.4839	0.8569	123.2699	9.9063
3.2159	1.0667	131.2962	9.9781
3.4957	1.148	139.8924	10.0319
4.4957	1.428	148.7971	10.0479
5.4957	1.701		
6.4957	1.956		
7.4957	2.198		
8.4957	2.428		
9.4957	2.649		
11.4957	3.063		
15.4957	3.789		
19.4957	4.429		
23.4957	4.984		
27.4957	5.480		

r_o = distance from point source to sonic sphere in radial flow

DISTRIBUTION

Copies of AGARD publications may be obtained in the various countries at the addresses given below.

On peut se procurer des exemplaires des publications de l'AGARD aux adresses suivantes.

BELGIUM BELGIQUE	Centre National d'Etudes et de Recherches Aéronautiques 11, rue d'Egmont Bruxelles.
CANADA	Director of Scientific Information Services, Defence Research Board Department of National Defence 'A' Building Ottawa, Ontario.
DENMARK DANEMARK	Military Research Board Defence Staff Kastellet Copenhagen Ø.
FRANCE	O.N.E.R.A. (Direction) 25, avenue de la Division-Leclerc Châtillon-sous-Bagneux (Seine)
GERMANY ALLEMAGNE	Wissenschaftliche Gesellschaft für Luftfahrt Zentralstelle der Luftfahrtdokumentation München 64, Flughafen Attn: Dr. H.J. Rautenberg
GREECE GRECE	Greek Nat. Def. Gen. Staff B. MEO Athens.
ICELAND ISLANDE	Director of Aviation C/o Flugrad Reykjavik Iceland
ITALY ITALIE	Centro Consultivo Studi e Ricerche Ministero Difesa - Aeronautica Rome.

LUXEMBURG LUXEMBOURG	Luxemburg Delegation to NATO Palais de Chaillot Paris 16.
NETHERLANDS PAYS BAS	Netherlands Delegation to AGARD 10 Kanaalstraat Delft, Holland.
NORWAY NORVEGE	Chief Engineering Division Royal Norwegian Air Force Deputy Chief of Staff/Material Myntgaten 2 Oslo, Norway Attn: Lt. Col. S. Heglund
PORTUGAL	Subsecretariado da Estado da Aeronautica Av. da Liberdade 252 Lisbon. Attn: Lt. Col. Jose Pereira do Nascimento
TURKEY TURQUIE	M. M. Vekaleti Erkaniharbiyei Umumiye Riyaseti Ilmi Istisare Kurulu Mudurlugu Ankara, Turkey Attn: Brigadier General Fuat Ulug
UNITED KINGDOM ROYAUME UNI	Ministry of Supply TIL, Room 009A First Avenue House High Holborn London, W.C.1.
UNITED STATES ETATS UNIS	National Aeronautics and Space Administration 1512 H Street, N.W. Washington 25, D.C.

Printed by Technical Editing and Reproduction Ltd
95 Great Portland St. London, W.1.

UNCLASSIFIED